UNIVERSITÀ POLITECNICA DELLE MARCHE

FACOLTÀ DI INGEGNERIA

Corso di Laurea Magistrale in Biomedical Engineering

Tesi di Laurea:

Brain interhemispheric connectivity: functional and structural analysis

Relatore:

Prof.ssa Mara Fabri

Tesi di laurea di:

Grazia Pia Perrotti

Correlatori:

Prof.ssa Laura Burattini

Dott.ssa Ilaria Marcantoni

A.A 2022/2023

Abstract

The aim of this thesis is to investigate whether bilateral activations occur in a callosotomised patient, and to identify possible pathways through which the exchange of information between the hemispheres takes place. The architecture of the brain is characterised by two hemispheres, left and right, which are constantly in communication with each other to allow the integration of information, necessary to perform several neural functions. This transfer of information takes place thanks to the corpus callosum (CC), a C-shaped structure of white matter and nerve pathways. The CC can be surgically severed through a procedure known as corpus callosotomy, introduced as a treatment option for epilepsy. Despite the various consequences and functional effects of callosal sectioning, patients underwent callosotomy provide a useful opportunity of research, as they constitute a good neuroanatomical model for understanding human neuroplasticity and the relationship between structural and functional connectivity. Structural connectivity represents the physical anatomical connections between different groups of neurons, while functional connectivity is defined as the temporal dependency of neuronal activation patterns of anatomically separated brain regions. This study is based on the analysis of data obtained from a healthy subject and a pathological one, underwent callosotomy about 20 years before. To perform structural and functional analysis of data, Brain Voyager, a powerful neuroimaging software package for data management and data analysis, was employed. In the analysis process, the evaluation of interhemispheric functional connectivity and the recognition of the resting state networks (RSNs) were performed by using the independent component analysis technique. Afterwards, the tractography was performed and the resulted white matter tracts, connecting the region of interests defined on the individuated RSNs, were reconstructed. White matter tracts constitute the structural highways of the brain, enabling information to travel quickly from one brain region to another. The tractography was performed taking into consideration three RSNs for the healthy subject and three RSNs for the patient. Tractography results have demonstrated, for the subject, the presence of anatomical callosal fibres connecting the functionally linked activated cortical areas. For the patient, the persistence in some cases of bilateral activation would suggest the presence of subcortical pathways alternative to the CC.

Contents

Introduction

Understanding the functioning and structural networks present in the brain has always been a topic that fascinating to many researchers. The development and advent of new imaging technologies has allowed to have better knowledge about cognitive brain functioning that occurs via the connections and interactions between different components of the brain. The human brain is defined as a complex biological network system characterized by a structural connectome of interconnected areas and a functional connectome of interregional neural activity. From a structural point of view the brain is divided into two main parts, called hemispheres, which communicate with each other to exchange information necessary to perform numerous neural functions. In fact, the brain is responsible for many sensory and motor functions, which are controlled by the right or left hemisphere according to the principle of hemispheric lateralization.

Interhemispheric communication is guaranteed by the presence of cerebral commissures that allow a continuous exchange of information. The largest and most important commissure is represented by the CC, a C-shaped structure of white matter and nerve pathways. This neural bridge is the largest white matter structure in the brain, composed by millions of nerve fibres. Damage to the CC can result in the inability of the hemispheres to communicate properly, causing the impairment of many functions such as changes to visual perception, speech and memory. However, the CC can be surgically severed through a procedure known as callosotomy, a treatment option for epilepsy to reduce spreading of seizures and their configuration in generalized.

William P. van Wagenen, chair of neurosurgery at the University of Rochester, identified a direct association between the frequency of epileptic attacks and the integrity of CC, thereby introducing the rationale behind corpus callosotomy in epilepsy management. Subsequently, numerous studies were conducted to investigate possible consequences and functional effects of callosotomy. These studies revealed the presence of numerous symptoms due to callosal sectioning in the human brain. This set of symptoms is considered a part of the spectrum of disconnection syndrome. However, patients underwent callosotomy represent a useful opportunity of research, as they constitute a good neuroanatomical model for understanding human neuroplasticity and the relationship between structural and functional connectivity.

Structural connectivity represents the physical anatomical connections between different groups of neurons, while functional connectivity is defined as the temporal dependency of neuronal activation patterns of anatomically separated brain regions.

The advent of new imaging technologies, such as resting state functional Magnetic Resonance Imaging (rs-fMRI) and Diffusion Tensor Imaging (DTI), has allowed researchers and clinicians to have a better knowledge about brain functioning and structural connections between different components of the brain. DTI technique enables the reconstruction of white matter tracts based on the direction of water molecules diffusion, useful to establish structural connectivity across brain regions. The fMRI indeed, relies on detecting the small changes in Blood Oxygen Level Dependent signal to produce resonance images associated with neuronal activity. In this study, functional and structural connectivity analysis were performed on both healthy and pathological subject. In healthy subjects, the transfer of information is supported by the presence of fibres passing through the CC, allowing the bilateral activation of areas in the brain. In some cases, the bilateral activations are also found in pathological subjects, despite they have underwent callosal resection. Therefore, the purpose of the DTI analysis is to support, from a structural point of view, the results obtained from the functional analysis. According to this, healthy subject is used as a term of comparison to show that, when bilateral activations are present even in pathological patients, communication between the right and left hemispheres takes place through different paths. The aim of this thesis is to investigate, by performing a DTI analysis, how bilateral activations occur in a callosotomised subject, to individuate possible alternative pathways to the CC, through which the exchange of information between the two hemispheres takes place.

Chapter 1 Anatomy and Physiology of the Human Brain

1.1 The Nervous System

The nervous system (NS) is made up of vast neural networks and contains numerous sensors, localized especially on the surface of the body, able to detect and integrate environmental stimuli into the nervous centres. This enables the organism to be in relation with the external world. (Ambrosi et al., 2010). Sensory and motor components are well coordinated to provide appropriate motor responses to the stimuli or sensory inputs that have been received, stored, and processed (Ludwig et al., 2022). Furthermore, thanks to the neuronal plasticity of its cells, the NS is able to adapt to situations never encountered before. It also has been shown that that neural stem cells are plastic and involved in creating new connections in adaptation and response to injury (Ludwig et al., 2022). The NS is divided topographically into two parts ***(Figure 1.1)***: the central nervous system (CNS) and the peripheral nervous system (PNS).

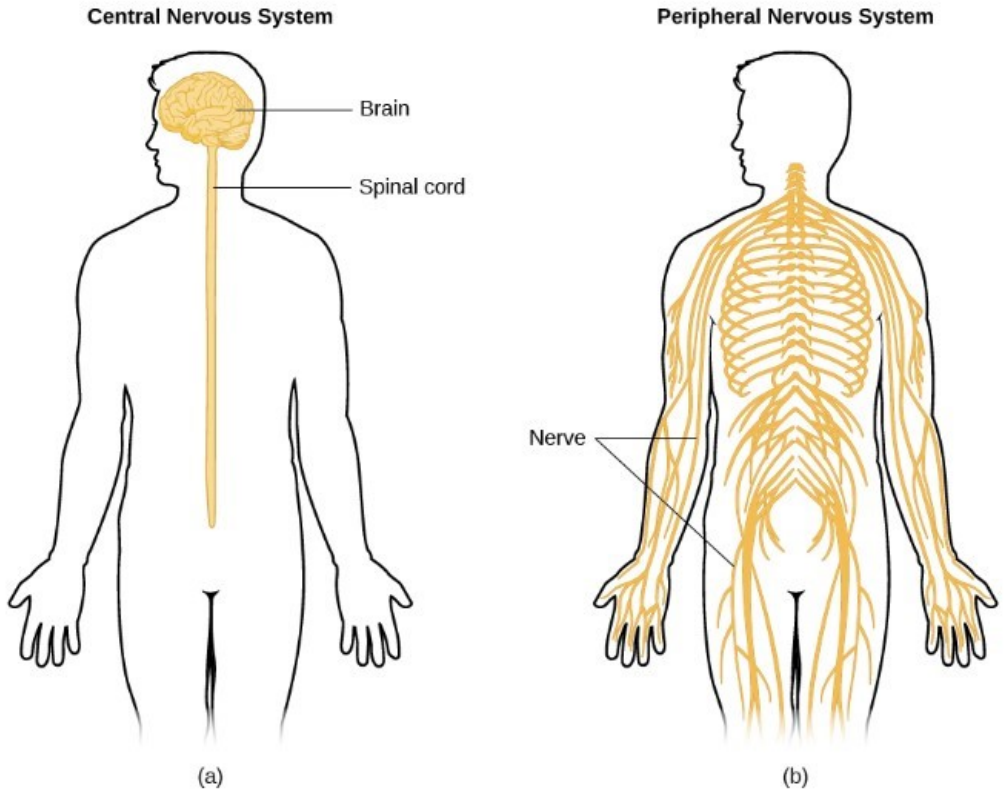

Figure 1.1 *The nervous system is divided into two major parts: (a) the Central Nervous System, brain and spinal cord, and (b) the Peripheral Nervous System, which encompasses nerves outside the brain and spinal cord (Spielman et al.,2021).*

From a functional point of view, however, the two systems are intimately connected and function in an integrated and coordinated manner. The CNS comprises the brain and spinal cord, while the PNS is made up of cranial and peripheral nerves and associated neurological structures (Bazira, 2021). Both the components of the CNS are surrounded by the bones of the axial skeleton: the brain stays in the cranial cavity of the skull and the spinal cord in the vertebral (spinal) canal (Bazira, 2021). The brain is the most complex part of the human body. This three-pound organ is the seat of intelligence, interpreter of the senses, initiator of body movement, and controller of behaviour. Lying in its bony shell and washed by protective fluid, the brain is the source of all the qualities that define our humanity (www.ninds.nih.gov). The spinal cord is a vital aspect of the CNS and is located within the vertebral column. The purpose of the spinal cord is to send motor commands from the brain to the peripheral body as well as to relay sensory information from the sensory organs to the brain. Spinal cord protection is insured by bone, meninges, and cerebrospinal fluids (Thau et al., 2022). The peripheral nerves in the PNS contain nerve fibres that carry information (stimuli) received by sensory receptors from the internal and external environment to the CNS (afferent nerve fibres), and other fibres carrying motor information from the CNS to effector structures (efferent nerve fibres) (Bazira, 2021). Functionally, the PNS is divided into the somatic and autonomic nervous systems. The autonomic nervous system regulates involuntary physiologic processes including heart rate, blood pressure, respiration, digestion, and sexual arousal (Waxenbaum et al., 2022). The somatic nervous system plays a major role in the voluntary control of the body movements via the use of skeletal muscles. It is responsible for all the functions we are aware of and can consciously influence. The somatic nervous system consists of both afferent (sensory) and efferent (motor) nerves (Akinrodoye and Lui, 2022). The autonomic nervous system can be further divided into sympathetic, parasympathetic, and enteric components. Activation of the sympathetic component leads to a state of overall elevated activity and attention: the “fight or flight” response, while the parasympathetic promotes the “rest and digest” processes (Waxenbaum al., 2022). The enteric nervous system is autonomous in its function, but this function can be upregulated or downregulated by the parasympathetic and sympathetic nervous systems (Bazira, 2021).

1.1.1 Cells of the Nervous System

Learning how the cells and organs (like the brain) function, helps us understand the biological basis behind human psychology (Spielman et al., 2021). Like the other organs in our body, the NS is made up of specialized cells: nerve cells (neurons) and glial cells (glia). Neurons represents the basic functional units of the NS, able to generate electric signal called action potential, allowing them to quickly transmit information over long distances. Indeed, glia are essential for the functioning of the NS, since they play a supporting role for neurons (www.khanacademy.org).

1.1.1.1 Glial cells

Glial cells provide scaffolding on which the NS is built, help neurons line up closely with each other to allow neuronal communication, provide insulation to neurons, transport nutrients and waste products, and mediate immune responses (Spielman et al., 2021). The most notable glial cells include (***Figure 1.2***): Oligodendrocytes, Schwann cells, Satellite cells, Astrocytes, Microglia, and Ependymal cells (Ludwig and Das, 2022). Four of these are found only in the CNS (Astrocytes, Oligodendrocytes, Microglia and Ependymal cells). Satellite and Schwann cells are found only in the PNS (qbi.uq.edu.au/brain-basics/).

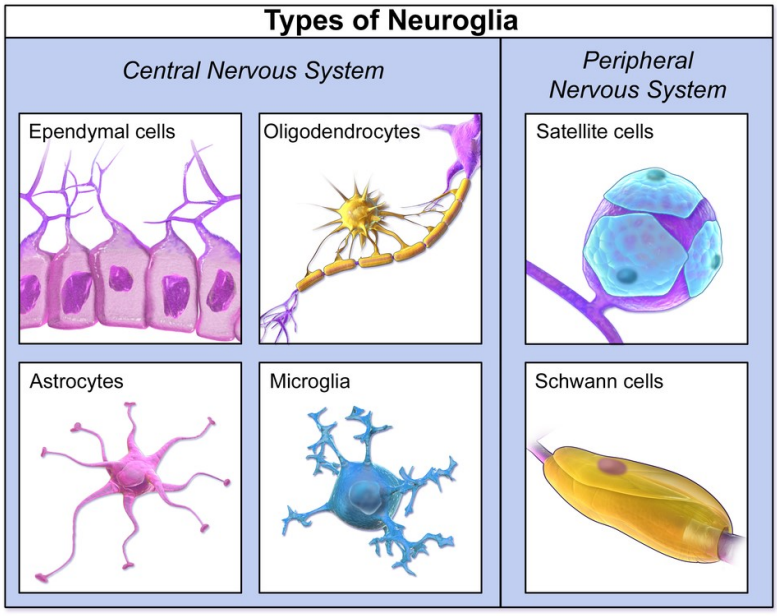

Figure 1.2 *Illustration of the glial cells. They include oligodendrocytes, astrocytes, microglia, and ependymal cells in the CNS and Schwann cells, satellite cells in the PNS (www.physio-pedia.com/Glial_Cells).*

Astrocytes are the most abundant cells in the brain. They are star-shaped glial cells that, thanks to their extensive branching, they are able to contact many neuronal soma, dendrites and axons simultaneously (Ludwig and Das, 2022). They communicate through gap junctions and are involved in the release and uptake of chemicals at synapses level **(**Ludwig and Das, 2022). They also contribute into the structure and functioning of the blood-brain barrier, which helps to protect the brain from potentially toxic substances in the blood (Ludwig and Das, 2022). Microglia are resident macrophages of the CNS, playing a role in removing foreign or damaged material, cells, or organisms (Ludwig and Das, 2022).

Schwann cells and Oligodendrocytes share a similar function, but in different places: the former are mainly found into the PNS, while the latter in the CNS. They both produce myelin, a substance composed of layered phospholipid membranes, useful to support and insulate axons, allowing for faster impulse transduction (Ludwig and Das, 2022). In the myelin sheath it is possible to find some gaps, the so-called Nodes of Ranvier that interrupt the insulation at intervals. This discontinuity enables impulses to jump from node to node in a process known as *saltatory conduction*, increasing the speed at which these impulses travel (www.britannica.com/science/node-of-Ranvier).

One of the differences between Oligodendrocytes and Schwann cells is that the first can myelinate multiple neurons at a time, but a single Schwann cell can only myelinate one neuron (www.kenhub.com/en/library/anatomy/histology-of-glial-cells). Another type of glial cells are the Satellite cells. Together with the Schwann cells represent the two major cell types in the PNS (www.kenhub.com/en/library/anatomy/histology-of-glial-cells). Satellite glial cells are unique cells whose most distinctive morphological feature is that they wrap around neuronal cell bodies, in most cases forming a complete envelope. They are found exclusively in peripheral ganglia —sensory, parasympathetic and sympathetic ganglia (Hanani and Spray, 2020). Ependymal cells form the epithelial lining of the ventricles and the central canal of the spinal cord. They possess hair-like structures, called cilia, that beat in a coordinate manner to facilitate the movement of the cerebrospinal fluid (CSF), guaranteeing the arrival of nutrients to neurons (www.britannica.com/science/ependymal-cell).

1.1.1.2 Neurons

Neurons are the central building blocks of the nervous system. Like all cells, neurons consist of several different parts, each one performing a specific function (Spielman et al., 2021). Externally the neuron is covered by a semipermeable membrane which allows smaller molecules to pass, while blocking larger ones. Structurally the neuron consists of three major components: the soma, axon and dendrites (***Figure 1.3***). The soma or 'cell body' contains the nucleus of the neuron and it is characterised by branching extensions called dendrites. The neuron is considered a small information processor, and dendrites serve as input sites where signals are received from other neurons. These signals are then transmitted electrically across the soma and down the axon, a major extension from the body cell, which ends with multiple terminal buttons. They contain synaptic vesicles that house neurotransmitters, the chemical messengers of the nervous system (Spielman et al., 2021). When the signal propagates and reaches synaptic vescicles, they release neurotransmitter into the synapse, a very little space between two contiguous neurons, in which communication occurs. Once neurotransmitters are released into the synapse, they travel across the small space and bind with corresponding receptors on the dendrite of the adjacent neuron. Receptors match different neurotransmitters, according to a lock and key relationship (Spielman et al., 2021).

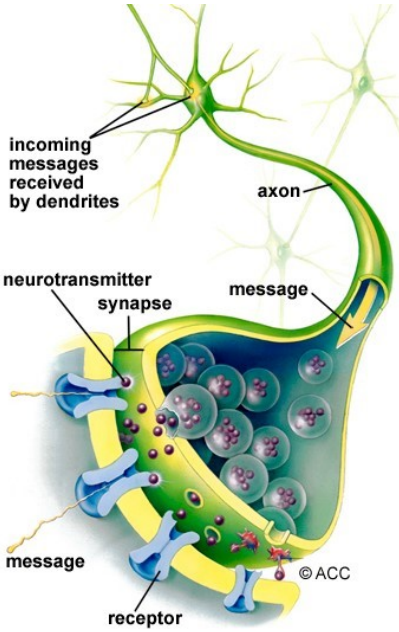

Figure 1.3 *Representation of the nerve cells components: cell body, dendrites and axon. Neurons communicate with each other by exchanging neurotransmitters across a tiny gap called synapse (mayfieldclinic.com).*

1.1.1.2.1 Types of Neurons

Based on their roles, the neurons found in the NS can be divided into three main classes: sensory neurons, motor neurons, and interneurons (***Figure 1.4***) (www.khanacademy.org).

Sensory neurons

Sensory neurons are nerve cells that are activated by sensory inputs from the environment. Inputs can be physical or chemical, corresponding to all five of our senses (qbi.uq.edu.au/brain/brain-anatomy/). They are found in receptors such as the eyes, ears, tongue, nose and skin, and carry nerve impulses to the spinal cord and brain. When these nerve impulses reach the brain, they are translated into 'sensations', such as vision, hearing, taste, olfaction and touch. They get information about what's going on inside and outside of the body and bring that information to the CNS, where it can be processed (www.khanacademy.org).

Motor neurons

Motor neurons are a specialized type of cells located into the brain and spinal cord. These neurons transmit impulses from the spinal cord to skeletal and smooth muscles directly controlling all muscle movements.

When stimulated, motor neurons release Acetylcholine as neurotransmitter, that bind to the receptors on muscles to trigger a response, leading to muscle contraction and eventually to movement execution (nba.uth.tmc.edu/neuroscience/m/s3/chapter01.html). For instance, if you picked up a hot coal, the motor neurons innervating the muscles in your arm would cause your hand to let go (www.khanacademy.org).

Interneurons

Interneurons or relay neurons are found in the brain and spinal cord and allow sensory and motor neurons to communicate. Interneurons are the most abundant class of neurons and are involved in processing information. They receive information from other neurons (either sensory neurons or interneurons) and transmit information to other neurons (either motor neurons or interneurons). It would be combinations of interneurons in your brain that would allow you to draw the conclusion that things that looked like hot coals weren't good to pick up, and, hopefully, retain that information for future reference (www.khanacademy.org).

Considering all the functions listed above it is possible to make a generalization by assuming that all neurons perform three basic functions (www.khanacademy.org):

1. Receive signals (or information).
2. Integrate incoming signals (to determine whether or not the information should be passed along).
3. Communicate signals to target cells (other neurons or muscles or glands).

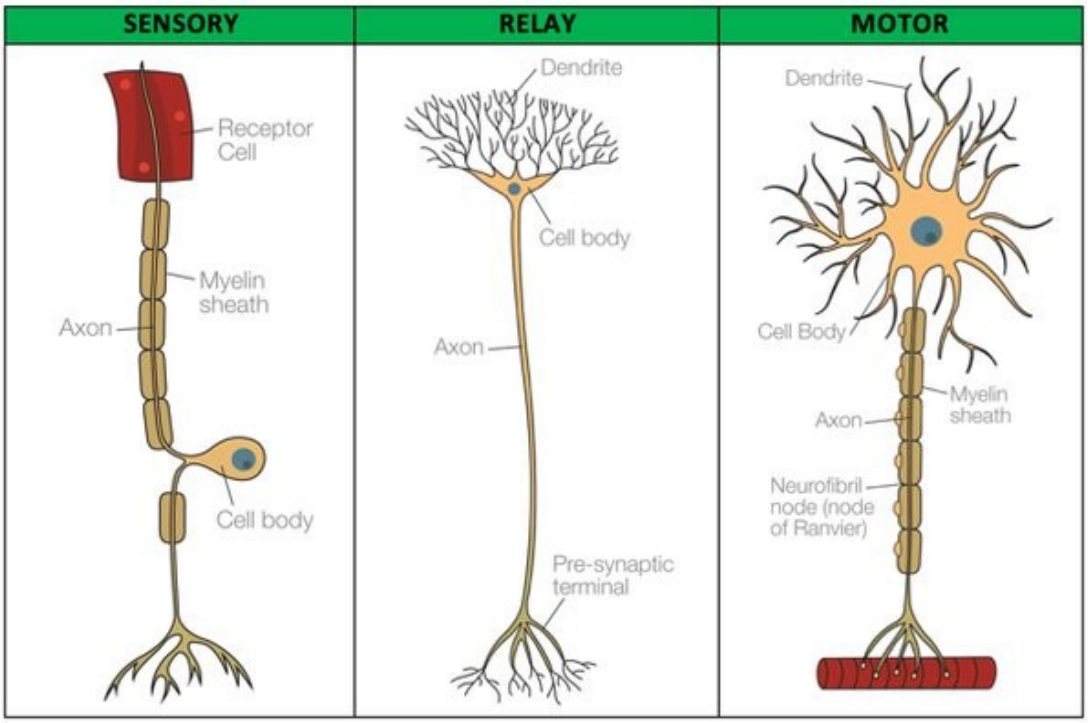

Figure 1.4 *Sensory Neurons, Relay Neurons and Motor Neurons morphology (Anastasi et al., 2012).*

1.1.1.2.2 Neuronal Action Potential

The neuron is surrounded by extracellular fluid, and inside it contains intracellular fluid, called cytoplasm. Being their ionic composition different, there will be a difference in charge across the membrane, called membrane potential (Spielman et al., 2021). The electrical charge of the fluids is caused by charged molecules (ions) dissolved inside. Being the neuronal membrane semipermeable, it restricts the movement of these charged molecules and, as a result, some of them tend to become more concentrated inside the cell, other outside. When the neuron is not active, membrane's potential is held in a state of readiness, called the resting potential.

In resting state, the inside of the cell is slightly negatively charged compared to the outside, since sodium and potassium are more concentrated outside and inside the cell, respectively (Spielman et al., 2021).When the signal arrives at the neuron, the sodium voltage-gated channels and slightly later, also the potassium voltage-gated channels open, allowing ions on each side of the membrane to move according to their electrochemical gradient. Therefore, ions move from high-concentration to low-concentration areas, and positive ions move towards areas with a negative charge (Spielman et al., 2021). During this period, Na^+ ions will move into the cell, causing an influx of positive charges, that makes the inside of the cell more positive (Spielman et al., 2021). To fully activate the neuron, the potential must reach a certain level, called threshold of excitation. If this is not reached, the action potential will not be generated. For this reason, the action potential is defined as all-or-none phenomenon (Spielman et al., 2021). Many additional channels open, causing a massive influx of Na^+ ions resulting in a spike of the membrane potential. This positive spike constitutes the action potential (***Figure 1.5***): the electrical signal that typically moves from the cell body down the axon to the axon terminals. At the peak of the action potential, the sodium gates close and the potassium gates remain still open. As positively charged potassium ions leave, the cell quickly begins repolarization. At first, it hyperpolarizes, becoming slightly more negative than the resting potential, and then it levels off, returning to the resting potential (Spielman et al., 2021). The action potential propagates along the axon and when reaches the terminals, the signal is transmitted to neighbouring neurons through synapses (Spielman et al., 2021).

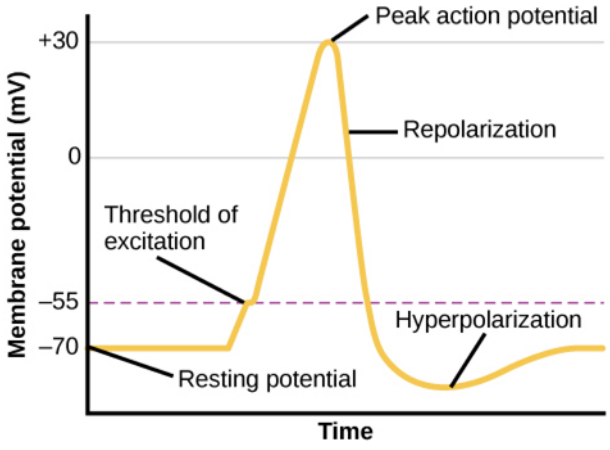

Figure 1.5 *Different phases of the neuronal action potential (Spielman et al.,2021).*

1.2 Human Brain

The brain is one of the most complex organs of the human body responsible for responses, sensation, movement, emotions, communication, thought processing, and all processes regulating our body. The nervous tissue is extremely delicate, in that it can be easily damaged by the smallest amount of force. According to this, the human brain is contained inside the skull and surrounded by meninges and CSF, which plays a protective role. In addition, a blood-brain barrier protects the brain from any harmful substance that could be floating in the blood (Thau et al., 2022). The brain consists of three parts: the cerebrum, cerebellum, and brainstem (***Figure 1.6***).

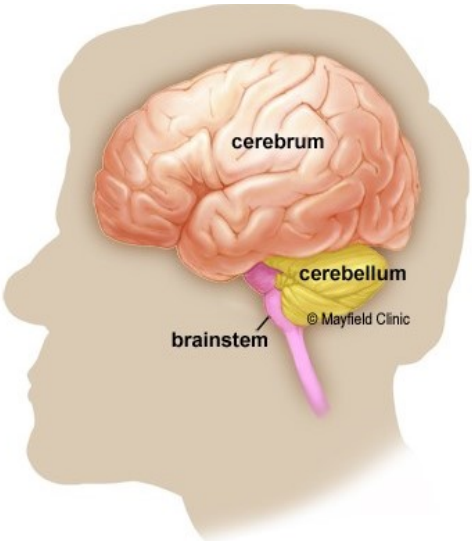

Figure 1.6 *Anatomy of the human brain. It can be divided in 3 parts: cerebrum, cerebellum and brainstem (mayfieldclinic.com).*

The cerebrum takes up more brain volume and it is responsible for the control of somatosensory, motor, language, cognitive thought, memory, emotions, hearing, and vision functions. Structurally it can be divided into two halves by a deep longitudinal fissure: the left and right hemispheres, that communicate each other through the CC (Bui and Das, 2022). Although they are in constant communication, the left and right hemisphere are responsible for different behaviours. The left hemisphere is more dominant with language, logic, and math abilities. The right hemisphere is more creative, being dominant in artistic and musical situations, and intuition. This phenomenon is known as brain lateralization (Thau et al., 2022). Each hemisphere is further subdivided into four separate lobes *(**Figure 1.7**)* (frontal, parietal, occipital, and temporal lobe) by the central sulcus, parieto-occipital sulcus, and lateral fissure.

Each hemisphere performs different functions (Bui and Das, 2022). The cerebral hemisphere in which the comprehension and production of language is predominantly represented is referred to as the dominant hemisphere (Bazira, 2021).

1.2.1 Lobes

Each hemisphere is subdivided into four separate lobes: frontal, parietal, occipital, and temporal lobe.

Frontal Lobe

The frontal lobe is the largest lobe, located in the front of the head (***Figure 1.7).*** The principal functional areas in the frontal lobe are the prefrontal cortex, the primary motor cortex (and associated supplementary and premotor areas), the frontal eye field and the expressive speech area (Broca's area). It controls judgment, problem-solving, planning, behaviour, personality, speech, writing, speaking, concentration, self-awareness, and intelligence.

The primary motor cortex is present in the precentral gyrus of the frontal lobe and is positioned immediately anterior to the central sulcus. The premotor cortex is anterior to the primary motor cortex. This area controls the contralateral body and extremity movement (Bui and Das, 2022). The prefrontal cortex is responsible for a wide variety of higher cortical functions including personality, behaviour, abstract thought, decision making, inhibition (Bazira, 2021). As mentioned above, the frontal lobe contains Broca's area, responsible for speech. This area is not present in both hemispheres, but it is located within the inferior frontal gyrus of the dominant hemisphere (Bui and Das, 2022). The dominant hemisphere, in the vast majority of individuals, is the left one. Therefore, Broca's area is most common in the left inferior frontal gyrus (Bui and Das, 2022).

Parietal Lobe

The parietal lobe constitutes the middle part of the brain and controls perception and sensation. It helps a person identify objects and understand spatial relationships (***Figure 1.7***) (Vitti, 2023). The primary somatosensory cortex processes touch, temperature, and pain information from the contralateral body (Bui and Das, 2022).

Occipital Lobe

The occipital lobe lies posterior to the parietal and temporal lobes (Bazira, 2021). The occipital lobe occupies the back part of the head (***Figure 1.7***). This lobe interprets vision, distance, depth, colour, and objects recognition.

The occipital lobe receives information from both eyes relative to the contralateral visual field (i.e., the left occipital lobe receives and interprets information from the right visual field from both the left and right eye) (Bui and Das, 2022).

Temporal Lobe

The temporal lobe is located in the lower and lateral part of each hemisphere (***Figure 1.7***). The temporal lobe features the auditory cortex; it is concerned with the perception and processing of auditory stimuli. The cortical region just above and behind this area, is the receptive speech cortex (Wernicke's area) that is responsible for receptive aspects of language comprehension (Bazira, 2021). Similarly to Broca's area, Wernicke's area is found only in the dominant hemisphere, which is usually the left one (Bui and Das, 2022).

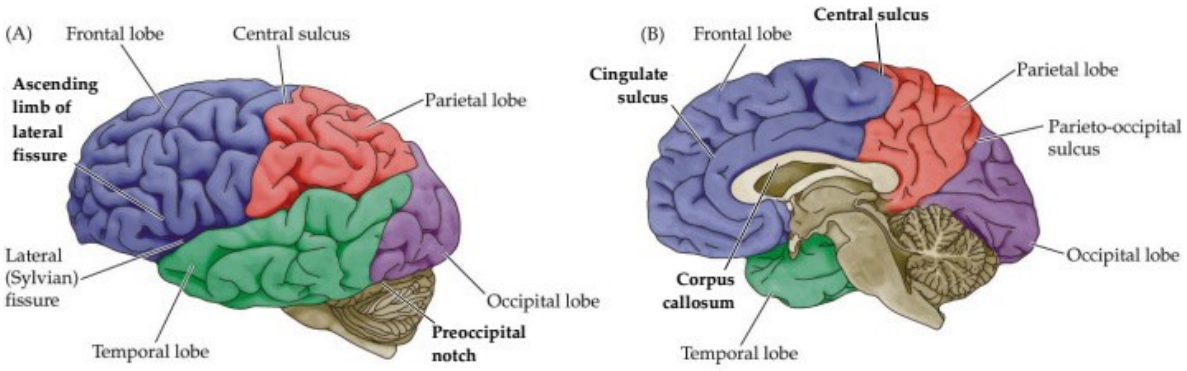

Figure 1.7 *Lateral and midsagittal views of the human brain, emphasizing the division of the cerebral cortex into four lobes (Purves et al., 2018).*

1.2.2 Cerebral Cortex

Each cerebral hemisphere comprises the cerebral cortex, the subcortical white matter, consisting of neural fibre tracts, and the basal nuclei (basal ganglia) (Bazira, 2021). The cerebral cortex is the outermost layer that surrounds the brain, composed of grey matter, and filled with billions of neurons (Thau et al., 2021). The folding of the cortex (***Figure 1.8***) forms ridges (gyri) and grooves (sulci) (Bui and Das, 2022), increasing the surface area of the brain to allow more neurons to fit inside the skull, enabling higher motor functions (mayfieldclinic.com) through the processing of sensory information and the integration of motor functions (Ludwig et al., 2022). The cerebral cortices of the two hemispheres communicate with each other through the fibres of the CC and the anterior commissure. Through the commissural fibres much information received from one hemisphere is also transferred to the other. Since most of the sensory and motor information flows through crossed nerve pathways, the functions of the left hemisphere correspond to the right half of the body and vice versa (Ambrosi et al., 2010). The grey matter constituting the cerebral cortex consists of nerve cell bodies, also including their terminal part (dendrites). It appears grey because that section of the nerve lacks the fatty covering substance called myelin (my.clevelandclinic.org/health/articles). The grey matter of the cortex interprets signals received from different parts of the body and then sends out a response signal. Below the cortex sits white matter, that appears white since the axons are myelinated. White matter receives and sends signals to and from the brain, allowing for fast communication between different part of the brain due to the presence of myelin (Bui and Das, 2022).

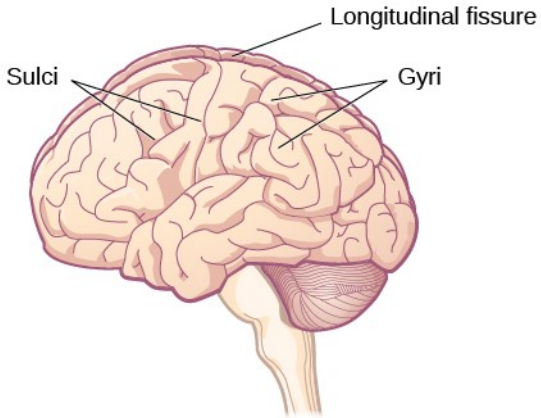

Figure 1.8 *The surface of the brain is covered with gyri and sulci. A deep sulcus is called a fissure, such as the longitudinal fissure that divides the brain into left and right hemispheres (Spielman et al.,2021).*

1.2.2.1 Cerebral Cortical Areas

Several studies performed on humans have shown that some cortical functions are compartmentalized, i.e., that different cortical areas correspond to different functions (Hall,2017). Korbinian Brodmann (1868–1918) can be defined as the founder of anatomical mapping of the brain. In 1909 he published his first studies on the cytoarchitecture of the cortex, in which he elaborated the mapping and subdivision of the cortex in areas with similar histological structure, resulting in the identification of 52 different regions in the cerebral cortex. The cortical areas can be divided into three groups, based on different purposes: associative, motor and sensory areas (***Figure 1.9***) (Bem et al., 2021).

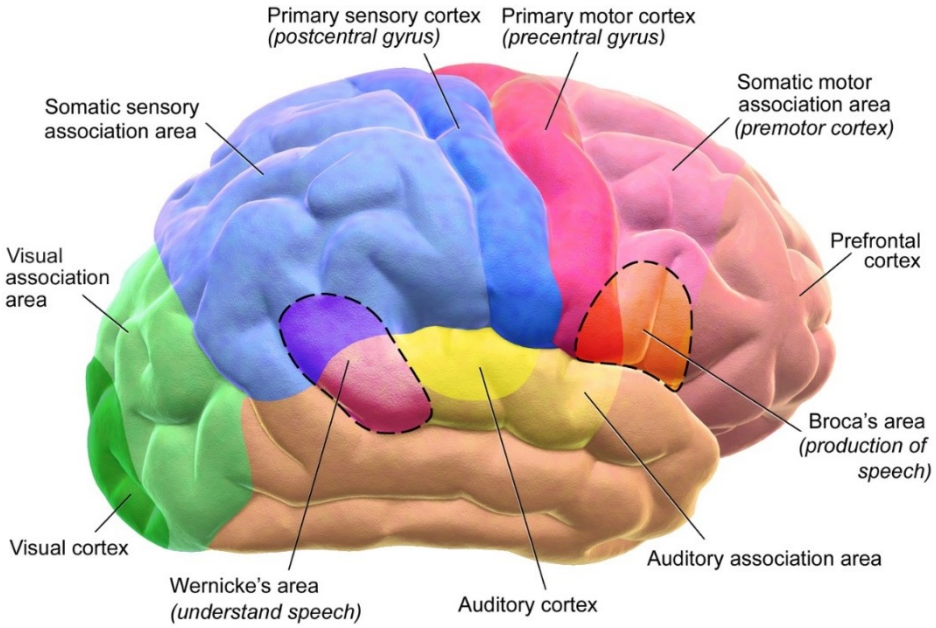

Figure 1.9 *Motor and Sensory regions of the Cerebral Cortex (Medical gallery of Blausen Medical).*

Sensory Areas

Sensory areas can be divided into primary and secondary areas (***Figure 1.10***). The primary areas are involved in the perception of elementary stimuli. The most extensive primary sensory area is the one responsible for general somatic sensitivity, the *primary somatosensory cortex*. Then there are secondary sensory areas that receive inputs from the homonymous primary cortices. They are involved in the coding and decoding of sensory stimuli, allowing their recognition following the attribution of a meaning to the stimulus based on experience. In some primary sensory areas specific pathways are projected from the thalamus, such as the optical, acoustic, gustatory and olfactory ones (Ambrosi et al., 2010).

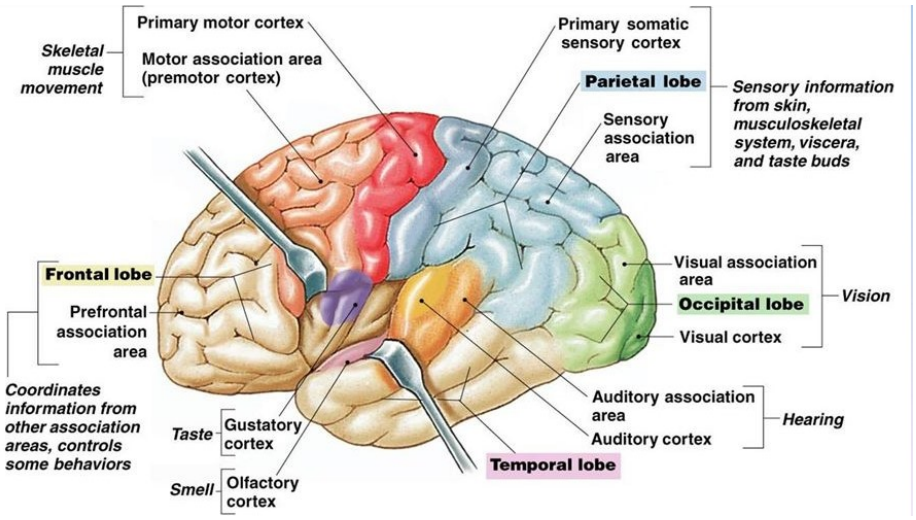

Figure1.10 *Sensory Areas of the Cerebral Cortex (Nacy et al., 2016).*

The *visual cortex* is the primary cortical region of the brain that receives, integrates, and processes visual information relayed from the retinas. It plays a fundamental role in object recognition (Ambrosi et al., 2010). It is in the occipital lobe of the primary cerebral cortex and divides into five different areas (V1 to V5) (Huff et al., 2022). Each hemisphere has its own visual cortex, which receives information from the contralateral visual field. In other words, the right cortical areas process information from the left visual field, and the left processes information from the right visual field (Huff et al., 2022).

The *primary somatosensory cortex* (S1) receives the peripheral sensory information but requires the secondary somatosensory cortex (S2) to store, process, and retain it. The S2 region make decisions on how to approach to the information from our environment by integrating our prior stored experience, factoring our current appraisal of the stimulus, and finally forming a reaction. The S1 region would be associated with identifying the aspects of touch, such as shape, size, texture and temperature. The S2 region would be associated with spatial and tactile memory associated with sensory experiences (Raju and Tadi, 2022).

The *auditory cortex* is located in the temporal lobe and intervenes in the discriminative and conscious perception of sounds (Ambrosi et al., 2010).

The *gustatory cortex*, or primary gustatory cortex, is a region of the cerebral cortex responsible for the perception of taste and flavour.

It is comprised of the anterior insula on the insular lobe and the frontal operculum on the frontal lobe (www.nature.com/subjects/gustatory-cortex).

The *olfactory cortex* is the portion of the cerebral cortex concerned with the sense of smell (www.physio-pedia.com/Olfactory_Cortex), located in the internal surface of temporal lobe.

Motor Areas

The primary function of the motor cortex is to plan and create electrical impulses that cause voluntary muscle contractions. It is composed of the primary motor cortex, premotor cortex, and the supplementary motor area (***Figure 1.11***).

The *primary motor cortex*, situated in Brodmann area 4, sends most electrical impulses coming out of the motor cortex. These fibres directly synapse with motor neurons or interneurons of the spinal cord (Yip and Lui, 2022). It is associated with the coordination and initiation of voluntary movements (Vitti, 2023).

The *premotor cortex* is situated just anterior to the primary motor cortex in Brodmann area 6. Its function is to prepare for movement, especially proximal musculature (Yip and Lui, 2022). The premotor cortex appears to be involved in the selection of appropriate motor plans for voluntary movements, whereas the primary motor cortex is involved in the execution of these voluntary movements (nba.uth.tmc.edu/neuroscience/m/s3/chapter03.html).

The *supplementary motor area* is in the medial surface of the longitudinal fissure. Although not fully understood, proposed functions include body postural stabilization and coordination (Yip and Lui, 2022). It is involved in programming complex sequences of movements and coordinating bilateral movements (nba.uth.tmc.edu/neuroscience/m/s3/chapter03.html).

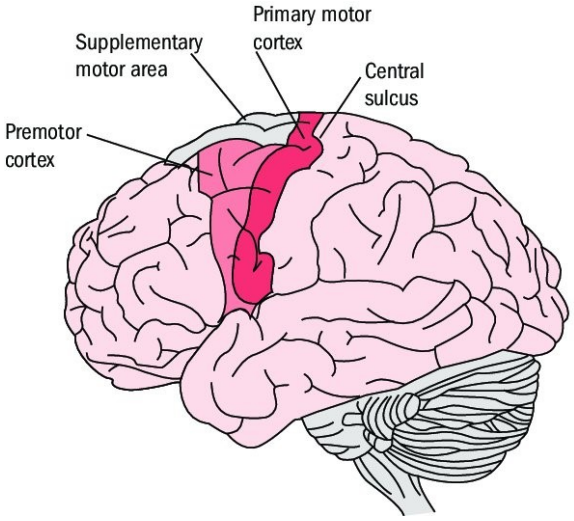

Figure 1.11 *Motor Areas of the Cerebral Cortex (Jefferys and Cooper, 2023).*

Associative Areas

The sum of the various primary and secondary sensory and motor areas constitutes less than half of the total cortical surface. The remaining surface constitutes the set of associative areas (Ambrosi et al., 2010). Important associative areas are: temporo-parieto-occipital area, prefrontal area and limbic area (***Figure 1.12***) (Hall, 2017).

The *temporo-parieto-occipital (TPO)* junction is located at the posterior end of the Sylvian fissure, where the temporal, parietal and occipital lobes meet. The TPO is a complex region of the brain through which various white matter fibres pass. These fibres are involved in several crucial high-level functions, such as language, visuo-spatial recognition, writing and reading (De Benedictis et al., 2014).

The *prefrontal association area* is closely linked and associated with the primary motor areas to plan the sequence of complex motor acts. It is also crucial for mental thought processing processes and for higher cognitive activities, such as judgment, discrimination and choice (Hall, 2017).

The *limbic association area* is involved into the control of the behaviour, emotions and motivations (Hall, 2017).

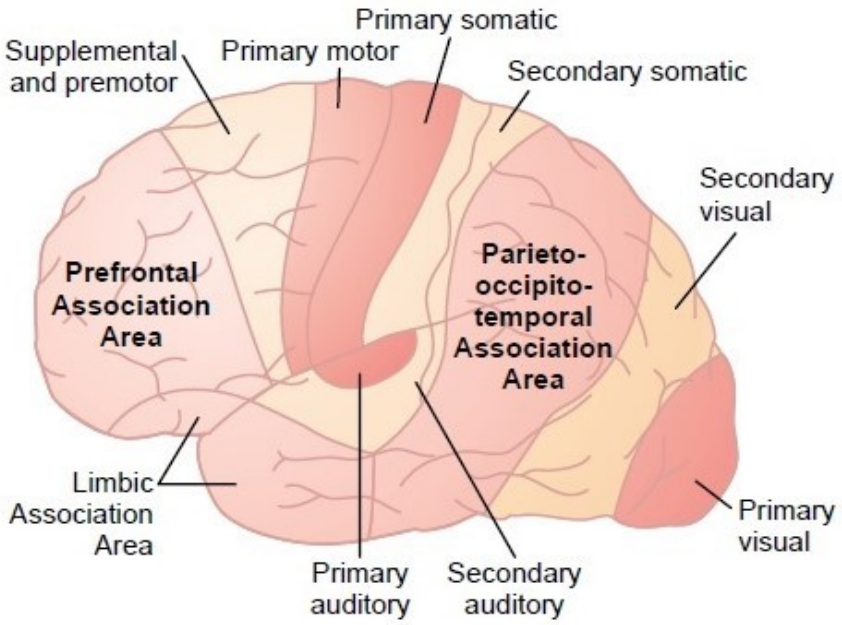

Figure 1.12 *Location of major association areas of the Cerebral Cortex (Hall, 2012).*

1.2.2.1.1 Broca's and Wernicke's Areas

Processing and producing language are complex processes, in which several structures within the brain participate, all playing a crucial role (Stinnett et al., 2022).

Broca's area (the motor speech centre) in the prefrontal cortex and Wernicke's area (the sensory speech centre) in the temporal lobe are the two most well-known cortical areas involved in the production and comprehension of speech (Chaplin et al., 2020). However, this classical model of neural basis of language has grown to a larger and more complex one based upon recent advancements in neuroscience, comprising the frontal, temporal, and parietal language areas (Fujii et al., 2016).

Broca's area

The Broca's area is important for the motor execution of speech, written and spoken. In fact, in this area the motor patterns used for the pronunciation of single words or short sentences are planned (Hall, 2017). The process of identifying the parts of the brain that are involved in language began in 1861, when Paul Broca, a French neurosurgeon, examined the brain of a recently deceased patient suffering from neurologic disorders. Though he was able to understand spoken language, each time he attempted to produce a complete sentence or answer to a question, he was unable to reproduce any words. The only articulate sound he could make was a single repetitive syllable "tan". During autopsy, a lesion on the surface of the frontal lobe was found. Subsequently, Broca studied eight other patients, with similar language deficits and lesions in their left frontal hemisphere. This led him to make his famous statement which claims that "we speak with the left hemisphere" and to identify, for the first time, the existence of a "language centre" in the posterior portion of the frontal lobe of this hemisphere. This is known as Broca's area, represented in Brodmann's (1909) cytoarchitectonic map as areas 44 and 45 (***Figure 1.13***) (Dronkers et al., 2007). Speech disorders resulting from lesions in Broca's area are known as motor aphasia. Clinical studies of Broca's aphasia often assume that the deficits in these patients are due entirely to dysfunction in Broca's area. Recent studies have instead suggested that other regions also play a role in speech production, some of which are medial to the area originally described by Broca on the lateral surface of the brain (Dronkers et al., 2007).

Wernicke's Area

Although the final product of speech is a series of muscle movements, the brain mechanisms involved in speech production should not be seen as limited to motor commands that move muscles. Before such commands can be sent, the speaker must momentarily activate knowledge about the sequence of consonant and vowel speech sounds (phonemes) that form the word to be spoken. This mental stage prior to articulation is known as *phonologic retrieval*. This process is required for all speech production tasks, including repetition, word retrieval (e.g., in spontaneous speech or naming), and reading aloud (Binder, 2015). Wernicke area was first discovered in 1874 by a German neurologist, Carl Wernicke. It has been identified as one of two areas found in the cerebral cortex that manages speech. Wernicke area is located in Brodmann area 22 (***Figure 1.13***), the posterior segment of the superior temporal gyrus in the dominant hemisphere. Since 95% of people have a left dominant hemisphere, the Wernicke area is usually found on the left side. Because the Wernicke area is responsible for the comprehension of written and spoken language, damage to this area results in a fluent but receptive aphasia, known as sensory aphasia (Ambrosi et al., 2010). Wernicke aphasia may be best described as one who is unable to comprehend/express written or spoken language. The patient will most commonly have fluent speech, but their words will lack meaning. They could speak, but their speech was often incoherent and made no sense (Javed et al., 2022). In conclusion, it is possible to state that Broca's and Wernicke's areas are the main brain centres, vital for language production and comprehension. However, to be able to read, speak, and write, other areas of the brain need to function in coordination (Moini and Piran, 2020).

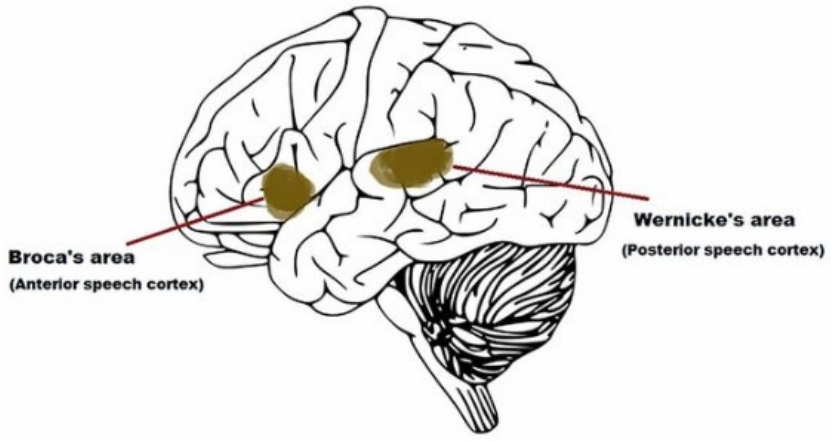

Figure 1.13 *Broca's and Wernicke's areas (Buğa,2016).*

1.2.3 Cerebellum

The cerebellum, also known as little brain, is the largest part of the embryological hindbrain and occupies most of the posterior cranial fossa (***Figure 1.14***). It is made up of the right and left cerebellar hemispheres and a median vermis. The principal function of the cerebellum is to regulate and maintain balance, to coordinate the timing and precision of body movements (Bazira, 2021). The cerebellum is in constant communication with the cerebral cortex, taking higher-level instructions about the brain's intentions, processing them through the cerebellar cortex, and then sending messages to the cerebral motor cortex to make voluntary muscle contractions (Thau et al., 2022). However, the cerebellum is incapable of initiating movement, but rather helps to refine and coordinate muscular contractions to make the movements more precise and accurate (Bazira, 2021).

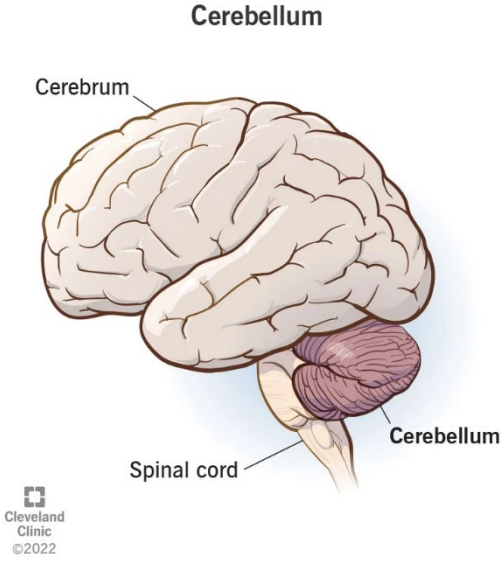

Figure 1.14 *Illustration of the cerebellum (my.clevelandclinic.org).*

The cerebellum is involved in the following functions (nba.uth.tmc.edu/neuroscience/m/s3/chapter05.html):

Maintenance of balance and posture. The cerebellum is important for making postural adjustments to maintain balance. Through its input from vestibular receptors and proprioceptors, it modulates commands to motor neurons to compensate for shifts in body position or changes in load upon muscles. Patients with cerebellar damage suffer from balance disorders, and they often develop stereotyped postural strategies to compensate for this problem (e.g., a wide-based stance).

Coordination of voluntary movements. Most movements are composed of several different muscle groups acting together in a temporally coordinated fashion. One major function of the cerebellum is to coordinate the timing and force of these different muscle groups to produce fluid limb or body movements.

Motor learning. The cerebellum plays a major role in adapting and fine-tuning motor programs to make accurate movements through a trial-and-error process (e.g., learning to hit a baseball).

Cognitive functions. Although the cerebellum is most understood in terms of its contributions to motor control, it is also involved in certain cognitive functions, such as language. Thus, like the basal ganglia, the cerebellum is historically considered as part of the motor system, but its functions extend beyond motor control in ways that are not yet well understood. In addition to its well-established role in motor function, the cerebellum has been shown to be a critical component of many cognitive and sensory-motor processes, including auditory pathways involved in functions such as speech recognition.

1.2.4 Brainstem

The brainstem is the structure that connects the cerebrum of the brain to the spinal cord and cerebellum. The brainstem is located in the posterior cranial fossa anterior to the cerebellum and extends from just above the tentorial hiatus to the foramen magnum (Bazira, 2021). It is composed of three sections in descending order: the midbrain, pons, and medulla (***Figure 1.15***). It is responsible for many vital functions, such as breathing, consciousness, blood pressure, heart rate, and sleep (Basinger and Hogg, 2022).

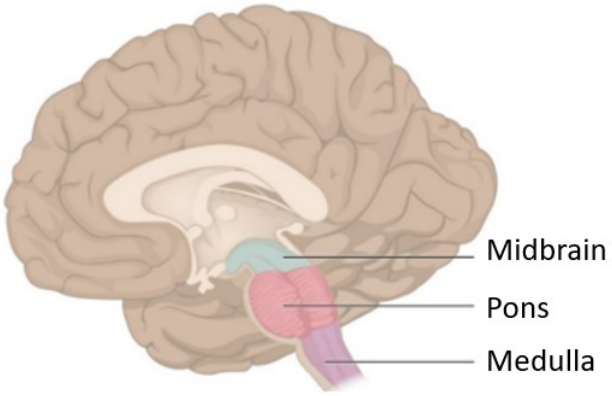

Figure 1.15 *Three major components of the brainstem: midbrain, pons and medulla (Wise et al., 2013).*

The three main components of the brainstem are:

- ***Midbrain.*** The midbrain is a very complex structure with a range of different neuron clusters (nuclei and colliculi), neural pathways and other structures. These features facilitate various functions, from hearing and movement to calculating responses and environmental changes (www.hopkinsmedicine.org).
- ***Pons.*** The pons is the origin for four of the twelve pairs of cranial nerves, which enable a range of activities such as tear production, chewing, blinking, focusing vision, balance, hearing and facial expression. Named for the Latin word for "bridge," the pons is the connection between the midbrain and the medulla (www.hopkinsmedicine.org).
- ***Medulla.*** At the bottom of the brainstem, the medulla represents the place where body and spinal cord meet. The medulla is essential to survival. Functions of the medulla regulate many body activities, including heart rhythm, breathing, blood flow, and oxygen and carbon dioxide levels. The medulla produces reflexive activities such as sneezing, vomiting, coughing and swallowing (www.hopkinsmedicine.org).

The brainstem contains the reticular formation (a fine and diffuse network of nerve cells and nerve fibres) and the reticular activating system, which regulate the individual's level of awareness and wakefulness. Damage to the reticular formation in the upper part of the braistem may cause the patient to be in a state of prolonged coma (Bazira, 2021).

1.2.5 Corpus Callosum

The two hemispheres in the brain are connected by a C-shaped structure of white matter and nerve pathways called CC that ensures the communication between the two sides of the brain (***Figure 1.16***). A combination of sensory, motor and cognitive information is constantly being transferred between hemispheres via this neural highway. This neural bridge is the largest white matter structure in the brain, being around 10 cm long at the midline and it is composed by millions of axons (nerve fibres). If the CC is severed, the brain's hemispheres are not able to communicate properly, causing the impairment of many functions such as changes to visual perception, speech and memory (qbi.uq.edu.au/brain/brain-anatomy/corpus-callosum). The CC is divided into four parts: rostrum, genu, body and splenium (***Figure 1.17***) **(**Baynes, 2002).

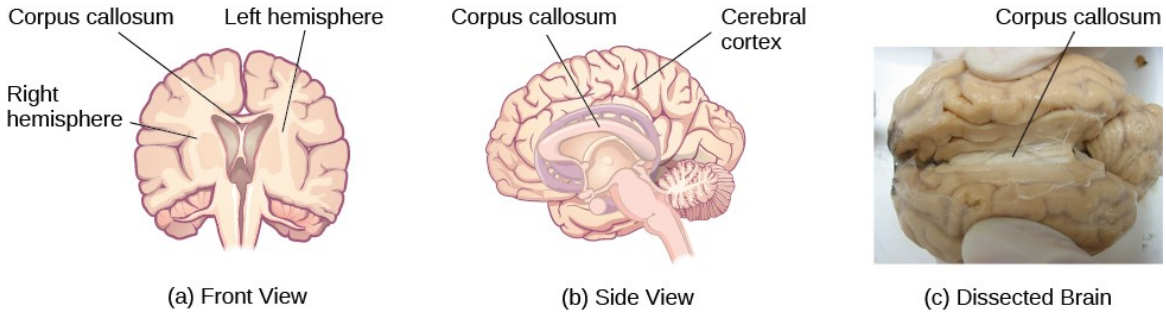

Figure 1.16 *(a, b) The corpus callosum connects the left and right hemispheres of the brain. (c) A scientist spreads this dissected sheep brain apart to show the corpus callosum between the hemispheres (Spielman et al.,2021).*

- The rostrum is the most anterior part of the CC.
- Just behind the rostrum, the CC bends to form the genu, or knee, and then extends posteriorly in the body (Baynes, 2002). The genu gives rise to a large fibre tract, the forceps that projects fibres from the genu to connect the frontal lobes (Richard et al., 2017).
- The body constricts slightly to become the isthmus and finally terminates in the slightly bulbous splenium (Baynes, 2002).
- The splenium gives rise to a large tract, the forceps major, which forms a prominence called the *bulb of callosum* (Richard et al., 2017). Forceps major projecting fibres from the splenium connect the two occipital lobes (Baynes, 2002).

White matter fibres projecting through the body and fibres through the splenium not included in the forceps major are known as the tapetum, that run along the entire lateral occipital and temporal horns. There are two types of connections: homotopic and heterotopic. Homotopic connections link similar regions in the left and right sides of the brain, while heterotopic connections connect dissimilar areas of the left and right sides of the brain. The main function of the CC is to guarantee the communication between the two hemispheres; the different parts of the CC connect homologous areas of each hemisphere. In this way these areas communicate in a way that harmonizes their functions (www.kenhub.com/en/library/anatomy/corpus-callosum).

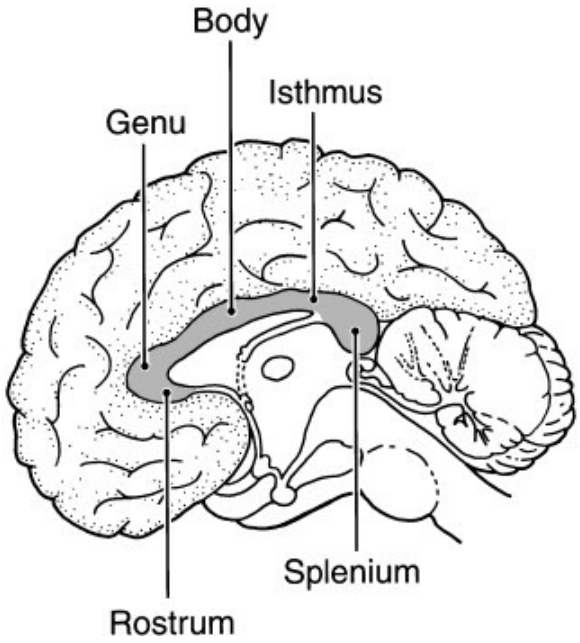

Figure 1.17 *Sagittal section of the brain with major division of the corpus callosum labelled (Bayens, 2002).*

1.2.5.1 Agenesis of the Corpus Callosum

The CC is the major interhemispheric bundle of commissural fibres in the brain that allows the transfer of motor, sensory, and cognitive information between the two hemispheres. Several abnormalities may affect the CC, including complete or partial agenesis, dysgenesis (an abnormal shape), or hypoplasia (decreased thickness) (***Figure 1.18***) (Rotmensch and Monteagudo, 2020).

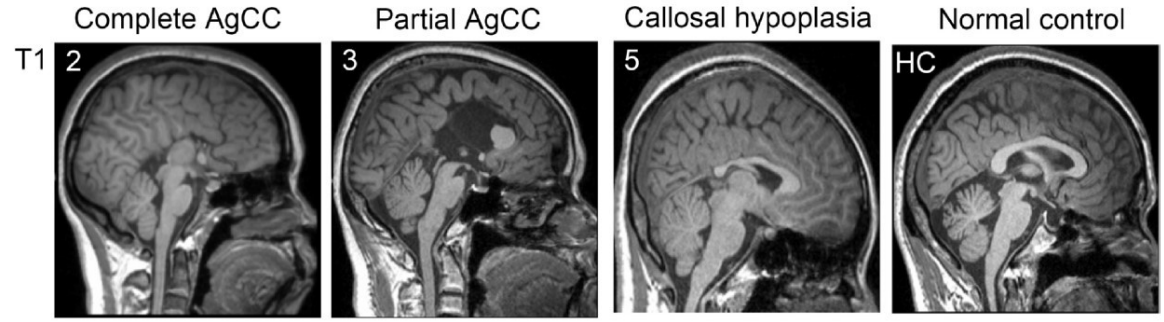

Figure 1.18 *T1-weighted MR images with midline sagittal view of four representative subjects. Three types of AgCC (the first column is patient n°2 with complete AgCC, the second column is patient n°3 with partial AgCC, the third column is patient n°5 with callosal hypoplasia) and one healthy control (the fourth column) are presented (*Yuan et al.,2020).

Agenesis of corpus callosum (AgCC) is a rare congenital malformation in which callosal fibres are congenitally partially or fully absent and is caused by different genetic or environmental factors during prenatal development (Yuan et al., 2020).

Neonatal and prenatal imaging studies suggest that AgCC occurs in at least 1:4000 live births. Agenesis of CC (AgCC) can be complete or partial. Complete AgCC is divided into type 1 and 2 according to the presence (type 1) or absence (type 2) of uncrossing axons forming the so-called Probst bundle (Unterberger et al., 2016). Despite the differences in white matter structure, several prior studies found no significant difference in basic cognition and intelligence between AgCC subjects and healthy controls (HC). Resting-state functional magnetic resonance (rs-fMRI) studies also found that global functional connectivity was nearly intact in AgCC, indicating that indirect or local polysynaptic pathways were utilized to preserve it in AgCC subjects. Thus, AgCC can serve as a good neuroanatomical model for understanding human neuroplasticity and the relationship between structural and functional connectivity in certain developmental abnormalities (Yuan et al., 2020).

1.2.6 Ventricular System of the Brain

The ventricular system of the brain is an interconnected series of cavities, filled with CSF that helps to protect the brain from injury (***Figure 1.19***) (Shenoy and Lui, 2022). CSF is primarily produced in the ventricular system by the secretory activity of the ependymal cells in the choroid plexuses. The choroid plexuses are vascular tufts that are invaginated into parts of the ventricular system in the lateral, 3rd and 4th ventricles. CSF is produced constantly at a rate of 0.5 ml/minute (Bazira, 2021). The cerebral ventricular system is made up of four ventricles that include two lateral ventricles (one in each cerebral hemisphere), the third ventricle in the diencephalon, and the fourth ventricle in the hindbrain. Inferiorly, it is continuous with the central canal of the spinal cord (Shenoy and Lui, 2022).

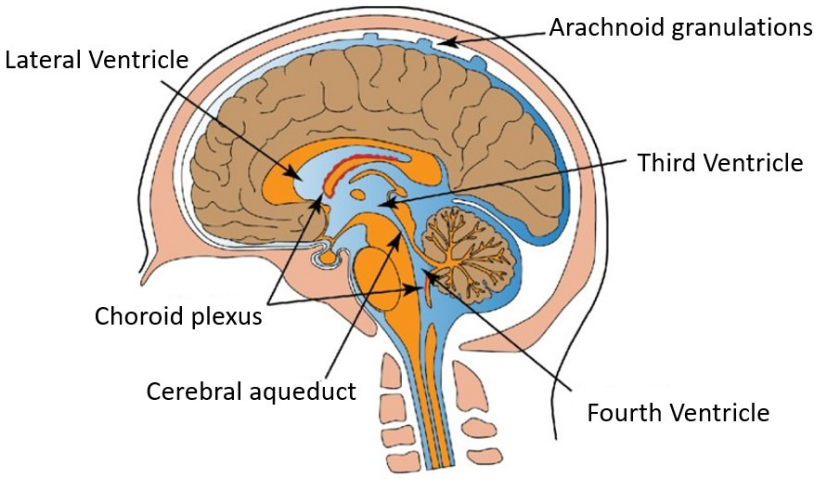

Figure 1.19 *The ventricular system of the human brain (Chou et al., 2014).*

Lateral Ventricles

The lateral ventricles are the largest in the series of four interconnecting fluid-filled cavities within the brain and are located within their respective hemisphere of the cerebrum (***Figure 1.20***) (www.kenhub.com/en/library/anatomy/lateral-ventricles). The lateral ventricles are paired C-shaped structures comprising a central part (body) and an atrium along with three projections into the frontal, temporal, and occipital lobes, termed "horns" (Scelsi et al., 2020). Depending on the lobe the three horns are called anterior, posterior and inferior horn. Each lateral ventricle is filled with CSF with an estimated capacity of 7 to 10 ml. The two lateral ventricles are separated from each other by a thin vertical sheet of nervous tissue called septum pellucidum covered on either side by ependyma. They communicate with the third ventricle through the interventricular foramen of Monro. On the coronal section, it appears triangular anteriorly and rectangular posteriorly (Shenoy and Lui, 2022). There exists an asymmetry between the lateral ventricles with an incidence of 5% to 12%. Studies have imputed this to various factors like brain dominance, early brain lesions, intrauterine, or postnatal compression skull (Scelsi et al., 2020).

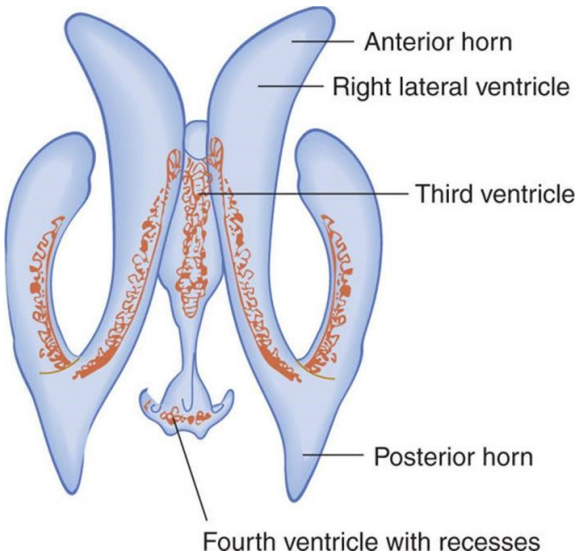

Figure 1.20 *Lateral Ventricles of the brain (Waxman, 2017).*

Central Part (Body)

The central part lies within the parietal lobe. It extends from the interventricular foramen anteriorly to the splenium of the CC posteriorly. The roof is formed by the inferior surface of the body of the CC. The medial wall is formed by the septum pellucidum majorly and the body of the fornix in the lower part. The lateral wall is formed by the caudate nucleus and thalamus (Scelsi et al., 2020).

Anterior Horn frontal

The frontal horn extends anteriorly from the foramina of Monro and communicates with the body of the lateral ventricle posteriorly (Scelsi et al., 2020).

Posterior Horn

This is also named occipital horn as it curves backward and medially to lie in the occipital lobe and is frequently asymmetrical.

Inferior Horn

The inferior (temporal) horn is the longest and largest horn, extending anteriorly from the atrium below the thalamus and terminating at the amygdala **(**Scelsi et al., 2020).

The area where the inferior horn and posterior horn diverge is called collateral trigone or atrium. The atrium is a triangular cavity that communicates with the body, temporal horn, and occipital horn (Scelsi et al., 2020).

Third Ventricle

The third ventricle is a median slit-like cavity situated between the left and right thalamus and part of the hypothalamus (***Figure 1.21***) It communicates with the lateral ventricles through the foramen of Monro and with the fourth ventricle through the cerebral aqueduct of Sylvius. The space of the third ventricle is lined by ependyma and is traversed by a mass of grey matter called interthalamic adhesion or Massa intermedia, located posterior to the foramen of Monroe and connecting the two thalami. The third ventricle is constituted by a roof, a floor, anterior and posterior wall, and two lateral walls. The third ventricle protrudes into the surrounding structure in the form of recesses (Shenoy and Lui, 2022).

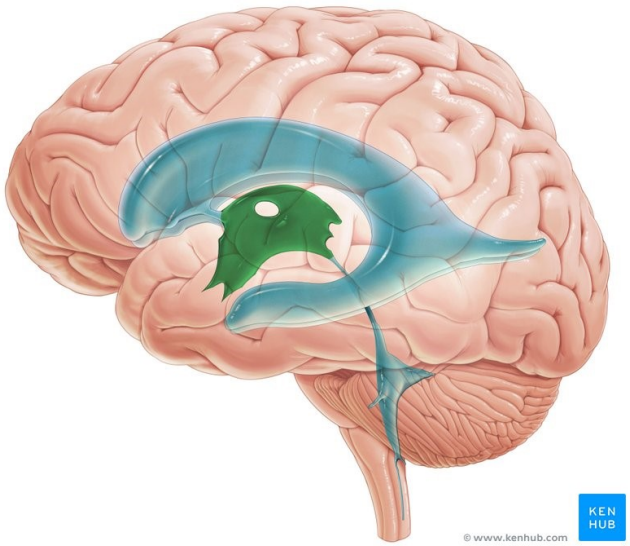

Figure 1.21 *Third ventricle in green (www.kenhub.com).*

Fourth Ventricle

The fourth ventricle is a broad, tent-like cavity of the hindbrain filled with CSF. It constitutes the last of the ventricular system which lies between the pons and medulla ventrally and the cerebellum dorsally (***Figure 1.22***). From the 3rd ventricle the CSF passes through a narrow channel in the midbrain, the aqueduct (of Sylvius), into the 4th ventricle. From the 4th ventricle the CSF flows into the subarachnoid space through three natural apertures in the membranous roof of the 4th ventricle, bathing the brain and spinal cord. After circulating through the ventricular system, CSF is absorbed back into the circulation by specialized evaginations of arachnoid, termed the arachnoid granulations (Bazira, 2021).

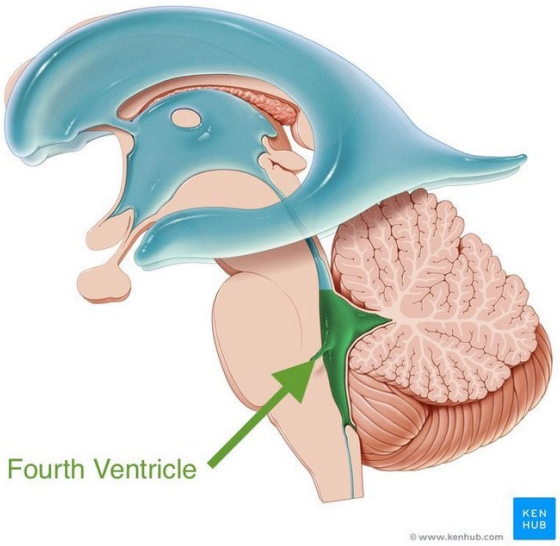

Figure 1.22 *Fourth ventricle in green (www.kenhub.com).*

Chapter 2 Callosotomy and consequences

2.1 Epilepsy

Epilepsy is one of the most common neurologic problems worldwide (Chang et al., 2003). It is defined as a chronic neurological disorder characterized by an enduring predisposition to generate epileptic seizures and the associated cognitive, psychological and social consequences. An epileptic seizure is a transient behavioural change that is characterised by objective signs or subjective symptoms (loss of awareness, stiffening, jerking or déjà vu), caused by abnormal excessive or synchronous neuronal activity in the brain (Devinsky et al., 2018). The diagnosis of epilepsy requires at least two unprovoked seizures occurring greater than twenty-four hours apart (Sarmast et al., 2020).

Epilepsy syndromes divide into two main categories: generalized and partial syndromes. In generalized epilepsy, seizures begin simultaneously in both cerebral hemispheres. In partial epilepsy, instead, seizures originate in one or more localized foci, although they can spread to involve the entire brain (***Figure 2.1***) (Chang et al., 2003).

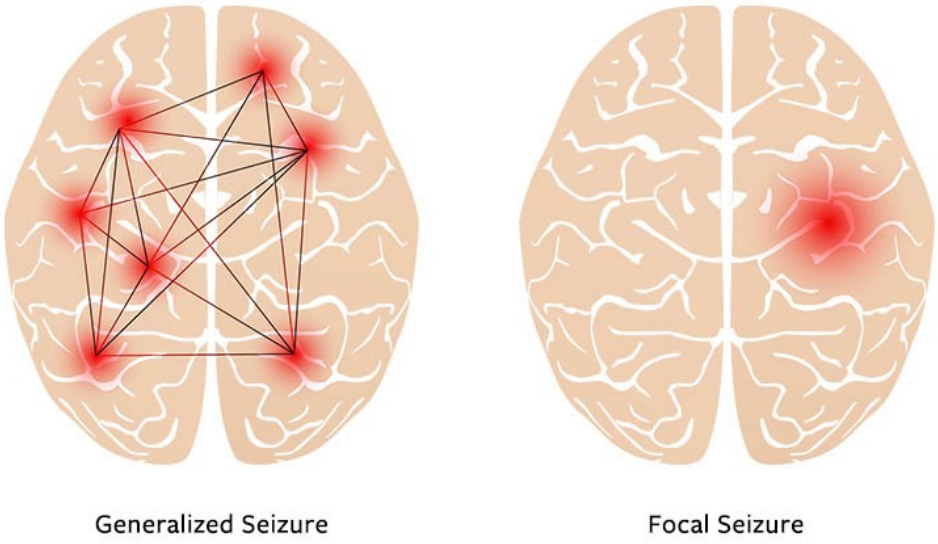

Figure 2.1 *Generalized seizures affect both sides of the brain whereas focal seizures happen in one area of the brain (magazine.medlineplus.gov).*

The study of epileptogenesis focuses on the cellular and molecular alterations caused by pathogenetic events that result in an active epileptic condition. These events can include brain injuries and genetic alterations. The study of ictogenesis, instead, investigates the causes of seizure generation and recurrence (Devinsky et al., 2018).

Epileptogenesis is initiated by a pathogenetic event ('an epileptogenic insult') or a genetic alteration, although many patients have an unknown cause. The process of epileptogenesis (***Figure 2.2***) occurs before and persists beyond the first unprovoked seizure; this process and the frequency and severity of spontaneous seizures can progress for years in humans, providing to the clinicians a broad window for anti-epileptogenic therapeutic interventions (Devinsky et al., 2018).

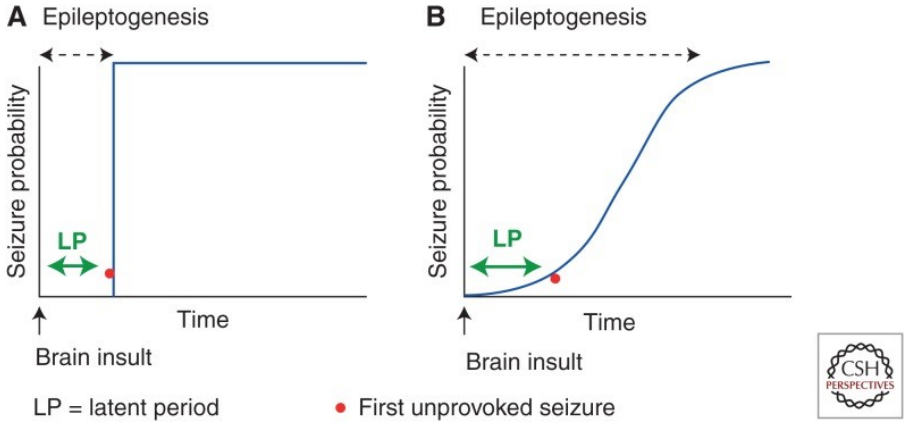

Figure 2.2 *Definitions of epileptogenesis. (A) Previously, epileptogenesis was represented by the latent period, which has been defined as the time between the precipitating insult and the occurrence of the first unprovoked clinical seizure. Thus, the temporal development of acquired epilepsy was previously considered to be a step function of time. (B) More recently, based on several experimental and clinical observations, epileptogenesis is now considered to extend beyond the latent period, which is still defined as the time from the precipitating injury and the first clinical seizure (Pitkänen et al., 2015).*

Discovering the pathogenetic alterations that occur during epileptogenesis and lead to seizure onset, recurrence and progression is essential for therapeutic innovations. Mechanisms of epileptogenesis include widespread alterations in both neuronal and non-neuronal cells at several levels in the brain, including genetic and epigenetic alterations and molecular and structural changes that result in the dysfunction of neuronal circuits (Devinsky et al., 2018). Focal seizures originate from a small group of neurons that form an epileptic focus, and therefore symptoms depend on where the focus is located within the brain (Kandel et al., 2014). If the activity of the seizure focus is intense enough, the electrical activity begins to spread involving other brain regions. In general, the abnormal electrical neuronal activity originating from the focus propagates through the same axonal pathways as normal cortical activity. The spread of focal activity can involve areas of the same hemisphere or it can affect, via the CC, areas of the contralateral hemisphere (Kandel et al., 2014).

At this point the patient may lose consciousness, fall to the floor, rigidly extend all extremities (tonic phase), and eventually exhibit jerky movements of all extremities (clonic phase). In this case the focal seizure becomes a secondary generalised seizure. Generalized epileptic seizures constitute the second category of epileptic accesses. They are not preceded by focal seizures and affect both hemispheres right away. Therefore, they are sometimes referred to as primary generalized epileptic seizures, to distinguish them from those that begin with a focus and then secondarily generalize (Kandel et al., 2014). The most recent classification of seizures and epilepsies refers to the International League Against Epilepsy (ILAE), 2017, published in March 2017 (***Figure 2.3***). In this current classification by ILAE, the clinical features of epilepsy are categorized into three levels: the seizures type, the epilepsy type, and the epilepsy syndromes.

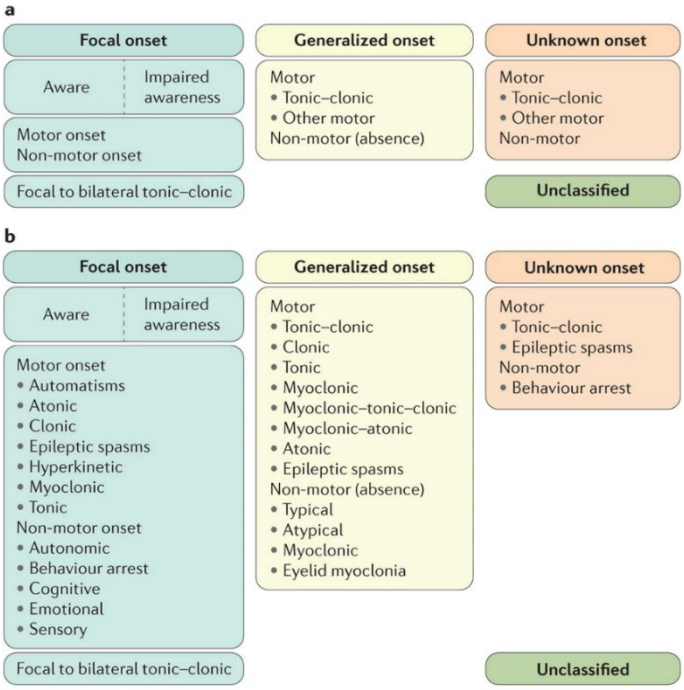

Figure 2.3 *According to the International League Against Epilepsy 2017 basic seizure classification, epileptic seizures can be classified as focal onset, generalized onset or unknown onset (Devinsky et al., 2018).*

This new classification is better organized with a clear elucidation of terminologies and list some new seizure types. The benefits of this model are represented by the achievement of a better and prompt diagnosis which will result into early management of seizure and epilepsy and consequently better patient outcomes (Sarmast et al., 2020).

2.2 Callosotomy as a treatment option in the management of epilepsy

The general anatomical organization of the human beings is such that each side of the sensory periphery is connected with neural structures in the opposite side of the brain. To ensure the interaction between the two halves of the brain, the integrity of the interhemispheric commissural formations, including the CC, is crucial (Conti et al., 2020). According to R.W. Sperry's principle of supplementary complementarity, the callosal connections serve to ensure the anatomical and functional continuity between the contralateral sensory and motor maps built in each half of the brain: the area of one side adds to that of the other a supplement of different information such as to make it complementary (Conti et al., 2020). If the CC is intact, the information from the sensory receptors, initially directed to one cerebral hemisphere, is made available to the other hemisphere within few milliseconds. Otherwise, integration takes longer or becomes completely impossible (Conti et al., 2020). CC and other interhemispheric connections were considered to transfer unilateral seizure activities to the contralateral hemisphere. MRI lesion mapping confirmed the genu of CC as the major pathway for seizure generalization. According to this, van Wagenen and Herren suggested a role for callosal section. The aim of this procedure is to prevent the seizures, originated from a focus located in the right or left hemisphere, from spreading throughout the brain (Unterberger et al., 2016).

2.2.1 Callosotomy: history and early research

Corpus callosotomy is a procedure adapted from cerebral commissurotomy that involves the resection of the CC (Vaddiparti et al., 2021). It is a surgical technique used in the palliative management of medically refractory cases of epilepsy in which focal resection surgery is not feasible. The procedure has also been used for patients with secondary generalized seizures from a unilateral focus not well controlled by medication. Corpus callosotomy has been shown to be a particularly efficacious approach to drop attacks caused by tonic/atonic seizures and childhood organic encephalopathic epilepsies such as Lennox-Gastaut syndrome, West syndrome, and severe epilepsy with multiple independent spike foci. William P. van Wagenen, chair of neurosurgery at the University of Rochester, identified a direct association between the frequency of epileptic attacks and the integrity of CC, thereby introducing the rationale behind corpus callosotomy in epilepsy management.

He hypothesized sectioning the CC to control convulsions based on four specific observations (Vaddiparti et al., 2021).

- The first observation involved the study of brain tumours, specifically glioblastomas of the CC, in which previously generalized seizures became less frequent and unilateral without the loss of consciousness as the tumours grew and destroyed the CC.
- The second observation was made in a patient with multiple meningiomas throughout the brain including the CC. The patient showed a decrease in seizure frequency as the disease progressed.
- The third observation was a postmortem brain study of a person with a 25-year history of epileptic attacks. The person was found to have a haemorrhagic scar interrupting nearly two thirds of the body and genu of the corpus CC. The presence of the scar made the patient completely free from seizures in the last years of his life.
- The final observation involved a patient with a long history of epilepsy who had a haemorrhagic accident. The accident resulted in the complete cessation of the patient's seizures.

Van Wagenen attributed these findings to the destruction of the association pathways in the CC caused by the growth of tumours or softening of the brain secondary to haemorrhage. On February 11, 1939, van Wagenen performed the first surgical division of the CC at the University of Rochester, Strong Memorial Hospital to limit the spread of the convulsive wave to one half of the cerebrum. In 1940, van Wagenen and Herren reported their findings and concluded that sectioning of the CC is a safe procedure to disrupt contralateral seizure propagation, preventing generalized seizures or loss of consciousness (Vaddiparti et al., 2021). Several studies were conducted on the use of callosotomy as a treatment option for epilepsy. By experimenting on cats and monkeys, Howard Curtis conclusively proved that the CC played a role in interhemispheric spread of neural activity. Curtis reported that cortical stimulation of one hemisphere evoked potentials at points on the opposite hemisphere. Furthermore he observed that, by performing the callosal resection, the potentials on the contralateral side previously observed were abolished, concluding that the CC mediated the signal propagation. Theodore Erickson simulated epileptic attacks in monkeys by electrically stimulating the cortex and then measuring the spread of neural activity. He subsequently repeated the experiment on monkeys subjected to callosotomy, observing that electric discharge was prevented from propagating to the contralateral hemisphere (Vaddiparti et al., 2021).

2.3 Split-brain disconnection syndrome

In late 1950s Roger Sperry began his research on split-brain to determine the function of the CC. He noted that humans with a severed CC did not show any significant difference in function from people with intact CC, even though their hemispheres could not communicate each other. Sperry postulated that there should be major consequences from cutting the CC and began designing experiments to document the effects of callosotomy. At the time, he knew that each hemisphere of the brain is responsible for movement and vision on the opposite side of the body, so the right hemisphere was responsible for the left visual field and viceversa (Lienhard, 2017). Sperry started to perform experiments on human volunteers, underwent callosal resection to treat drug-resistant epilepsy. From his previous experiments with cats and monkeys, Sperry learned that each hemisphere would only analyse information from the contralateral visual field, and that each hemisphere could not communicate to the other what it saw. Several experiments were designed to investigate changes occurred in callosotomised patients, by testing their language, vision, and motor skills. In the first test the patients had to look at a white screen with a black dot in the middle, which acts as a dividing point for the patient's visual field. In this way, the right hemisphere of the brain analysed everything to the left of the dot and the left hemisphere everything that appeared to the right of the dot (Lienhard, 2017). Then Sperry showed the participants a word on one side of the black dot for less than a second and asked them to say what they had read on the screen. After performing the test, he noticed that when the word was presented in the right visual field, the left hemisphere of the brain analysed it and patients were able to say what they saw (***Figure 2.4***).

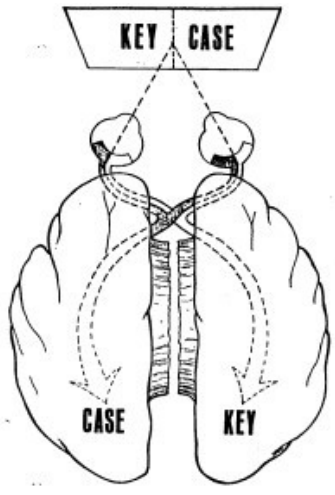

Figure 2.4 *Things seen in the left of a central fixation point with either eye are projected to the right hemisphere and vice-versa (Sperry, 1968).*

On the contrary, when the word was shown in the left visual field, and thus information was sent and processed by the right hemisphere, patients were unable to say what they saw. This led Sperry to state that the centre responsible for language processing is present only in the left hemisphere. Therefore, Sperry began to test the function of the right hemisphere. He asked the participants of the first experiment to close their eyes and draw the object with their left hand, processed by the right hemisphere. The patients were able to draw the word displayed on the left side of the screen, but when they looked at the drawing, they had no idea why the drawing did not correspond to the read word. Sperry carried out another experiment, to continue studying the right hemisphere's ability to recognize words, in which he asked the patients to place their left hand in a box full of different objects out of their sight. After that, a word indicated one object in the box, was shown on the left visual field and so processed by the right hemisphere. The patients were asked to take an object from the box by using the left hand, as showed in ***Figure 2.5***.

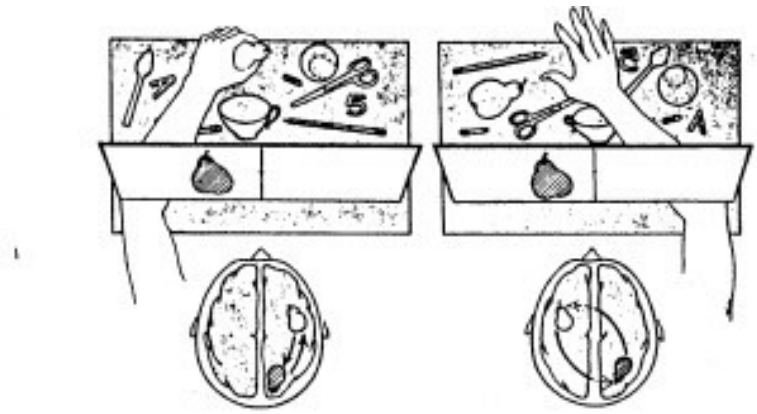

Figure 2.5 *Visuo-tactile associations between each half of the visual field and corresponding hand. They fail with crossed combinations in which visual and tactual stimuli are projected into opposite hemisphere (Sperry, 1968).*

Sperry noted that most of the patients picked up the object corresponding to the read word, without seeing it, but when Sperry asked them for the item's name, they could not tell and didn't know why they chose that object. However, he noticed that the patients, despite ignoring the object's name, were able to give a very rudimentary description of the object. At the end, Sperry discovered that the left hemisphere was responsible for language understanding and articulation and that also the right hemisphere had some speech recognition ability: it could recognize a word but could not articulate it. Sperry received the 1981 Nobel Prize in Physiology and Medicine for his research on split-brain patients and the findings on the functions of the CC (Lienhard et al., 2017).

Two decades later, Roger W. Sperry's split-brain studies inspired surgeons to re-examine the role of corpus callosotomy in the control of epileptic seizures. In 1962, Joseph Bogen and Philip Vogel performed complete corpus callosotomies in patients with a history of generalized seizures. The identification of a set of postsurgical disconnection symptoms and other neurologic deficits begged the improvement of the surgical technique (Vaddiparti et al., 2021). In fact, it was observed that most of the symptoms of both acute and chronic disconnection syndrome were absent in patients in whom the posterior one third of the CC, including the splenium, was spared. This finding led Bogen and Vogel to develop the surgical technique of partial commissurotomy to reduce the effects of dissociation symptoms (Vaddiparti et al., 2021).

Michael Gazzaniga, another doctoral student of Roger Sperry, conducted extensive research on all the patients of Bogen and Vogel who underwent corpus callosotomy (Vaddiparti et al., 2021). Like Sperry, Gazzaniga noticed the inability of right-handed patients to name or describe an object in their left hand; this phenomenon is called unilateral left tactile anomia. He also noticed that after projecting images to each hemisphere, patients who had undergone callosotomy were unable to read anything presented to the left visual field (unilateral left hemialexia) or write with the left hand (unilateral left agraphia). This set of symptoms is considered a part of the spectrum of disconnection syndrome. Bogen, Gazzaniga, and Sperry continued to research the patients who had undergone callosotomy and postulated various functional effects of callosal sectioning in the human brain.

2.4 Functional and Structural Connectivity

Understanding the functioning and structural networks present in the brain has always been a topic fascinating many researchers. The development and advent of new imaging technologies allowed to have better knowledge about cognitive brain functioning occurring via the connections and interactions between different components of the brain (Milano et al., 2019). The human brain is defined as a complex biological network system characterized by a structural connectome of interconnected areas and a functional connectome of interregional neural activity (Milano et al., 2019).

Structural connectivity represents the physical anatomical connections between different groups of neurons. At the scale of the human brain, these connections generally refer to white matter projections linking cortical and subcortical regions (Sporns, 2013). White matter tracts are the information highways of the brain, enabling transport of large amount of functional data between spatially separated regions (van den Heuvel et al., 2010).

Functional connectivity is defined as the temporal relationship of neuronal activation patterns of anatomically separated brain regions **(**van den Heuvel et al., 2010). It refers to statistical dependence between time series of electrophysiological activity and (de)oxygenated blood levels in distinct regions of the brain (Babaeeghazvini et al., 2021). This relationship reflects the level of functional communication between regions, representing an important factor in complex cognitive process, which relies on the continuous exchange and integration of information across different regions of the brain (van den Heuvel et al., 2010). In the past years an increasing body of neuroimaging studies has started to explore functional connectivity by measuring the level of co-activation of rs-MRI time-series between brain regions (van den Heuvel et al., 2010). If fluctuations in the resting state reflects the ongoing neuronal activity, one would at least expect the existence of anatomical connections between these functionally active regions. When the correlation of these rs-fMRI time series reflects the ongoing functional communication between anatomical separated brain regions, there should be a set of white matter connections allowing neuronal exchange of information (van den Heuvel et al., 2010). In last years, numerous studies have used the combination of two techniques, rs-fMRI and DTI, to describe the direct association between structural and functional connectivity (van den Heuvel et al., 2010) **(*Figure 2.6*).** DTI technique enables the reconstruction of white matter tracts based on the direction of water molecules diffusion. In white matter tracts they diffuse along a strong preferred direction due to the compact layout of axonal bundles (van den Heuvel et al., 2010).

DTI has been used extensively to map white matter tractography in the brain. Diffusion MRI (dMRI) raw data can be used to compute the probabilistic distribution of axonal orientations, which are then concatenated to establish structural connectivity across brain regions with tractography techniques (Milano et al., 2019). The fMRI indeed, relies on detecting the small changes in the Blood Oxygen Level Dependent (BOLD) signal to produce resonance images associated with neuronal activity.

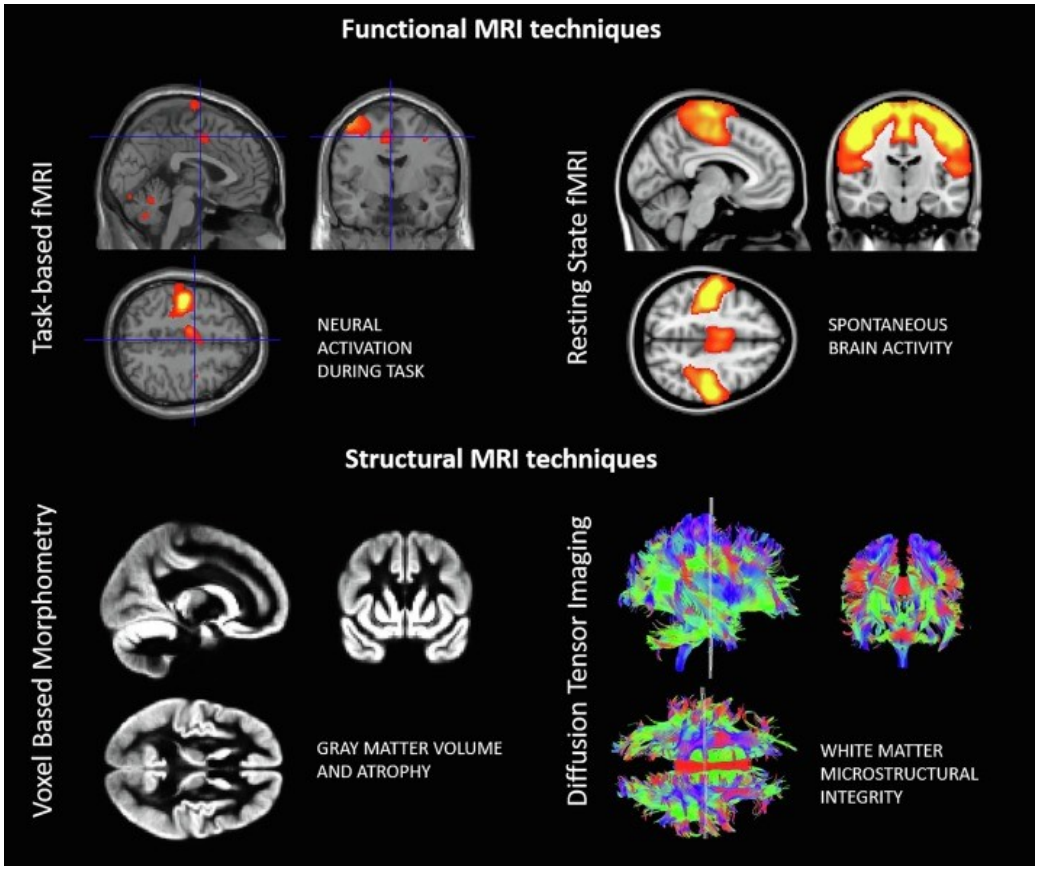

Figure 2.6 *Illustration of the main techniques to assess brain functional and structural connectivity (Tavazzi et al., 2022).*

Chapter 3 *Imaging techniques for structural and functional analysis of the brain*

3.1 Magnetic Resonance Imaging: physical principles

The nuclear magnetic resonance (NMR) phenomenon was first described experimentally by both Bloch and Purcell in 1946, for which they both were awarded the Nobel Prize for Physics in 1952 (Grover et al., 2015). The magnetic resonance imaging uses the NMR phenomena, whose working principle is based on the magnetization properties of certain atomic nuclei within the body. The atoms consist of three fundamental particles. Electrons surrounding the nucleus have negative charge, while the protons and neutrons have respectively positive and no charge. Water, contained in most of the biological tissues, contains hydrogen atoms which represents the most suitable chemical species for the MRI studies. Indeed, due to the impaired proton contained in the nucleus, hydrogen atoms have an intrinsic quantum property known as 'spin', or also indicated with angular momentum. The angular momentum vector coincides with the axis of proton, making it to rotate around its own axis. Due to the electric charge possessed by the proton, the spinning movement causes a magnetic moment that makes the proton to behave like a tiny magnetic dipole with a random orientation in space (***Figure 3.1***) (Grover et al., 2015).

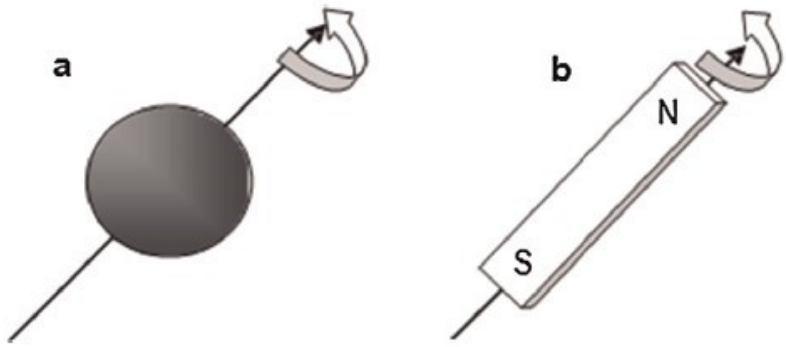

Figure 3.1 *Nuclear spin. The ''spinning'' nucleus (a) induces a magnetic field, behaving like a bar magnet (b). N and S represent north and south respectively. The directions of the arrows represent the direction of the magnetic field (Grover et al.,2015).*

To obtain the final image several steps are required to be performed: nuclear alignment, radiofrequency (RF) excitation, spatial encoding, and image formation.

To this aim an MRI system must incorporate 5 major components (Hidalgo-Tobon, 2010):

- a magnet,
- gradient systems,
- an RF coil system,
- a receiver
- a computer system.

The first step requires the application of a strong magnetic field B_0 (z direction) that makes the hydrogen atoms to align parallel or antiparallel to the external field. The anti-parallel state is characterised by a higher energy state with respect the parallel one (Grover et al., 2015). A greater proportion of protons align parallel to the primary magnetic field and therefore the vector sum of all the spin vectors is greater than zero, aligned in the direction of the primary field B_0 (***Figure 3.2***). This is called longitudinal magnetization.

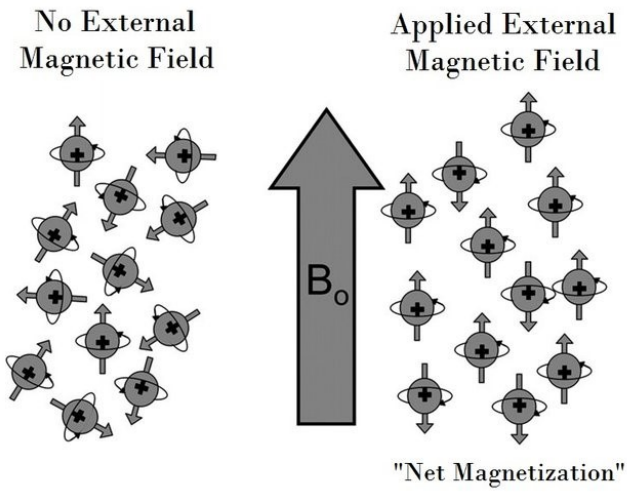

Figure 3.2 *Alignment of protons due to an external magnetic field (Caligari Conti, 2016).*

When a person is lying inside the magnet, each point within their body, represented in the final image as a particular 'pixel' (*picture element*) or 'voxel' (*volume element*) will have a certain number of protons, proportional to the water content of the tissue, aligned with the primary magnetic field (Amaro et al., 2006).

Regardless of the parallel or antiparallel alignment of the protons, the nucleus has an angular momentum due to its rotation, so it will process around the direction of the magnetic field B_0 with a specific frequency (known as *the Larmor frequency*), directly dependent on the magnitude of the primary magnetic field (***Figure 3.3***) (Grover et al., 2015).
Larmor equation:

$$\omega = \gamma \cdot B_0 \quad (1)$$

where ω is the precessional frequency, B_0 is the strength of magnetic field, and γ is the gyromagnetic ratio of the nucleus.

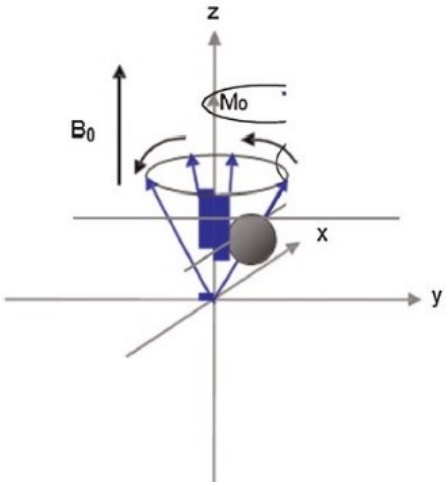

Figure 3.3 *Nucleus precessing around an external magnetic field (B_0). M_0 = direction of net magnetization (Grover et al.,2015).*

Consequently, a second RF magnetic field B_1 is applied perpendicular to B_0. The RF energy is usually emitted in short pulses, each lasting microseconds, with a frequency matching the precession one. It results in a disturbance of the proton alignment and the absorption of energy by the nucleus makes the protons to process in phase and the transition from higher to lower energy levels (Grover et al., 2015). This causes a decrease of longitudinal magnetization (aligned with the magnetic field B_0) and consequently the net magnetization vector turns towards the transverse plane (right angles with respect B_0). This is known as transversal magnetization (***Figure 3.4***).

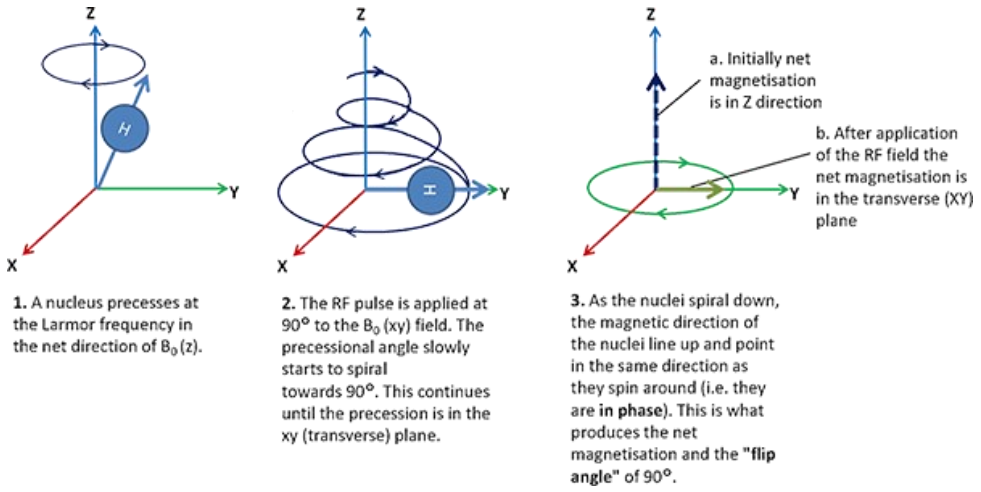

Figure 3.4 *Application of RF pulses makes the net magnetization vector to flip 90° (Clarke and Abdulla, 2020).*

After the RF pulse ceases, the protons slowly return to their original orientation. The process through which a proton returns to its equilibrium condition after the absorption of RF energy is called relaxation. There are two types of relaxation, longitudinal and transverse relaxations (***Figure 3.5***), and these are described by the time constants, T_1 and T_2, respectively (Grover et al., 2015).

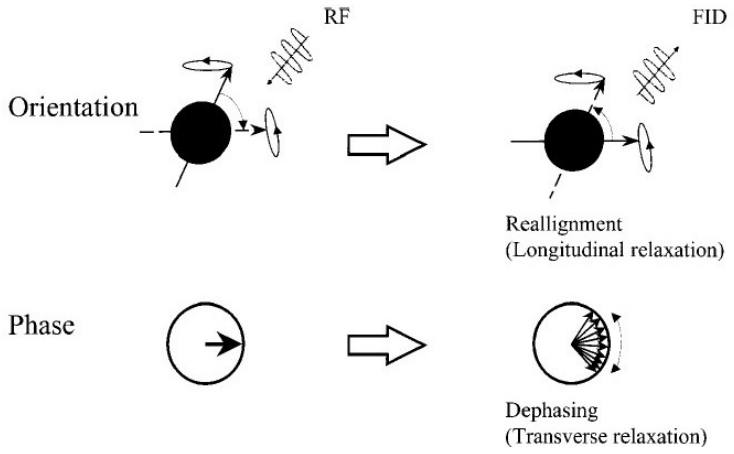

Figure 3.5 *During relaxation, two processes exist: longitudinal relaxation and transverse relaxation. Longitudinal relaxation (upper row) is the realignment of the net magnetization to the external magnetic field. Transverse relaxation is the dephasing of the precessing spins illustrated in the lower row (van Geuns et al., 1999).*

- T_1 relaxation or spin lattice relaxation (***Figure 3.6***) → there is a realignment to the external magnetic field in which several protons flip back to their low energy state, releasing energy to the surrounding nucleus environment. This results in changes in the longitudinal component of the net magnetization vector. The time constant T_1 represents the time needed for the system to return to the 63% of its equilibrium value.

- T_2 relaxation or spin-spin relaxation (***Figure 3.6***) → the process of dephasing of the spinning protons results in changes in the transverse component of the net magnetization vector, that decreases over time and returns to its initial magnetization state. It drops 37% of its original magnitude after one-time constant T_2. The spins dephase much quicker than T2 because of inhomogeneity in the magnetic field B_0. Their combination gives T_2^*.

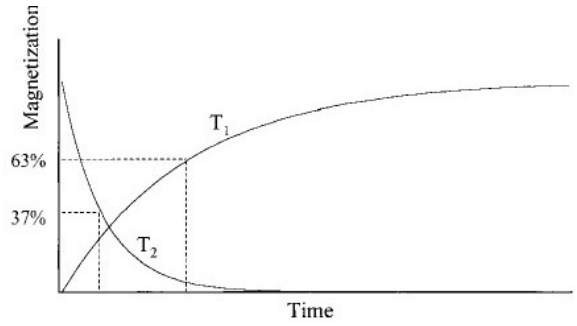

Figure 3.6 *Longitudinal relaxation is characterized by the T1 relaxation time, which is the time to recover 63% of the original net magnetization vector. Transverse relaxation is characterized by the T2 time, which is the time it takes to decay the signal to 37% of the original signal (van Geuns et al., 1999).*

Both T_1 and T_2 can vary depending on tissue composition and structure (***Table 1***). T_2 relaxation time varies between tissues: in water T_2 takes longer. T_1 can be manipulated by varying the repetition time (TR), defined as the time interval between consecutive RF pulses. Water and CSF have long T_1 values (3000–5000 ms), and thus they appear dark on T_1-weighted images, while fat has a short T_1 value (260 ms) and appears bright on T_1-weighted images (Grover et al., 2015).

Table 1 *Different T_1 values for various types of tissues (van Geuns et al., 1999).*

Tissue	**T_1 (ms)**	**T_2 (ms)**
Skeletal Muscle	870	47
Myocardium	600	40
Liver	490	43
Fat	260	84
Blood	1210	35
Venous arterial blood	1210	250

The contrast obtained in the final image is the result of the specific magnetic relaxation properties of the hydrogen atoms present in the water (Amaro et al., 2006). In imaging, contrast can be defined as the difference in signal intensity between a region of interest (ROI) and its surroundings, within the field of view under observation (Alzola-Aldamizetxebarria et al., 2022). It is possible to choose different contrast mechanisms by appropriately selecting the right pulse sequence parameters. There are 2 principal time variables that influence the image contrast: repetition time (TR) and echo time (TE) (***Figure 3.7***). Repetition time, measured in ms, is the time between successive RF excitation pulses applied to a given volume of tissue. Echo time, measured in ms, is the time between the excitation pulse and the echo (signal maximum) (Chan et al., 2019).

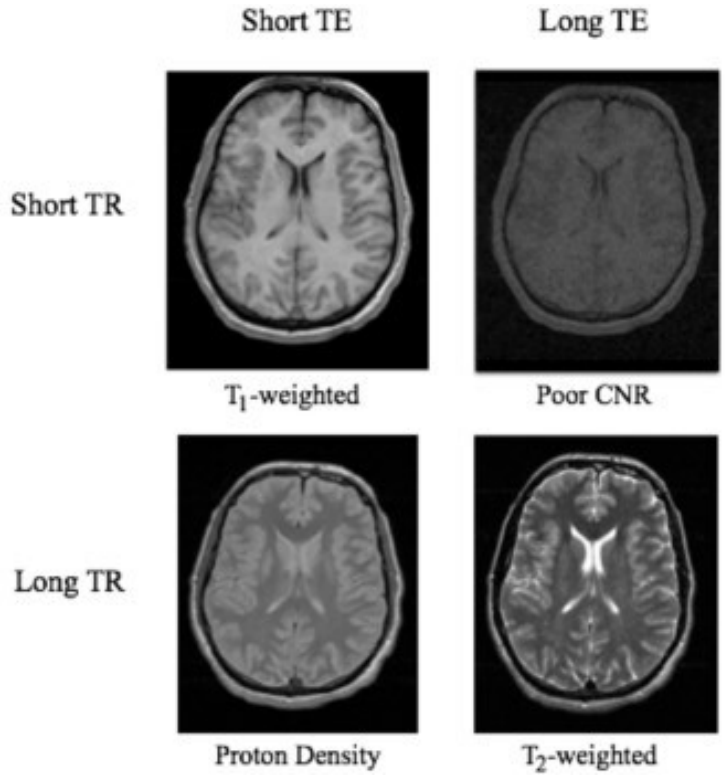

Figure 3.7 *Contrast mechanism. The choice of TE and TR determines the type of weighting (contrast) seen in the final image. Short values of TR and TE are common in images exhibiting T_1 contrast (T_1-Weighted Image). Long values of TR and TE are common in images exhibiting T_2 contrast (T_2-Weighted Image). Long TR values and short TE values are common for density weighted contrast (Proton Density Weighted Image) (Chappell et al.,2018).*

Consequently, to the application of the RF pulses, the nuclei absorb energy and then release it inducing an electric signal (voltage), called Free Induction Decay (FID) (***Figure 3.8***). It can be detected by a suitable antenna receiver coil, placed around the patient.

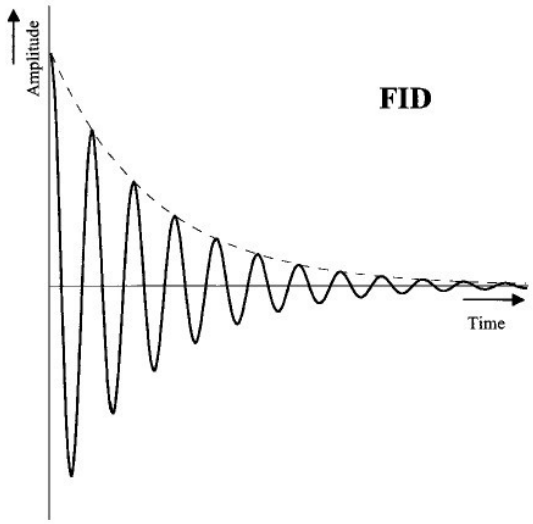

Figure 3.8 *The received signal detected by the receiver coil, the FID, decreases over time when the net magnetization vector returns to its original orientation (van Geuns et al., 1999).*

Multiple RF pulses are applied to obtain multiple FIDs, which are then averaged to improve the signal-to-noise ratio (SNR). The signal-averaged FID is a time-domain signal. The signal-averaged FID can be resolved by a mathematical process known as Fourier transformation, into either an image (MRI) or a frequency spectrum, providing biochemical information (Grover et al., 2015).

To form the final image, it is also necessary to perform spatial localization of the MR signal, achieved through gradient coils. A gradient spatially encodes the positions of the nuclei of hydrogen within a sample by causing a variation in Larmor frequency as a function of their position (Hidalgo-Tobon, 2010). Each MR scanner has three sets of spatial encoding electrical coils able to produce magnetic fields in the *x*, *y*, and *z* directions. These coils can be adjusted to produce a gradient field (***Figure 3.9***), i.e., a magnetic field that changes in strength depending on the position, varying linearly across the x, y, or z direction (***Figure 3.10***).

- Z gradient runs along longitudinal axis to produce axial images
- Y gradient runs along the vertical axis to produce coronal images
- X gradient along the horizontal axis to produce sagittal images

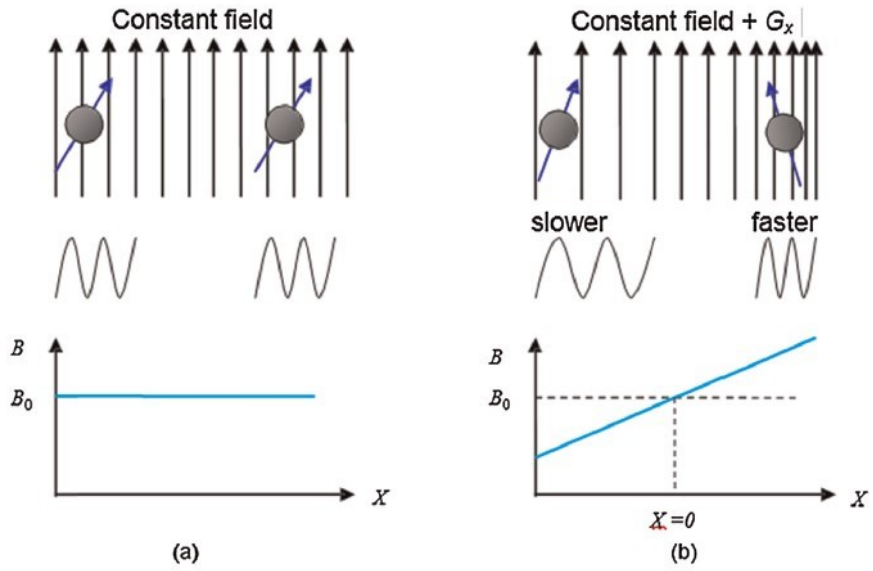

Figure 3.9 *Effect of field gradient on nuclei. (a) B_0 only, all nuclei precess at the same frequency. (b) B_0 with gradient Gx. Further along the x direction the field increases and thus the protons resonate faster. Precession frequency depends upon position (Grover et al., 2015).*

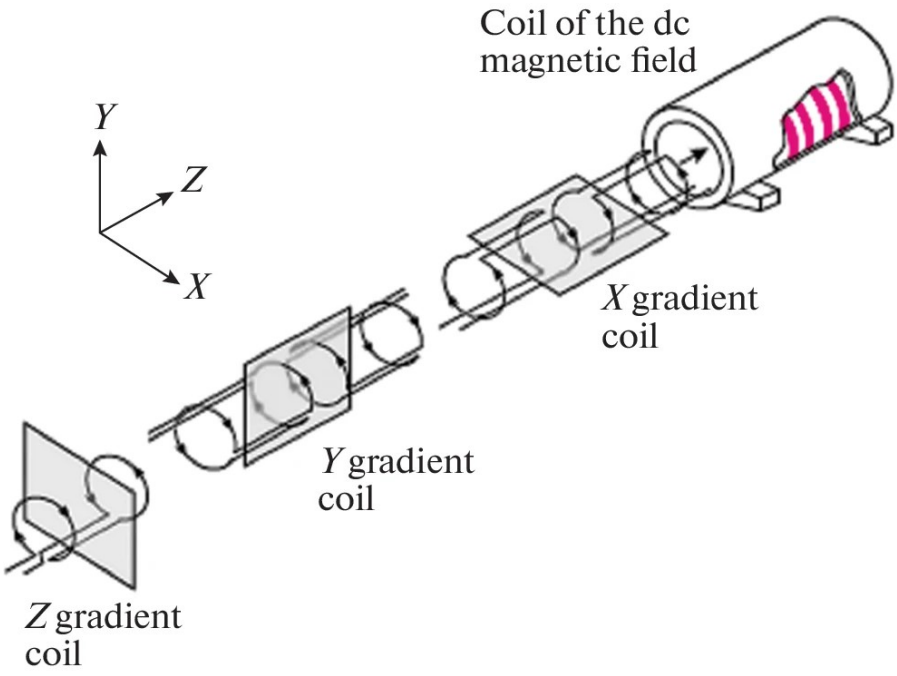

Figure 3.10 *X, Y and Z gradient coils to obtain respectively sagittal, coronal and axial images (Bagdinova et al., 2022).*

Being the gradients magnetic field variable in the space, the protons will experience a different magnetic field depending on their position and the *precession frequency* of the protons will vary as well, according to the Larmor equation.

In this way, the scanner can select a particular slice to image by turning on the slice-select gradient and then altering the frequency of the excitation pulses to match the frequency at the desired slice position (***Figure 3.11***). Protons not in the slice will not get excited since their Larmor frequency will not match the frequency of the pulse**.** As a mnemonic rule, the complete process is reflected in the technique's name: *magnetic* (nuclear magnetic spins) *resonance* (the matching of frequency between the RF pulse and the precession of the spins) *imaging* (the process by which the signal measured by the MR scanner is spatially encoded and the computer algorithm that produces the images) (***Figure 3.12***) (Amaro et al., 2006).

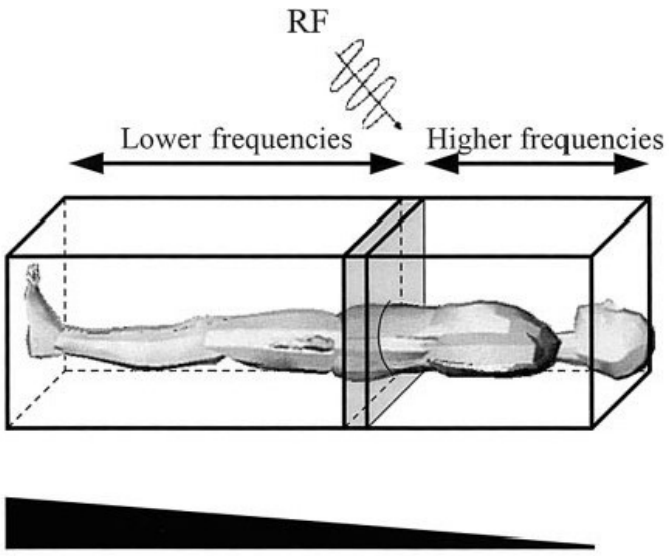

Figure 3.11 *A single slice through the body is selected in MRI by superimposing a small magnetic gradient on the main magnetic field in cranial-caudal direction. A RF pulse will only exite the spins, where the RF pulse matches the local precessing frequency determined by the Larmor equation (van Geuns et al., 1999).*

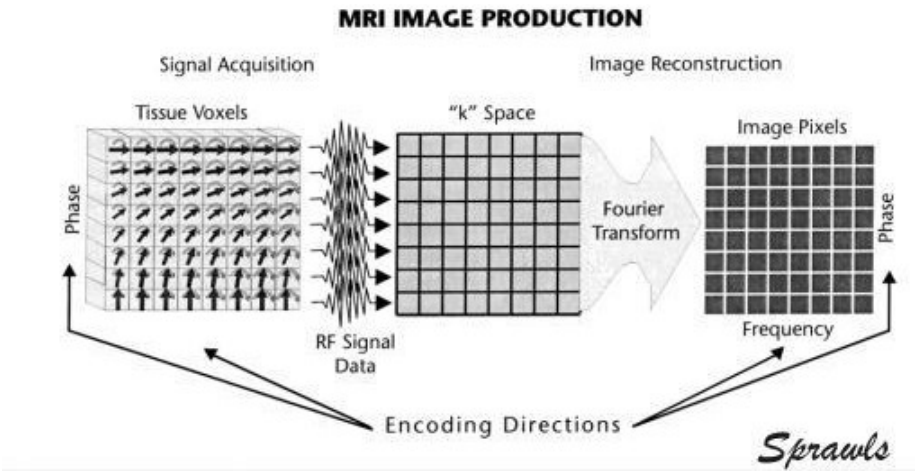

Figure 3.12 *Signal acquisition and Image reconstruction to obtain the final MRI scan (Sprawls, 2000).*

3.1.1 Definition of bioimage

A bioimage is the representation of the internal structure or function of an anatomic region in the form of an array of picture elements called voxels, which are the three-dimensional analogues of pixels. It is a discrete representation resulting from a sampling/reconstruction process that maps numerical values to positions of the space (Larobina and Murino, 2014). For the visualization it is necessary to represent the numbers in the image in terms of grey values (as is common for anatomical MRI images such as in ***Figure 3.13***). In a computer, images are represented as *binary* data, which means that the representation takes the form of ones and zeros.

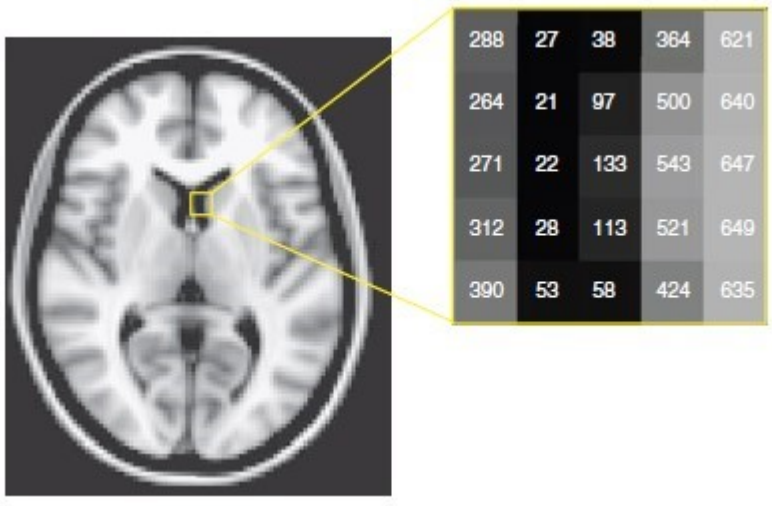

Figure 3.13 *The illustration of the image as a graphical representation of a matrix. The grey scale values in the image (left) correspond to numbers for a set of selected voxels (Poldrack et al., 2011).*

In addition to the voxel values, it is also critical to store other information about the image, known generally as *metadata* (Poldrack et al., 2011). Metadata are *information that describes the image*. This information is typically stored at the beginning of the file as a header and contains at least the image matrix dimensions, the spatial resolution and the pixel depth. Thanks to metadata, a software application recognizes and correctly open an image in a supported file format. Images coming from diagnostic modalities typically have information about how the image was produced. For example, a magnetic resonance image will contain parameters related to the pulse sequence used (e.g., timing information, flip angle, number of acquisitions, etc) (Larobina and Murino, 2014).

Structural MRI images generally comprise a single three-dimensional image and are stored as 3D data files. fMRI data, instead, consist of a time series of three-dimensional images (Poldrack et al., 2011).

They can be stored in two ways:

- a series of separate 3D data files.
- a single 4D file, in which the entire time series can be saved in a single data file, with time as the fourth dimension.

It is generally preferable to store data as a single 4D file since it minimizes the number of files to deal with. However, some analysis packages cannot handle four-dimensional files.

In the neuroimaging field there has been a variety of different image formats; several of these are described in ***Table 2*** (Poldrack et al., 2011). The file formats currently used in biomedical imaging are: Analyze, Neuroimaging Informatics Technology Initiative (NIfTI), Minc, and Digital Imaging and Communications in Medicine (DICOM) (Larobina and Murino, 2014).

Table 2 *Description of some medical image data formats (Poldrack et al., 2011).*

Format Name	File Extension	Origin
Analyze	.img/.hdr	Analyze software,Mayo Clinic
DICOM	none	ACR/NEMA consortium
NIfTI	.nii or .img/.hdr	NIH Neuroimaging Informatics Tools Initiative
MINC	.mnc	MontrealN eurologicalI nstitute (extension of NetCDF)
AFNI brick	.BRIK	AFNI software,MedicalC ollege of Wisconsin/NIMH

3.1.1.1 Coordinate systems

In imaging it is common to use standard terms for the different planes that are employed to virtually slice through the brain. The terms for these planes are *sagittal* (showing superior-inferior and anterior-posterior), *axial* (showing anterior-posterior and left-right) and *coronal* (showing superior-inferior and left-right) ***(Figure 3.14)*** (Jenkinson and Chappell, 2018). The use of coordinate system allows to relate the data points in the image to spatial location in the physical object. The data matrix for a single brain image is usually three-dimensional, such that each dimension in the matrix corresponds to a dimension in space. By convention, these dimensions (or *axes*) are called *X*, *Y*, and *Z*. In the standard space used for neuroimaging data, *X* represents the left–right dimension, *Y* represents the anterior–posterior dimension, and *Z* represents the inferior–superior dimension (***Figure 3.15***). In the data matrix, a specific voxel can be indexed as [*Xvox*, *Yvox*, *Zvox*], where these three coordinates specify its position in the matrix (Poldrack et al., 2011).

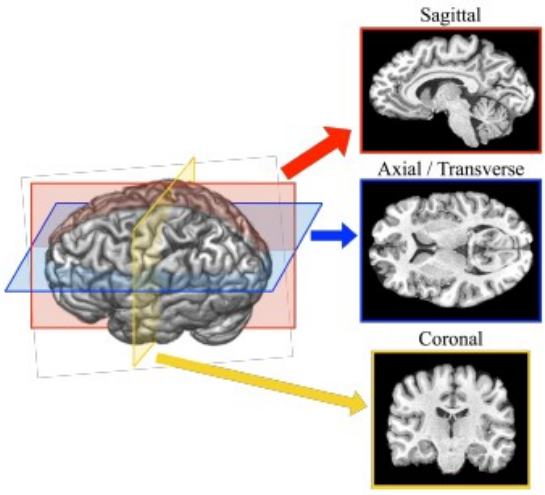

Figure 3.14 *Illustration of the three cross-sectional planes commonly used in imaging (Jenkinson and Chappell, 2018).*

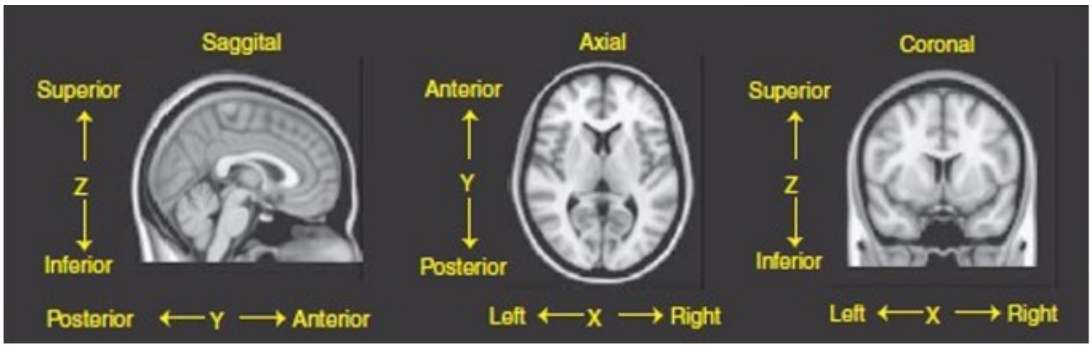

Figure 3.15 *A depiction of the three main axes used in the standard coordinate space for MRI (Poldrack et al., 2011).*

3.1.1.2 Radiological and neurological conventions

Fields of scientific research often have their own conventions for presentation of data. The storage and display of brain images also have a set of inconsistent conventions, which grew out of historical differences in the preferences of radiologists and neurologists. The two main conventions used in the brain imaging field are called 'radiological' and 'neurological' conventions ***(Figure 3.16)*** (Poldrack et al., 2011). The first one intends to visualize the images with the left–right dimension reversed. Radiologists, in fact, prefer to view images with the right side of the brain on the left side of the image, so that the orientation of the structures in the film matches the body when viewed from the foot of the bed. Neurologist on the contrary prefer to visualize the images without flipping the left–right dimension (i.e., the left side of the brain is on the left side of the image).

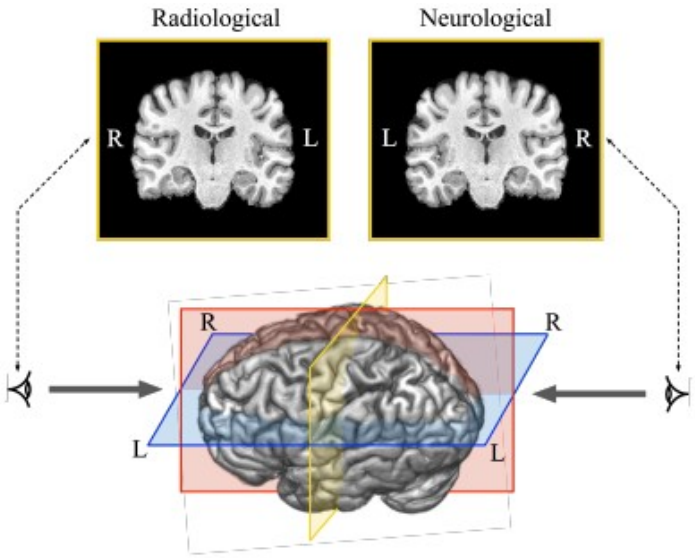

Figure 3.16 *Illustration of radiological and neurological conventions for viewing images, based on whether the brain is viewed from the front (radiological) or from behind (neurological) (Jenkinson and Chappell, 2018).*

Unfortunately, there is no consistent convention for the storage or display of images in brain imaging. In accordance with this, difficulties arise in identifying with certainty the right and left sides of the brain image, given the left– right symmetry of the human brain (Poldrack et al., 2011). Anatomical differences between the two hemispheres are subtle and inconsistent across individuals and do not provide a sufficient means to identify the left and right hemispheres from an image. For the anterior–posterior and inferior–superior dimensions, no convention is needed because it is obvious which direction is up/down or forward/backward due to the anatomy (Poldrack et al., 2011).

3.1.1.3 Standard coordinate spaces

The coordinate systems previously discussed provide a link between the physical structures in the brain and the coordinates in the image. The original image coordinate system derived from the MRI acquisition is called the native space of the image. Although the native space allows to relate image coordinates to physical structures, it is not suitable when it is necessary the comparison between images of the same subject, scanned on different occasions, or between images of different individuals (Poldrack et al., 2011). They will not necessarily line up in native space since each subject will have different brain sizes and even when the same person is scanned multiple times, the brain will be in different places in the image depending on the exact position in the scanner. Therefore, to combine data across individuals, it is necessary to state a common space in which different subjects can be aligned. The need for the establishment of a standardized space mainly arises from neurosurgeons to be able to perform stereotactic neurosurgery. Such spaces are now referred to as *standard spaces* or *stereotactic spaces* (Poldrack et al., 2011). The most famous of these has been developed by Jean Talairach (Talairach, 1967). More recently, a stereotactic coordinate space developed at the Montreal Neurological Institute (MNI), based on a large number of MRI images, has become a standard in the field (Poldrack et al., 2011).

3.2 Functional Magnetic Resonance Imaging technique

Functional MRI has enjoyed an exciting development course with an exponential growth in published studies since its inception in the early 90's (Glover and Gary, 2011) when Ogawa and colleagues (Ogawa et al., 1990) obtained the first MRI images containing info about cerebral activity, based on the BOLD effect described many years before by Pauling (Pauling and Coryell, 1936; Huettel et al., 2004). Nowadays, this technique has become commonplace for clinical uses such as presurgical planning, fundamental cognitive neuroscience investigations, behaviour modification and training. Thanks to the fMRI advent more precise and detailed modelling of brain networks have been developed, leading to a better knowledge of the human brain (Glover and Gary, 2011). It represents one of most sophisticated techniques that exploit the hemodynamic variations related to the neuronal activity to identify the corresponding brain activated areas (Lv et al., 2018). The basic concept of fMRI is to collect BOLD images while the person inside the scanner performs a motor or cognitive tasks, or receives a sensory stimulation (Amaro et al., 2006). A set of images covering the whole brain (a brain volume) is typically acquired every 2–3 s, and (to increase sensitivity) hundreds of brain volumes are typically accumulated during the execution of a complete fMRI scan, lasting around 2»10 min (Amaro et al., 2006). Functional MRI represents a very powerful tool able to probe brain responses to different kinds of tasks. Due to its non-invasiveness and high spatial resolution, it is one of the most widely used technology in the functional brain research (Amaro et al., 2006).

Furthermore, with respect to the nuclear medicine, it allows the acquisition of both functional and structural images in the same session without the use of ionizing radiations or external contrast agents (Huettel et al., 2004). The main limitation is represented by the low temporal resolution. In fact, there is a finite amount of time, a delay between neuronal activation and a detectable increase in the BOLD signal (Glover and Gary, 2011).

3.2.1 Functional Magnetic Resonance Imaging: basic principles

This technique is used to better understand what are the mechanisms on which the brain functioning is based, both in healthy and pathological conditions. It's also useful to detect the brain activation in response to an external sensory input or to a performed task (Jackson et al., 2012). To better understand the mechanisms that make the fMRI possible it's necessary to investigate the physiological and biochemical properties of the brain and blood (Sokoloff, 2008).

The normal functioning of our cells is guaranteed by a steady source of energy, represented by the glucose in the brain, which can be metabolized with the oxygen to obtain energy. Most active tissues in the body, such as liver and muscles, possess energy stores that can be accessed during periods of high demand. However, the brain is the most metabolically active organ in our body, without any local oxygen reserve: therefore, it is highly dependent on a local blood supply (Takahashi, 2022). The local blood supply to a group of resting neurons is sufficient to support the basal metabolic needs of the cells. In the arterioles the incoming blood is highly oxygenated, while in the venules the blood becomes deoxygenated. When a group of neurons activate to perform a particular task, local biochemical changes cause the regional arterioles to dilate and thus to supply the necessary energy substrate and oxygen to the activated neurons. The fMRI technique is based on what is known as BOLD effect, sensitive to changes in the state of oxygenation of the haemoglobin (Amaro et al., 2006). The BOLD signal represents the ratio between oxygenated and deoxygenated haemoglobin.

3.2.1.1 Blood Oxygen Level Dependent effect

Within any imaging voxel (representing a small part of the brain) the proportion of deoxyhaemoglobin relative to oxyhaemoglobin dictates how the MR signal will behave in a BOLD image: areas with high concentration of oxyhaemoglobin give a higher signal (a brighter image) than areas with low concentration (Amaro et al., 2006). NMR signal characteristics of oxy- and deoxyhaemoglobin can be used to indirectly determine brain regional activity. The two haemoglobin states have different magnetic properties (***Figure 3.17***). The magnetic properties of an element or molecule is largely influenced by the number of unpaired electrons in the valence shell (Sparacia, 2019).

Oxyhaemoglobin → has no unpaired electrons and is weakly diamagnetic; it doesn't provoke any distortion in the MR signal (Sparacia, 2019).

Deoxyhaemoglobin → when oxygen is released to form deoxyhaemoglobin, four unpaired electrons are exposed at each iron centre, causing the molecule to become strongly paramagnetic. The presence of paramagnetic deoxyhaemoglobin within red blood cells creates local magnetic field distortions in and around blood vessels (Sparacia, 2019).

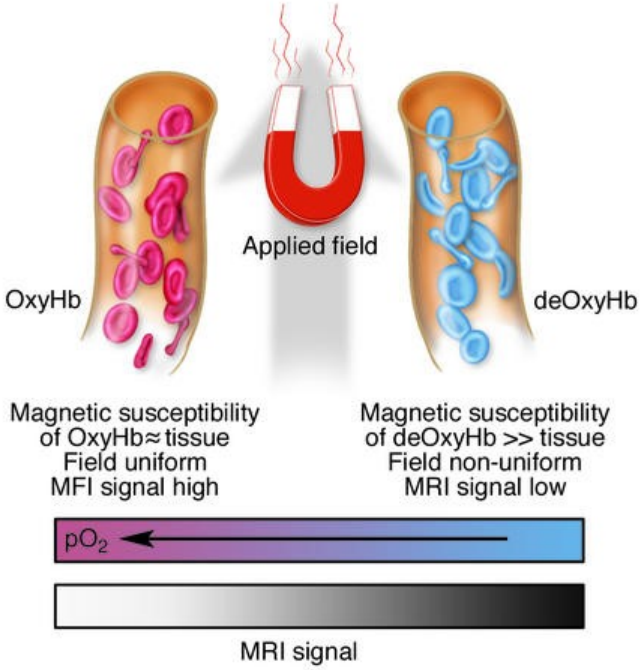

Figure 3.17 *Schematic illustration of the origin of the BOLD effect in fMRI (Gore, 2003).*

The increase in blood flow related to neuronal activation is also accompanied by an increase in oxyhaemoglobin concentration in that 'activated' area of the brain (Amaro et al., 2006). Since the paramagnetic properties of the deoxyhaemoglobin, when neurons are activated and the level of oxyhaemoglobin increases, the consequently decrease of deoxyhaemoglobin has a direct effect on the final NMR signal. Vessels containing oxygenated blood thus cause little or no distortion to the magnetic field in the surrounding tissue, while capillaries and veins containing blood that is partially deoxygenated distort the magnetic field in their vicinity (Matthews and Pezzard, 2004). To understand how tissue oxygenation is related to neuronal activity we must return to experiments performed in the 19th century, when it was noted that there is "an automatic mechanism by which the blood supply of any part of the cerebral tissue is varied in accordance with the activity of the chemical changes which underlie the functional action of that part. Bearing in mind that strong evidence exists of localization of function in the brain, we are of the opinion that an automatic mechanism, of the kind just referred to, is well fitted to provide for a local variation of the blood supply in accordance with local variations of the functional activity." (Roy & Sherrington, 1890). This mechanism is known as *neurovascular coupling* and it's based on hemodynamic responses (HR) related to neuronal activity (Amaro et al., 2006). The hemodynamic response function (HRF) represents the transfer function linking neural activity with the BOLD fMRI signal, modelling neurovascular coupling (Rangaprakash et al., 2021).

In fact, the HR produced by the neuronal activity makes the fMRI able to identify the brain area activated by the performance of a particular task. The temporal evolution of the BOLD effect from a brief stimulus presentation is not static. Rather it is a dynamic process that can be modelled using mathematical functions, providing different parameters regarding the neurovascular coupling (Amaro et al., 2006). The temporal evolution of BOLD signal changes has the form of a characteristic curve called the HRF (Jackson et al., 2012). The trend of the BOLD signal is strictly related to the metabolic phenomena involved in neuronal activation (Siero et al., 2013). During the first moments following the stimulus, the BOLD signal and the oxyhaemoglobin concentration decrease briefly, while there is a transient increase in deoxyhaemoglobin concentration (Jackson et al., 2012). This is called initial dip which is thought to reflect an increase in metabolism and oxygen extraction before blood flow increases to the area (Yacoub et al., 2001). Following the initial dip phase, the increase in cerebral blood flow and cerebral blood volume gives rise to an increase in BOLD signal (Jackson et al., 2012). This positive BOLD effect is proportional to the neuronal activity and, if the stimulus is maintained for a sufficient time, the signal reaches a plateau (Amaro et al., 2006). After the cessation of the stimulus, there is a return to the baseline, eventually dipping temporarily below baseline: the post-stimulus undershoot (Jackson et al., 2012).

This effect is believed to derive from the venous bed capacity, which tends to cause the regional blood volume to normalize at a slower rate than the changes in blood flow, thus leading to relatively high deoxy-haemoglobin concentration. These events are depicted in ***Figure 3.18*** (Amaro et al., 2006). By using BOLD images, is it therefore possible to indirectly detect the increase the neuronal activity when the subject performs a specific task, compared to another moment in which no task is performed (Amaro et al., 2006).

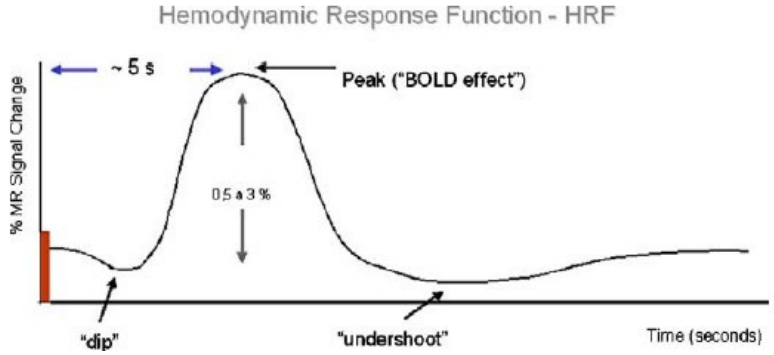

Figure 3.18 *Hemodynamic response function from a hypothetical short duration stimulus (grey bar—red bar in the web version); the BOLD effect peaks after circa 3 s from the start of stimulus presentation (black bar) (Amaro et al., 2006).*

3.3 Resting-state functional Magnetic Resonance Imaging

The study of the hemodynamic response following the neuronal activation in response to a task or a stimulus, represents one of the main arguments dealt in functional neuroscience studies (Fox and Raichle, 2007). Many researchers have tried to understand how different regions of the brain work together to accomplish the many functions that the brain performs (Seitzman et al., 2019). The paradigm most often used in studying the brain with fMRI is that of imposing a cognitive, sensory, or motor task and subsequently observing the change in BOLD signal (Seitzman et al., 2019). Numerous tasks have been studied and reported in the literature, providing us a wide understanding of the many different systems that function across the brain (Seitzman et al., 2019). One important finding deduced from these studies is that the increase in the neuronal metabolism is only minimally altered during the performance of a task, accounting for only less than 5% of the total oxygen consumption at rest (Fox and Raichle, 2007). The implication of this observation is that the intrinsic activity of the brain at rest uses a substantial amount of energy, and thus must be of great importance for the normal function of the brain (Seitzman et al., 2019). According to this, to have a full knowledge of the brain functioning it's important to focus also on the component responsible for the highest metabolic demand, known as spontaneous neuronal activity (Fox and Raichle, 2007).

3.3.1 Resting-state networks

The observation that spontaneous BOLD activity is specifically organized in the resting human brain has generated a great interest in studying the so called rs-fMRI (Fox and Raichle, 2007). Many investigators suspected that the signal in absence of task was mainly due to noise, inferring that there was little to be gained by studying such data (Power et al., 2014). Biswal and colleagues in 1995 were the first who changed this perspective by demonstrating that fluctuations in the fMRI signal, in the absence of a task, were highly and specifically correlated among functionally related brain regions (Power et al., 2014). In their study (schematically illustrated in ***Figure 3.19***), the resting-state timeseries of a voxel in the motor network was correlated with the resting-state time-series of all other brain voxels, revealing a high correlation between the spontaneous neuronal activation patterns of these regions (van den Heuvel et al., 2010).

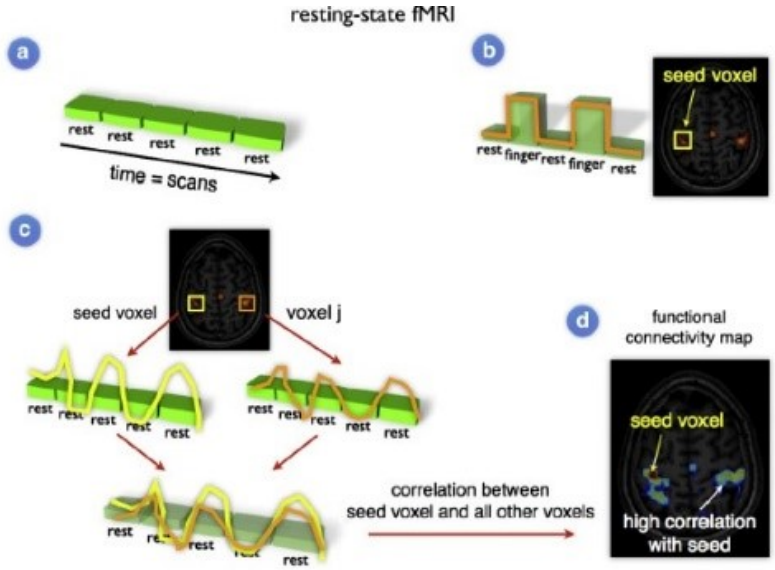

Figure 3.19 *Resting-state fMRI studies are focused on measuring the correlation between spontaneous activation patterns of brain regions. Within a resting-state experiment, subjects are placed into the scanner and asked to close their eyes and to think of nothing, without falling asleep. Like conventional task-related fMRI, the BOLD fMRI signal is measured throughout the experiment (panel a). Conventional task-dependent fMRI can be used to select a seed region of interest (panel b). To examine the level of functional connectivity between the selected seed voxel i and a second brain region j (for example a region in the contralateral motor cortex), the resting-state time-series of the seed voxel is correlated with the resting-state time-series of region j (panel c). A high correlation between the time-series of voxel i and voxel j is reflecting a high level of functional connectivity between these regions. Furthermore, to map out all functional connections of the selected seed region, the time-series of the seed voxel i can be correlated with the time-series of all other voxels in the brain, resulting in a functional connectivity map that reflects the regions that show a high level of functional connectivity with the selected seed region (panel d) (van den Heuvel et al., 2010).*

Several studies have replicated these pioneering results, showing a high level of functional connectivity between the left and right hemispheric motor cortex, but also between regions of other known functional networks, like the primary visual network, auditory network, and higher order cognitive networks (van den Heuvel et al., 2010). In accordance with these studies, it was possible to demonstrate that during rest the brain network is not idle but is characterised by spontaneous activity highly correlated between different brain regions (van den Heuvel et al., 2010). Brain areas demonstrating synchronous activity have been called RSNs. The topography of RSNs closely corresponds to responses elicited by a wide variety of sensory, motor, and cognitive tasks (Seitzman et al., 2019). The RSNs are a pivotal element for understanding the dynamics and organization of the brain basal activity in health and disease (Diez et al., 2015). The spontaneous activity during the execution of a task shows an anatomical distribution like that observed during the rest phase. Smith and his colleagues

(Smith et al., 2009) suggested that the measured neuronal responses represent an approximately linear overlap of task-related neuronal activity and spontaneous activity. The correlation between two or more regions equally activated by the execution of a task increases during the conditions of activity, and the correlation between the other regions decreases. Therefore, the correlation between brain structures remains constant during the rest and task phase and the observed changes in the correlations are simple due to a superimposition of spontaneous and task-related activity (Fox and Raichle, 2007). In contrast to the traditional task-based approach, resting state studies observe the brain in the absence of task performance or external stimulation. Subjects are asked to lie quietly keeping the eyes closed, or opened fixing at a point, while the spontaneous fluctuations of BOLD signal are recorded (Fox and Greicius et al., 2010). Recent studies have focused on the identification of the possible origin of the slow variations present in the measured BOLD signal. Various researchers have suggested that these signal variations, temporally correlated across the brain, are of neuronal origin and correspond to functional RSNs which jointly characterize the neuronal baseline activity of the human brain in the absence of externally stimulated neuronal activity and may reflect functionally distinct networks (Beckmann et al., 2005). In the study of Beckmann et al, which involved the analysis of 10 healthy subjects during rest condition, have been identified 8 RSNs shown in ***Figure 3.20*** (Beckmann et al., 2005).

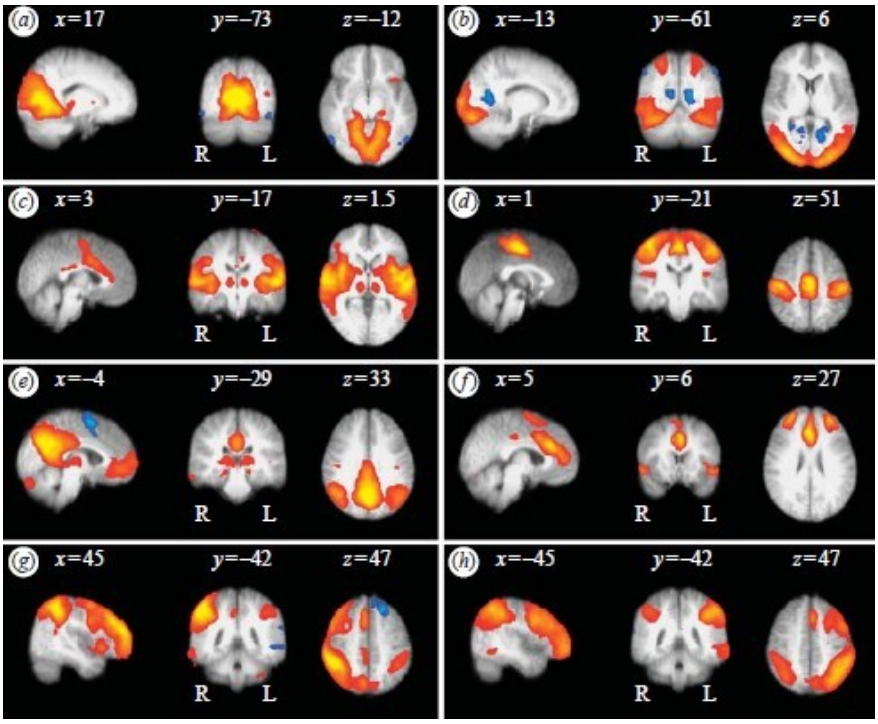

Figure 3.20 *Different estimated resting patterns: sagittal, coronal and axial views of different spatial maps associated with low frequency resting patterns estimated from a group of 10 subjects (Beckmann et al. 2005).*

Another important contribution was given by the study of Smith and his colleagues in 2009, in which they identified 10 RSNs (Smith et al., 2009). The analysis consisted in comparing the networks of 36 healthy subjects activated during resting condition with the networks of a large database of brain map, acquired during task fMRI, to identify any correlation between resting state networks and those under stimulation. The 10 maps are shown in ***Figure 3.21*** and include the 8 RSN maps found by Beckmann, an additional cerebellar map and 2 maps obtained by the split of the lateral visual cortical area (***Figure 3.21***). The results obtained derive from the Independent Component Analysis (ICA) decomposition of subject data of the Brain-map database and separately from the analysis of the resting fMRI data. The 10 maps correspond to interpretable functional categories and can be considered the ‘‘major representative’’ functional networks as derived independently from both activation meta-analysis and resting data.

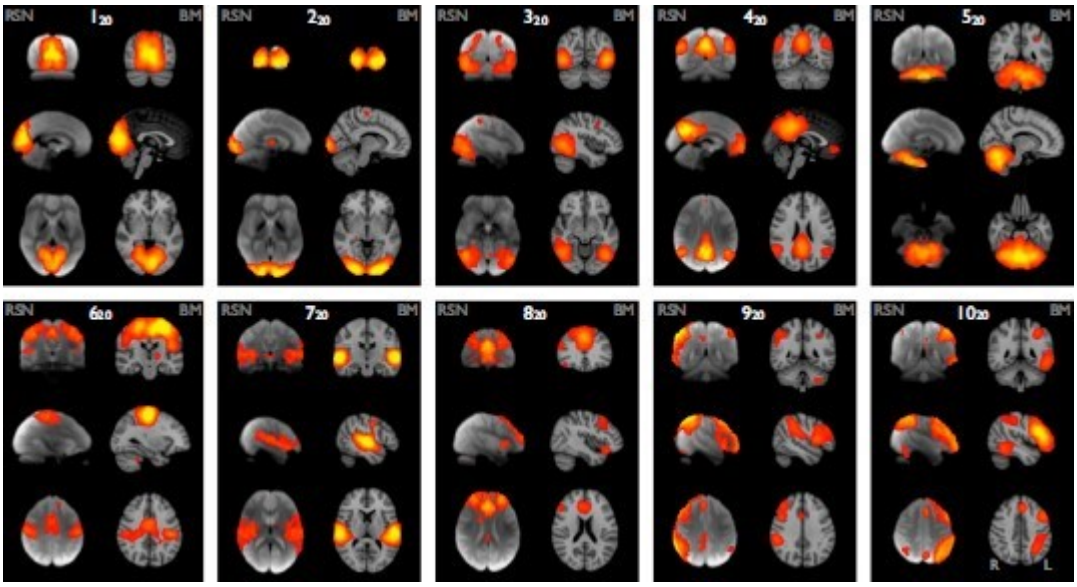

Figure 3.21 *The 10 maps obtained by Smith and co-workers represented in three planes: sagittal, coronal, and axial. Left column of each pair corresponds to the resting fMRI data overlayed onto the mean fMRI image from all subjects. Right column of each pair corresponds to the network from specific task fMRI (Smith et al., 2009).*

• Maps 1_{20}, 2_{20} and 3_{20} ('visual'): they correspond to medial, occipital pole, and lateral visual areas.

• Map 4_{20}('default mode network'): this is often referred to as the default mode network and is possibly the most widely studied RSNs in the rs-fMRI literature.

• Map 5_{20}('cerebellum'): it covers the cerebellum. This corresponds most strongly to action–execution and perception–somesthesis– pain domains.

• Map 6_{20}: it includes supplementary motor area, sensorimotor cortex, and secondary somatosensory cortex. This corresponds most strongly to the action–execution and perception–somesthesis paradigms.

• Map 7_{20}('auditory'): It includes primary and association *auditory cortices*. This corresponds most strongly to action–execution–speech, cognition–language–speech, and perception–audition paradigms.

• Map 8_{20}: ("executive control"): it covers several medial–frontal areas. This corresponds to action–inhibition, emotion, and perception–somesthesis–pain.

• Maps 9_{20} and 10_{20} ('frontoparietal'): they cover several frontoparietal areas, right and left respectively. They correspond to several cognition/language paradigms.

In addition, map 9_{20} corresponds strongly to perception–somesthesis–pain.

Map 10_{20} corresponds strongly to cognition–language paradigms, which is consistent with the Broca's and Wernicke's areas seen in the map.

3.4 Diffusion Tensor Imaging technique

The possibility to perform virtual dissections of white matter tracts and visualize pathways in the living human brain is one of the most promising applications of DTI tractography (Catani et al., 2008). DTI revolutionized the field of white matter mapping, thus becoming one of the most popular MRI techniques in brain research, as well as in clinical practice. This MRI-based methodology, originally presented in 1994, takes advantage of the macroscopic geometrical arrangement of white matter bundles that becomes apparent through diffusion MRI measurements. In general, diffusion MRI measures the three-dimensional displacement of water molecules. Since the early diffusion MRI measurements, it has been observed that water displacement in white matter has anisotropic nature. In particular, the water molecules' diffusion was found to be much faster along the white matter fibres than perpendicular to them. The DTI technique is based on the difference between these two motions, parallel and perpendicular to the fibres. This phenomenon is known as diffusion anisotropy (Assaf and Pasternak, 2008). DTI provides a quantification of the diffusion properties of white matter, mathematically characterized by an effective diffusion tensor consisting of nine matrix elements (Dijkhuizen et al., 2012). Using tensor decomposition, it is possible to extract the diffusivities parallel and perpendicular to the fibres (also termed principal diffusivities, $\lambda//$ and $\lambda\perp$), used later for calculation of summation indices. One of them is the fractional anisotropy (FA), which represents the normalized standard deviation of the diffusivities. Nowadays, the FA index is the most widely used parameter of DTI to represent the motional anisotropy of water molecules, being sensitive to the presence and integrity of white matter fibres.

FA provides a greyscale, 2D map, enhancing diffusion anisotropy differences with intensity limits between zero and one (Assaf and Pasternak, 2008). Since white matter tracts are composed of highly oriented fibres, which cause relatively high anisotropy of diffusing tissue water, DTI is very suitable to measure effects on white matter integrity.

3.4.1 Basic Concept of Diffusion

Diffusion is considered as a three-dimensional phenomenon with a direction and shape. The shape and magnitude of water molecules diffusion differ between various brain structures since it is influenced by the microstructural architecture as well as physiologic factors (Huisman,2010). Diffusion in white matter tracts is, for example, predominantly along the direction parallel to the long axis of tracts and limited in the perpendicular direction. This directional diffusion can be graphically represented as an ellipsoid or cigar and is known as *anisotropic diffusion* (***Figure 3.22a***). When the degree of diffusion is equal in all directions in space such as in CSF, where no cell membranes limit diffusion, the three-dimensional shape of diffusion can be graphically represented by a sphere and is known as *isotropic diffusion* (***Figure 3.22b***) (Huisman,2010).

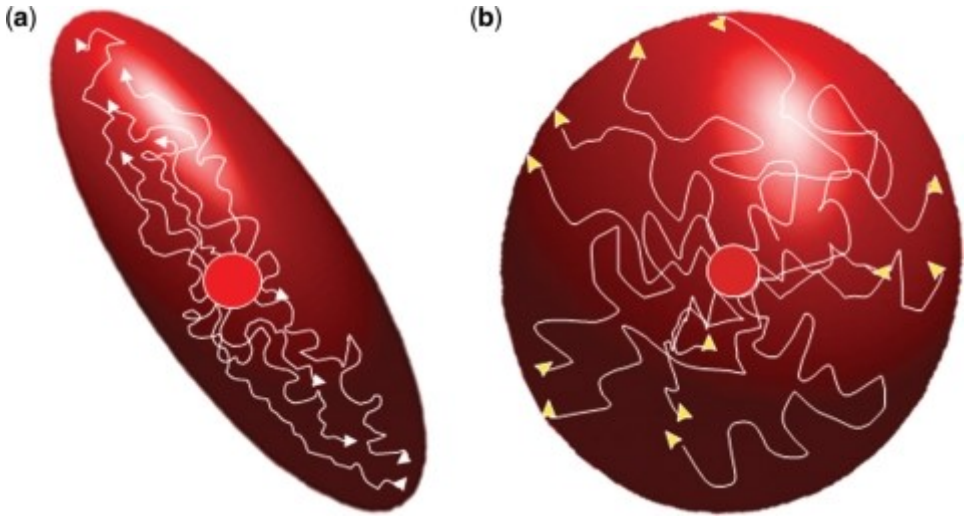

Figure 3.22 *Anisotropic diffusion (a) represented by a three-dimensional ellipsoid in space with predominant diffusion of molecules along the main axis of the ellipsoid and restricted diffusion perpendicular to the ellipsoid. Isotropic diffusion (b) can be represented by a sphere with equal diffusion in all directions in space. The arrows indicate the motion of individual molecules (Huisman, 2010).*

DTI analyses the three-dimensional shape of the diffusion, also known as diffusion tensor. The diffusion tensor contains information about the microstructure of brain tissue. Through DTI technique, it is possible to estimate several parameters of water diffusion, such as mean diffusivity (MD) and FA (Huisman, 2010). The MD describes the overall diffusion and is calculated as the mean of the three eigenvalues of the diffusion tensor (the mean amount of diffusion in each of the principal directions calculated in the tensor) (Salat, 2014).

The FA is defined as the ratio of the anisotropic component of the diffusion tensor to the whole diffusion tensor and serves as a rotationally invariant scalar that quantifies the shape of the diffusion tensor. FA varies between zero and one. Zero represents maximal isotropic diffusion as in a perfect sphere; one represents maximal anisotropic diffusion as in the hypothetical case of a long cylinder of minimal diameter (***Figure 3.23***). The FA values can also be calculated on a voxel-by-voxel basis and mapped accordingly. Areas with a high degree of anisotropic diffusion (high FA value) are bright (e.g., CC, internal capsule), and areas with low anisotropic diffusion are dark (e.g., CSF or grey matter) (Huisman,2010).

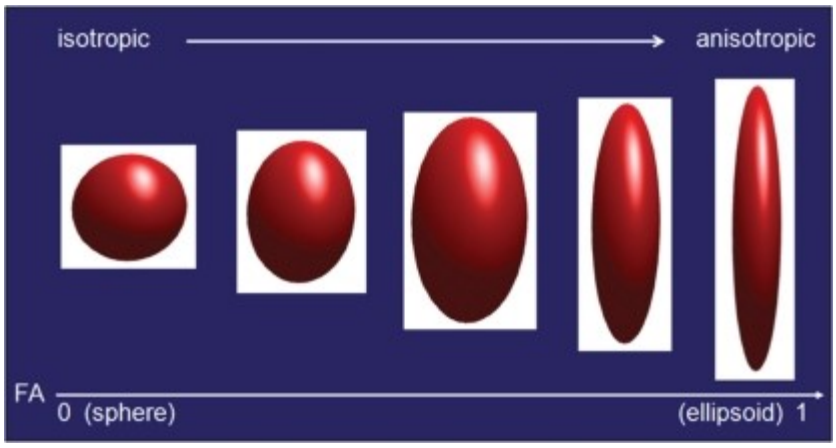

Figure 3.23 *Graphical display of the range of FA values between isotropic and anisotropic diffusion. A FA value of zero represents complete isotropic diffusion (perfect sphere); a FA value of one represents the hypothetical case of complete anisotropic diffusion (narrow ellipsoid) (Huisman,2010).*

Sampling the diffusion tensor also gives information about the principal direction of diffusion (***Figure 3.24a***) that can also be mapped together with the degree of anisotropic diffusion.
The DTI-derived diffusion anisotropy and principal diffusion direction in white matter tissue can be used to model the architecture of neuronal fibres, visualized by orientation based color-coded FA maps or three-dimensional fibre tract maps computed with tractography algorithms (Dijkhuizen et al., 2012). The most basic red–green–blue (RGB) color-coded scheme attributes a colour for each orientation of the fibres ***(Figure 3.25)***: fibres crossing from left to right are visualized in red, fibres crossing anteriorly–posteriorly are visualized in green, and fibres crossing inferiorly–superiorly are visualized in blue (Assaf and Pasternak, 2008). This colour coding facilitates recognition of major normal and aberrant white matter tracts.

By combining the directional information and magnitude of anisotropic diffusion of the individual voxels, the course of white matter tracts can be reconstructed. This technique relies on the assumption that voxels with a similar orientation of their principal anisotropic diffusion direction are part of the same white matter tract (Huisman, 2010).

After localization and reconstruction of white matter tracts, powerful postprocessing mathematical algorithms can be used to study and visualize these tracts in vivo. This technique is also known as tractography (***Figure 3.24b***). By increasing the number of diffusion-encoding gradients, complex crossings of white matter tracts within one voxel can be identified (Huisman, 2010).

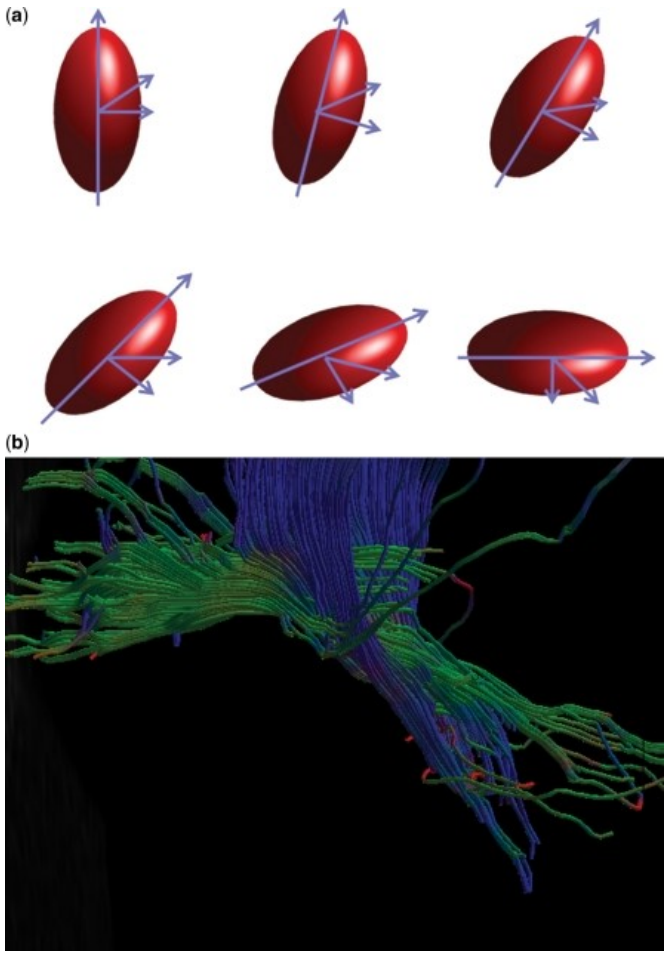

Figure 3.24 *(a) DTI allows the calculation of the diffusion tensor shape in space (e.g., ellipsoid) but also gives the orientation of the tensor in space. The tensor is represented by the three principal eigenvectors both in direction (orientation of the vector) and magnitude (length of the vector). Various orientations of the diffusion tensor are displayed, which provide information about the orientation of white matter tracts in the brain. (b) Based on the DTI data, fibre tracts can be reconstructed from the DTI data based on the identified direction and magnitude of the anisotropic diffusion within the individual voxels (Huisman,2010).*

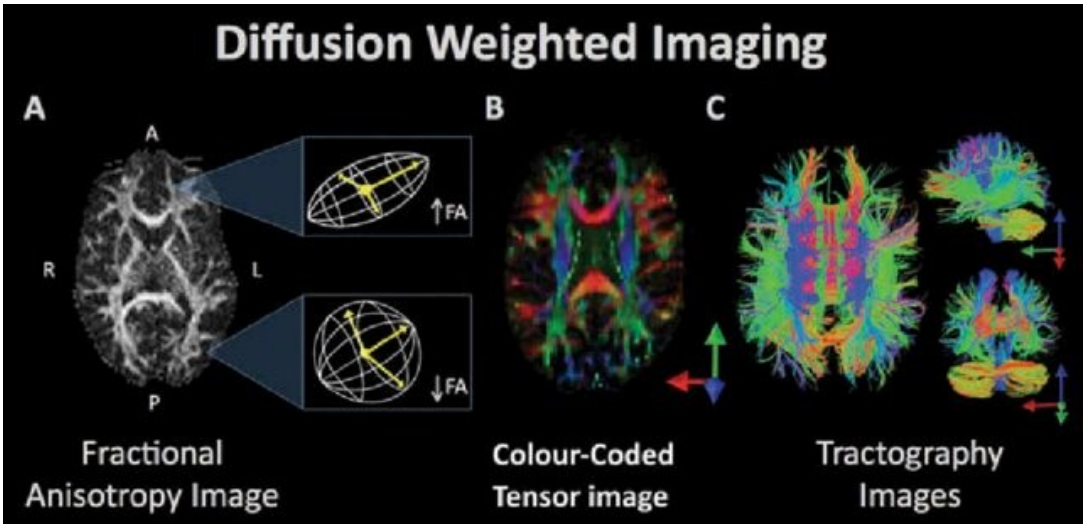

Figure 3.25 *(A) The white matter tracts of a single subject's brain, reconstructed from the FA values where high FA represents regions of strict, directed water diffusion (along the borders of white matter bundles) and low FA indicates regions with isotropic water diffusion. (B) The white matter tracts from FA values are color-coded to indicate the direction of water diffusion to illustrate the arrangement and organization of bundles of white matter. (C) Visualization of diffusion tensor imaging (DTI) data in the axial (left), sagittal (top right), and coronal plane (bottom right). Fiber bundle directionality is indicated by colour: red = right to left/left to right (e.g., CC), green = posterior to anterior/anterior to posterior (e.g., cingulum bundle), blue = inferior to superior/superior to inferior (e.g., corticospinal tracts) (Salat et al., 2009).*

Diffusion tensor imaging is considered a functional technique because it is based on a phenomenon changing over time, i.e., the water molecules diffusion in different brain regions. Since the water diffusion is conditioned by the physical structure inside the brain, the trajectories of water molecules allow to identify the structural connections inside the brain. Therefore, the image obtained from a DTI analysis represent physical structure although they are based on a dynamic process.

3.5 Magnetic Resonance Imaging modalities

There are many types of images that can be acquired on an MRI scanner. These different images capture different information about the brain, and are called modalities (Jenkinson and Chappell, 2018). The most used modalities in neuroimaging research are the following: structural, diffusion, and functional imaging ***(Figure 3.26).*** The structural imaging provides information about anatomical structures of the brain. The diffusion-weighted imaging (DWI), or dMRI, provides information about microstructure and anatomical connectivity within the brain (Jenkinson and Chappell, 2018). The third, functional imaging or fMRI, provides information about the activity of groups of neurons in the brain, either in response to specific stimuli or tasks (task fMRI) or in relation to the spontaneous activity of the brain (rs-fMRI). Information from several modalities can be combined to perform more specific and complete analyses, as the anatomical connectivity associated with a particular functional area.

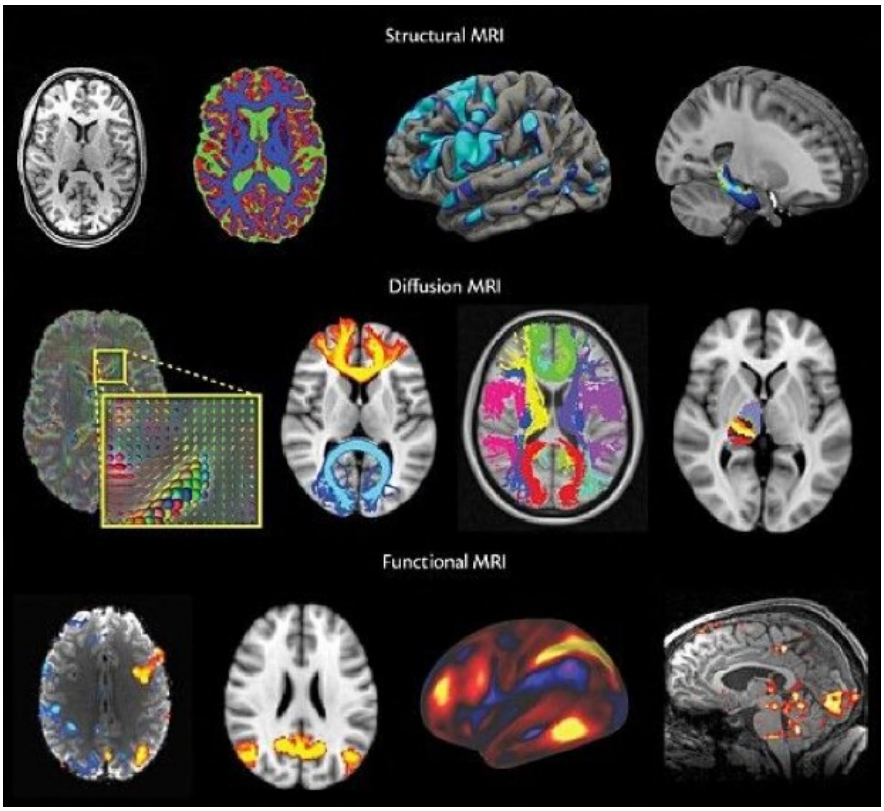

Figure 3.26 *Illustrations of the three main MRI modalities to be covered in this primer and examples of various analysis outputs. These include tissue and structure delineation (structural), estimation of white matter tracts and connectivity-based parcellation (diffusion), and functional activations and connectivity networks (functional) (Jenkinson and Chappell, 2018).*

Structural imaging

Structural images give a static image (no change over time), useful to detect different shape and dimension of grey and white matter, or differences between them. These structural images do not give any information about what it is happening at each location in the brain, but they provide high spatial resolution that enables analysis of the brain anatomy.
Structural MRI results in a single ***volume*** represented by a 3D box corresponding to the area scanned by the MRI machine. This volume is composed of individual ***voxels*** which are like three-dimensional pixels (the green and blue boxes in ***Figure 3.27***). Voxels are the basic spatial unit of MRI acquisition; in structural MRI they are usually 1mm x 1mm x 1mm. A single volume is obtained from the structural MRI since the anatomy is not expected to change across the timescale of the scanning session.

Functional imaging

Functional images are the data acquired during the fMRI. The fMRI technique is employed to detect changes in the BOLD signal. The BOLD signal derives from changes in the oxygen level of blood that are related to neural activity. Although the spatial resolution of fMRI is much worse than structural MRI, fMRI measures a signal that changes over time, providing an indirect measurement of neural activity. Functional MRI data also contains volumes composed of individual voxels. In fMRI these voxels tend to have a size of 3mm x 3mm x 3mm but, unlike structural MRI, a measurement from each voxel at each timestep of the experiment is obtained. The unit of time in MRI is the TR, which is the time required for a single measurement from each voxel in the volume. In fMRI this is usually in the range of 1 to 3 s. In contrast to structural MRI, whose measured signal is used to distinguish different tissue types from each other, fMRI is measuring the BOLD signal which changes at each moment in time in response to nearby neural activity. This means that an fMRI dataset is four-dimensional since it contains a volume of N voxels measured at each of T timepoints. Then, for each voxel (defined by the x, y, z coordinate in the 3D volume) there is a timeseries of BOLD activation measured during the acquisition.

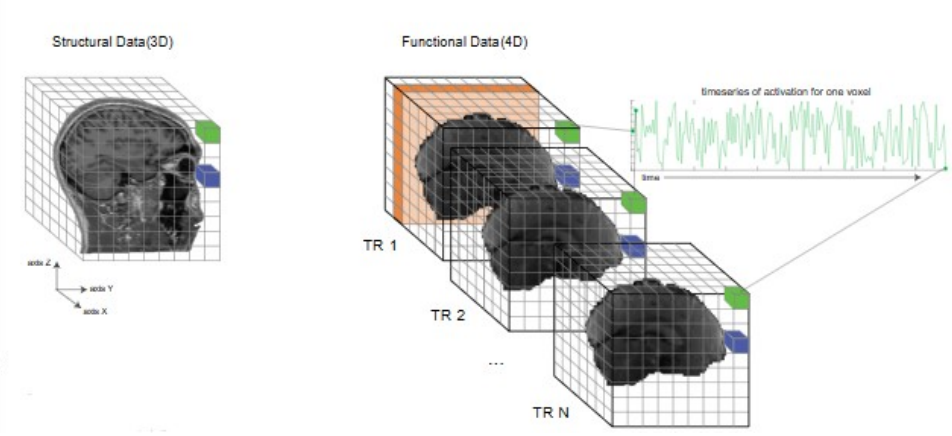

Figure 3.27 *Representation of Structural (3D) and Functional (4D) data. The entire 3D grid covering the space imaged by the MRI scanner is indicated as the 'volume', composed in turn by several voxels (green and blue cubes). Each voxel has coordinates in the 3D volume. All the voxels in a 2D plane taken from the 3D volume represent the slice (orange). One volume is scanned with an acquisition interval equal to TR (cims.nyu.edu/~brenden/courses/labincp/chapters/17/00-mri.html).*

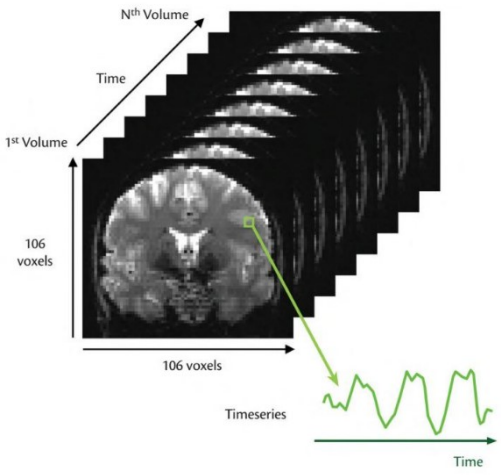

Figure 3.28 *Representation of the functional data (4D) and its associated timeseries (Jenkinson and Chappell, 2018).*

Diffusion imaging

The major difference of this modality in comparison to structural and functional imaging is the use of special gradient fields, called diffusion-encoding gradients. Diffusion-weighted images are routinely accomplished by applying strong pulsed "diffusion" gradients during the evolution of the MR signal (Holdsworth et al., 2008). These magnetic fields are created by the gradient coils in the scanner (the same ones used to figure out the spatial locations of the signal) but are made especially strong and applied right at the beginning of each slice acquisition. Since each single 3D image only gives information about diffusion in one direction, it is necessary to acquire many images with different diffusion-encoding directions, to build up a picture of how the diffusion varies with direction (Jenkinson and Chappell, 2018). In addition to the number of directions, it is also important to specify their orientation in space. In addition to the directions, the acquisition is affected by the strength and the timing of the diffusion-encoding gradients. The key combination of these is measured by the b-value, which expresses how strongly a given amount of diffusion will affect the MR signal (i.e., the image intensity) (Jenkinson and Chappell, 2018). The b-value is a function of the gradient-related parameters: strength, duration, and the period between diffusion gradients (Holdsworth et al., 2008). Typically, b-values of 1000-1500 s/mm^2 are used as a trade-off between having high sensitivity to diffusion and good SNR ***(Figure 3.29)***. Regardless of the type of acquisition scheme used, it is also necessary to collect several images without using the diffusion-encoding gradients, that contain no diffusion weighting ***(Figure 3.29).*** These are referred to as "b = 0" or just "b0" scans. Such images provide a crucial baseline for being able to extract quantitative information (such as MD, FA, etc.) from the diffusion MR intensities. This baseline is necessary to know how much the diffusion of the water molecules has reduced the signal intensity when the diffusion-encoding gradients are used (Jenkinson and Chappell, 2018).

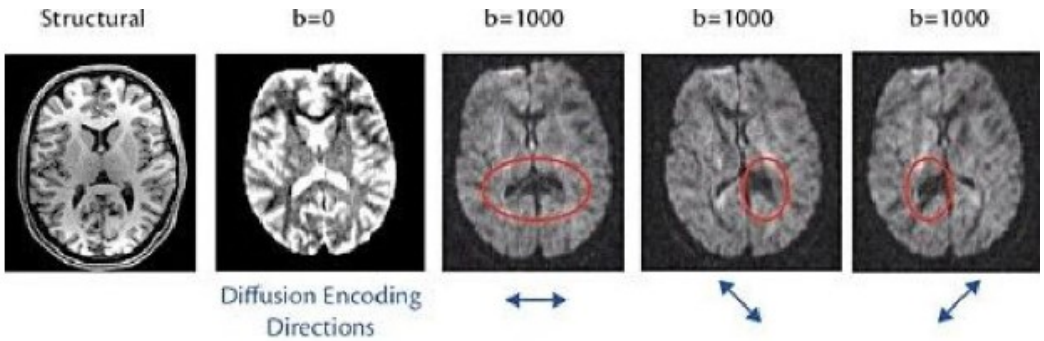

Figure 3.29 *From the left: T1-weighted structural image; non-diffusion weighted (b = o) image; and three diffusion MRI images (all with b = 1000 s/mm^2) with different diffusion encoding directions (Jenkinson and Chappell, 2018).*

Diffusion magnetic resonance images may suffer from geometric distortions. The rapid echo planar imaging techniques and high gradient fields typically used for dMRI cause geometric mismatch with anatomical images and ultimately affect subsequent quantification of connectivity indices (Jenkinson and Chappell, 2018). In ***Figure 3.30*** is it possible to observe the amount of the geometric distortions, resulting on the final scan. Acquiring a pair of images, with different encoding directions (posterior-anterior, P-A, and anterior-posterior, A-P), is very useful for correcting the geometric distortion in the analysis.

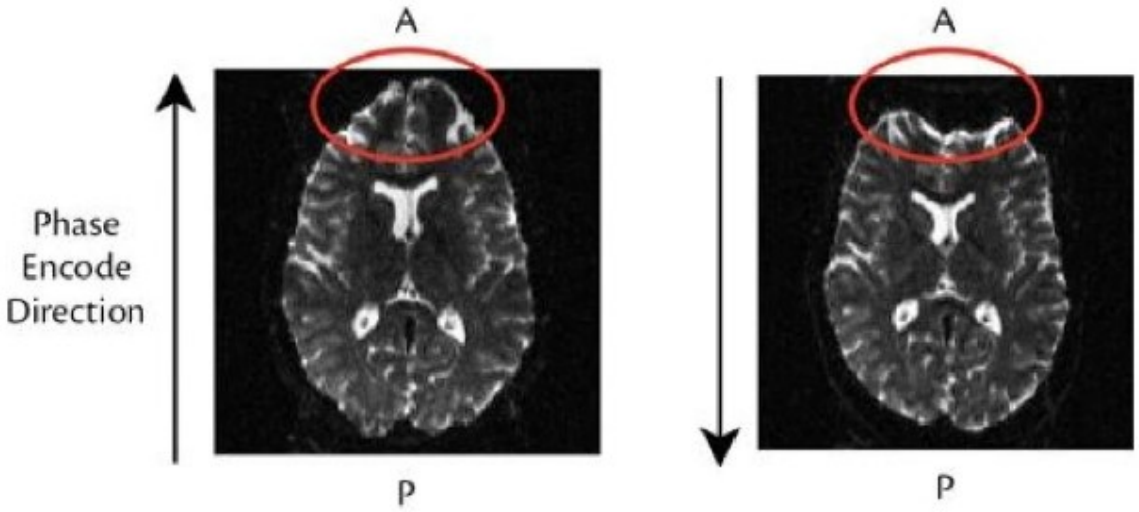

Figure 3.30 *Example of axial images from a dMRI experiment. Two b = O images with opposite phase encode directions (P-A and A-P), demonstrating the reversed geometric distortions (red circles) directions (Jenkinson and Chappell, 2018).*

Another artifact that is common in diffusion imaging is eddy-current distortion. This is a consequence of using strong diffusion- encoding gradients that are rapidly turned on and off, which then induce electrical currents in the nearby metallic surfaces of the scanner. These currents are known as eddy currents, and they arise for the same reason why moving a magnet in a coil of wire can generate electrical current. The eddy currents then, in turn, create unwanted magnetic fields (using the same principle as an electromagnet), and these fields linger and interfere with the imaging gradient fields necessary to determine the spatial locations of the signals. Therefore, the spatial locations are incorrectly assigned, and the images are geometrically distorted, which need to be corrected for the analysis.

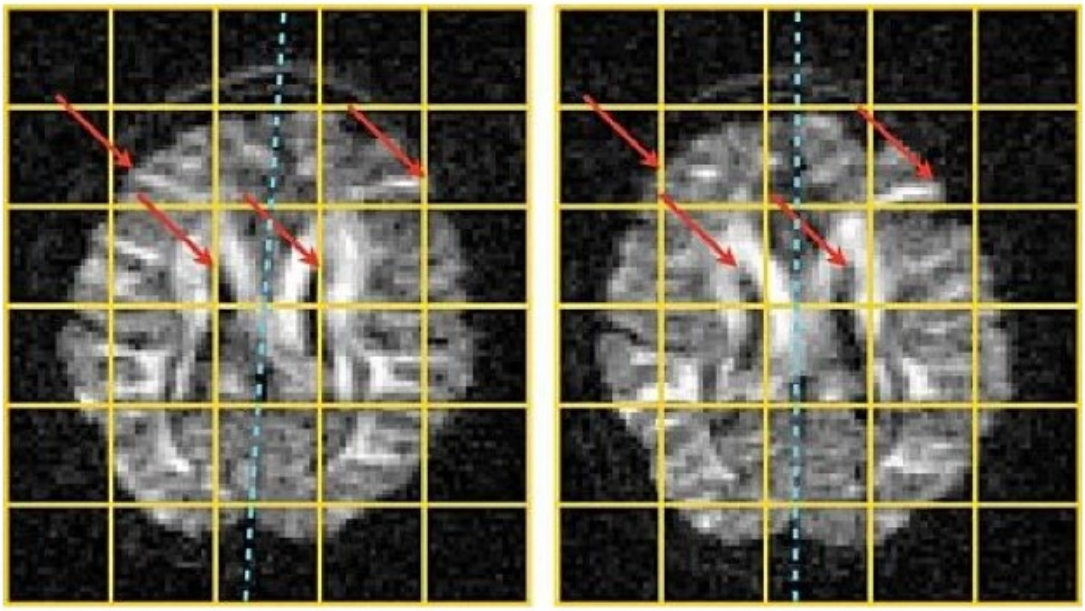

Figure 3.31 *An example of eddy current distortions in dMRI. Two diffusion-encoded images (from the same 4D acquisition) with different diffusion encoding directions are shown, demonstrating the geometric distortions caused by the different eddy currents on the image. The red arrows indicate corresponding anatomical locations that are clearly shifted due to the eddy current distortions. The blue dotted line indicates the approximate inter-hemispheric plane, which illustrates the magnitude of the geometric distortion directions (Jenkinson and Chappell, 2018).*

Chapter 4 *Materials and Methods*

4.1 Data acquisition

For the current study, resting-state BOLD fMRI data, T1-weighted structural images and DWI data were acquired using a 1.5 Signa HDxt GE Medical System MRI scanner. Data were collected from one healthy subject S1 and one patient named P2, according to the study of Fabri and Polonara (Fabri and Polonara, 2023).

During the resting-state fMRI acquisition subjects were instructed to lie down and stay still as much as possible, to keep their eyes open, to relax without falling asleep and without focusing on anything. Functional images were acquired using a gradient-echo EPI sequence. In addition to functional acquisitions, a T1 weighted structural image covering the whole brain (high resolution scan) was acquired for better anatomical localization and co-registration with functional data. A MPRAGE sequence was used. For the diffusion MRI data, instead, acquisition was performed using a SE-EPI pulse sequence. These acquisition techniques are better explained in the Appendix A. All the parameters used during the three acquisitions are listed in ***Table 3*** and ***Table 4***.

Table 3 *Parameters used for the DWI, Functional and Structural acquisitions in subject S1.*

S1	***Parameters***	***DWI***	***Functional***	***Structural***
	TE (ms)	*89*	*50*	*6,7*
	TR (ms)	*6500*	*3000*	*14,7*
	FOV	*260x260*	*240x240*	*256x256*
	FLIP ANGLE (°)	*90°*	*90°*	*15°*
	MATRIX SIZE	*256x256*	*64x64*	*512x512*
	NUMBER OF VOLUMES	*26*	*300*	*1*
	NUMBER OF SLICES	*27*	*35*	*158*
	SLICE THICKNESS (mm)	*5*	*5*	*1*
	VOXEL RESOLUTION (mm)	*1,0156x1,0156x5*	*3,75x3,75x5*	*1x1x1*
	DURATION (min)	*5-6 min*	*15 min*	*8 min*

Table 4 *Parameters used for the DWI, Functional and Structural acquisitions in patient P2.*

P2	***Parameters***	***DWI***	***Functional***	***Structural***
	TE (ms)	*91*	*50*	*6,7*
	TR (ms)	*6500*	*3000*	*14,7*
	FOV	*260x260*	*192x192*	*256x256*
	FLIP ANGLE (°)	*90°*	*90°*	*15°*
	MATRIX SIZE	*256x256*	*64x64*	*512x512*
	NUMBER OF VOLUMES	*26*	*300*	*1*
	NUMBER OF SLICES	*28*	*35*	*158*
	SLICE THICKNESS (mm)	*5*	*4*	*1*
	VOXEL RESOLUTION (mm)	*1,0156x1,0156x5*	*3x3x4*	*1x1x1*
	DURATION (min)	*5-6 min*	*15 min*	*8 min*

All these parameters are obtained by the so called json file, which contains information about the acquisition. This file can be recovered by the conversion from the DICOM to the NifTi format. The conversion is performed through the MriCron software (people.cas.sc.edu/ rorden/mricron/install.html). In addition to the json file, for the DWI data, others two files are necessary to perform the analysis: the bval and the bvec files. The bval contains a single number per volume that indicates the strength and the timing of the diffusion gradients, applied to the data; the bvec file contains a triplet of numbers per volume that shows in what directions the gradients were applied.

4.2 Pre-Processing

After data acquisition, all the images were processed using dedicated software to obtain the information necessary for the subsequent analysis. The software used in this study is Brain Voyager (BV), version 2.4. BV is a powerful neuroimaging software package for data management and data analysis. It started as a tool for the analysis of anatomical and functional MRI data sets but has evolved over the years into a multi-modal analysis tool for fMRI, DTI, electroencephalography (EEG), and magnetoencephalography (MEG) data (www.brainvoyager.com). The program runs on all major computer platforms including Windows, Linux, and Mac OS X. BV QX provides an easy-to-use, interactive graphical user interface (GUI) on all platforms (Goebel et al., 2006). All the steps performed during the data analysis are described in detail in Appendix B and Appendix C.

The MRI images were acquired in DICOM format. Although DICOM is the standard format for data output from MRI scanners, it is often necessary to convert DICOM to other format before data analysis. The main reason is that DICOM datasets are unwieldy, owing to the storage of each slice as a separate file. This can soon lead to massive numbers of small files that clog file systems and slow analysis (Poldrack et al., 2011) According to this, for the BOLD data, a 4D volume is obtained in Nifti format from a specific number of DICOM images. The total number of DICOM images results from the number of slices and the number of acquired volumes from each slice. However, version 2.4 of BV takes in input the DICOM format and therefore there is no need for conversion to the NifTi format. Consequently, some form of quality control is applied to the resting state fMRI data, by visually checking all the images. Therefore, the data preprocessing, which represents the first stage of data analysis, is performed. This procedure represents an essential step since its purpose is to prepare the resting state data for subsequent functional connectivity analysis, by reducing the influence of artifacts and other types of structured noise (Smith et al., 2017). Preprocessing of fMRI data varies substantially between different software packages, but there is a standard set of steps to be performed. ***Figure 4.1*** provides an overview of the various noise-reduction steps commonly used commonly in any fMRI study (Smith et al., 2017). It is also important to adopt the appropriate quality controls at each step to verify the effectiveness of the pre-processing procedure to prevent the error propagation (Smith et al., 2017).

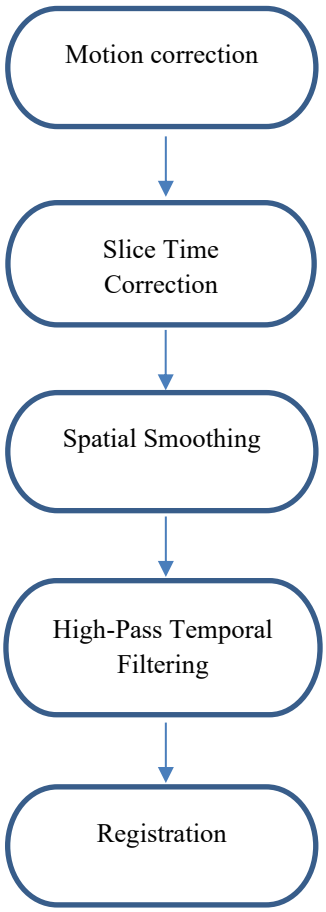

Figure 4.1 *Flowchart of the standard fMRI preprocessing stream.*

4.2.1 Brain Extraction

The first step is called Brain Extraction. It is performed on the T1-weighed structural image and consists in differentiating brain from non-brain tissue. By removing all non-brain tissue, the registration robustness is improved (Smith, 2002).

- ***BV***: to increase the accuracy of the results of co-registration and segmentation steps, the quality of anatomical dataset was improved by applying the intensity inhomogeneity correction procedure. It is an automatic method which consists of 4 different steps: background cleaning, brain extraction, white matter detection and bias field estimation within white matter voxels (Goebel et al., 2011).

4.2.2 Pre-statistical processing

Before to perform the pre-processing steps, the fMRI data need to be selected.

- ***BV***: by creating a new FMR project, the DICOM file were selected, and the number of volumes and slices were set. In this case the first 2 volumes have been deleted.

To reduce artifact and noise-related signal components, a series of operations is typically performed on raw functional data sets prior to statistical analysis. The most essential steps of these pre-processing operations are (www.brainvoyager.com):

- slice scan timing correction
- head motion detection and correction
- spatial and temporal smoothing

4.2.2.1 Motion Correction

The goal of motion correction (also known as *realignment*) is to reduce the misalignment between images in an fMRI time series that occurs due to head motion (Poldrack et al., 2011). The Motion Correction is an important issue in the analysis because even slight movements of the patient can induce large artifacts, potentially of greater intensity than the BOLD signal particularly at tissue boundaries, at the edge of the brain or near major vessels (Smith et al., 2004). Motion correction tools generally assume that head motion can be described using a rigid body transformation, which means that the position of the head can change (by translation or rotation along each of the three axes) but that the shape of the head cannot change. In brief, each image in the fMRI time series is aligned to a common reference scan using an image registration method, and the images are then resliced to create realigned versions of the original data (Poldrack et al., 2011). Subjects' head motion can result in a misalignment of successive slices leading to incorrect anatomical positions between voxels of subsequent images.

- ***BV***: in the "Analysis" menu select "FMR Data Preprocessing" and it was selected "3D motion correction". All the other values have been left by default (Formisano et al., 2005).

4.2.2.2 Slice Time Correction

Slice timing correction is a temporal correction procedure of the acquired volumes as the individual slices are recorded at different time instants.

The problem of different slice scanning times stems from the fact that a functional volume (e.g., whole brain) is usually not covered at once but with a series of successively measured 2D slices. To correct for different slice scan timings, the time series of individual slices are "shifted" in time to match a reference time point, e.g., the first or middle slice of a functional volume. This temporal shift depends on the order in which the individual slices of a volume are scanned. Slices can be acquired sequentially (ascending or descending order) or in an interleaved way (www.brainvoyager.com).

- ***BV***: in the "FMR Data Preprocessing" Slice scan time correction was selected, and the cubic spline was chosen as interpolation function, with ascending order.

4.2.2.3 Spatial Smoothing

The *Spatial Smoothing,* also called spatial filtering, is commonly applied in most fMRI studies and consists in calculating, at each voxel, a weighted average over multiple neighbouring voxels resulting in blurring of images (Bijsterbosch et al., 2017). This has the effect of a low-pass filter: high frequencies of the signal are removed from the data while prevailing the low frequencies information, typical of resting neural activity.

The result is that sharp "edges" of the images are blurred and spatial correlation within the data becomes more pronounced. Among the benefits associated with the application of spatial smoothing there is the improvement of the SNR. Although it represents an advantage, the application of the spatial smoothing has some drawbacks: it results in reduced spatial resolution of data and further along the edges of the brain, brain voxels are smoothed with non-brain voxels, resulting in a dark ring around the brain which might be mistaken for hypoactivity (***Figure 4.2***) (www.brainvoyager.com).

Figure 2 *The effect of the spatial smoothing on the image with different values. The higher the filter, the blurrier is the image (Bijsterbosch et al., 2017).*

The standard procedure of spatial smoothing is employed by performing the convolution of the fMRI signal with a three-dimensional Gaussian filter, or kernel, of a specific width. This Gaussian kernel has the shape of a normal distribution curve (Poldrack et al., 2011). The amount of smoothing imposed by a Gaussian kernel is determined by the width of the distribution. In statistics this is generally described in terms of the standard deviation, whereas in image processing the width of the distribution is described by the full width at half-maximum (or *FWHM*).

This measures the width of the distribution at the point where it is at half of its maximum; it is related to the standard deviation (σ) by the equation $FWHM = 2\sigma\sqrt{2ln\,(2)}$, or approximately $2.55 * \sigma$. The larger *FWHM*, the greater the smoothing (Poldrack et al., 2011). It is important to clarify that the *smoothness* of an image is not necessarily identical to the *smoothing* that has been applied to the image. Smoothness describes the correlations between neighbouring voxels. When smoothing is applied to an image, the smoothness of the resulting image is:

$$FWHM = \sqrt{FWHM_{intrinsic}^2 + FWHM_{applied}^2} \quad (2)$$

The amount of smoothing depends on the type of analysis that is being conducted. In general, it is recommended to use the minimum value to achieve a given result: it should be twice the voxel dimensions (Poldrack et al., 2011).

- ***BV***: in the FMR Data Preprocessing the Spatial smoothing option is selected with a FWHM = 5mm for the healthy subject. For the patient a double smoothing was selected with a FWHM=4 in the first step and then with a FWHM=8mm.

4.2.2.4 Temporal Filtering

The *Temporal Filtering* is used to remove the unwanted signal from the times series of each voxel without removing the desired signal. Most commonly, fMRI data are high-pass filtered, which means that the lowest frequencies are removed from the data. The amount of temporal filtering applied is expressed using a cutoff frequency (in Hertz) or a cutoff period (in seconds) and depends on the quality of the data. For high quality datasets it is possible to set higher cutoff frequency (0.001 Hz) to remove less and retain more data, while for lower quality datasets, lower cutoff frequency (0.01 Hz) is often used to remove more noise (Smith et al., 2017).

- ***BV***: to apply a high-pass filter during preprocessing of FMR projects, Temporal filtering must be enabled in the Preprocessing options field of the FMR Preprocessing dialog. The selected high-pass filtering method was the General Linear Model (GLM) with N° of cycles=7.

4.2.2.5 Registration

Both functional and structural images are in the native space, the original space in which they have been acquired. To perform group-level analysis it is necessary to register all subjects 'brains to a common 'standard' space, in a common coordinate system used to describe locations in the brain. The most common standard spaces are Talairach and MNI space (Smith et al., 2017). It is very important to remember that these three spaces (functional, structural and standard) usually are characterized by different image sizes and voxel dimensions: the brain region covered by a certain voxel in a space will not correspond to the same brain region in the other spaces (Smith et al., 2017). The collected anatomical and functional images generally do not match each other due to different MR contrasts and acquisitions, causing problems in mapping activity from functional data to the anatomical image (Glover et al., 2015). In fact, both functional and structural images, are acquired in the same imaging session but in different time windows. The problem of different slice scanning times stems from the fact that functional images represent a signal that changes over time; a functional volume (e.g. whole brain) is usually not covered at once but with a series of successively measured 2D slices (www.brainvoyager.com). To overcome this problem and match up spatial structures of the images, to calculate the transformations between different spaces, the registration step is necessary. Furthermore, the registration is essential to solve the group-level comparison issue.

Through this procedure is it possible to place into the standard space statistical images obtained from a subject-level analysis performed in functional space, to perform intra e inter subject analysis (Smith et al., 2017). In the current study the resting state functional images and a T1-weighted structural image were acquired in the same session. Since the human brain differs across subjects both in size and shape, to perform a group-level analysis across different subjects or different acquisition performed on the same subject, it is needed to align the functional and anatomical images of each subject with the standard space. Although it may seem reasonable to simply align the functional images directly to the template, in practice that doesn't work properly. The structural image in fact has a higher spatial resolution than the functional image and therefore less likely to match up with the anatomical details of the template. The anatomical image, i.e., a 2D or 3D anatomical image is a better candidate. To delimit and precisely recognize the regions of interest within the functional image, to interpret the results and understand in which brain region is active, it is necessary to perform the alignment between the functional and the T1-weighted structural image of the respective subject (Andy's Brain Book, 2019 GitHub).

The registration is a two-step process. The first step is called co-registration, in which the pre-processed functional image and the corresponding T1-weighted image are aligned. Through this procedure the information contained in the functional images can be superimposed on the structural one, where it is possible to discriminate between different anatomical brain regions. The second step is known as normalization, in which both functional and structural images are brought into a standardized space through the registration to a template. The goal of spatial normalization is to transform the brain images from each individual to reduce the variability between individuals and allow meaningful group analyses to be successfully performed (Poldrack et al., 2011). During the normalization step the brain images need to be aligned to an atlas, to make possible the comparison between different subjects. Transformations from one space (subject) to an atlas space provide localization of structural, functional, and physiological data into a well-understood template space (Mandal et al., 2012). The terms "brain atlas" and "brain template" have both been used commonly in the literature to date, although they may have different meanings in some situations (Dickie et al., 2017). In this study the term atlas and template have been used with different meanings. Individual brain scans from several individuals can be combined to form a brain image bank, which can in turn be used to form a brain atlas—an anatomical representation of the brain showing group-wise or study population global or regional brain features (Dickie et al., 2017).

An *atlas* provides a guide to the location of anatomical features in a coordinate space (Poldrack et al., 2011). They may be used in research as registration targets for functional activation, segmentation, and statistical mapping, for example in analysis of population imaging datasets (Dickie et al., 2017). A *template* is an image that is representative of the atlas and provides a target to which individual images can be aligned. A template can comprise an image from a single individual or an average of many individuals. Atlases are useful for localization of activation and interpretation of results; templates play a central role in the spatial normalization of MRI data (Poldrack et al., 2011).
The most used brain atlases and templates and their characteristic features of each brain template are presented below:

- the Talairach atlas, was published by Talairach and Tournoux in 1988. It was constructed from the single post-mortem brain of a 60-year-old French woman. This atlas has become one of the standard reference systems in human brain mapping. Talairach thought it was necessary to define a reference frame in which to place the different individuals. Therefore, he introduced a coordinate system, a "three-dimensional proportional grid", to identify and label different brain regions which was based on a set of anatomical landmarks: The anterior commissure (AC), and posterior commissure (PC), the midline sagittal plane, and the exterior boundaries of the brain at each edge. Given these landmarks, the origin (zero-point) in the three-dimensional space is defined as the point where the AC intersects the midline sagittal plane. In addition, the space has a *bounding box* that specifies the extent of the space in each dimension, which is defined by the most extreme portions of the brain in each direction (Poldrack et al., 2011).

- the MNI templates are the most common templates within the fMRI literature used for spatial normalization, developed at the Montreal Neurological Institute. These templates were created to provide an MRI-based template that would allow automated registration rather than landmark-based registration (Poldrack et al., 2011). The most famous is the MNI-152 template created in 2001 from 3D brain MRI images of 152 normal subjects. To construct the MNI-152 brain template, automated image registration (AIR) algorithms were used to align brain MRI images with the reference brain image. The brain MRI images were linearly registered to the target image (using a 9-parameter affine transformation) followed by a non-linear registration to overcome the inter-subject anatomical differences in shape, size, and relative orientation

(Mandal et al., 2012). The steps carried out during the registration phase in the BV software are shown below.

Registration from functional space to standard space is a two-step process.

- ***BV***: in the first step the co-registration of functional images (FMR) and the structural image (VMR) is performed. By opening the "3D Volume Tools" in the co-registration section, the pre-processed functional file was selected and aligned with the structural file, by running both the Initial Alignment and Fine-Tuning Alignment. The second step is the normalization. The structural data are registered into Talairach space by using the manual transformation in which landmark points need to be identified. First, the AC was identified, then the PC and the AC-PC plane, and finally the other points, such as AP (the most anterior point of the cerebrum), PP (the most posterior point), SP (the superior point), IP (the inferior point), RP (the rightest point) and LP (the most left point) (Goebel et al., 2011).

4.2.2.5.1 Drawbacks of the Talairach and Tournoux atlas

Although it played a fundamental role in the development of neuroimaging, the Talairach and Tournoux atlas and the coordinate space associated with it are characterised by some problems (Poldrack et al., 2011):

- The brain used by Talairach and Tournoux was relatively smaller and furthermore, this atlas is based on a single subject. It was created from a postmortem brain of a 60-year-old woman, and therefore is not representative of either the population as a whole nor any individuals (Poldrack et al., 2011).
- The slice thickness was large (2–5 mm), and almost fifteen slices were left unaccounted in the creation of the atlas. This generated wide gaps in the atlas and hence, did not reflect the complete neuro-anatomical features (Mandal et al., 2012).
- The atlas is based on a single left hemisphere that was reflected to model the other hemisphere. However, there are well-known hemispheric asymmetries in normal individuals (e.g., location of Heschl's gyrus, length of precentral gyrus), such that assuming symmetry across hemispheres will result in additional inaccuracy (Poldrack et al., 2011).
- No 3D image of the original brain was used for atlas construction and consequently, an accurate template cannot be created (Poldracket al., 2011). According to this, the

normalization to the template requires the identification of anatomical landmarks that are then used to guide the procedure (Poldrack et al., 2011). These anatomical locations can only be identified by comparing the Talairach and Tournoux brain atlas with the Brodmann map (Mandal et al., 2012).

4.3 Independent Component Analysis

Functional connectivity refers to correlations between activity in spatially remote brain regions, which can arise for several reasons (Poldrack et al., 2011). Numerous methodologies have been developed to study functional connectivity such as data-driven methods, which are very useful for resting-state fMRI studies where no prior information about the spatial or temporal pattern is known. Among them many are based on decomposition techniques (Kaiming et al., 2009). There are several ways to decompose a matrix into separate components, which can be used to identify coherently active networks from fMRI data. These methods assumes that the data are composed of several underlying components mixed together to form the observed data. One of best-known methods for matrix decomposition is the Independent Component Analysis. Independent components analysis was developed to allow the detection of unknown signals in a dataset, sometimes called the *blind source separation* problem (Poldrack et al., 2011). It has proven to be a successful technique for detecting consistent spatial components and separating signal from noise. ICA decomposes the 4D (space X time) data into multiple components, each described by a single 3D spatial map and an associated time course. Ideally, some components purely reflect BOLD signal, and others purely reflect artefactual processes (Griffanti et al., 2014). Once a set of artefactual components is identified, those components can be removed from the data, creating a "denoised" dataset. Several approaches have been proposed for the automatic classification of the independent components (ICs) as signal or noise (Griffanti et al., 2014)**,** which may provide more reliable identification of artifact-related components than manual classification (Poldrack et al., 2011). Identification of artefactual component by hand has some drawbacks, in that is it time consuming, operator dependent and requires expert knowledge about signal and noise fluctuations' spatial and temporal characteristics (Griffanti et al., 2014).

Formally, the ICA model is defined as:

$$x=As \tag{3}$$

where **x** is the signal that we are trying to decompose, **s** is a set of unknown sources (or *components*), and **A** is the unknown *mixing matrix* that combines the components to obtain the observed signal (Poldrack et al., 2011).

Because both **A** and **s** are both unknown, some assumptions must be done about the relation between the different components in **s** (Poldrack et al., 2011).

Fundamental assumptions on ICA:

- Source signals are statistically independent.
- Independent components are not Gaussian.

The entire 4-dimensional data set containing the observed BOLD signal is rearranged into a 2-dimensional matrix by arranging all voxels for each timepoint into a single row (i.e., one row per 3D functional image). This data set is then decomposed into two new matrices, the first one containing a time course of an underlying signal in each column and the second matrix containing a spatial component's map in each row (***Figure 4.3***). Thus, spatial independent component analysis can be viewed as a way of finding *temporal* basis vectors so that the associated spatial maps are sparse and statistically independent (Beckmann et al., 2012).

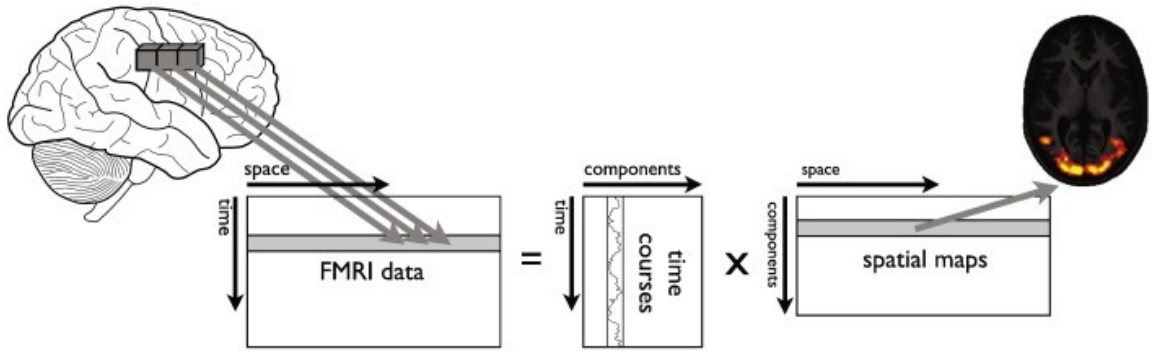

Figure 4.3 *Schematic illustration of the data representation and the spatial decomposition performed by spatial ICA on FMRI data (Beckmann et al., 2012).*

4.3.1 Independent Component Analysis on Brain Voyager

ICA is a data-driven method to analyse fMRI data. For fMRI data, spatial ICA (sICA) is normally applied as opposed to temporal ICA. There are different ICA algorithms to estimate a set of spatial components. In BV, the spatial decomposition of the data is performed using "FastICA". It consists of a fixed-point ICA which minimizes the mutual information of the components using a robust approximation of the negentropy as a contrast function and a fast, iterative algorithm for its maximization. (Formisano et al., 2004). There are two ways to run FastICA, the deflation approach and the symmetric approach. Usually, the deflation approach is recommended and used as default. For what concerns the nonlinearity function the Gaussian option was set, and the number of components was left by default equal to 30. Before applying spatial ICA, the temporal dimension of the data set may be optionally reduced using Principal Component Analysis (PCA). In this way it is possible to limit the ICA decomposition of a functional data to the selected voxels, within a specified region with respect to the cortical sheet (Formisano et al., 2004).
This restriction to the relevant voxels not only reduces calculation time substantially but also improves the resulting decomposition by "focusing" the ICA to the relevant voxel time courses. The restriction is implemented by applying a cortical mask file to the volume time course (VTC) data, which can be derived easily after standard cortex segmentation procedures. The spatial ICA restricted to cortical voxels is indicated with the term *cortex-based ICA* or *cbICA* (Formisano et al., 2004). After the creation of a functional project the fMRI data were pre-processed to improve data quality. Besides this, it is also necessary to put the data into a normalized 3D space called VTC files. The files from a single subject are usually linked to the subject's normalized anatomical VMR data set creating VMR-VTC projects. At the end of these procedures ICA can be performed on a group of subjects, thus making it possible to compare the ICs across subjects.

- ***BV***: to run FastICa the deflation approach and Gaussian option as Nonlinearity function were used. The number of components was by default kept 30. The input file to perform the spatial ICA is a VTC (volume time course) data set. The threshold value was 10 and Z>2.

4.3.2 Hand Classification of signal and noise independent components

Spatial ICA has proven to be a powerful tool for blind source separation of fMRI data into 3D spatial maps and 1D time courses. ICA is a very good procedure in the context of artifact removal, also called 'data denoising' or 'data cleanup', since it can separate neural-related signal from different sources of noise (Griffanti et al., 2017). In fact, fMRI data contain two kinds of noises: structured and stochastic; in the context of ICA-based denoising the term noise refers to the structured one, since ICA decomposition aims to un-mixing data into non-Gaussian sources. ICA produces many different spatiotemporal components, such as noise independent components (N-ICs), i.e., the components characterized by a noise/artefact signal, and the neural signals independent components (S-ICs), which represent the signals of interest (Griffanti et al., 2017). The information represented in the ICA decomposition is used to recognize and separate the N-ICs by the neural signals. Independently from the denoising method adopted, the biggest challenge remains the identification of the N-ICs. Several approaches have been proposed to achieve this aim, exploiting the fact that signal components S-ICs and N-IC differ in terms of spatial, temporal and spectral characteristics (Griffanti et al., 2017). Many of these approaches are fully automated, especially when dealing with a large population. Beside this, the gold standard for component classification remains the visual inspection of the components, particularly useful in case of small sample size or unusual characteristics of the dataset. On the other hand, manual labelling is time consuming and requires expertise (Griffanti et al., 2017).

For the classification of the signal and noise components it is necessary to have the following three complementary information: the IC spatial map, its time series and its power spectral density.

- Spatial map, characterised by the presence of clusters which, depending on their number and size, suggest the presence of signal or noise components. The localisation of clusters in the grey matter suggests the neural-related origin of the component, while clusters mainly located in the white matter, cerebrospinal fluid and blood vessels are usually related to physiological noise (respiration, pulsation). The presence of clusters near brain edges suggests the presence of motion-related artefact (Griffanti et al., 2017).
- Time series, which checks the overall aspect, if there are one or more sudden peaks or if it shows a saw-tooth pattern (sharply and regularly alternating up-and-down time course) (Robert et al., 2010; Griffanti et al., 2017).

- Power spectrum, which checks the distribution of power in the frequency domain. Depending on where the distribution of power occurs, in low or high frequencies, is it possible to discriminate the signal of interest from the noise (Griffanti et al., 2017).

The main features that can be visually evaluated during the classification are listed in ***Table 5.***

Table 5 *Features of signal and noise-related independent components (Griffanti et al., 2017).*

Features	***S-IC characteristic***	***N-IC characteristic***
	Spatial	
Number and dimension of clusters	Low number of large clusters	Large number of small clusters
Overlap with GM	Clusters' peaks in GM and overall good overlap of the clusters with GM.	Indiscriminate overlap with non-GM tissues, or clusters' peaks in WM/CSF
Overlap with WM, CSF, blood vessels	Very low or absent overlap with WM, CSF, blood vessels	High overlap with one or more of WM, CSF, blood vessels
Overlap with brain boundaries or areas close to the edges of the FOV.	Very low or absent overlap with brain boundaries. Clusters follow known anatomical (e.g., structural/ histological) boundaries.	Ring-like or crescent shape or stripes near the edges of the field-of-view
Location near area of susceptibility induced signal loss (e.g., orbitofrontal)	Generally located away from these areas	Located within the region of signal loss (e.g., areas of air-tissue interface)
Non-biological, acquisition-related patterns	Patterns have no relation to acquisition parameters	Often show banding patterns in slice direction or streaks along the phase encoding direction, accelerated sequences may have centrally located artefacts
	Temporal (and spectral) features	
Overall aspect of the time series	Fairly regular/oscillatory time course	Large jumps and/or sudden change of oscillation pattern.
Distribution of power in frequency domain	Predominantly low frequency (at least one strong peak within 0.01 – 0.1 Hz)	Predominantly high frequency, very low frequency, or pan frequency
Legend: GM = grey matter; WM = white matter; CSF = cerebrospinal fluid.		

4.4 Diffusion Tensor Imaging Analysis

The diffusion tensor is estimated based on the raw diffusion measurements and the associated direction information provided from the gradient directions and b values table. The estimation process results in three eigenvectors and associated eigenvalues specifying an ellipsoid characterizing the direction of diffusion and the amount of anisotropy in the respective voxel. After having calculated the diffusion tensor at each voxel, the MD and the FA diffusion maps can be calculated. The main assumption of DTI is that diffusion is predominant along the major axis of fibre bundles than in other directions, therefore it may be used to detect the direction of white matter fibre tracts running through a voxel. For the final visualization of the fibre bundles, the eigenvector orientations in neighbouring voxels must be connected in a proper way. This connecting process is called "fibre tracking" and was performed through a probabilistic approach.

Probabilistic fibre tracking measures the probability that a seed region is connected to a second region. This technique has the advantage that individual connectivity probability maps can be compared between subjects, enabling a statistical group analysis. However, probabilistic fibre tracking does not directly measure the true structural connections between brain regions, but rather the probability that two regions are connected (van Den Heuvel et al., 2009). All the steps performed in the analysis are explained in the Appendix C.

Chapter 5 Results

All the results obtained from the analysis described in the ***Chapter 4*** are reported. Firstly, the results of the motion correction and registration steps are examined, to verify that the procedures have been correctly performed. If the requirements are satisfied, it is possible to proceed with the inspection and classification of ICs. After the recognition and separation of N-ICs from the S-ICs, the RSNs were detected through a comparison with the RSNs identified by Smith and coworkers (Smith et al., 2009).

5.1 Functional pre-processing results

As described in ***Chapter 4***, to reduce artifact and noise-related signal components, a series of operations is typically performed on raw functional data sets prior to statistical analysis. In ***Figure 5.1*** and ***Figure 5.2*** the results obtained by the Motion Correction step are reported. Motion correction tools generally assume that head motion can be described using a rigid body transformation, in which the head movement is described by translations or rotations along each of the three axes. The following figures represent the head movement of the subject and patient respectively. From the ***Figure 5.1*** it is possible to notice that the movement of the S1 is very low. The ***Figure 5.2***, instead, shows a significant rotation around x-axis (yellow) and around z-axis (cyan), but without relevant and sudden peaks. The x-axis indicates the volumes and the y-axis the entity of movement expressed in mm.

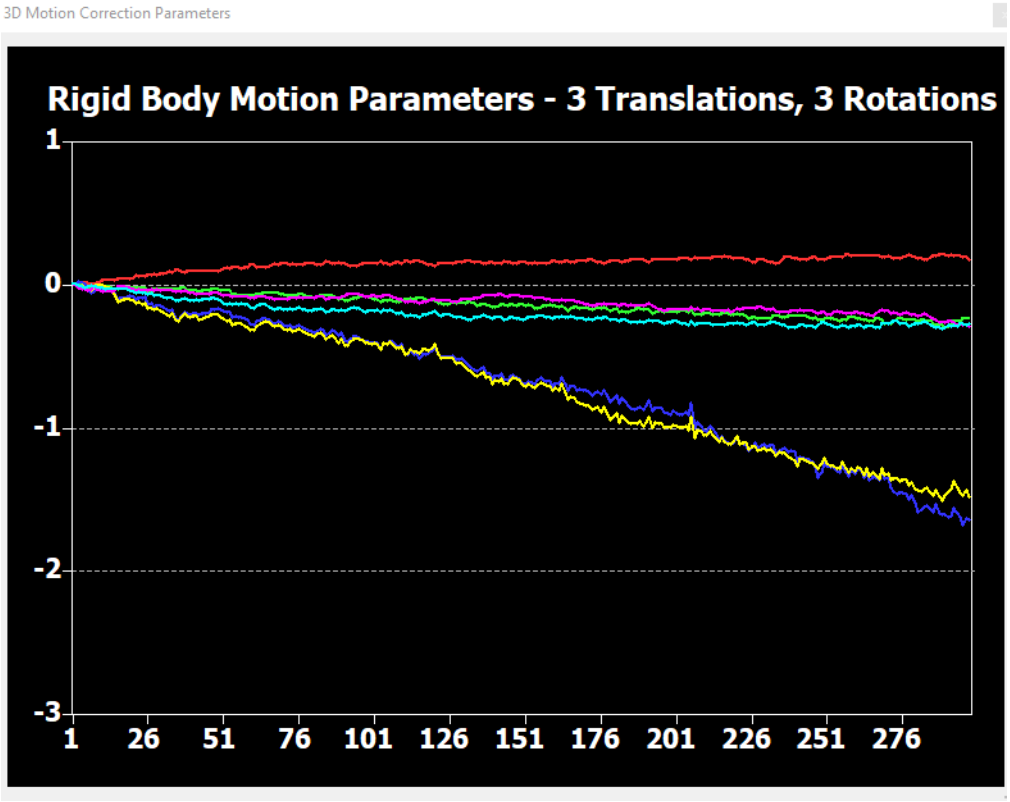

Figure 5.1 *Displacement detected in subject S1. The panel indicates the rotation movement around the axes and the translation movement along the axes.*

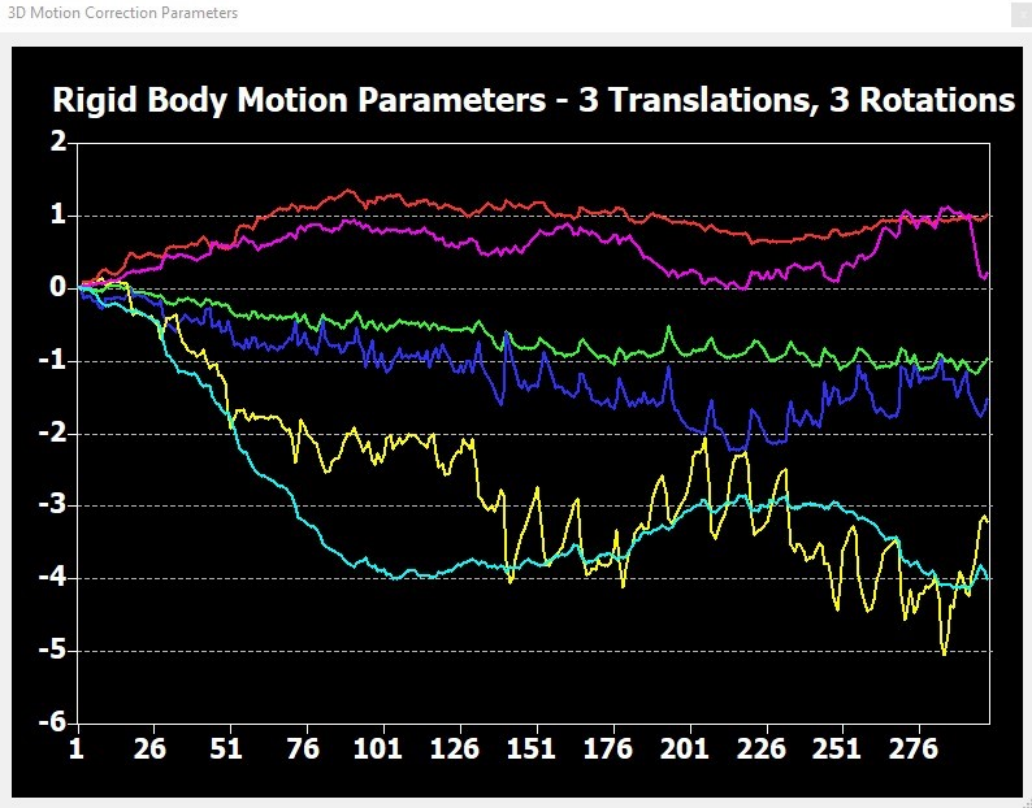

Figure 5.2 *The displacement detected in patient P2. The panel indicates the rotation movement around the axes and the translation movement along the axes.*

Successively, the inspection of the results derived from the registration step is performed. The registration was successful for both subject S1 and patient P2. The registration is a two-step process. In the co-registration, the pre-processed functional image and the corresponding T1-weighted image are aligned. In the second one, known as normalization, both functional and structural images are brought into a standardized space through the registration to a template. ***Figure 5.3*** shows the results obtained from the co-registration step, ***Figure 5.4*** depicts the transformation of structural and functional images to the Talairach space.

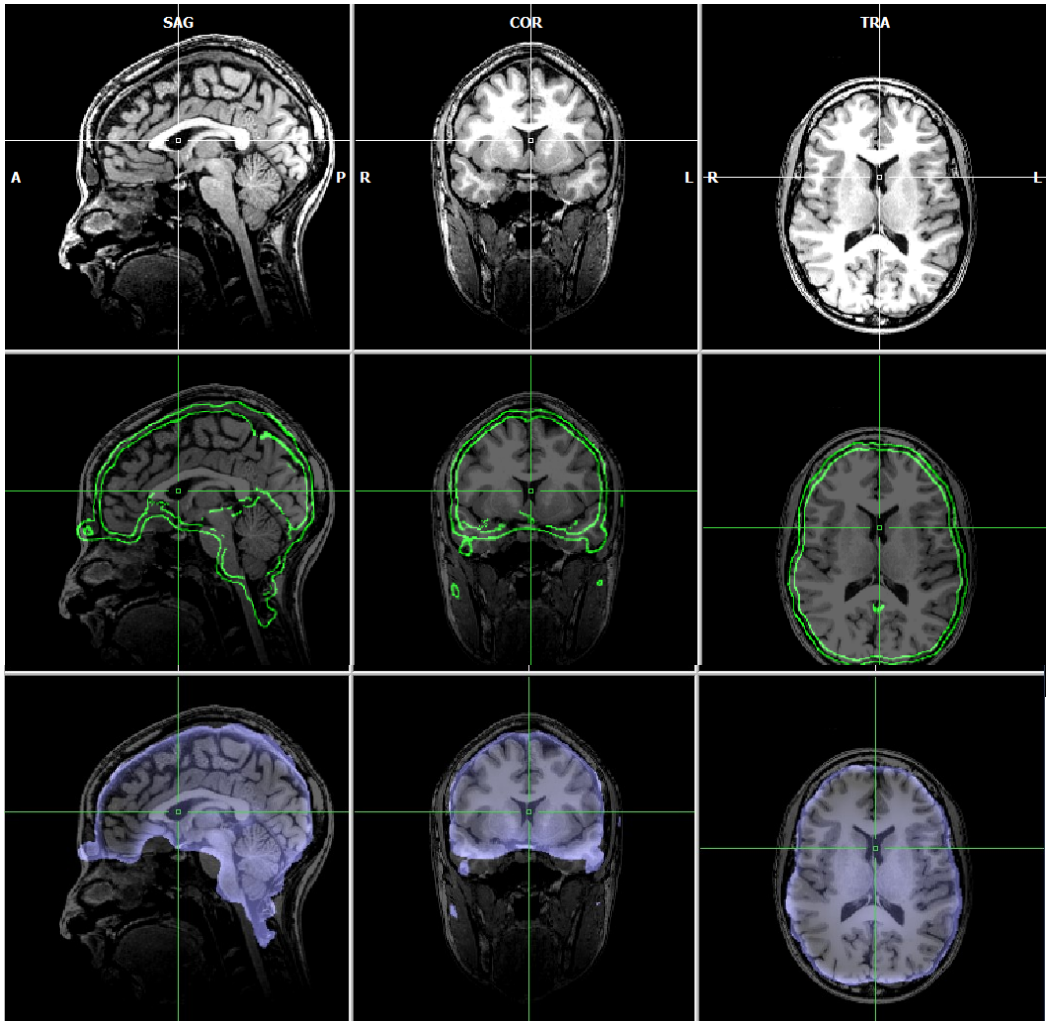

Figure 5.3 *The top panel represents the structural ISO image of the subject S1. The middle and bottom panel represent the co-registration between the functional pre-processed file and structural ISO image, visualised with the Edges Option (middle panel) and Transparent Option (bottom panel).*

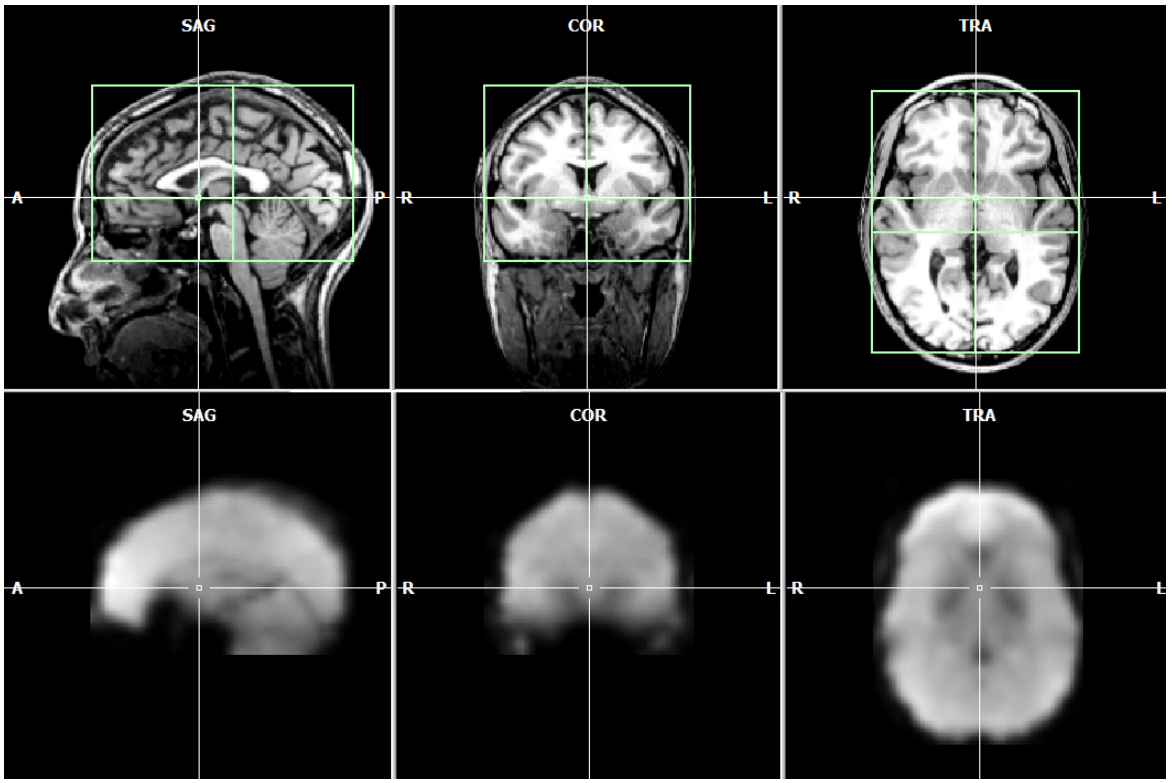

Figure 5.4 *The top panel represents the structural ISO image of the subject S1 in Talairach space (green lines). The bottom panel represents the normalization of functional image (in grey) in the Talairach space.*

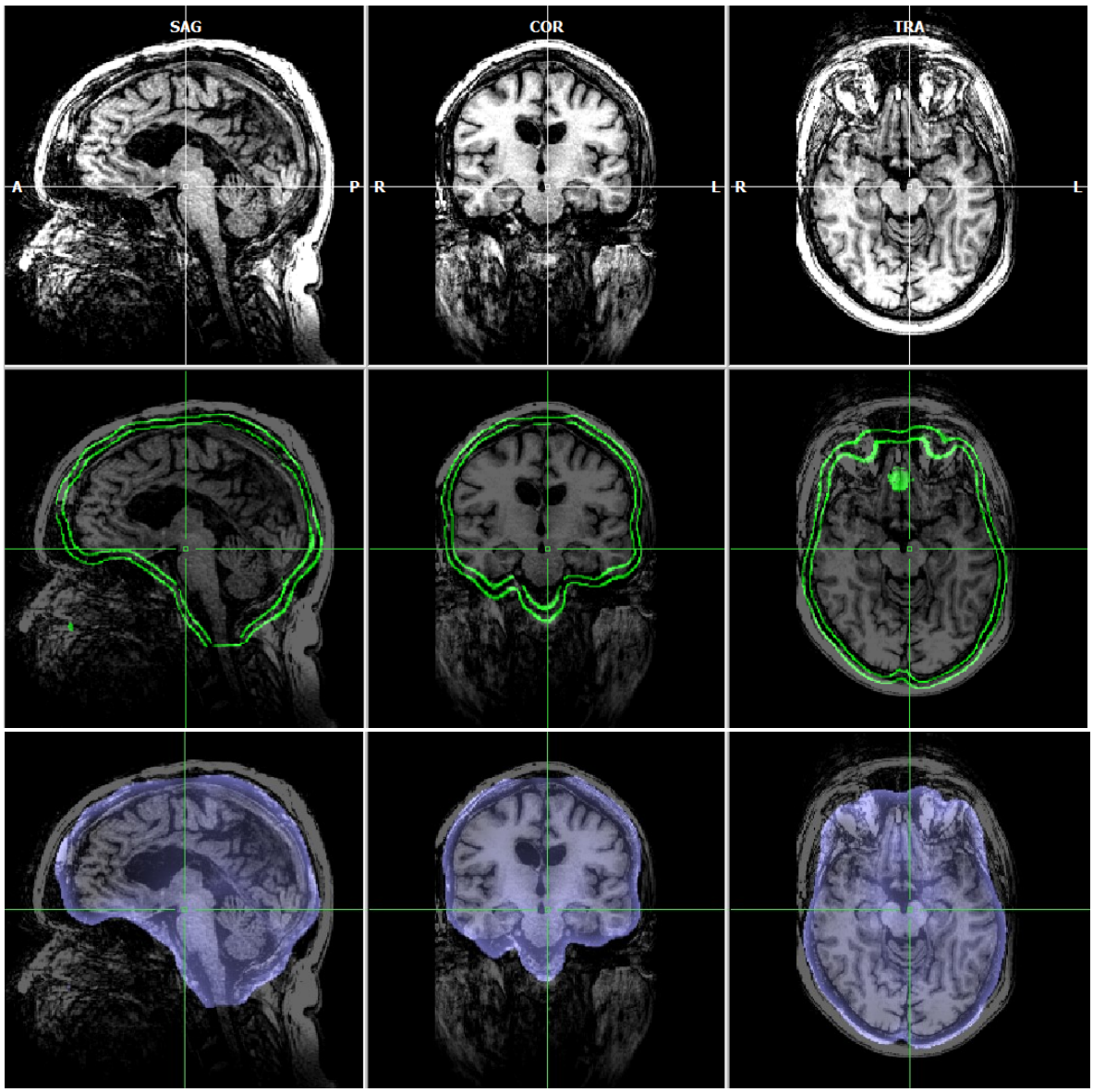

Figure 5.5 *The top panel represents the structural ISO image of the patient P2. The middle and bottom panel represent the co-registration between the functional pre-processed file and structural ISO image, visualised with the Edges Option (middle panel) and Transparent Option (bottom panel).*

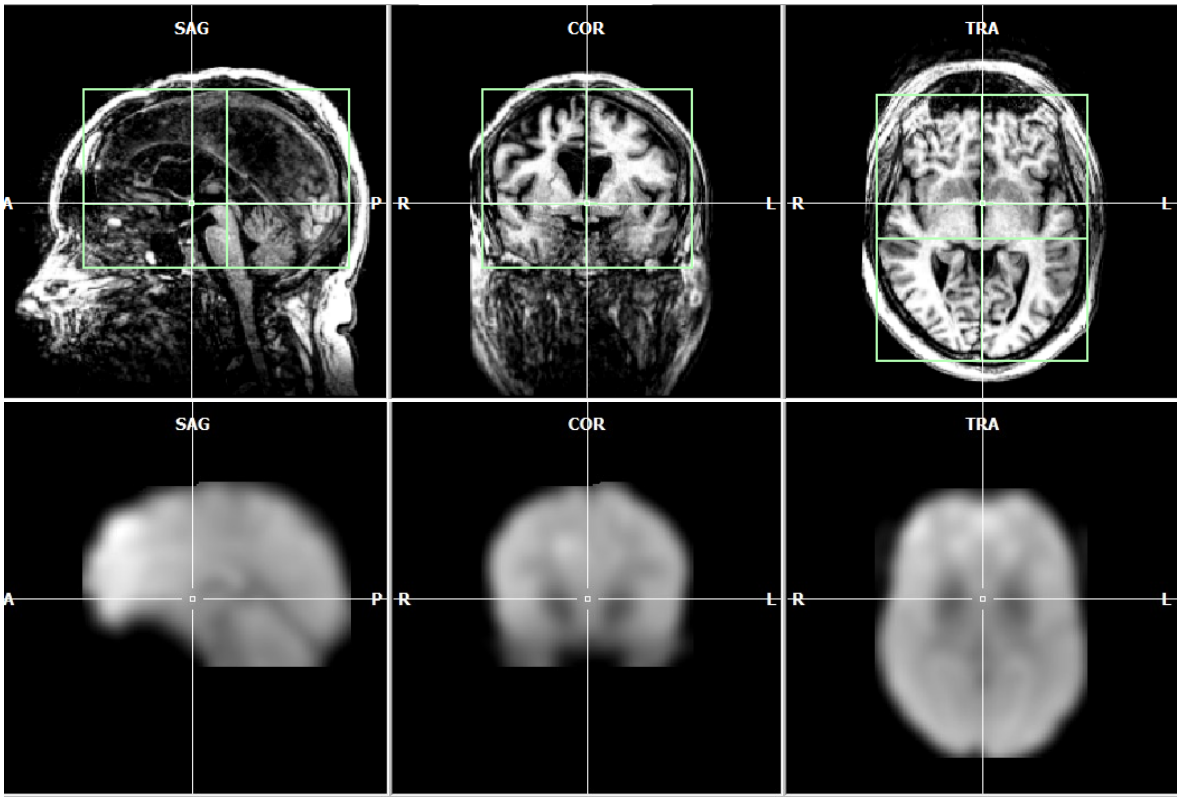

Figure 5.6 *The top panel represents the structural ISO image of the patient P2 in Talairach space (green lines). The bottom panel represents the normalization of functional image (in grey) in the Talairach space.*

5.2 Independent Component Analysis on BrainVoyager

The ICs estimated within BV software were 60 in total: 30 for the subject and 30 for the patient. According to the labelling rules defined by Griffanti and coworkers (Griffanti et al., 2017), the spatial map and the time series of each component were examined to be subsequently classified as signal (S-IC) or noise (N-IC). ***Figure 5.7*** and ***Figure 5.8*** show respectively a N-IC and a S-IC. In both figures the ortho view (top panel) and the time series (bottom panel) are shown. The functional activations are superimposed on the structural image of the subject and the patient, transformed in Talairach space.

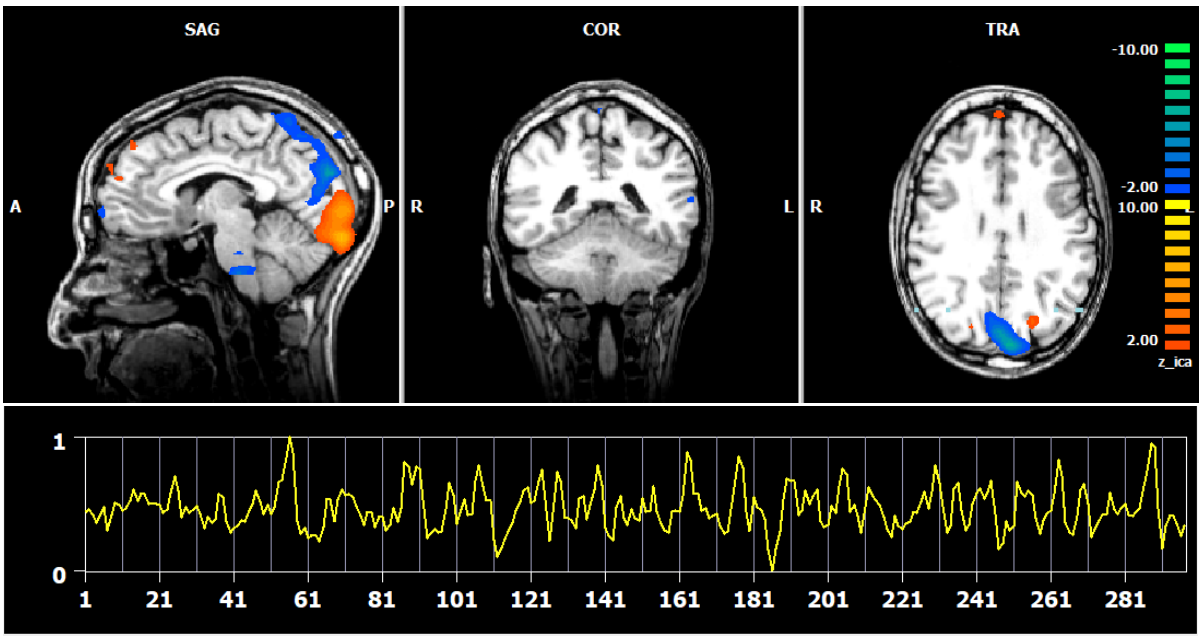

Figure 5.7 *An example of signal component identified on the subject S1data (IC 19). The clusters in the spatial map are in the grey matter (top panel). The time series shows a typical saw-tooth pattern (bottom panel). The positive activations are shown in red, the negatives in blue.*

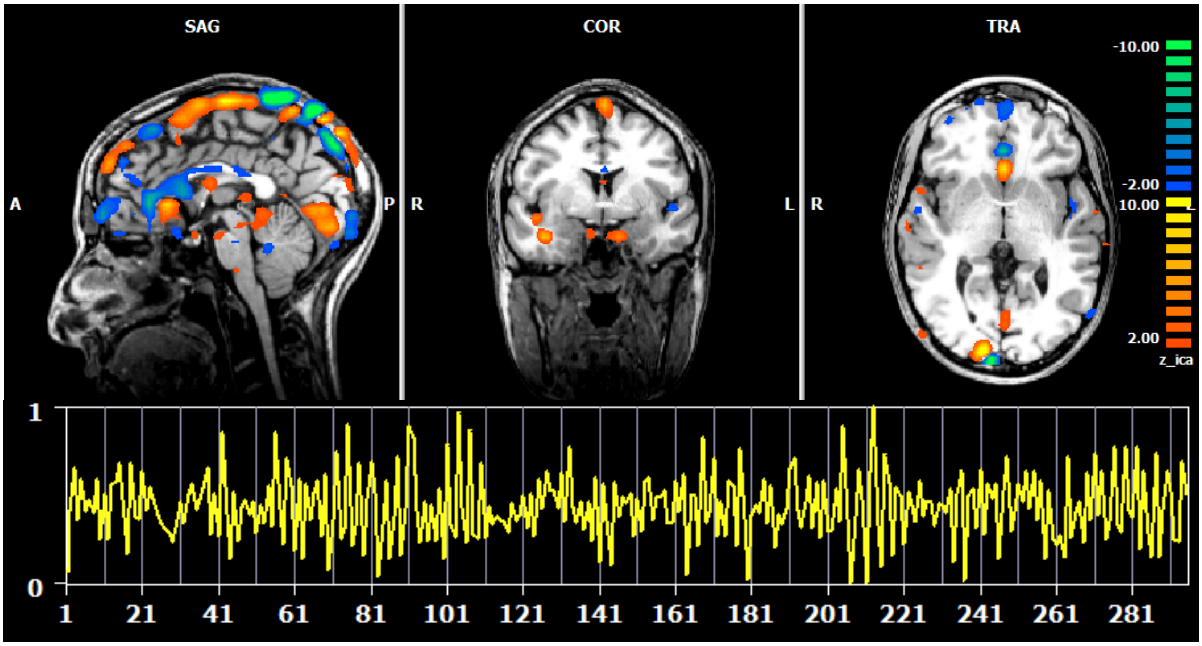

Figure 5.8 *An example of artefact component identified on the subject S1data (IC 18). In the spatial map the clusters are localised in the white matter (top panel). The time series shows a high oscillation. The positive activations are shown in red, the negatives in blue.*

The S-ICs obtained are visually inspected to identify those corresponding to well-established RSNs, according to the study of Smith (Smith et al., 2009). The images are shown in radiological convention and each network is shown in the sagittal, coronal, and axial view. In ***Figure 5.9*** and ***Figure 5.10*** are reported the resting state networks identified in healthy subject S1.

From the analysis performed on subject S1 and on patient P2 the following networks were identified (***Table 6***).

Table 6 *RSNs identified in the subject S1 and patient P2 by using BrainVoyager software.*

Resting State Network	**S1**	**P2**
Medial Visual Area	✓	✓
Occipital Visual Area	✓	✓
Lateral Visual Area		
Default Mode Network	✓	✓
Sensorymotor System		✓
Auditory System		
Executive Control	✓	✓
Frontoparietal Right	✓	
Frontoparietal Left		✓
Cerebellum Area	✓	

DEFAULT MODE NETWORK

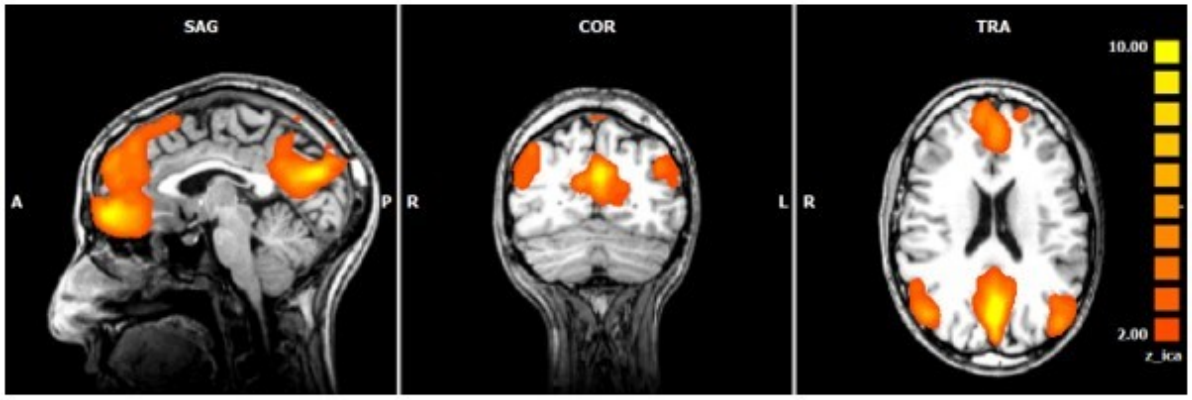

OCCIPITAL VISUAL AREA

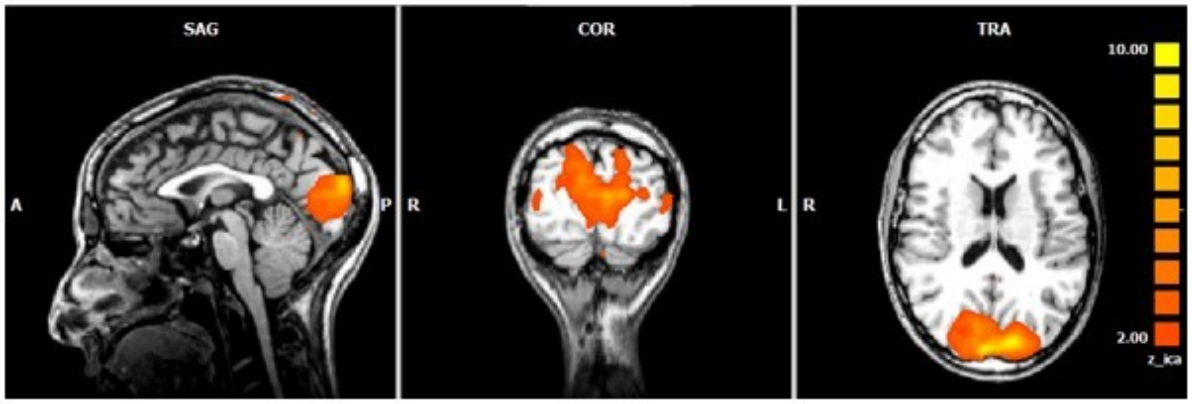

MEDIAL VISUAL AREA

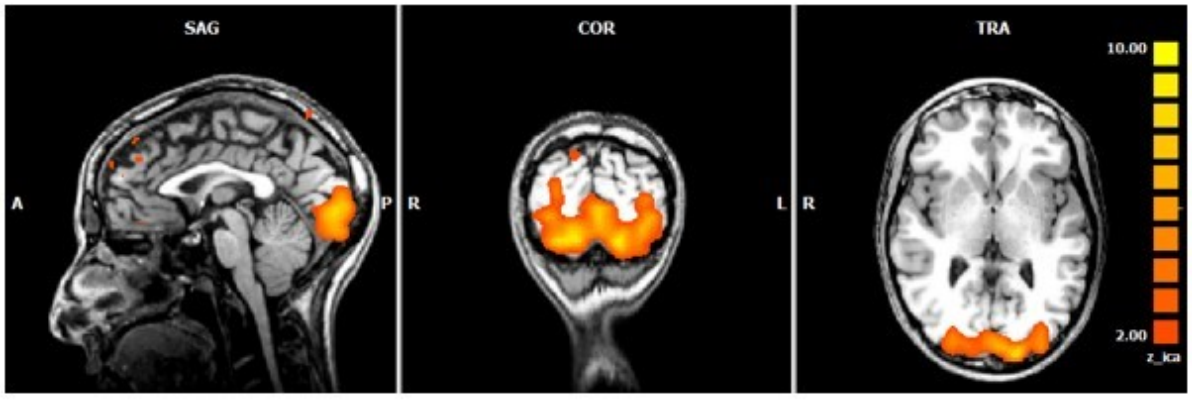

Figure 5.9 *Resting state networks identified in healthy subject S1. In the top panel is illustrated the Default Mode Network, in the middle panel the Occipital Visual Area and in the bottom one the Medial Visual Area.*

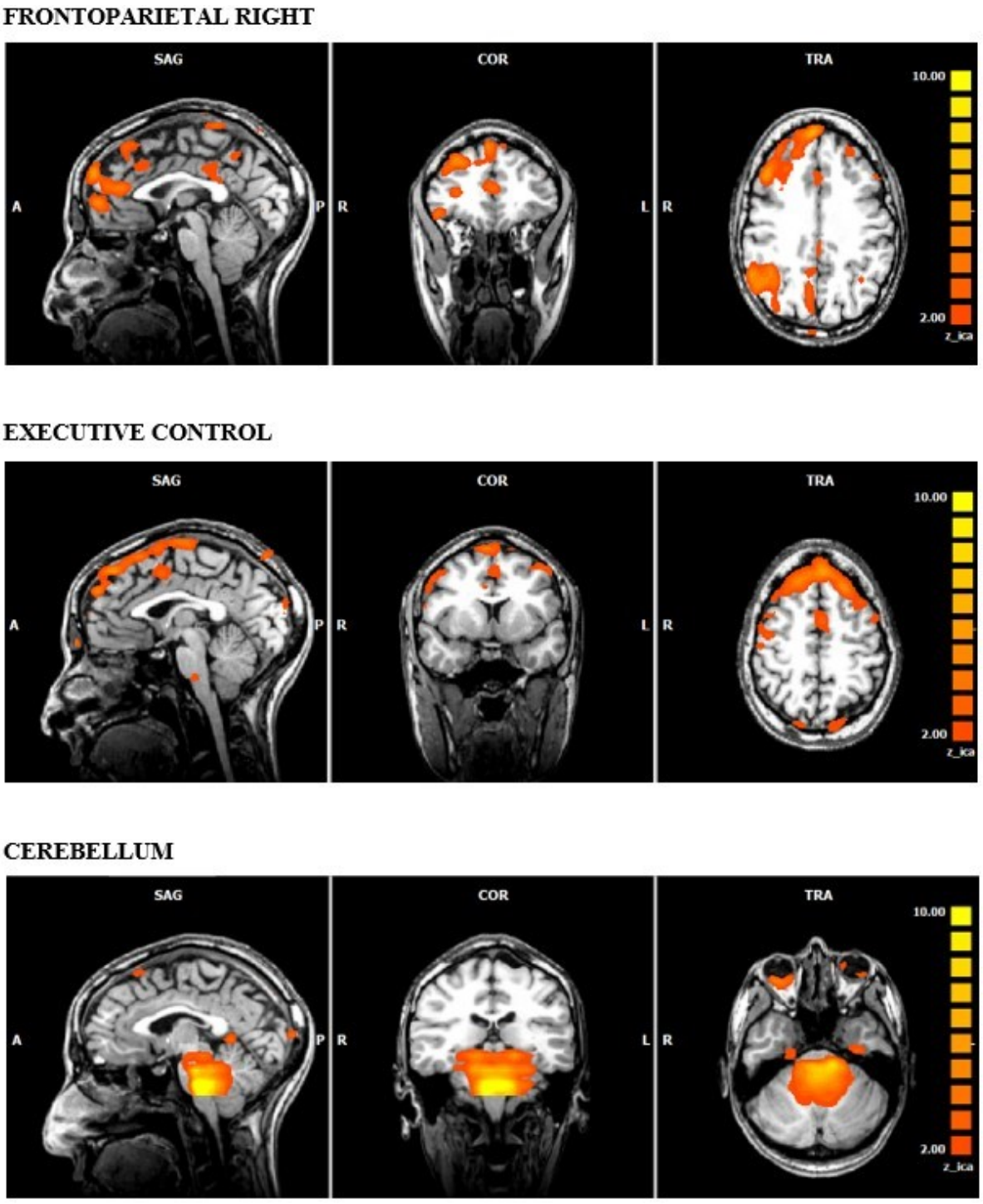

Figure 5.10 *Resting state networks identified in healthy subject S1. In the top panel is illustrated the Frontoparietal Right, in the middle panel the Executive Control and in the bottom one the Cerebellum.*

In ***Figure 5.11*** and ***Figure 5.12*** are reported the resting state networks identified in patient P2.

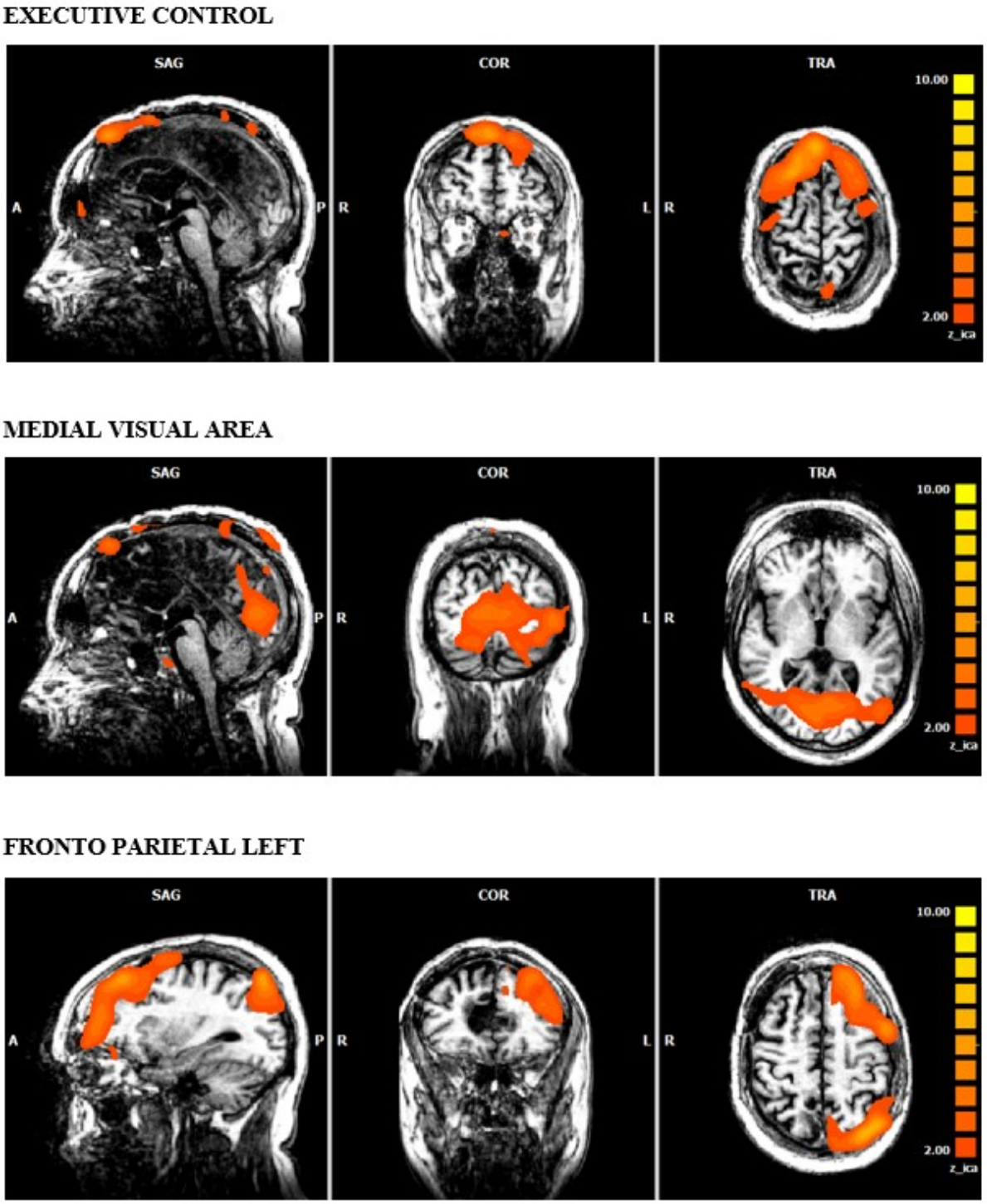

Figure 5.11 *Resting state networks identified in patient P2. In the top panel is illustrated the Executive Control, in the middle panel the Medial Visual Area and in the bottom one the Frontoparietal Left*

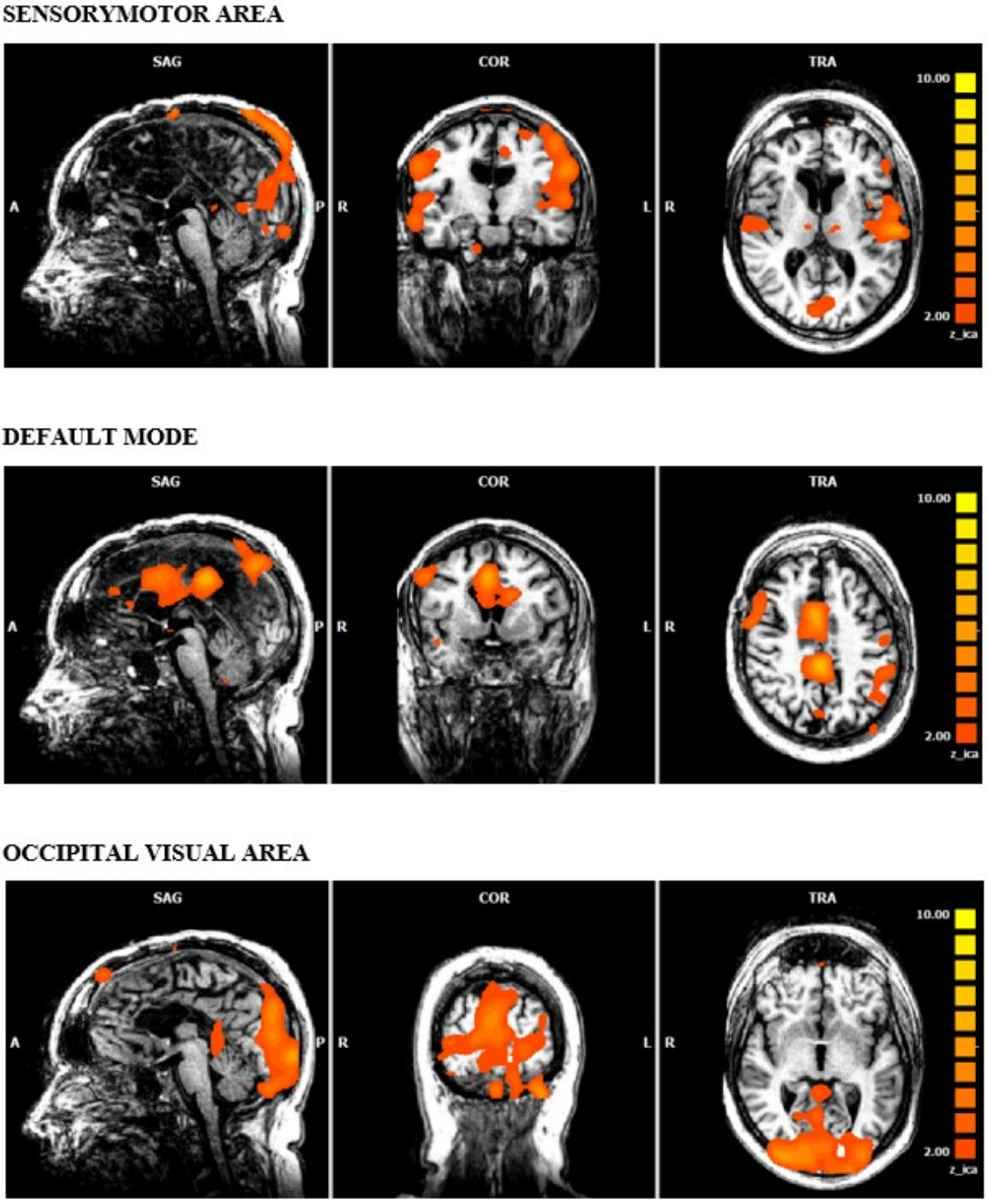

Figure 5.12 *Resting state networks identified in patient P2. In the top panel is illustrated the Sensorymotor Area, in the middle panel the Default Mode Network and in the bottom one the Occipital Visual Area.*

5.3 Diffusion Tensor Imaging pre-processing results

In ***Figure 5.13*** the results obtained from the co-registration between the structural and the diffusion weighted image of the subject S1 are shown.

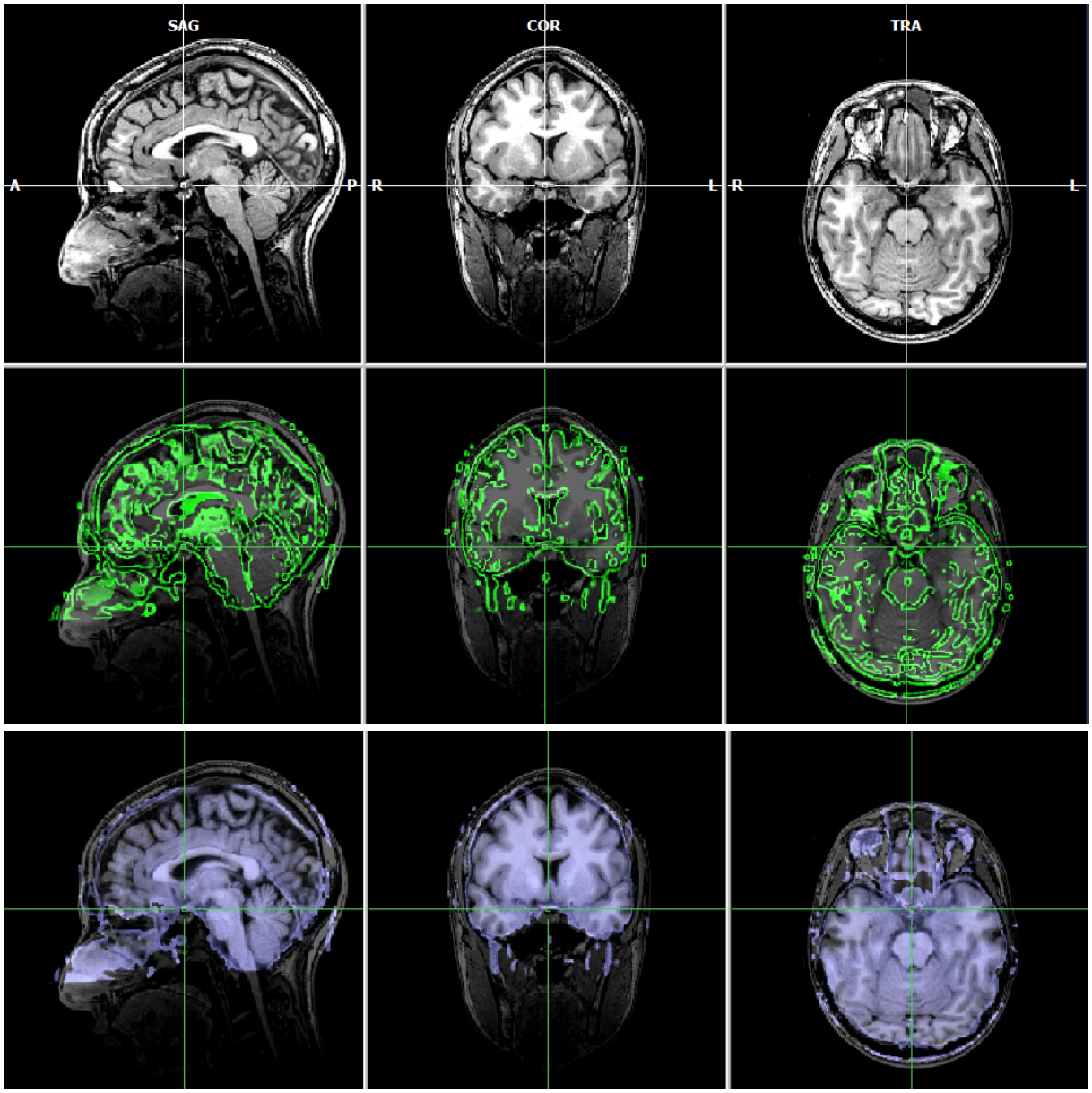

Figure 5.13 *The top panel represents the structural ISO image of the subject S1. The middle and bottom panel represent the co-registration between diffusion weighted image and structural ISO image, visualised with the Edges Option (middle panel) and Transparent Option (bottom panel).*

Figure 5.14 illustrates the results obtained from the co-registration between the structural and the diffusion weighted image of the patient P2.

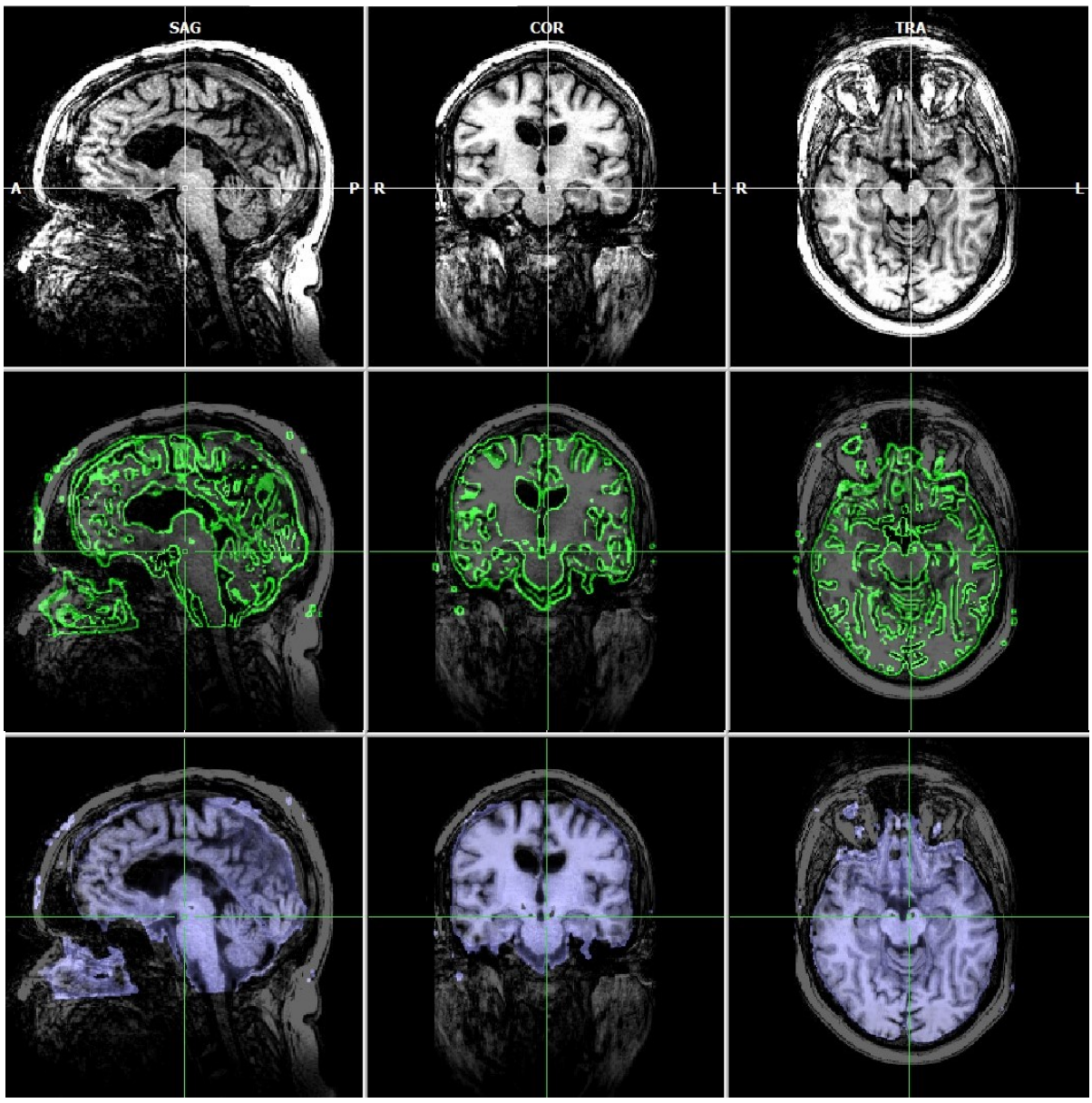

Figure 5.14 *The top panel represents the structural ISO image of the patient P2. The middle and bottom panel represent the co-registration between diffusion weighted image and structural ISO image, visualised with the Edges Option (middle panel) and Transparent Option (bottom panel).*

Figure 5.15 illustrates the Color Direction Map according to the RGB coding.

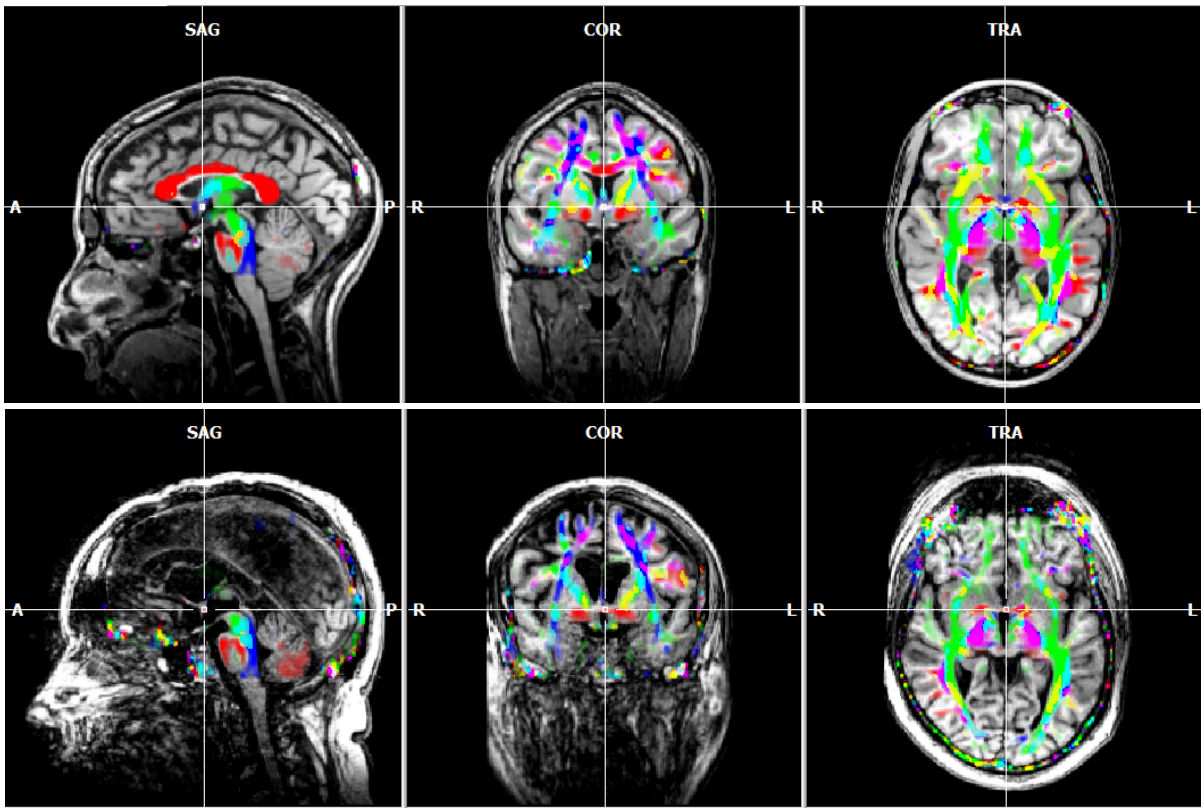

Figure 5.15 *Visualisation of the Color Direction Map of the subject S1 (top panel) and of the patient P2 (bottom panel) according to the RGB coding.*

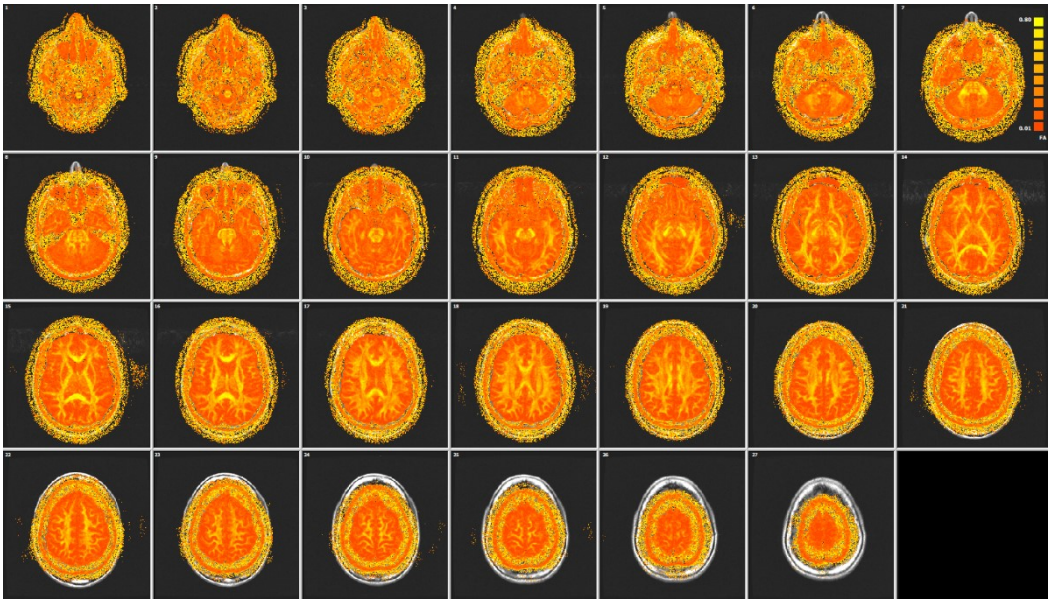

Figure 5.16 *Visualisation of the FA map of the subject S1. On the top right is it possible to visualize the range of values of the FA: higher values (yellow) in white matter and lower (orange) in grey matter.*

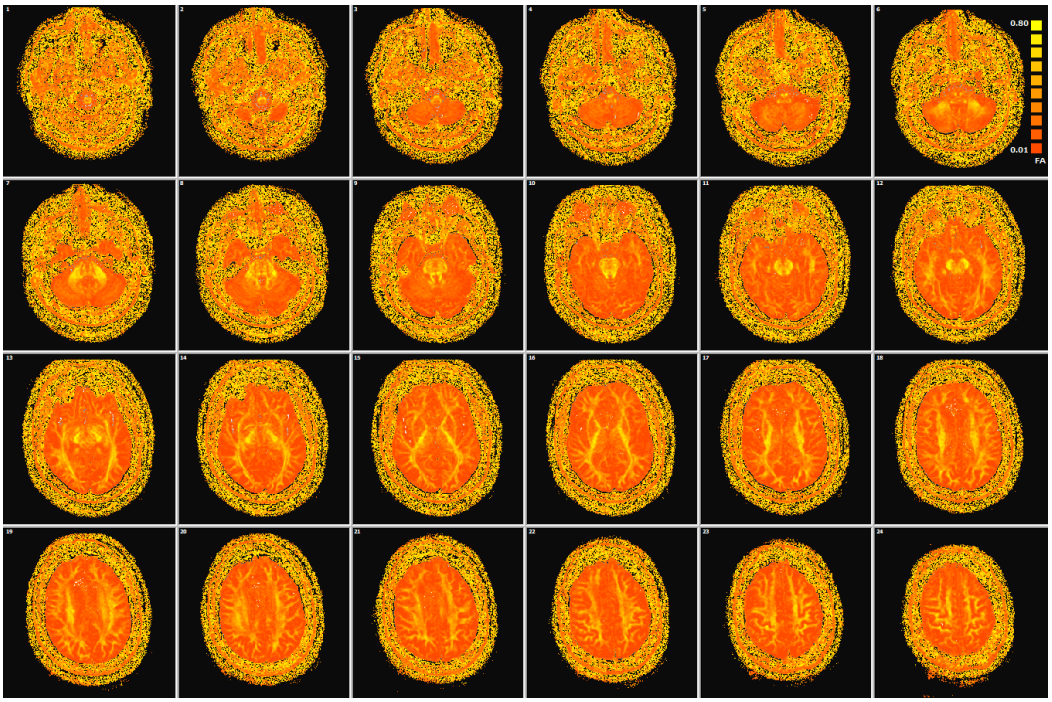

Figure 5.17 *Visualization of the FA map of the patient P2. On the top right is it possible to visualize the range of values of the FA: in this case the areas with higher FA values are less than those of the subject S1.*

The results obtained from the tractography, performed on the three networks identified in the healthy subject S1, are reported below.

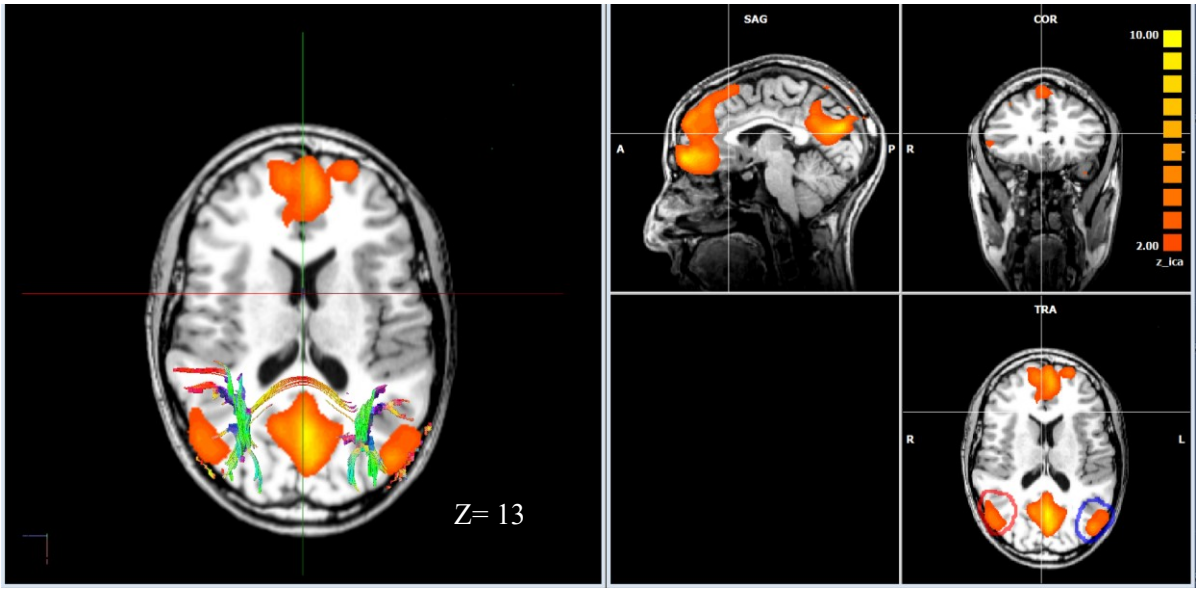

Figure 5.18 *Visualization of the ROIs defined on two activated areas of the Default Mode Network, on the transversal slice (right panel). The fibres resulting from the intersection of these two ROIs are shown on the left panel, in bottom view at level Z=13.*

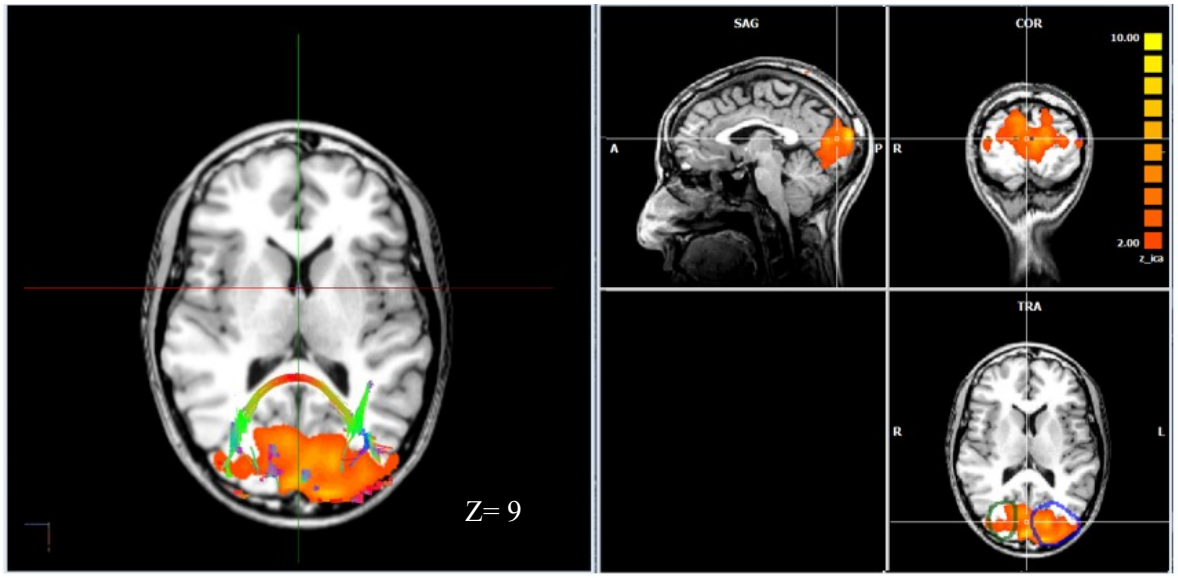

Figure 5.19 *Visualization of the ROIS defined on two activation areas of the Occipital Visual Area, on the transversal slice (right panel). The fibres resulting from the intersection of these two ROIs are shown on the left panel, in bottom view at level (Z=9).*

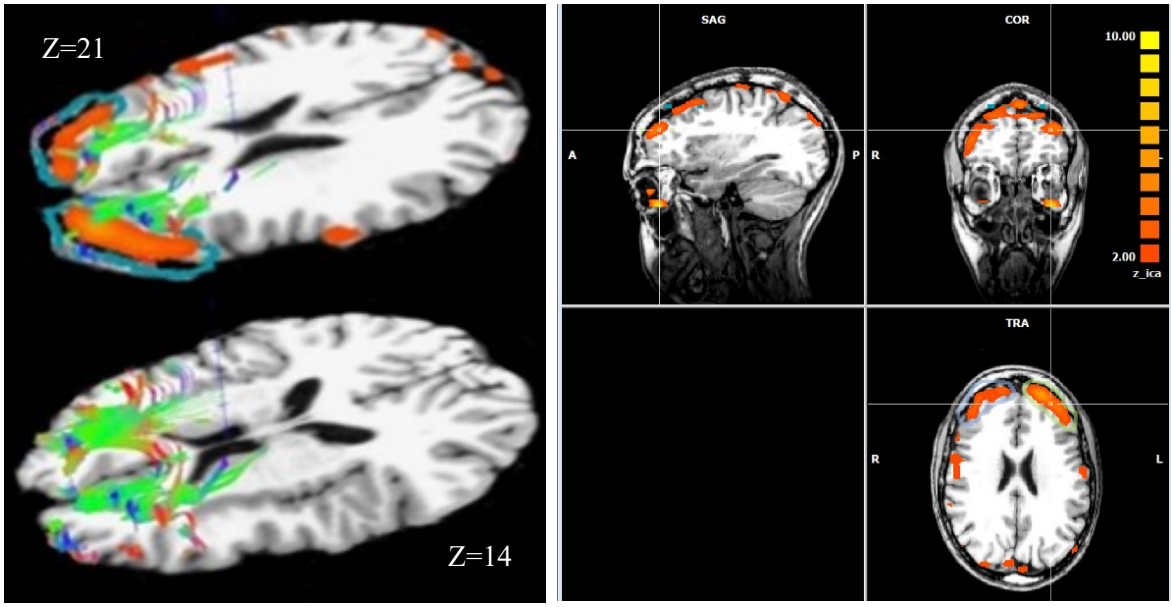

Figure 5.20 *Visualization of the ROIs defined on two activation areas of the Executive Control Network, on the transversal slice (right panel). The fibres resulting from the intersection of these ROIs are shown on the left panel, in two levels. The top image shows a perspective view of the fibres arising from the two ROIs defined on the activation areas, at level Z=21. The bottom panel shows the fibres running towards the corpus callosum, visualized in a more ventral plane (lower z coordinate) at level (Z=14).*

The results obtained from the tractography, performed on the three networks identified in the patient P2, are reported below.

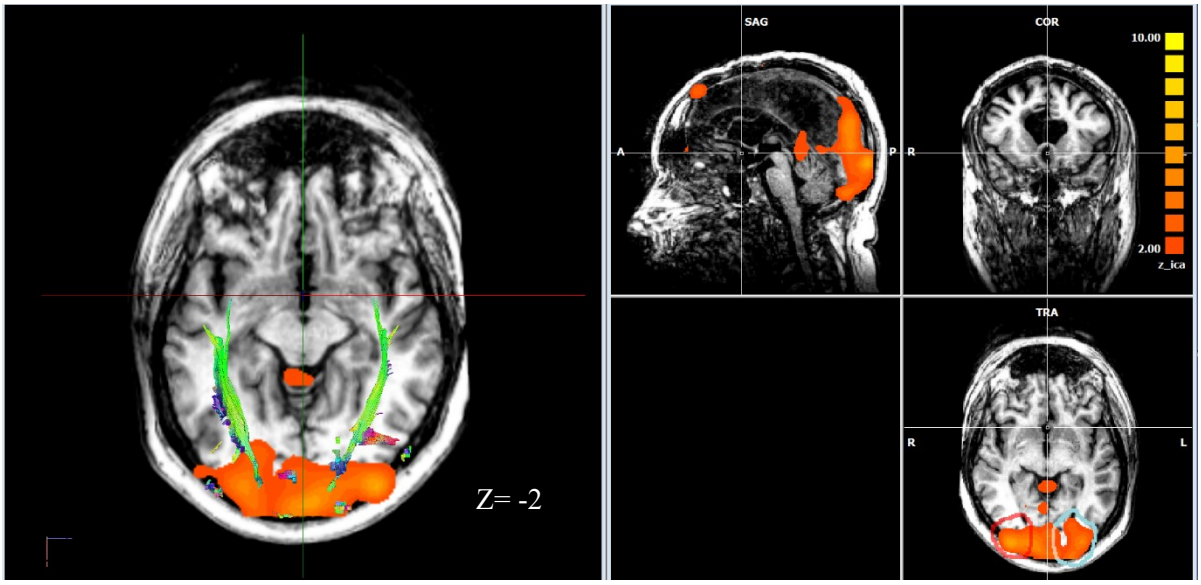

Figure 5.21 *Visualization of the two ROIs defined on two activation areas of the Occipital Visual Area, on the transversal slice (right panel). The fibres resulting from the intersection of these two ROIs are shown on the left panel, in bottom view at level* Z= -2.

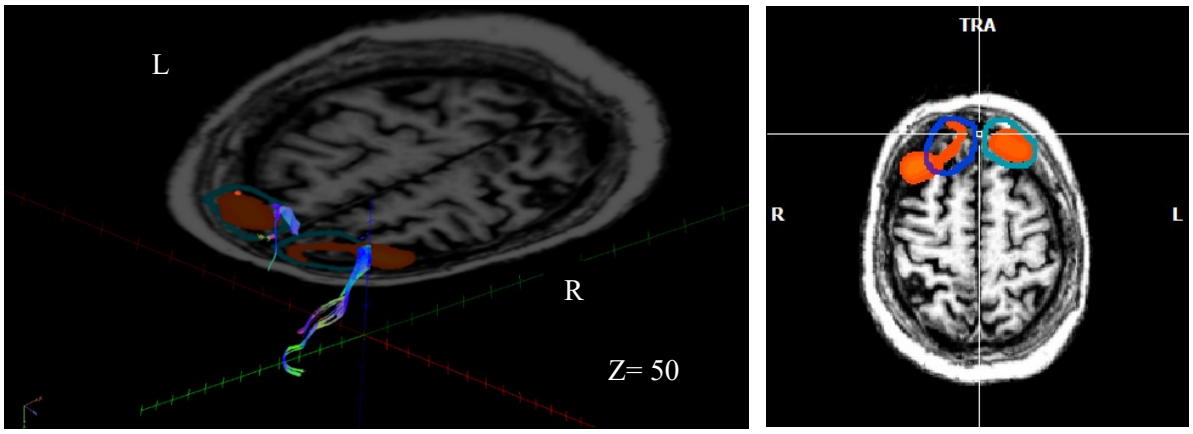

Figure 5.22 *Visualization of the two ROIs defined on two activation areas of the Executive Control Network, on the transversal slice (right panel). The fibres resulting from the intersection of these two ROIs are shown on the left panel, in bottom perspective view at level Z=50. The choice of this visualization allows to better appreciate the fibres that start from the two ROIs and then head downwards. Right hemisphere is on the right side of the panel.*

In ***Table 7*** the RSNs and the corresponding structural connections, linking the functionally linked regions are described.

Table 7 *Description of the functionally linked regions of the three RSNs and the interconnecting structural white matter pathways.*

Resting state network	*Functionally linked regions*	*Structural connections*
Default Mode Network	Left PPC	 Splenium of the CC
	Right PPC	
Occipital Visual Area	Left PVC	 Splenium of the CC
	Right PVC	
Executive Control	Left MFC	 Genu of the CC
	Right MFC	
MFC= Medial Frontal Cortex PPC= Posterior Parietal Cortex PVC= Primary Visual Cortex		

Discussion

The aim of this thesis was to investigate, by performing a DTI analysis, how bilateral activations occur in a callosotomised subject, to individuate possible alternative pathways to the corpus callosum through which the exchange of information, between the two hemispheres, takes place. The results are based on the analysis of rs-fMRI data, through the ICA procedure, and the analysis of the DWI data, both performed on BrainVoyager. BrainVoyager is a powerful neuroimaging software package for the analysis and visualization of structural and functional MRI data. The analysis involved one healthy subject and one patient, underwent callosotomy about 20 years before. Patients undergoing complete commissurotomy represent a unique opportunity for neuroscientists to examine the mechanisms of interhemispheric interactions, neuroplasticity, and compensatory reorganization (Uddin et al., 2008).

Even during rest, multiple cortical brain regions show a vast amount of spontaneous neuronal activity and are functionally linked to each other, forming the so called RSNs. This high level of functional connectivity within RSNs suggests the existence of direct neuroanatomical connections between these functionally linked brain regions, which facilitate the neuronal communication. After the ICA classification, in which the S-ICs are separated from the N-ICs, the S-ICs were visually inspected to detect some RSNs. The RSNs individuation was performed through the comparison to those present in literature, obtained in the study of Smith and coworkers (Smith et al., 2009). For the healthy subject six RSNs were identified: Default Mode Network, Medial Visual Area, Occipital Visual Area, Executive Control, Frontoparietal Right and Cerebellum Area. Instead, in the patient were identified the following RSNs: Default Mode Network, Medial Visual Area, Occipital Visual Area, Sensorymotor System, Executive Control and Frontoparietal Left. For a more accurate individuation of the patient RSNs, a double step of smoothing was performed. This represents an essential step, since the neuronal activations were less defined with respect those found in the healthy subject. Without any smoothing, most of the components would have been classified as noise with the risk to lose the recognition of some RSNs in the patient. The networks of the patient characterised by bilateral activations are the Occipital Visual Area, Sensorymotor System and the Executive Control. In both the healthy subject and the patient, the Default Mode Network has been identified: it results to be unilateral in the patient with respect to healthy subject in which it is strongly bilateral. This can be probably due to the effects of callosotomy or to the drug treatment for epilepsy.

According to this, the functional connectivity of this network results slightly altered. Subsequently, the white matter tracts, linking activation areas of the RSNs, have been reconstructed. White matter tracts constitute the structural highways of the brain, enabling information to travel quickly from one brain region to another (van den Heuvel et al.,2009). The tractography was performed taking into consideration three RSNs for the patient (Occipital Visual Area, Executive Control and Sensorymotor System) and three RSNs (Default Mode Network, Occipital Visual Area and Executive Control) for the healthy subject. Based on the tractography results, it is possible to affirm that the functionally linked activation areas within the RSNs are interconnected by anatomical white matter tracts. In particular, the white matter tracts identified in the subject have been compared to those found in the study of van den Heuvel (van den Heuvel et al., 2009) and of Figley (Figley et al., 2015). For each network, two ROIs were defined on the bilateral activation areas. The active areas of the Default Mode Network were interconnected through the splenium of the corpus callosum, as reported in the study of Figley and coworkers (Figley et al., 2015): images from the Figley's paper (2015) and from present study showing the closest z coordinate have been compared, by considering both cortical activations and reconstructed fibres tracts. Tracts crossing the splenium of the CC were also found to interconnect the regions of the primary visual network according to the results of van den Heuvel and colleagues (van den Heuvel et al., 2009). Fibres passing the genu of the CC were found to interconnect the left and right prefrontal cortical regions, in agreement with van den Heuvel and colleagues (van den Heuvel et al., 2009). The results obtained from the tractography performed on the RSNs of the patient, would suggest the presence of alternative pathways to the CC. For the Occipital Visual Area, the tracts originating from the two activated areas, seems to get to the lateral geniculate nucleus. For the Executive Control, the fibres start from the two cortical activated areas and proceed downwards. It is not possible to understand where they cross, but probably they initially will follow a path similar to that in the corresponding RSN of the healthy subject, and then proceed along some subcortical pathways. In the Sensorymotor System network, it was not possible to individuate and reconstruct any possible pathways that can justify the presence of bilateral activations. This is probably because patients undergone callosotomy display lower values of FA, as it can be appreciable by inspecting the FA map obtained in the patient. Therefore, the low values of FA indicate a worsening of the conduction of information between different areas of the brain, thus negatively affecting functional connectivity. This constitutes a limitation for the software because it becomes more difficult to identify and reconstruct the white matter tracts that connect functionally linked brain areas.

The presence of alternative pathways to the callosal fibres has been hypothesized in the study of Fabri and coworkers (Fabri et al., 2006). In this study the presence of bilateral activations of the post-central gyrus (PCG) and PO (parietal operculum) in the callosotomised patients has been demonstrated. These results suggested the presence of a subcortical neural mechanism responsible for the bilateral cortical activations (Fabri et al., 2006).

Comparison with other studies

In the literature various studies have been conducted on human characterised by the absence of the corpus callosum, which can be due either to callosal agenesis or to callosal resection. Resting-state fMRI studies found that global functional connectivity was nearly intact in AgCC, indicating that indirect or local polysynaptic pathways were utilized to preserve it in AgCC subjects (Yuan et al., 2020). In the study of Tyszka and colleagues (Tyszka et al., 2011), the presence of a strong functional connectivity between homotopic cortical brain regions in the AgCC group has been demonstrated, with no significant differences with respect to the control group. Furthermore, RSNs identified in the AgCC group were very similar to those identified in the control group and corresponded to the networks consistently identified in the resting-state literature in healthy adult subjects. Moreover, the spatial ICs of the AgCC group showed a high presence of bilateral activations, as those found in controls. This observation, together with the entirely intact functional connectivity between cortical regions, demonstrates that interhemispheric functional integration can occur in the absence of the corpus callosum (Tyszka et al., 2011). In addition, other studies were carried out on patients in which the CC was resected to treat drug-resistant epilepsy. Functional connectivity is thought to reflect structural connectivity. Given the known structural connectivity existing between homologous regions in each cerebral hemisphere, cortical commissural fibres have long been considered to mediate most interhemispheric interactions. However, in split-brain patients, when interhemispheric coordination exists, it must be mediated by extra-callosal pathways. As shown in the study of Uddin and coworkers (Uddin et al. 2008), it is generally accepted that some interhemispheric transfer exists in the split-brain patients, because it is possible that specific RSNs maintain bilateral presence after complete commissurotomy, suggesting that their coordination is subcortical in origin. Therefore, the comparison with intact brains suggests that in healthy subjects' brain a possible dual mechanism exists (Uddin et al., 2008). This means that cortical and sub-cortical mechanisms work together to coordinate neural activity and that the corpus callosum is not the only pathway involved in the connections between the two hemispheres.

The key concept is that in the intact brain, commissural connections exert a greater influence, but in the absence of such connections, the subcortical mechanism takes over (Uddin et al., 2008).

Limitations

The main limitation of this study is given by the reduced number of involved patients, in the present description only one individual. These patients are rare, in that the complete commissurotomy represented a solution performed in the past as treatment for intractable epilepsy. Nowadays this has been largely replaced by pharmacological interventions (Uddin et al., 2018). Another limitation of this study is represented by the manual classification of ICs as signal or noise. If not carefully visualized and classified, the ICs can be misinterpreted and some noise components can be erroneously not rejected, compromising the signal of interest. The manual classification has been performed by the supervision of an expert since this stage was crucial for the successive analysis. Nevertheless, this procedure is preferred over automatic classification because the data set analysed in this study corresponds to a group of subjects characterised by altered neural activity.

Conclusions

In conclusion, it is possible to affirm that the presence of commissural fibres plays a vital role for guaranteeing interhemispheric functional connectivity in healthy subject. Furthermore, in the comparison between intact-brain and split-brain subjects, it was found that the callosal connections do have a role when present, but in case of callosal resection, a subcortical route for transferring information may be involved. In fact, the persistence of interhemispheric coordination in split-brain patients, can be justified by the possible presence of subcortical pathways. The present study highlighted, in the split-brain patient, patterns of bilateral cortical activations comparable to those of healthy subject. This demonstrates the presence of functional interhemispheric connectivity even in subjects undergone the resection of the corpus callosum. The results of the DTI analysis would suggest the recruitment of sub-cortical connections, alternative to the callosal pathways, able to guarantee the structural connection between the two cerebral hemispheres.

A future improvement could be given by the acquisition of task-related activation data. This would allow to investigate interhemispheric communication during task performance, to have a global valuation of the functional connectivity in callosotomised patients. The results obtained from this preliminary work encourage the development of future studies involving a larger cohort of callosotomised patients. Furthermore, a comparison with a healthy control group, would represent an important contribute for this work, because it would give some statistical significance.

Bibliography

Akinrodoye MA, Lui F. Neuroanatomy, Somatic Nervous System. [Updated 2022 Nov 7]. In: StatPearls [Internet]. Treasure Island (FL): StatPearls Publishing; 2022 Jan-.

Alzola-Aldamizetxebarria, Saioa et al. “A Comprehensive Introduction to Magnetic Resonance Imaging Relaxometry and Contrast Agents.” *ACS omega* vol. 7,42 36905-36917. 13 Oct. 2022.

Amaro, Edson Jr, and Gareth J Barker. “Study design in fMRI: basic principles.” *Brain and cognition”* vol. 60,3 (2006): 220-32.

Ambrosi G., Cantino D., Castano P., et al., *“Anatomia dell’uomo”*, Chapter 14-SistemaNervoso Centrale, Pages 313-401, Edi-Ermes, Milano 2010.

Andersson, Jesper LR, Mark Jenkinson, and Stephen Smith. "Non-linear registration, aka Spatial normalisation FMRIB technical report TR07JA2." *FMRIB Analysis Group of the University of Oxford* 2.1 (2007): e21.

Andy’s Brain Book, 2019 GitHub.

Assaf, Yaniv, and Ofer Pasternak. “Diffusion tensor imaging (DTI)-based white matter mapping in brain research: a review.” *Journal of molecular neuroscience: MN* vol. 34,1 (2008): 51-61.

Babaeeghazvini, Parinaz et al. “Brain Structural and Functional Connectivity: A Review of Combined Works of Diffusion Magnetic Resonance Imaging and Electro-Encephalography.” *Frontiers in human neuroscience* vol. 15 721206. 7 Oct. 2021.

Basinger H, Hogg JP. Neuroanatomy, Brainstem. [Updated 2022 Jul 6]. In: StatPearls [Internet]. Treasure Island (FL): StatPearls Publishing; 2022 Jan-.

Baynes K., Corpus Callosum, in *“Encyclopedia of the Human Brain”*, Chapter: I Anatomy, 2002.

Bazira PJ. An overview of the nervous system. *Surgery* 2021.

Beckmann, Christian F et al. “Investigations into resting-state connectivity using independent component analysis.” *Philosophical transactions of the Royal Society of London. Series B, Biological sciences* vol. 360,1457 (2005): 1001-13.

Beckmann, Christian F. “Modelling with independent components.” *NeuroImage* vol. 62,2 (2012): 891-901.

Bem Junior, Luiz Severo et al. “The anatomy of the brain - learned over the centuries.” *Surgical neurology international* vol. 12 319. 28 Jun. 2021.Binder, Jeffrey R. “The Wernicke area: Modern evidence and a reinterpretation.” *Neurology* vol. 85,24 (2015): 2170-5.

Bijsterbosch J., Smith S.M., Beckmann C. *“Introduction to Resting State fMRI Functional Connectivity”,* Oxford University Press, 2017.

Bui T, M Das J. Neuroanatomy, Cerebral Hemisphere. 2022 Jul 25. In: StatPearls [Internet]. Treasure Island (FL): StatPearls Publishing; 2022 Jan–.

Buxton, Richard B. “The physics of functional magnetic resonance imaging (fMRI).” *Reports on progress in physics. Physical Society (Great Britain)* vol. 76,9 (2013): 096601.

Catani, Marco, and Michel Thiebaut de Schotten. “A diffusion tensor imaging tractography atlas for virtual in vivo dissections.” *Cortex: a journal devoted to the study of the nervous system and behavior* vol. 44,8 (2008): 1105-32.

Chan Rachel W., Justin Y.C. Lau, Wilfred W. Lam, Angus Z. Lau, Magnetic Resonance Imaging, Editor(s): Roger Narayan, Encyclopedia of Biomedical Engineering, Elsevier, 2019, Pages 574-587.

Chang, Bernard S, and Daniel H Lowenstein. “Epilepsy.” *The New England journal of medicine* vol. 349,13 (2003): 1257-66.

Chaplin T.A., Rosa M.G.P., Yu H., Chapter 22 – *“Scaling Up the Simian Primate Cortex: A Conserved Pattern of Expansion Across Brain Sizes”,* Evolutionary Neuroscience (Second Edition), 2020: 533-545.

Chappell M., Okell T., Jenkinson M., *“Short Introduction to MRI Physics for neuroimaging”,* Oxford University Press, 2018.

Chen Jean, and Julien Cohen-Adad. "Functional magnetic resonance imaging." (2019): 533-544.

Chen, Jingyuan E, and Gary H Glover. “Functional Magnetic Resonance Imaging Methods.” *Neuropsychology review* vol. 25,3 (2015): 289-313.

Conti Fiorenzo et al., "*Fisiologia Medica*" (Third edition), Vol.1, Edi-Ermes, Milano 2020.

De Benedictis, Alessandro et al. "Anatomo-functional study of the temporo-parieto-occipital region: dissection, tractographic and brain mapping evidence from a neurosurgical perspective." *Journal of anatomy* vol. 225,2 (2014): 132-51.

Devinsky, Orrin et al. "Epilepsy." *Nature reviews. Disease primers* vol. 4 18024. 3 May. 2018.

Dickie, David Alexander et al. "Whole Brain Magnetic Resonance Image Atlases: A Systematic Review of Existing Atlases and Caveats for Use in Population Imaging." *Frontiers in neuroinformatics* vol. 11 1. 19 Jan. 2017.

Diez, Ibai et al. "Information Flow Between Resting-State Networks." *Brain connectivity* vol. 5,9 (2015): 554-64.

Dijkhuizen, Rick M et al. "Functional MRI and diffusion tensor imaging of brain reorganization after experimental stroke." *Translational stroke research* vol. 3,1 (2012): 36-43.

Dronkers, N F et al. "Paul Broca's historic cases: high resolution MR imaging of the brains of Leborgne and Lelong." *Brain : a journal of neurology* vol. 130,Pt 5 (2007): 1432-41.

Fabri, Mara, and Gabriele Polonara. "Functional topography of the corpus callosum as revealed by fMRI and behavioural studies of control subjects and patients with callosal resection." Neuropsychologia vol. 183 (2023): 108533.

Fabri, M et al. "Contribution of the corpus callosum to bilateral representation of the trunk midline in the human brain: an fMRI study of callosotomized patients." *The European journal of neuroscience* vol. 23,11 (2006): 3139-48.

Figley, Teresa D., et al. "Probabilistic atlases of default mode, executive control and salience network white matter tracts: an fMRI-guided diffusion tensor imaging and tractography study." *Frontiers in human neuroscience* 9 (2015): 585.

Formisano E, Di Salle F, Goebel R. Fundamentals of Data Analysis Methods in Functional MRI. Advanced Image Processing in Magnetic Resonance Imaging, 2005, 481-503.

Formisano, Elia et al. "Cortex-based independent component analysis of fMRI time series." *Magnetic resonance imaging* vol. 22,10 (2004): 1493-504.

Fox, Michael D, and Marcus E Raichle. “Spontaneous fluctuations in brain activity observed with functional magnetic resonance imaging.” *Nature reviews. Neuroscience* vol. 8,9 (2007): 700-11.

Fox, Michael D, and Michael Greicius. “Clinical applications of resting state functional connectivity.” *Frontiers in systems neuroscience* vol. 4 19. 17 Jun. 2010.

Fujii, Masazumi et al. “Neural Basis of Language: An Overview of An Evolving Model.” *Neurologia medico-chirurgica* vol. 56,7 (2016): 379-86.

Glover, Gary H. “Overview of functional magnetic resonance imaging.” *Neurosurgery clinics of North America* vol. 22,2 (2011): 133-9.

Goebel, R., Esposito, F. Formisano, E. (2006). Analysis of functional image analysis contest (FIAC) data with Brainvoyager QX: From single-subject to cortically aligned group general linear model analysis and self-organizing group independent component analysis. *Human Brain Mapping*, **27**, 392-401.

Goebel R, Jansma H, Eck J. BrainVoyager QX Getting Started Guide (version 2.10 for BVQX 2.4). Brain Innovation B.V.

Gore, John C. “Principles and practice of functional MRI of the human brain.” *The Journal of clinical investigation* vol. 112,1 (2003): 4-9.

Griffanti, Ludovica et al. “Hand classification of fMRI ICA noise components.” *NeuroImage* vol. 154 (2017): 188-205.

Griffanti, Ludovica et al. “ICA-based artefact removal and accelerated fMRI acquisition for improved resting state network imaging.” *NeuroImage* vol. 95 (2014): 232-47.

Grover, Vijay P B et al. “Magnetic Resonance Imaging: Principles and Techniques: Lessons for Clinicians.” *Journal of clinical and experimental hepatology* vol. 5,3 (2015): 246-55.

Hall J. E., “*Guyton e Hall Fisiologia medica*” (13th Edition), Chapter 58, Edra,Milano 2017.

Hanani, Menachem, and David C Spray. “Emerging importance of satellite glia in nervous system function and dysfunction.” *Nature reviews. Neuroscience* vol. 21,9 (2020): 485-498.

Hidalgo-Tobón, Silvia S. “Theory of gradient coil design methods for magnetic resonance imaging.” *Concepts in Magnetic Resonance Part A* 36 (2010): 223-242.

Holdsworth, Samantha J, and Roland Bammer. “Magnetic resonance imaging techniques: fMRI, DWI, and PWI.” *Seminars in neurology* vol. 28,4 (2008): 395-406.

Huettel S. A., Song A. W., McCarthy G., “Functional magnetic resonance imaging”, Volume 1, Sinauer Associates Sunderland (2004).

Huff T, Mahabadi N, Tadi P. Neuroanatomy, Visual Cortex. 2022 Jul 25. In: StatPearls [Internet]. Treasure Island (FL): StatPearls Publishing; 2022 Jan–.

Huisman, T A G M. “Diffusion-weighted and diffusion tensor imaging of the brain, made easy.” *Cancer imaging: the official publication of the International Cancer Imaging Society* vol. 10 Spec no A,1A S163-71. 4 Oct. 2010.

Jackson, Graeme D et al. “Functional magnetic resonance imaging: focus localization.” *Handbook of clinical neurology* vol. 107 (2012): 369-85.

Javed K, Reddy V, M Das J, et al. Neuroanatomy, Wernicke Area. [Updated 2022 Jul 25]. In: StatPearls [Internet]. Treasure Island (FL): StatPearls Publishing; 2022 Jan-.Kandel E.R. et al., “*Principi di Neuroscienze*” (4th Edition), Chapter 50, Casa Editrice Ambrosiana, Milano 2014.

Jenkinson, Mark, and Michael Chappell. “*Introduction to neuroimaging analysis”*, Oxford University Press, 2018.

Jenkinson M., Chappell M., *“Short introduction to Brain Anatomy for Neuroimaging”,* Oxford University Press, 2018.

Kaiming, Li et al. “Review of methods for functional brain connectivity detection using fMRI.” *Computerized medical imaging and graphics: the official journal of the Computerized Medical Imaging Society* vol. 33,2 (2009): 131-9.

Kelly, Robert E Jr et al. “Visual inspection of independent components: defining a procedure for artifact removal from fMRI data.” *Journal of neuroscience methods* vol. 189,2 (2010): 233-45.

Larobina, M., and Murino, L. “Medical image file formats.” *Journal of digital imaging* vol. 27,2 (2014): 200-6.

Ludwig PE, M Das J. Histology, Glial Cells. 2022 May 8. In: StatPearls [Internet]. Treasure Island (FL): StatPearls Publishing; 2022 Jan–.

Ludwig PE, Reddy V, Varacallo M. Neuroanatomy, Central Nervous System (CNS) [Updated 2022 Oct 10]. In: StatPearls [Internet]. Treasure Island (FL): StatPearls Publishing; 2022 Jan-.

Lv, H et al. "Resting-State Functional MRI: Everything That Nonexperts Have Always Wanted to Know." *AJNR. American journal of neuroradiology* vol. 39,8 (2018): 1390-1399.

Mandal, Pravat K et al. "Structural brain atlases: design, rationale, and applications in normal and pathological cohorts." *Journal of Alzheimer's disease: JAD* vol. 31 Suppl 3,0 3 (2012): S169-88.

Matthews, P M, and P Jezzard. "Functional magnetic resonance imaging." *Journal of neurology, neurosurgery, and psychiatry*" vol. 75,1 (2004): 6-12.

Milano, M et al. "Network building and analysis in connectomics studies: a review of algorithms, databases and technologies." *Network Modeling Analysis Health Informatics and Bioinformatics* 8, 13 (2019).

Moini J., Piran P., *"Cerebral cortex, Functional and Clinical Neuroanatomy, A Guide for Health Care Professionals"*, Chapter 6, Pages 177-240, 2020.

Ogawa, S et al. "Brain magnetic resonance imaging with contrast dependent on blood oxygenation." *Proceedings of the National Academy of Sciences of the United States of America* vol. 87,24 (1990): 9868-72.

Pauling, L, and C D Coryell. "The Magnetic Properties and Structure of Hemoglobin, Oxyhemoglobin and Carbonmonoxyhemoglobin." *Proceedings of the National Academy of Sciences of the United States of America* vol. 22,4 (1936): 210-6.

Poldrack, R., Mumford, J., & Nichols, T. "*Handbook of Functional MRI Data Analysis*" Cambridge: Cambridge University Press. (2011).

Power, Jonathan D et al. "Studying brain organization via spontaneous fMRI signal." *Neuron* vol. 84,4 (2014): 681-96.

R.W. Chan, J.Y.C. Lau, W.W. Lam, A.Z. Lau, Magnetic resonance imaging, in: R. Narayan (Ed.), Encyclopedia of Biomedical Engineering, Elsevier, Oxford, 2019, pp. 574–587.

Raju H, Tadi P. Neuroanatomy, Somatosensory Cortex. 2022 Nov 7. In: StatPearls [Internet]. Treasure Island (FL): StatPearls Publishing; 2022 Jan–.

Rangaprakash, D et al. “FMRI hemodynamic response function (HRF) as a novel marker of brain function: applications for understanding obsessive-compulsive disorder pathology and treatment response.” *Brain imaging and behavior* vol. 15,3 (2021): 1622-1640.

Roy, C S, and C S Sherrington. “On the Regulation of the Blood-supply of the Brain.” *The Journal of physiology* vol. 11,1-2 (1890): 85-158.17.

Sarmast, Shah T et al. “Current Classification of Seizures and Epilepsies: Scope, Limitations and Recommendations for Future Action.” *Cureus* vol. 12,9 e10549. 20 Sep. 2020.

Scelsi, C L et al. “The Lateral Ventricles: A Detailed Review of Anatomy, Development, and Anatomic Variations.” *AJNR. American journal of neuroradiology* vol. 41,4 (2020): 566-572.

Scheffer, Ingrid E et al. “ILAE classification of the epilepsies: Position paper of the ILAE Commission for Classification and Terminology.” *Epilepsia* vol. 58,4 (2017): 512-521.

Seitzman, Benjamin A et al. “The State of Resting State Networks.” *Topics in magnetic resonance imaging: TMRI* vol. 28,4 (2019): 189-196.

Shenoy SS, Lui F. Neuroanatomy, Ventricular System. [Updated 2022 Jul 25]. In: StatPearls [Internet]. Treasure Island (FL): StatPearls Publishing; 2022 Jan-.

Shenoy SS, Lui F. Neuroanatomy, Ventricular System. [Updated 2022 Jul 25]. In: StatPearls [Internet]. Treasure Island (FL): StatPearls Publishing; 2022 Jan-.

Siero, Jeroen C W et al. “Blood Oxygenation Level-dependent/Functional Magnetic Resonance Imaging: Underpinnings, Practice, and Perspectives.” *PET clinics* vol. 8,3 (2013): 329-44.

Smith, Stephen M et al. “Correspondence of the brain's functional architecture during activation and rest.” *Proceedings of the National Academy of Sciences of the United States of America* vol. 106,31 (2009): 13040-5.

Smith, Stephen M. “Fast robust automated brain extraction.” *Human brain mapping* vol. 17,3 (2002): 143-55.

Smith, Stephen M et al. “Advances in functional and structural MR image analysis and implementation as FSL.” *NeuroImage* vol. 23 Suppl 1 (2004): S208-19.

Smith, Stephen M., et al. “An Introduction to Resting State FMRI Functional Connectivity”. Regno Unito, Oxford University Press, 2017.

Society for Maternal-Fetal Medicine (SMFM), Rotmensch, S., & Monteagudo, A. (2020). Agenesis of the Corpus Callosum. *American journal of obstetrics and gynecology*, *223*(6), B17–B22.

Sokoloff, Louis. "The physiological and biochemical bases of functional brain imaging." *Cognitive neurodynamics* vol. 2,1 (2008): 1-5.

Sparacia, Gianvincenzo et al. "Resting-State Functional Magnetic Resonance Imaging for Brain Tumor Surgical Planning: Feasibility in Clinical Setting." *World neurosurgery* vol. 131 (2019): 356-363.

Spielman, R., Jenkins, W., & Lovett, M. (2021). *Psychology*. BCcampus.

Sporns, Olaf. "Structure and function of complex brain networks." *Dialogues in clinical neuroscience* vol. 15,3 (2013): 247-62.

Sprawls, Perry. "*Magnetic Resonance Imaging Principles, Methods and Techniques"*. Medical Physics Publishing, 2000.

Stinnett TJ, Reddy V, Zabel MK. Neuroanatomy, Broca Area. [Updated 2022 Aug 8]. In: StatPearls [Internet]. Treasure Island (FL): StatPearls Publishing; 2022 Jan-.

Symms M, Jäger HR, Schmierer K, et al. "A review of structural magnetic resonance neuroimaging" *Journal of Neurology, Neurosurgery & Psychiatry* 2004;**75:**1235-1244.

Takahashi, Shinichi. "Metabolic Contribution and Cerebral Blood Flow Regulation by Astrocytes in the Neurovascular Unit." *Cells* vol. 11,5 813. 25 Feb. 2022.

Thau L, Reddy V, Singh P. Anatomy, Central Nervous System. 2022 Oct 10. In: StatPearls [Internet]. Treasure Island (FL): StatPearls Publishing; 2022 Jan–.

Thau L, Reddy V, Singh P. Anatomy, Central Nervous System. 2022 Oct 10. In: StatPearls [Internet]. Treasure Island (FL): StatPearls Publishing; 2022 Jan–.

Tyszka, J Michael et al. "Intact bilateral resting-state networks in the absence of the corpus callosum." *The Journal of neuroscience: the official journal of the Society for Neuroscience* vol. 31,42 (2011): 15154-62.

Uddin, Lucina Q et al. "Residual functional connectivity in the split-brain revealed with resting-state functional MRI." *Neuroreport* vol. 19,7 (2008): 703-9.

Unterberger, Iris et al. “Corpus callosum and epilepsies.” *Seizure* vol. 37 (2016): 55-60.

Vaddiparti, Aparna et al. “The Evolution of Corpus Callosotomy for Epilepsy Management.” *World neurosurgery* vol. 145 (2021): 455-461.

van Den Heuvel, Martijn P., et al. "Functionally linked resting-state networks reflect the underlying structural connectivity architecture of the human brain." *Human brain mapping* 30.10 (2009): 3127-3141.

van den Heuvel et al., “Exploring the brain network: a review on resting-state fMRI functional connectivity.” *European neuropsychopharmacology: the journal of the European College of Neuropsychopharmacology* vol. 20,8 (2010): 519-34.

Vitti Elena, “*Analysis of functional connectivity in healthy subjects with intact brain and in patients with surgical resection of the corpus callosum”, Master Degree in Biomedical Engineering, Ancona* Università Politecnica delle Marche, 2023.

Waxenbaum JA, Reddy V, Varacallo M. Anatomy, Autonomic Nervous System. [Updated 2022 Jul 25] In: StatPearls [Internet]. Treasure Island (FL): StatPearls Publishing; 2022 Jan-.

Yacoub, E et al. “Investigation of the initial dip in fMRI at 7 Tesla.” *NMR in biomedicine* vol. 14,7-8 (2001): 408-12.

Yip DW, Lui F. Physiology, Motor Cortical. [Updated 2022 Sep 12]. In: StatPearls [Internet]. Treasure Island (FL): StatPearls Publishing; 2022 Jan-.

Yuan, Junliang et al. “The structural basis for interhemispheric functional connectivity: Evidence from individuals with agenesis of the corpus callosum.” *NeuroImage. Clinical* vol. 28 (2020): 102425.

Sitography

BrainVoyager User's Guide.
www.brainvoyager.com/bv/doc/UsersGuide (Accessed April 2023)

National Institute of Neurological Disorders and Stroke, Brain Basics: Know Your Brain.
www.ninds.nih.gov/health-information/public-education/brain-basics/brain-basics-know-your-brain (Accessed February 2023)

Khan Academy, Overview of neuron structure and function.
www.khanacademy.org/science/biology/human-biology/neuron-nervous-system/a/overview-of-neuron-structure-and-function (Accessed February 2023)

Queensland Brain Institute, Types of glia.
qbi.uq.edu.au/brain-basics/brain/brain-physiology/types-glia (Accessed February 2023)

Kenhub, Glial cell histology.
www.kenhub.com/en/library/anatomy/histology-of-glial-cells (Accessed February 2023)

Britannica, node of Ranvier.
www.britannica.com/science/node-of-Ranvier (Accessed February 2023)

Britannica, ependymal cell.
www.britannica.com/science/ependymal-cell (Accessed February 2023)

Queensland Brain Institute, Types of neurons.
qbi.uq.edu.au/brain/brain-anatomy/types-neurons (Accessed February 2023)

Johns Hopkins Medicine, Brain Anatomy and How the Brain Works. www.hopkinsmedicine.org/health/conditions-and-diseases/anatomy-of-the-brain (Accessed March 2023).

Mayfield, Anatomy of the Brain.

mayfieldclinic.com/pe-anatbrain.htm (Accessed February 2023)

Cleveland Clinic, Cerebral Cortex.
my.clevelandclinic.org/health/articles/23073-cerebral-cortex (Accessed March 2023)

Kenhub, Lateral Ventricles.
www.kenhub.com/en/library/anatomy/lateral-ventricles (Accessed March 2023)

Cleveland Clinic, Medulla Oblongata.
my.clevelandclinic.org/health/body/23001-medulla-oblongata (Accessed February 2023)

Queensland Brain Institute, Corpus Callosum.
qbi.uq.edu.au/brain/brain-anatomy/corpus-callosum (Accessed February 2023)

Kenhub, Corpus callosum.
www.kenhub.com/en/library/anatomy/corpus-callosum (Accessed February 2023)

Nature portfolio, Gustatory cortex.
(www.nature.com/subjects/gustatory-cortex (Accessed March 2023)

Physiopedia, Olfactory Cortex.
www.physio-pedia.com/Olfactory_Cortex (Accessed March 2023)

The University of Texas Health Science Center at Houston, Motor Cortex.
nba.uth.tmc.edu/neuroscience/m/s3/chapter03.html (Accessed February 2023)

The University of Texas Health Science Center at Houston, Motor Units and Muscle Receptors.
nba.uth.tmc.edu/neuroscience/m/s3/chapter01.html (Accessed February 2023)

The University of Texas Health Science Center at Houston, Functions of the Cerebellum.
nba.uth.tmc.edu/neuroscience/m/s3/chapter05.html (Accessed March 2023)

Bibliography Images

Amaro, Edson Jr, and Gareth J Barker. “Study design in fMRI: basic principles.” *Brain and cognition* vol. 60,3 (2006): 220-32.

Anastasi G., Capitani S., Carnazza M.L., et al., “Trattato di anatomia umana”, Chapter:14, Edi-Ermes (2012).

Bagdinova, A.N., Rybakov, A.S., Demikhov, E.I. et al. *Simulation of a Gradient System for a Helium-Free Magnetic Resonance Imager. Instrum Exp Tech 65, 113–122 (2022).*

Baynes K., Corpus Callosum, in *“Encyclopedia of the Human Brain”*, 2002, Chapter: I Anatomy.

Beckmann, Christian F et al. “Investigations into resting-state connectivity using independent component analysis.” *Philosophical transactions of the Royal Society of London. Series B, Biological sciences* vol. 360,1457 (2005): 1001-13.

Blausen.com staff (2014)*"Medical gallery of Blausen Medical 2014".WikiJournal of Medicine 1*

Buğa, D. *Central Language Hypothesis in the Decision-Making Process. In B. Christiansen & E. Lechman (Eds.), Neuroeconomics and the Decision-making Process (pp. 66–85). Hershey, PA: IGI Global.* (2016).

Caligari Conti, Daphne. *Magnetic Resonance Imaging. (2016).*

Chou, Dean & Vardakis, John & Ventikos, Yiannis. *Multiscale Modelling for Cerebrospinal Fluid Dynamics: Multicompartmental Poroelasticity and the Role of AQP4. Journal of Biosciences and Medicines. (2014).*

Clarke, Christopher, and Abdulla, Sarah. *FRCR Physics Notes: Medical Imaging Physics for the First FRCR Examination. Regno Unito, Radiology Cafe Publishing, 2020.*

Gore, John C. “Principles and practice of functional MRI of the human brain.” *The Journal of clinical investigation* vol. 112,1 (2003): 4-9.

Grover, Vijay P B et al. “Magnetic Resonance Imaging: Principles and Techniques: Lessons for Clinicians.” *Journal of clinical and experimental hepatology* vol. 5,3 (2015): 246-55.

Jefferys, John & Cooper, Alison. *Brain basics (2023).*

John, E. H., Guyton and Hall Textbook of Medical Physiology, 12th Ed., Saunders, 2012.

Kim, Moon Sun and Dae Cheol Kweon. "Blood Flow Measurement with Phase Contrast MRI According to Flip Angle in the Ascending Aorta." Journal of Korean Medical Science 26 (2016): 142-148.

Larobina, Michele, and Loredana Murino. "Medical image file formats." *Journal of digital imaging* vol. 27,2 (2014): 200-6.

Nacy, Somer M. et al. "Controlling a Servo Motor Using EEG Signals from the Primary Motor Cortex." *American Journal of Biomedical Engineering* 6 (2016): 139-146.

Pitkänen, Asla et al. *"Epileptogenesis." Cold Spring Harbor perspectives in medicine vol. 5,10 a022822. 18 Sep. 2015.*

Poldrack, R., Mumford, J., & Nichols, T. *Handbook of Functional MRI Data Analysis*. Cambridge: Cambridge University Press. (2011).

Purves, D., et al. Neuroscience. 6th Edition, Sinauer Associates, New York (2018).

Salat, David H et al. "Neuroimaging of deployment-associated traumatic brain injury (TBI) with a focus on mild TBI (mTBI) since 2009." *Brain injury* vol. 31,9 (2017): 1204-1219.

Salat David H., Chapter 12 – "Diffusion Tensor Imaging in the Study of Aging and Age-Associated Neural Disease", Editor(s): Heidi Johansen-Berg, Timothy E.J. Behrens,Diffusion MRI (Second Edition), Academic Press, 2014, Pages 257-281.

Smith, Stephen M et al. "Correspondence of the brain's functional architecture during activation and rest." *Proceedings of the National Academy of Sciences of the United States of America* vol. 106,31 (2009): 13040-5.

Sperry, R W. "Hemisphere deconnection and unity in conscious awareness." *The American psychologist* vol. 23,10 (1968): 723-33.

Spielman, R., Jenkins, W., & Lovett, M. (2021). *Psychology*. BCcampus. https://opentextbc.ca/h5ppsychology/.

Sprawls, Perry. *Magnetic Resonance Imaging Principles, Methods and Techniques*. Medical Physics Publishing, 2000.

Tavazzi, E et al. *"MRI markers of functional connectivity and tissue microstructure in stroke-related motor rehabilitation: A systematic review." NeuroImage. Clinical vol. 33 (2022): 102931.*

van den Heuvel et al., "Exploring the brain network: a review on resting-state fMRI functional connectivity." *European neuropsychopharmacology: the journal of the European College of Neuropsychopharmacology* vol. 20,8 (2010): 519-34.

van Geuns, R J et al. "Basic principles of magnetic resonance imaging." *Progress in cardiovascular diseases* vol. 42,2 (1999): 149-56.

Waxman Stephen G. *"Ventricles and Coverings of the Brain." Clinical Neuroanatomy, 28e Ed. McGraw Hill,* 2017.

Wise, James A., et al. "Anatomy and Physiology" N.p., OpenStax, 2013.

Yuan, Junliang et al. "The structural basis for interhemispheric functional connectivity: Evidence from individuals with agenesis of the corpus callosum." *NeuroImage. Clinical* vol. 28 (2020): 102425.

Sitography Images

Mayfield, Anatomy of the Brain.
mayfieldclinic.com/pe-anatbrain.htm (Accessed February 2023)

Cleveland Clinic, Cerebellum.
my.clevelandclinic.org/health/body/23418-cerebellum (Accessed March 2023)

National Library of Medicine MedlinePlus magazine, Understanding different kinds of seizures
magazine.medlineplus.gov/article/understanding-different-kinds-of-seizures
(Accessed February 2023)

Kenhub, Ventricles of the brain.
www.kenhub.com/en/library/anatomy/ventricular-system-of-the-brain (Accessed March 2023)

Physiopedia, Glial Cells.
www.physio-pedia.com/Glial_Cells (Accessed March 2023)

Lab in Cognition and Perception
cims.nyu.edu/~brenden/courses/labincp/chapters/17/00-mri.html (Accessed April 2023)

Appendix A The Imaging Process

The MRI process is characterised by two major functions (***Figure A.1***). The first is the *acquisition* of RF signals from the patient's body, the second is the mathematical *reconstruction* of the image from the acquired signals (Sprawls, 2000). A single image of the brain (one volume) is obtained by sequentially acquiring images of all the slices that compose the brain (Smith et al., 2017). The time required for a complete acquisition is determined by the duration of the acquisition of a single slice multiplied by the number of slices contained in that volume. The duration of a single slice acquisition cycle is called TR, which represents one of the adjustable scanning parameters used to select the different types of image contrast (Sprawls, 2000). The image reconstruction process is usually fast compared to the acquisition process and generally does not require any decisions or adjustments by the operator. At the end of this process, the final MR scan is obtained. It appears as a matrix of picture elements, or pixels, each of them representing corresponding voxel of tissue within the slice. The size of a voxel has a significant effect on image quality. The amount of image blurring depends on the dimensions of the individual voxels, determined in turn by three basic imaging factors, as illustrated in ***Figure A.2.*** The dimension of a voxel in the plan of the image is determined by the ratio of the field of view (FOV) and the size of the matrix: smaller image FOVs and smaller voxels produce more detailed images. Matrix size refers to the number of voxels in the rows or columns of the matrix and is selected by the operator before the acquisition. Typical matrix dimensions are in the range of 128 to 512 mm (Sprawls, 2000).

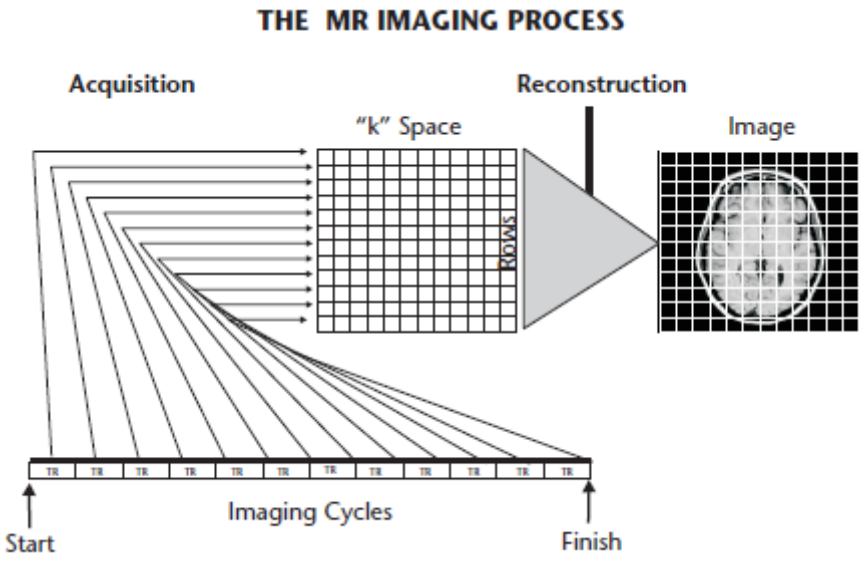

Figure A.1 *Acquisition and reconstruction phases that make up the MR image production process (Sprawls, 2000).*

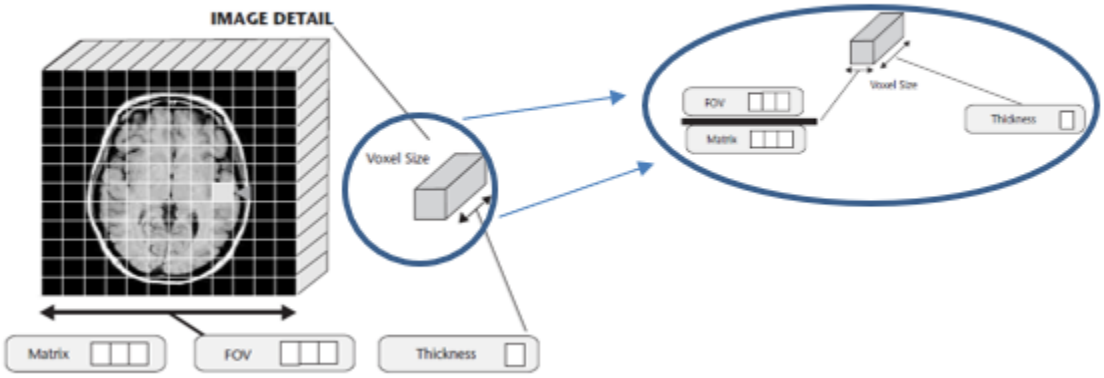

Figure A.2 *Voxel size and detail in MR images is determined by the values selected for the 3 protocol factors: FOV, matrix size, and slice thickness (Sprawls, 2000).*

A.1 Imaging Methods

There are several different imaging methods that can be used to create MR images (***Figure 3***). The main difference among these methods is the sequence in which the RF pulses and gradients are applied during the acquisition process. Therefore, the different methods are often referred to as the different *pulse sequences*. For each imaging method there is a set of factors that must be adjusted by the user to produce specific image characteristics (e.g., TR, ET, flip angle). The selection of a specific imaging method and factor values is generally based on the type of contrast required for a specific tissue (Sprawls, 2000). The most common imaging sequence used for fMRI is *echo planar imaging* (EPI). EPI is a fast-imaging technique whereby a two-dimensional (2D) image can be obtained in less than a second, by quickly switching the magnetic gradients back and forth after a single excitation pulse (Chen et al., 2019). The type of contrast generated is determined according to the choice of a *spin echo* or *gradient echo* preparation (Holdsworth et al., 2008). The image contrast can also be manipulated by two key pulse sequence parameters, such as TE and TR (Rachel et al., 2019).

Repetition time

TR is defined as the time interval between successive RF excitation pulses.

Echo time

TE is the time between the middle instant of the RF excitation pulse and the instant in which the signal is maximum. The TE corresponds to the time when the echo is detected or 'read out' (Rachel et al., 2019).

All the imaging methods belong to one of the two major families*, spin echo* or *gradient echo* ***(Figure A.3).*** The difference is due to the process used to create the echo event at the end of each imaging cycle. The transverse magnetization phase terminates with the echo event, which produces the signal emitted by the tissue, used to form the final image. For the spin echo methods, the echo event is produced by the application of a 180° RF pulse; for the gradient echo methods, the event is produced by applying a magnetic field gradient (Sprawls, 2000).

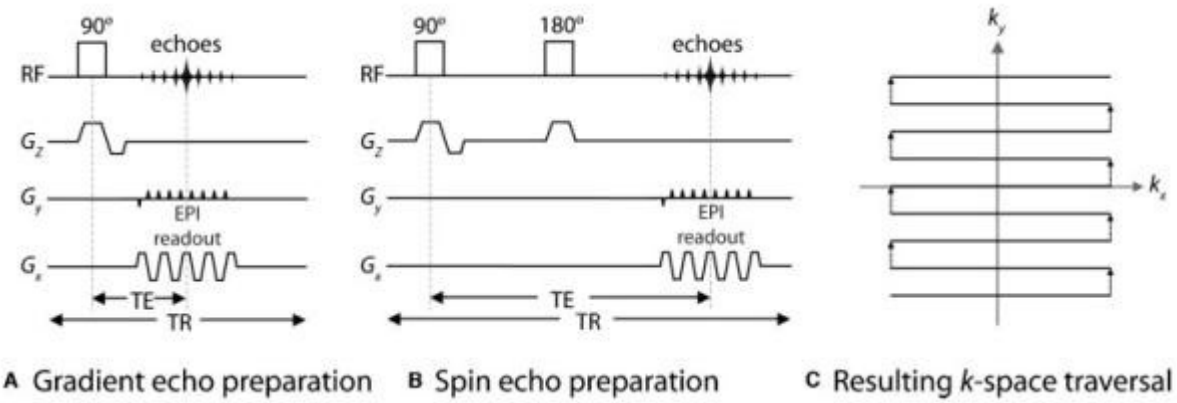

Figure A.3 *A typical echo planar pulse sequence timing diagram (EPI) from a gradient echo (A) and a spin echo RF excitation (B). Resulting imaging data, known as the EPI "k-space trajectory." (C). The gradients in Gz are the slice-select gradients. In the readout direction (Gx), the gradients oscillate rapidly between positive and negative values, corresponding to moving in opposite directions along the kx-axis. A strong "blip" in Gy (the phase-encoding direction) moves the k-space trajectory from one line to the next. Thus, the whole of k-space, corresponding to one complete image, is filled in one repetition (TR). TE is the echo time, determined by the distance from the middle of the 90-degree RF pulse to the centre of the largest echo (i.e., the centre of k-space). RF, radiofrequency (Holdsworth et al., 2008).*

Flip angle

Another parameter commonly used to describe an RF pulse is the flip angle. The flip angle is measured in radians or degrees and describes the nutation angle produced by the pulse ***(Figure A.4)***. For example, an excitation pulse that tips the longitudinal magnetization completely into the transverse plane has a flip angle of 90 degrees or n/2 rad. The application of an RF pulse generates a transition from the longitudinal magnetization phase to the transverse magnetization phase. This is generally known as the excitation process because the transverse magnetization represents a more unstable or "excited" state than longitudinal magnetization. The excitation pulse is characterized by a flip angle. A 90° excitation pulse converts all the existing longitudinal magnetization into transverse magnetization. This type of pulse is used in the spin echo process. However, there are methods that use excitation pulses with flip less than 90° (Sprawls, 2000). In fact, the gradient echo technique is generally used in combination with an RF excitation pulse that has a small flip angle of less than 90°. Small flip angles (<90°) convert only a fraction of the existing longitudinal magnetization into transverse magnetization and are used primarily to make the TR shorter and this, in turn, produces faster image acquisition.

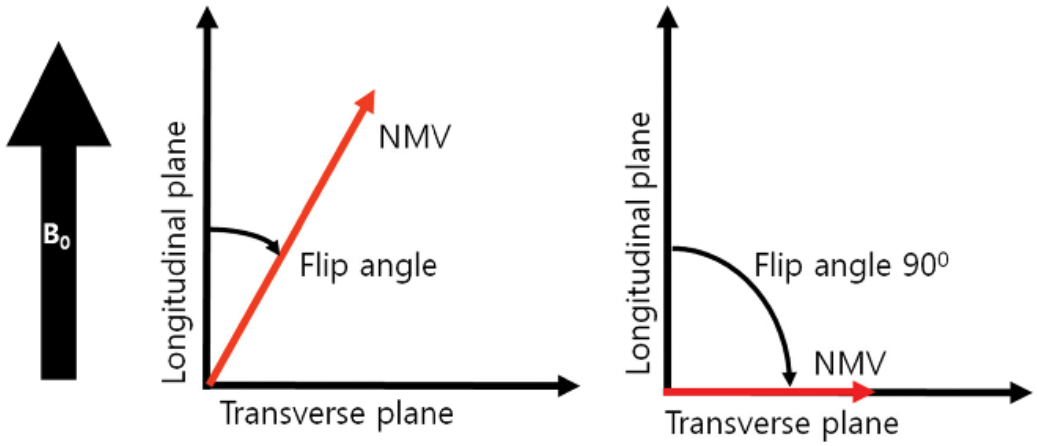

Figure A.4 *Different configurations of the flip angle (Kim and Kweon, 2016).*

A.2 Spin-echo process

The basic pulse sequence for the spin echo method is shown in ***Figure A.5.*** Each cycle begins with a 90° excitation pulse that produces the initial transverse magnetization and a later 180° pulse that rephases the protons to produce the echo event. The time between the initial excitation and the echo signal is TE (Sprawls, 2000).

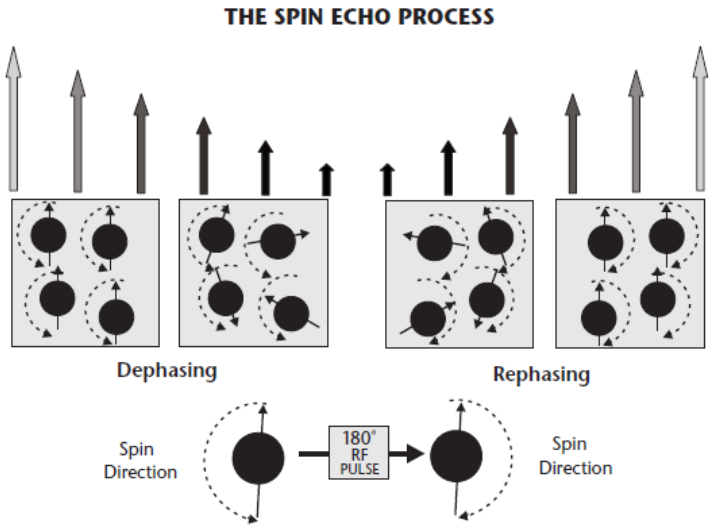

Figure A.5 *The 180° pulse sets up the protons so that they rephase (Sprawls, 2000).*

A.3 Gradient Echo Method

It is possible to produce an echo event by applying a magnetic field gradient to the tissue without using a 180° RF pulse, as in the spin echo methods. The primary advantage is that gradient echo methods perform faster image acquisitions. With the spin echo technique, an RF pulse is used to rephase the protons after they have been dephased by inherent magnetic field inhomogeneities and susceptibility effects within the tissue. With the gradient echo technique, the protons are first dephased, on purpose, by turning on a gradient and then rephased by reversing the direction of the gradient, as shown in ***Figure A.6***. First, transverse magnetization is produced by the excitation pulse and then immediately begins to decay (the free induction decay, FID, process) because of the magnetic field inhomogeneities within each individual voxel. A short time after the excitation pulse a gradient is applied, which produces a very rapid dephasing of the protons and reduction in the transverse magnetization, since a gradient is a forced inhomogeneity in the magnetic field. Subsequently the direction of the applied gradient is reversed. Even though this still represents an inhomogeneity in the magnetic field, it is in the opposite direction causing the rephasing of the protons and the production of an echo event. The TE is determined by adjusting the time interval between the excitation pulse and the gradients that produce the echo event (Sprawls, 2000).

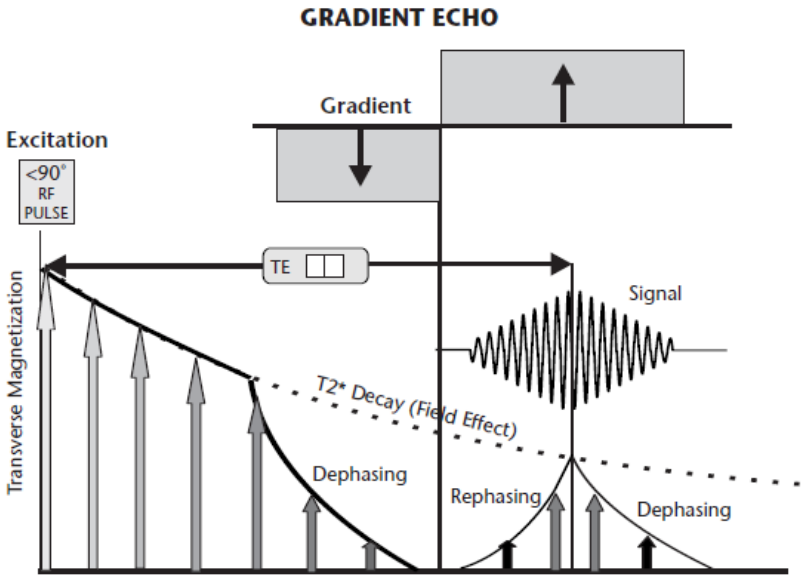

Figure A.6 *The gradient echo process using a magnetic field gradient to produce an echo event during the FID (Sprawls, 2000).*

A.4 Echo-planar imaging

The EPI technique was proposed by the British physicist Peter Mansfield in 1976. Echo-planar imaging collected data from an entire image slice at one time, by sending one electromagnetic pulse from a transmitter coil and then introducing rapidly changing magnetic field gradients while recording the MR signal. The resulting complex MR signal could be reconstructed into an image using Fourier analysis techniques. Echo-planar imaging reduced the time needed to collect a single image from minutes down to fractions of a second greatly improving the feasibility of clinical imaging. Concepts derived from echo-planar imaging underlie the most important approaches to MRI even today, especially for fMRI studies, due to the need for fast imaging to measure changes in brain function (Huettel et al., 2008). For anatomical images of the brain, contrast is more important than speed of acquisition, since structural parameters such as size and shape change little over the course of a single scanning session. However, understanding the function of the brain requires images to be acquired very rapidly, at approximately the same rate as the physiological changes of interest. Fast pulse sequences have been developed that acquire a very large number of images within a short period of time (Huettel et al., 2008). The EPI method consists of rapid, multiple gradient echo acquisitions executed during a single spin echo event. The unique characteristic of this method is that each gradient echo signal receives a different spatial encoding and is directed into a different row of k space (Sprawls, 2000). This ultra-fast technique can produce video-frequency tomographic images (15-30 images per second). The scan sequence commonly used in fMRI studies of the brain is the *Gradient-Echo Echo Planar Imaging* (GE-EPI) sequence. The cycle usually begins with a spin echo pulse sequence that produces a spin echo event consisting of a period of transverse magnetization. In conventional spin echo imaging, only one signal (fill one row of k space) is obtained from this period of magnetization. Through this technique one spin echo event is split into many shorter gradient echo events. The signals from each gradient echo event will receive different spatial encodings and fill different rows of k space (Sprawls, 2000).

Appendix B Functional Processing

B.1 Creation of an AMR project

In this Appendix, all the steps performed on the functional data are shown. Before to proceed with the steps, it is necessary to create the anatomical project (AMR) ***(Figures B.1-B.4)*** and the volumetric one (VMR). A new AMR Project can be created by selecting in the menu **File → Create Project Wizard.** A window will appear, and the AMR project option should be selected. After choosing the correct data type, it is necessary to set the name of the project and select the folder in which data file is contained.

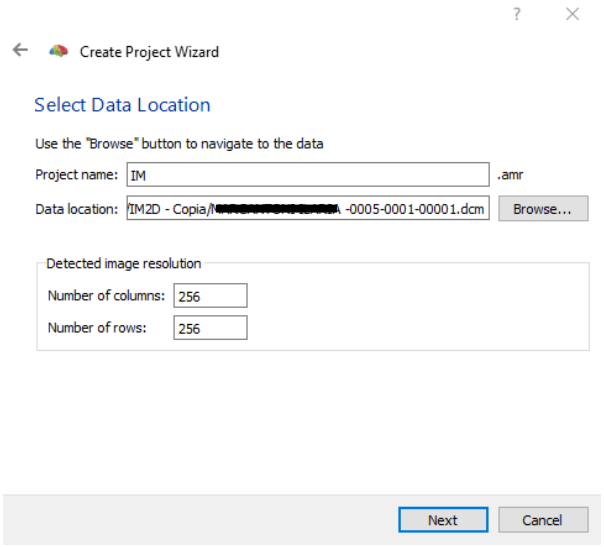

Figure B.1 *The figure shows the creation of the AMR project. Project name and the folder which contains the DICOM files are set.*

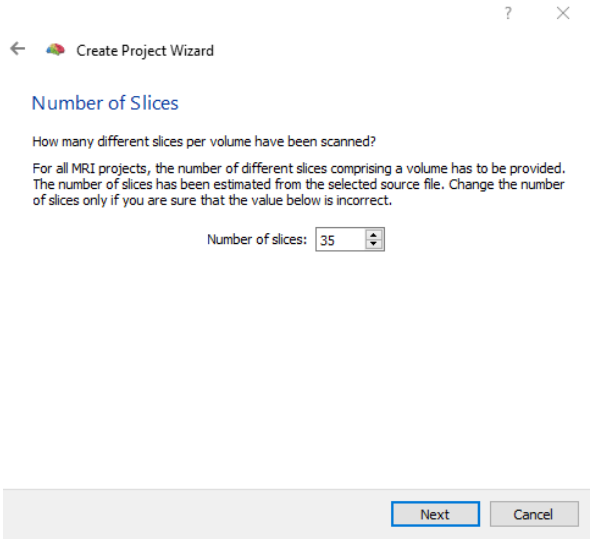

Figure B.2 *Number of slices contained into the 2D data acquisition.*

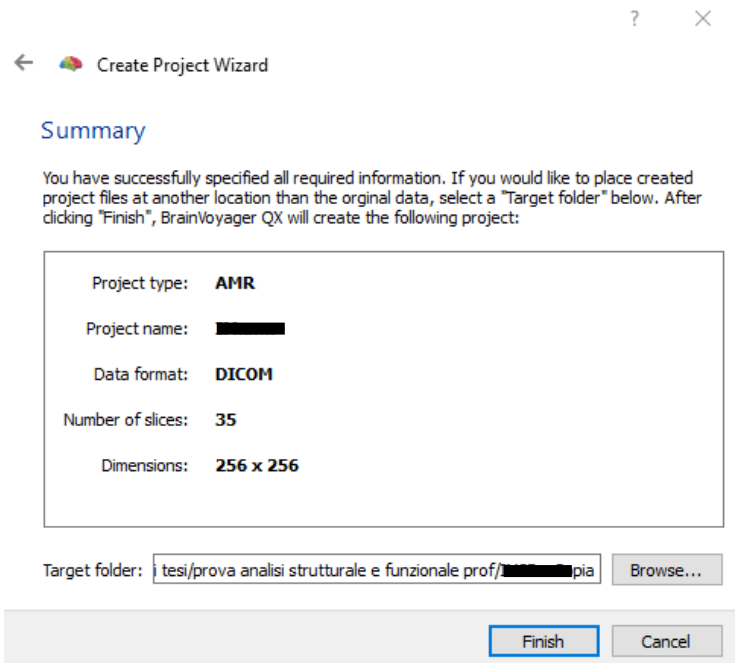

Figure B.3 *Summary of the AMR project.*

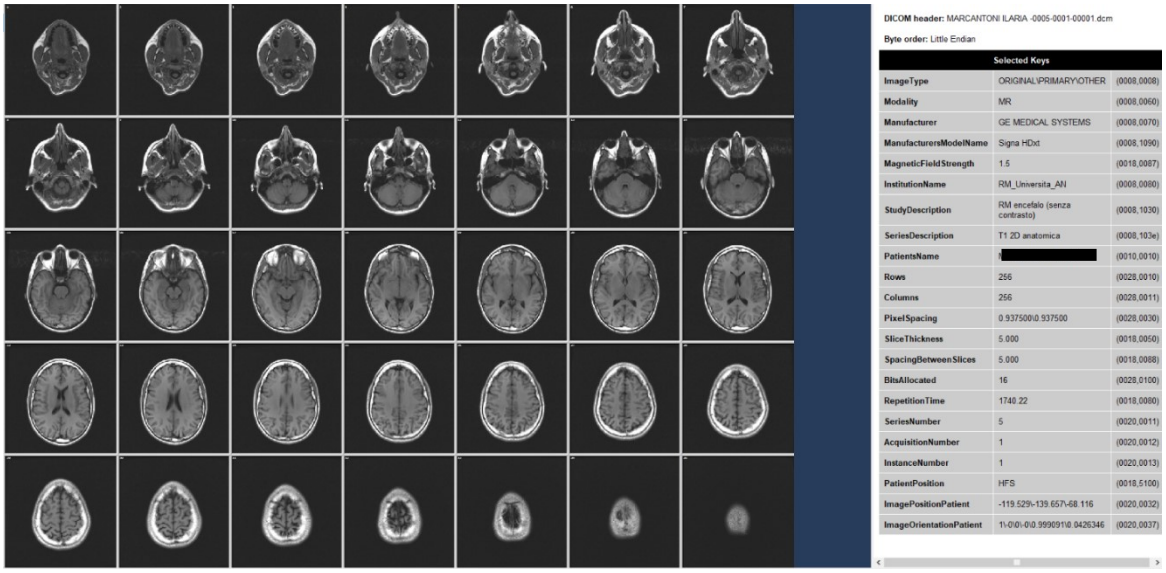

Figure B.4 *Visualization of the AMR project data (left panel) and related information (right panel).*

B.2 Creation of a VMR project

In this step a 3D anatomical project will be created ***(Figures B.5-B.7)***. The 3D data set will be used for co-registration with the functional data.

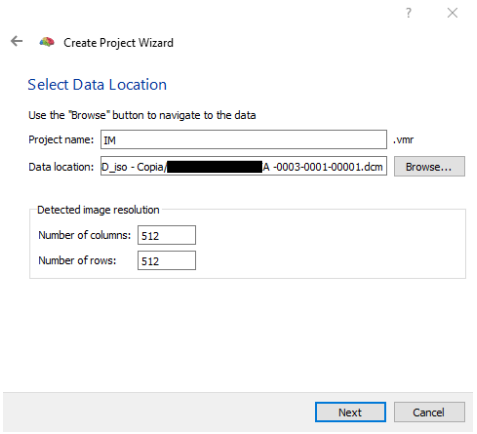

Figure B.5 *The figure shows the creation of the VMR project. Project name and the folder which contains the DICOM files are set.*

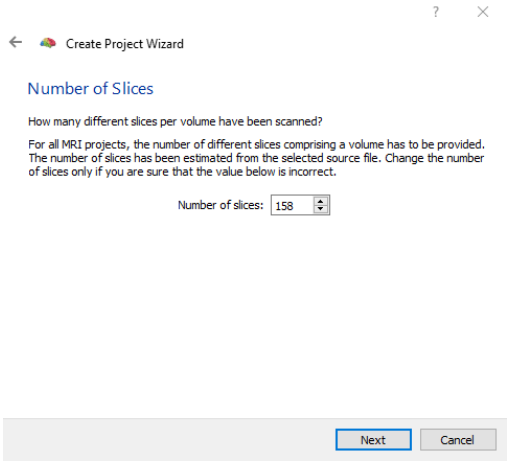

Figure B.6 *Number of slices contained into the 3D data acquisition.*

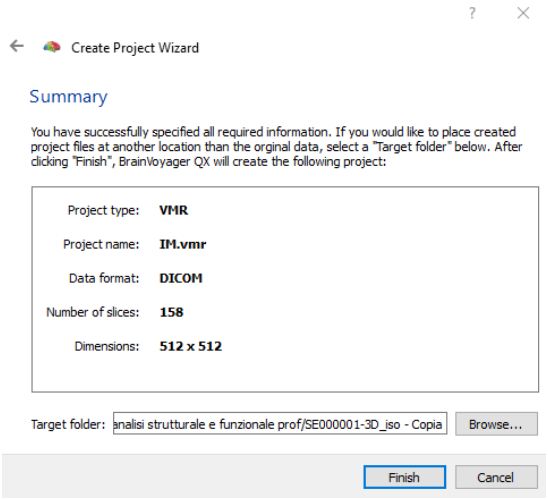

Figure B.7 *Summary of the VMR project.*

After the creation of a VMR project, the following image will appear. It is possible to note that the voxel dimensions are not equal in the x, y and z directions. According to this, an iso-voxel transformation must be performed ***(Figure B.8)***.

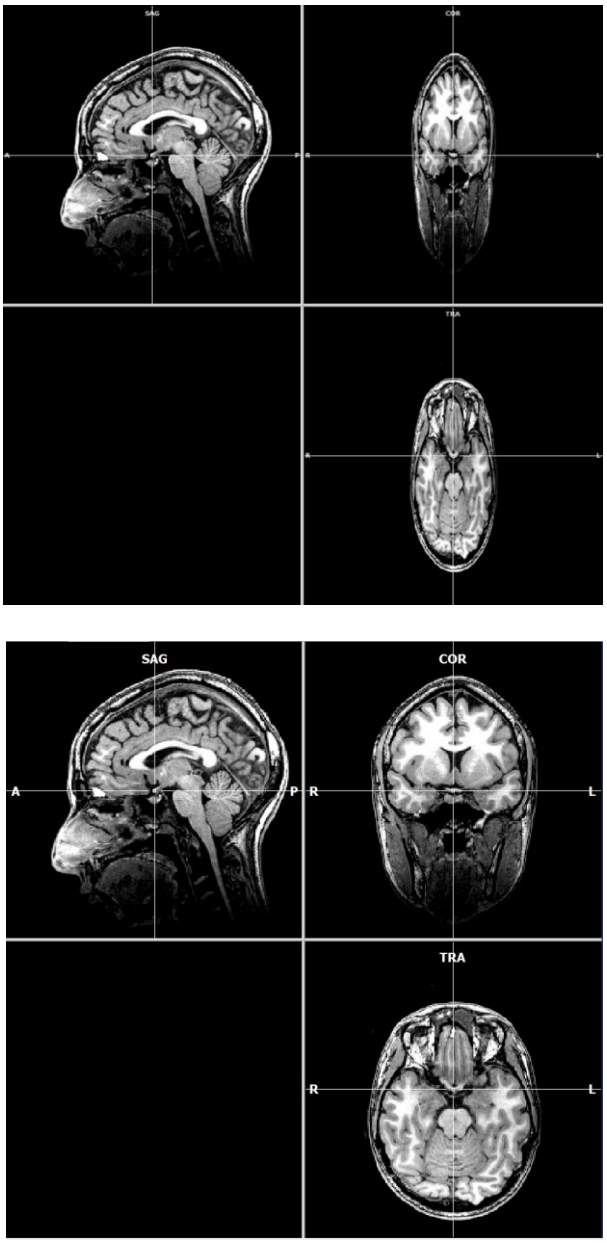

Figure B.8 *ISO-Voxel transformation. Top panel shows data before transformation, while the bottom panel illustrates the image after the iso-voxel transformation. The interpolation option used was the Trilinear.*

B.3 Intensity inhomogeneity correction

Intensity inhomogeneities in the image might have negative effects on the outcome of co-registration and segmentation procedures. According to this, the quality of anatomical data set must be improved by applying automatic intensity inhomogeneity correction ***(Figures B.9, B.10)***. Select the file ISO.vmr and click on **"Intensity inhomogeneity correction"** in the **"Volumes"** menu.

The automatic intensity inhomogeneity correction includes 4 steps:

1. Background cleaning (all intensities of voxels in the background are set to 0)
2. Brain extraction (the brain is segregated from the head tissue)
3. White matter detection
4. Bias field estimation within white matter voxels (voxels labelled as white matter are used to estimate the variability of white matter intensities across 3D image space).

The white matter detection and bias field estimation is usually applied several times to improve the result; by default, the **"No. of cycles:"** entry in the **"Intensity inhomogeneity correction (IIHC)"** field, is 2. Click the **"GO"** button to start the inhomogeneity correction.

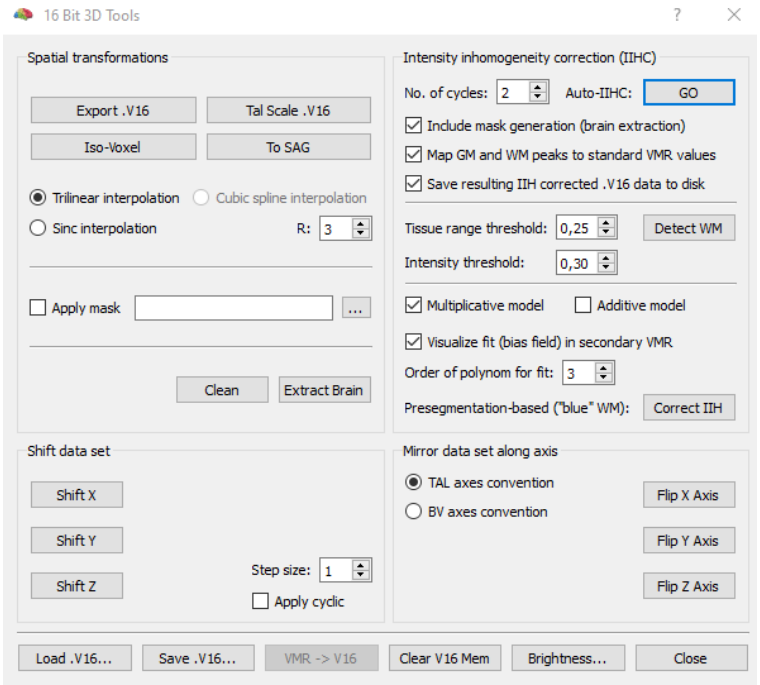

Figure B.9 *Intensity inhomogeneity correction panel.*

For each step of the intensity inhomogeneity correction process BV saves one new file in the same folder as the original .vmr file. The result of the intensity inhomogeneity correction procedure is a more homogeneous and peeled VMR data set.

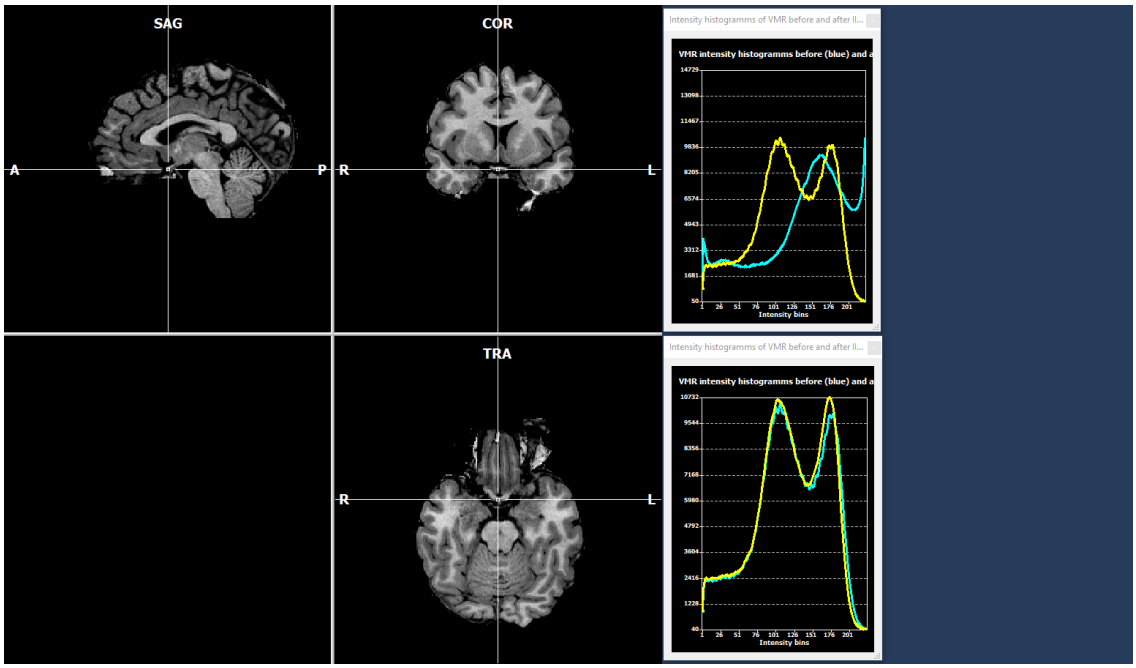

Figure B.10 *Results of the IIHC step.*

B.4 Functional analysis steps

The first step consists of importing the data into BV QX by creating a project. Select **"File" → "Create Project Wizard..."** in the toolbar ***(Figure B.11)***.

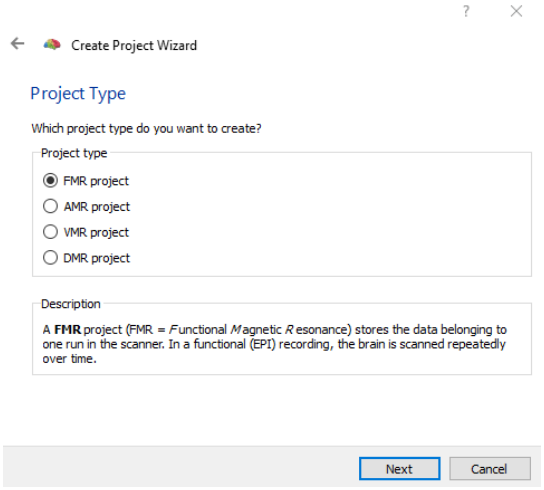

Figure B.11 *Creation of a new FMR project.*

After choosing the correct data type, it is necessary to set the name of the project and select the folder in which data file is contained. In the next window the number of recognised volumes is shown. Since the first volume scans in a functional run contain data with very high intensity values (due to T1 saturation), it is recommended to skip a few volumes (e.g., 2-4) ***(Figure B.12)***. Despite skipping volumes for analysis, BV QX will use the first volume for display since it contains more anatomical information than later volume scans (Goebel et al.,2011).

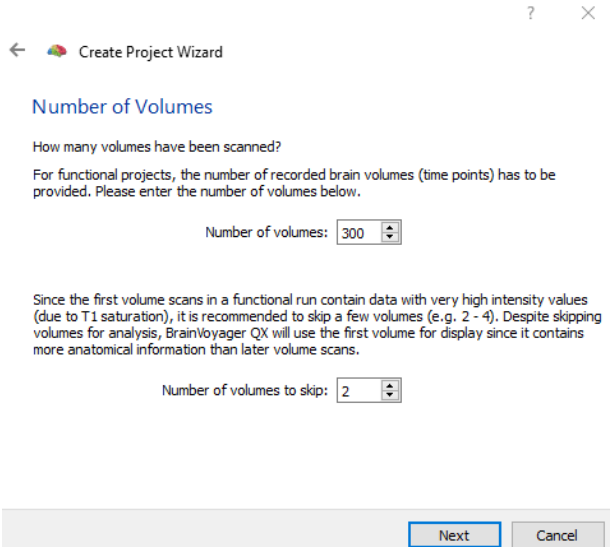

Figure B.12 *Number of volumes contained in the functional data and the number of volumes that it is recommended to skip.*

The Create Project Wizard ends with an overview containing the most important settings ***(Figures B.13, B.14)***.

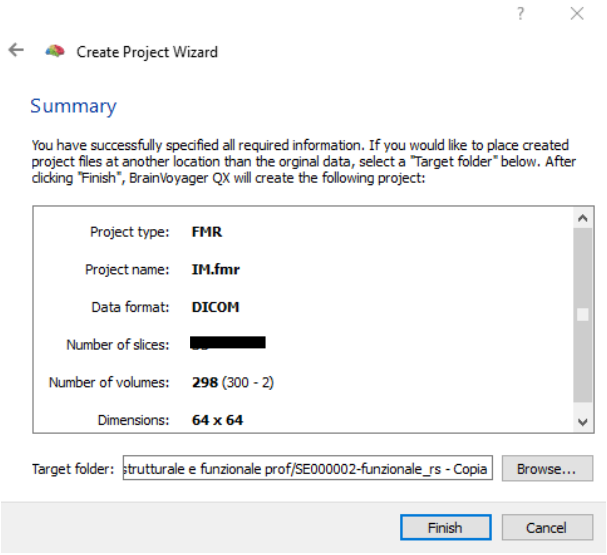

Figure B.13 *Summary of the FMR project.*

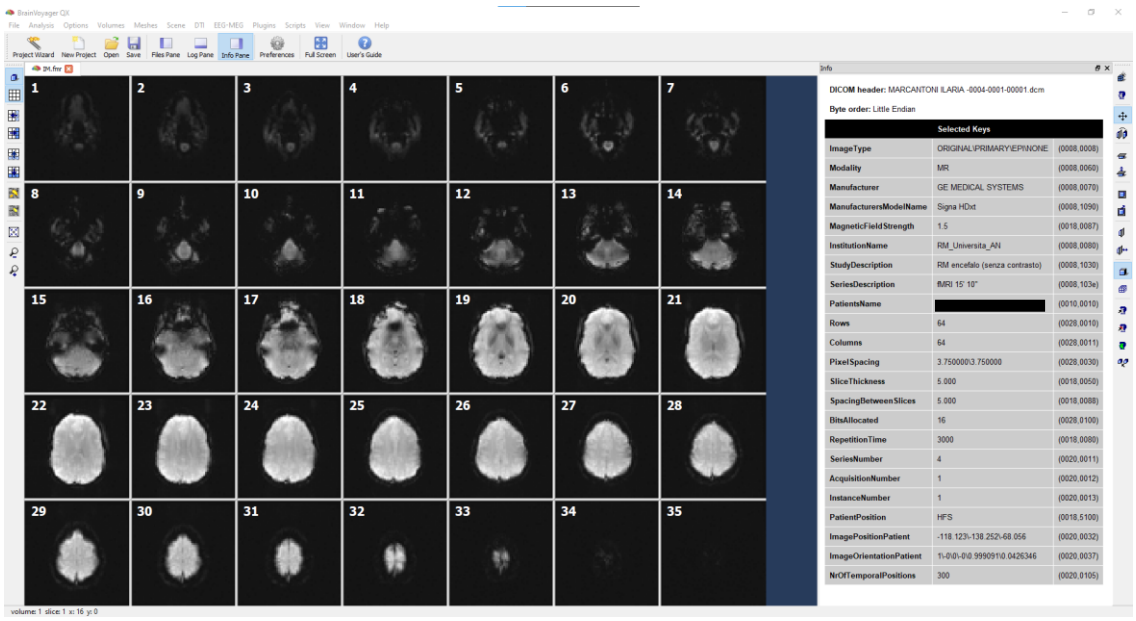

Figure B.14 *Illustration of the functional data (right panel) and related information (left panel).*

After the creation of the FMR project, the **"FMR Properties"** dialog, shown above, is opened automatically. This dialog allows you to inspect and modify the relevant information of the FMR project ***(Figure B.15)***. You can call this dialog at any time via the menu item: **"File" → "FMR Properties..."**.

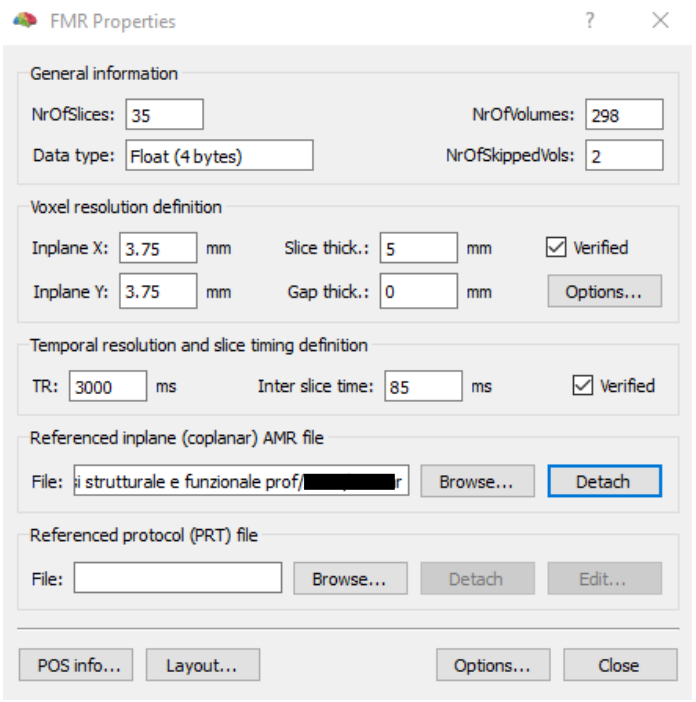

Figure B.15 *FMR Properties panel.*

A reference inplane AMR file must be linked to the functional project, by selecting the file created before ***(Figure B.16)***.

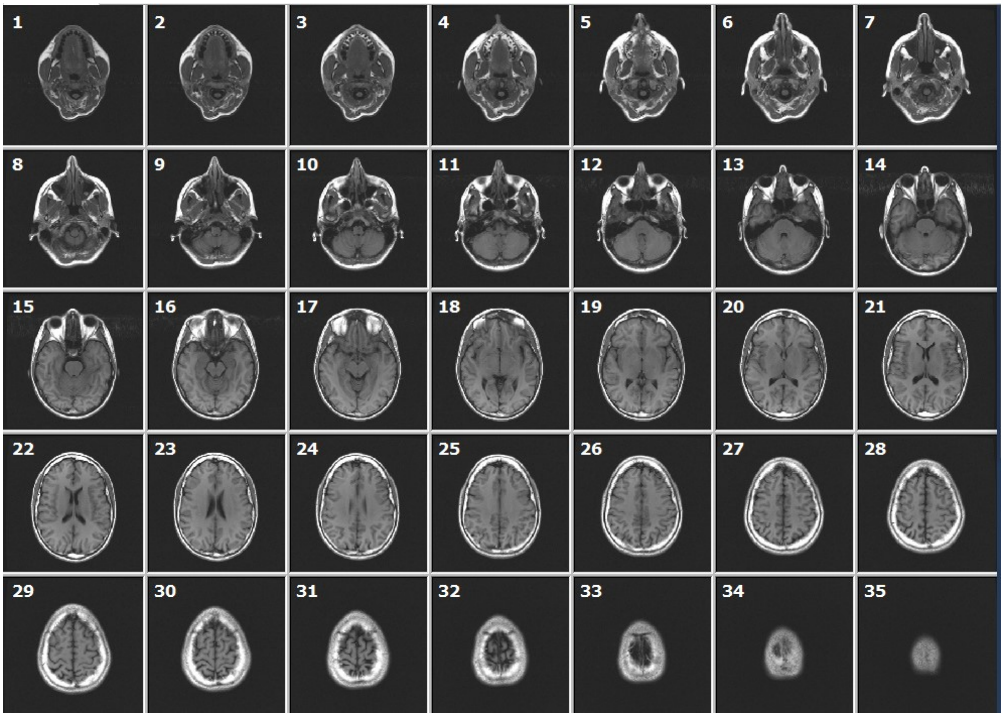

Figure B.16 *Visualization of the FMR Project with the linked AMR.*

B.5 Functional data Preprocessing

To improve the quality of the data, the preprocessing must be performed. Select **"FMR Data Preprocessing..."** in the **"Analysis" menu.** This will invoke the "**FMR Data Preprocessing**" dialog. There are several preprocessing options like **"Slice scan time correction"**, **"3D motion correction"** and so on ***(Figure B.17)***.

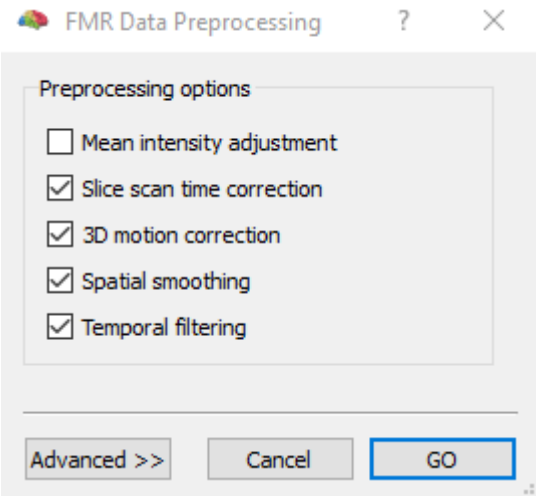

Figure B.17 *FMR Data Preprocessing panel.*

The expanded dialog ***(Figure B.18)*** shows more detailed information about the chosen preprocessing options: 3D motion correction will be performed on our functional data; in addition, it will be spatially smoothed and linear (and nonlinear) trends ("drifts") in the data will be removed. Click the **"GO"** button to run the specified preprocessing options.

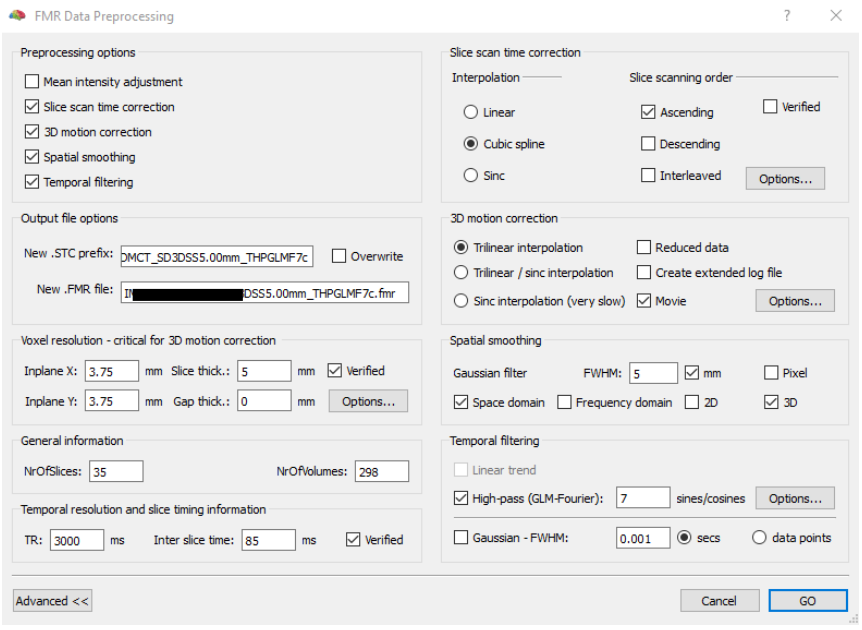

Figure B.18 *Parameters used for each Preprocessing step.*

Parameters used during pre-processing are included in the name of the resulting file.

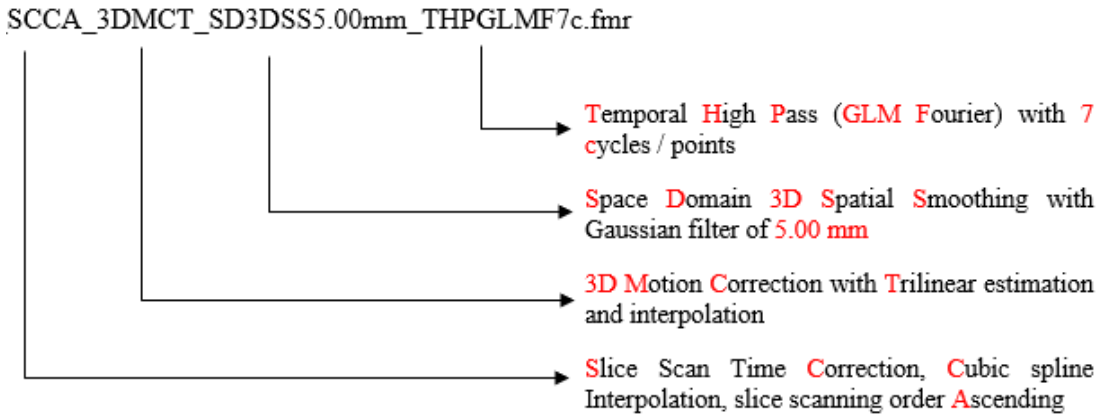

BV QX shows a graphical representation of the ongoing 3D motion correction. A specified volume serves as the reference (the first as default) to which all other volumes are aligned in space by rigid body transformations. The detected head motion of a volume with respect to the reference volume results in 3 translation and 3 rotation parameters. The six estimated parameters are displayed incrementally in a time course graph ***(Figure B.19)***. The 3 translation and 3 rotation parameters are color-coded as follows:

red -> translation in X direction,
green -> translation in Y direction,
blue -> translation in Z direction,
yellow -> rotation around X axis,
magenta -> rotation around Y axis,
cyan -> rotation around Z axis.

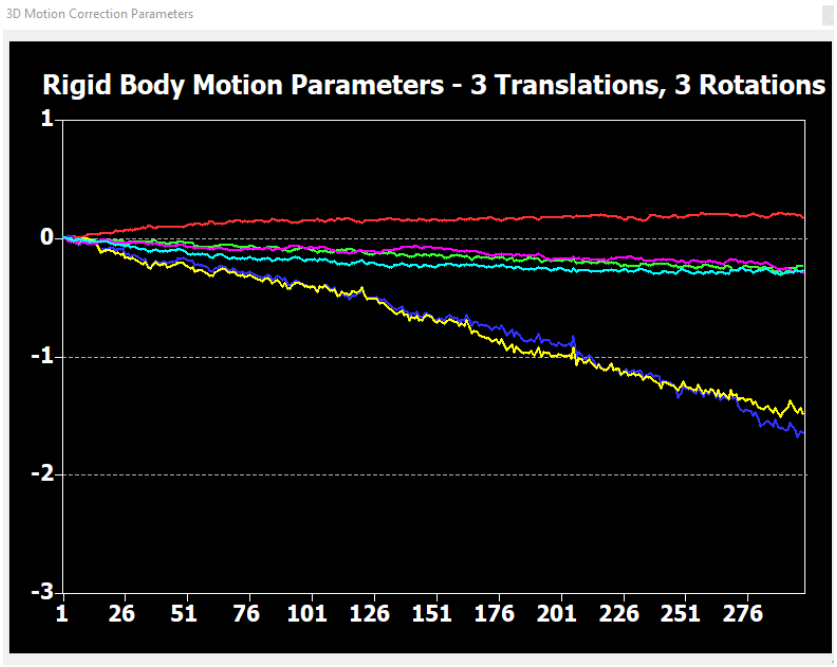

Figure B.19 *Visualization of the six estimated parameters, during the Motion Correction step.*

The axes are defined in image space (i.e., not in Talairach space): X refers to the image left-to-right direction, Y refers to top-to-bottom direction and Z refers to direction across slices (first-to-last image).

B.6 Coregistration of functional and anatomical data

In this step, functional slice-based data of an FMR project are aligned with a 3D data set. This allows us to relate brain activity more easily to anatomical locations and it prepares the transformation of the functional data into stereotaxic (Talairach) space (Goebel et al., 2011). Open the IIHC.vmr file, created before, and by clicking on the "**3D Volume Tools**" dialog, select the **"Coregistration"** tab to switch to the options needed for the task ***(Figure B.20)***.

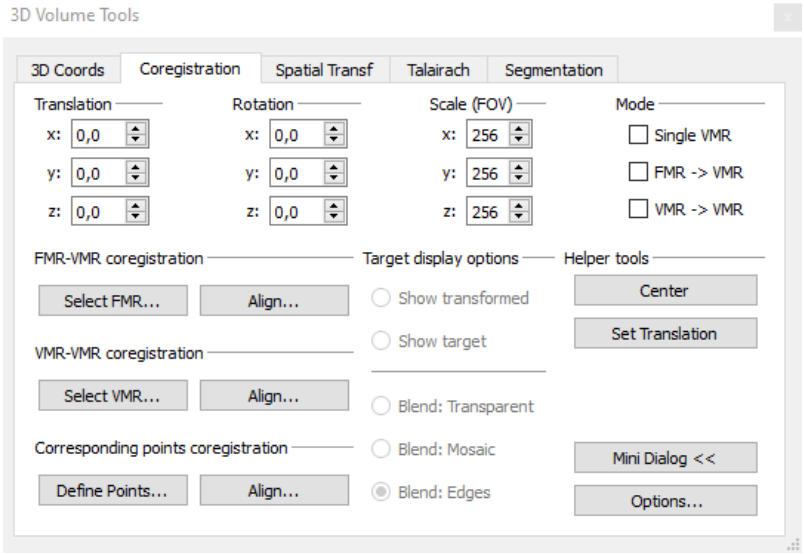

Figure B.20 *3D Volume Tools dialog.*

Click the **"Select FMR..."** button in the **"FMR-VMR coregistration"** field and then select the .fmr file. After selecting the file, the functional data is still in a different orientation than the anatomical data set. This will be corrected by clicking the **"Align"** button in the **"FMR-VMR coregistration"** field. BV QX automatically proposes file names for the .trf files that will hold the information of the Initial Alignment and Fine-Tuning Alignment ***(Figure B.21)***. These files will be saved when the alignment is finished. To start the mathematical initial alignment and the gradient-based affine alignment (for fine-tuning), press the **"GO"** button.

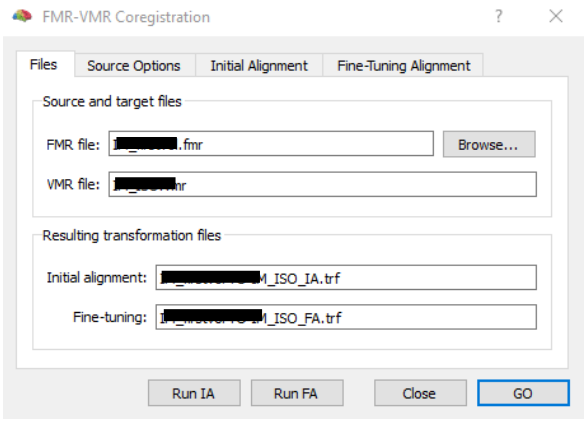

Figure B.21 *FMR-VMR Coregistration panel.*

It is important to evaluate the co-registration by checking whether the co-registered functional data indeed matches the corresponding anatomical data. This can be done by browsing to various regions in the data set and by switching between different display views. The display option **"Blend: Edges"** is marked by default, which shows the "edge" display of the co-registered functional data overlayed in green on top of the anatomical data in the co-registration row ***(Figure B.22)***.

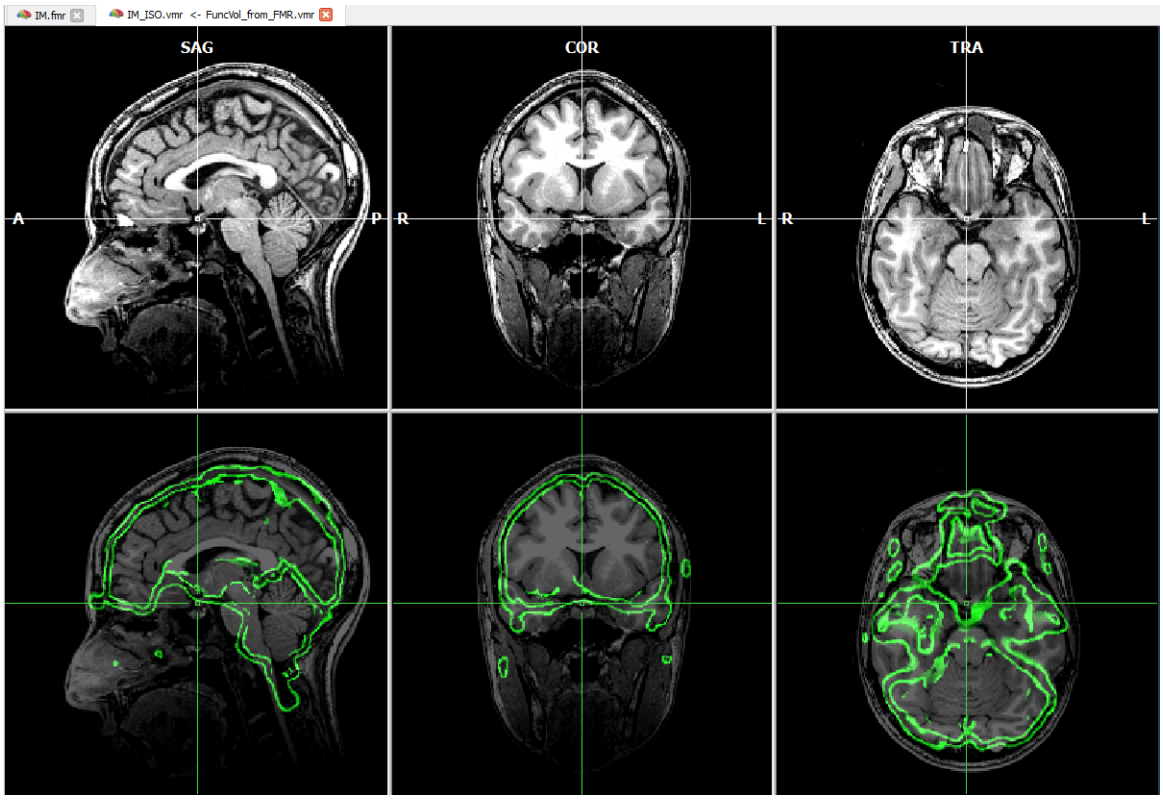

Figure B.22 *Results of the co-registration step.*

B.7 Manual Talairach transformation

In this step, the 3D data set will be transformed into Talairach space, which is a commonly used "standard" space for reporting locations of activated brain regions and for averaging data across subjects (Goebel et al., 2011). Talairach transformation is performed in two major steps. In the first step, the cerebrum is translated and rotated into the AC-PC plane (AC = anterior commissure, PC = posterior commissure). In the second step, the borders of the cerebrum are identified; in addition, with the AC and PC points, the size of the brain is fitted into standard space. These steps are performed in the **"Talairach"** tab of the **"3D Volume Tools"** dialog. Switch to the **"Talairach"** tab of the **"3D Volume Tools"** dialog and switch from **"Automatic"** to **"Manual"** AC-PC transformation ***(Figure B.23)***.

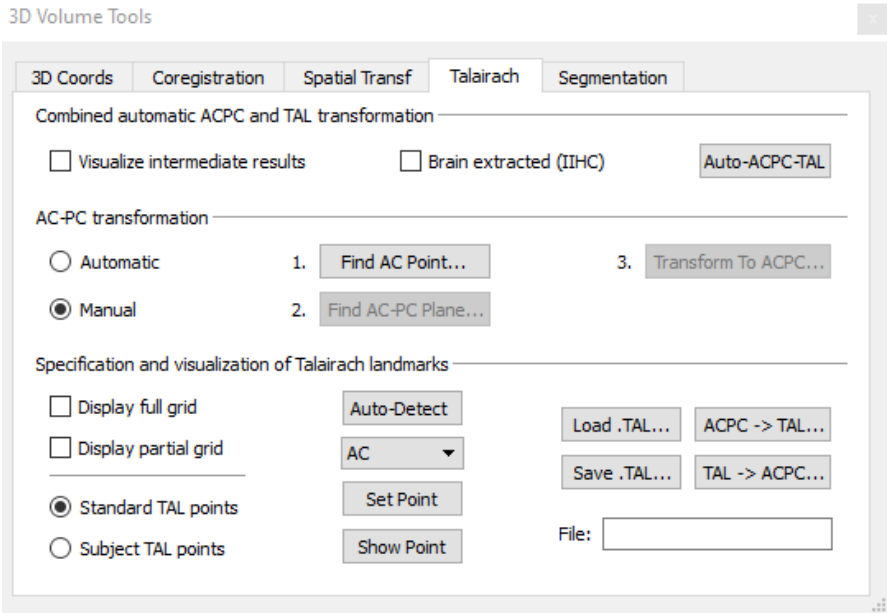

Figure B.23 *Talairach tab of the 3D Volume Tools. The "manual" AC-PC transformation must be selected.*

Click the **"Find AC Point…"** button in the **"Talairach"** tab of the **"3D Volume Tools"** dialog. Now is it possible to define translation parameters, necessary to move the original centre of the 3D data set to the AC point, which will become the new centre of the transformed data set ***(Figure B.24)***.

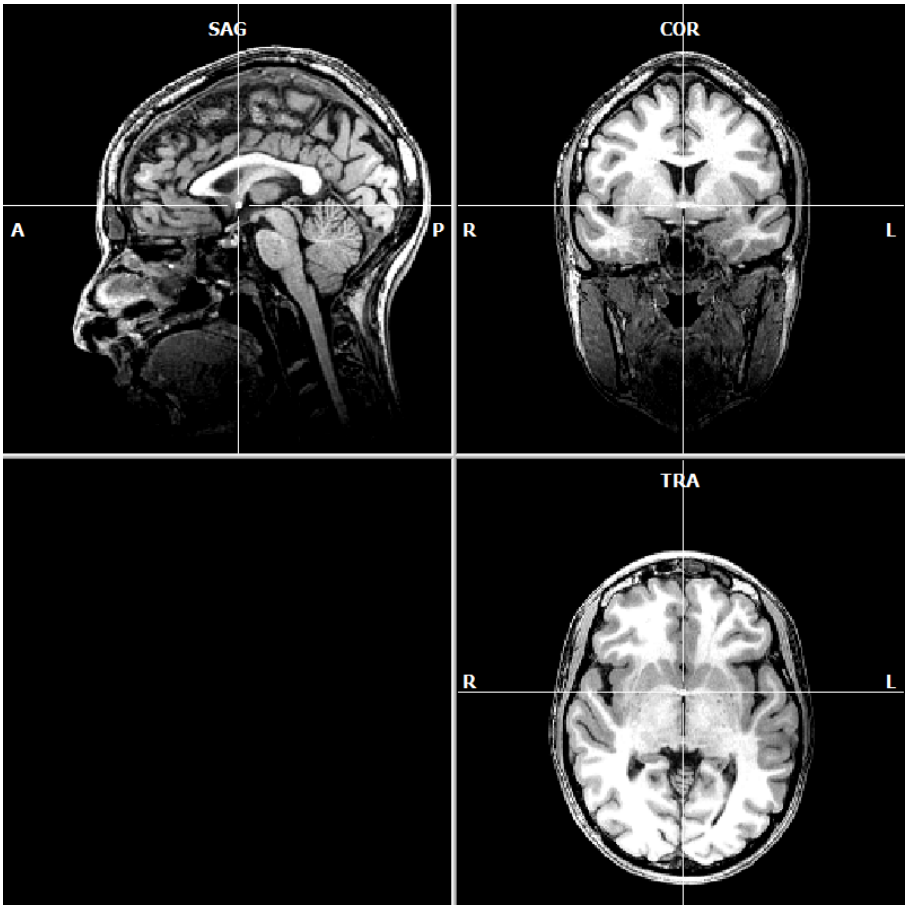

Figure B.24 *Visualization of the AC point.*

After having specified the AC point, the **"Find AC Point"** button is disabled and the **"Find AC-PC Plane..."** button is enabled. The next task is to rotate the data set in such a way that we also see the posterior commissure in the axial slice. To find the posterior commissure, click the **"Find AC-PC Plane..."** button ***(Figure B.25)***.

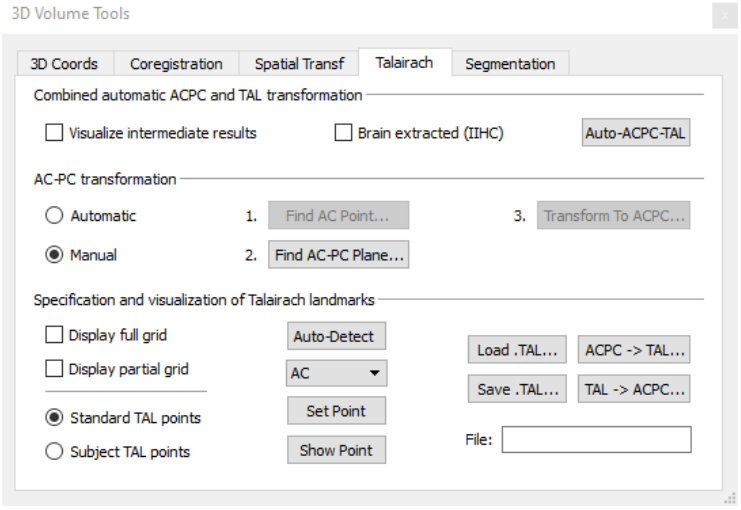

Figure B.25 *Talairach tab of the 3D Volume Tools. The "Find AC-PC plane" option must be selected.*

Use the **"x"** spin control in the **"Rotation"** field to rotate the dataset in the sagittal plane (lower left in ***Figure B.26***), until the view shows the posterior commissure. Then, by using the **"y"** and **"z"** spin controls, the dataset is rotated in the coronal and axial planes, respectively, to correctly position the brain in the Talairach space.

AC- PC PLANE

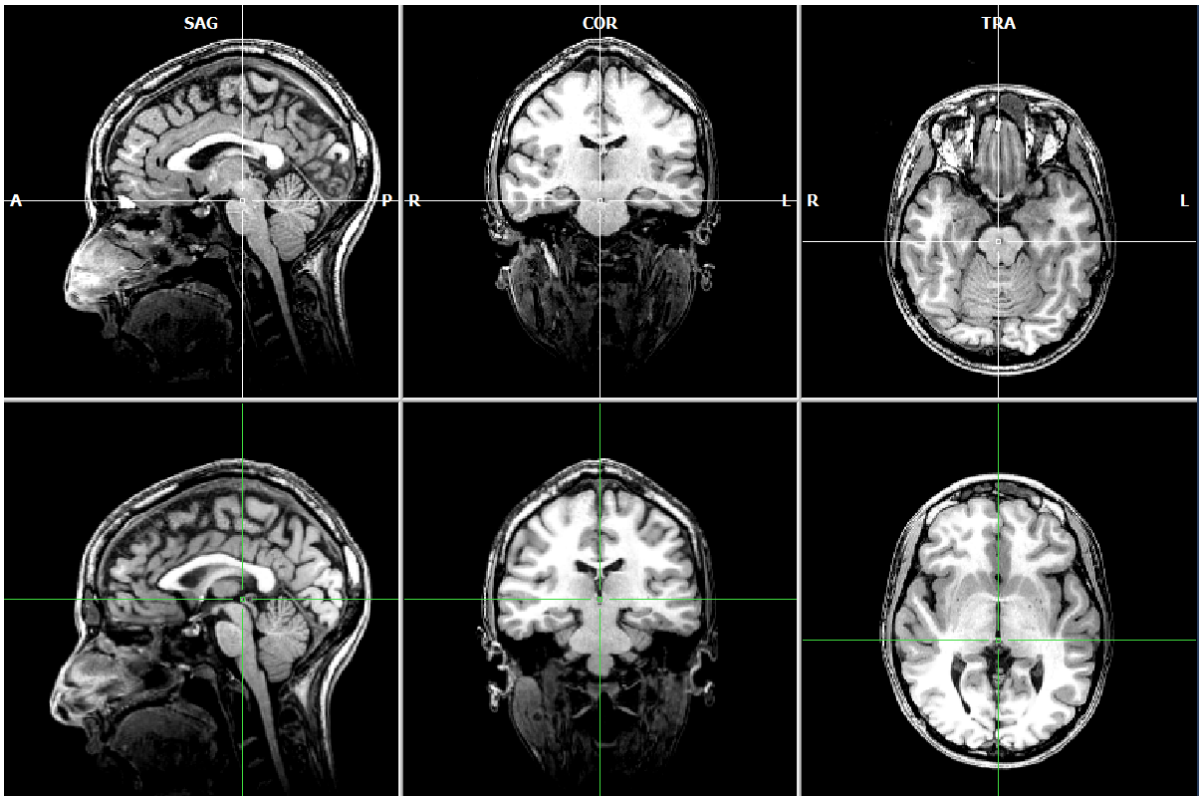

Figure B.26 *Individuation of the AC-PC plane.*

After having specified the AC-PC plane, the **"Find AC-PC Plane"** button is disabled and the **"Transform to ACPC"** button in the **"AC-PC transformation"** field of the **"Talairach"** tab is enabled. To save the specified transformation (translation and rotation values) and to apply them to the 3D data set, click the **"Transform to ACPC..."** button. After clicking the **"Transform to ACPC..."** button a **"Spatial Transformation of VMR"** dialog opens automatically. BV QX will suggest the filename (ACPC suffix), which is used to name both the spatial transformation (TRF) file as well as the resulting VMR file ***(Figure B.27)***. The TRF file *specifies* a desired spatial (rigid body) transformation while the resulting VMR file is the result of the *application* of the spatial transformation (Goebel et al.,2011). After a few seconds the resulting new 3D volume it is shown automatically in a new window. The centre of the new data set is now the AC point, and the brain is located in the AC-PC plane ***(Figure B.28)***.

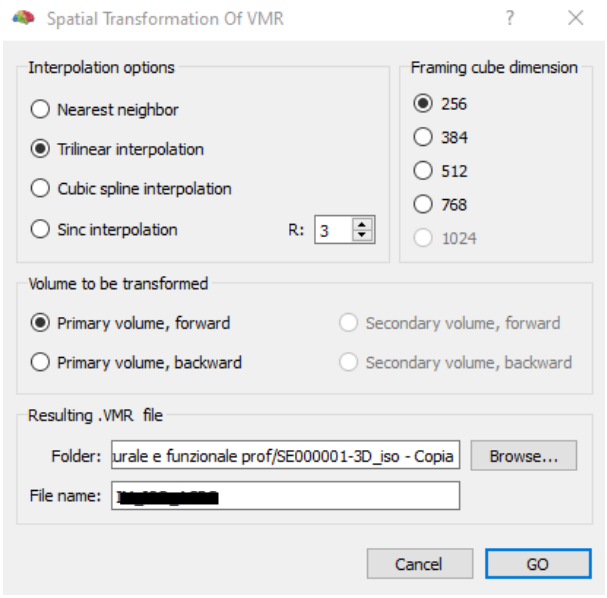

Figure B.27 *AC-PC spatial transformation window.*

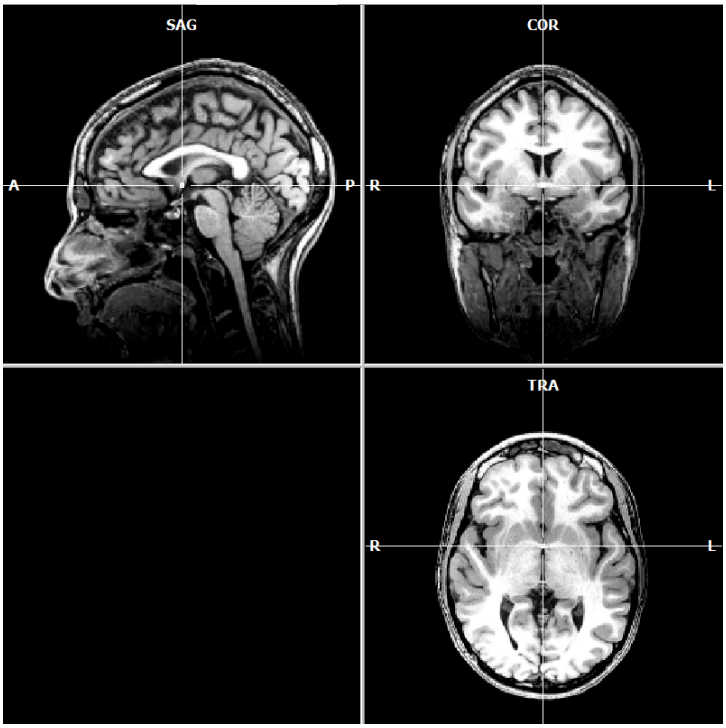

Figure B.28 *Visualization of the resulting new 3D volume. The centre of the new data set is the AC point, and the brain is located in the AC-PC plane.*

In the second step of Talairach transformation, eight *reference points* have to be specified within the ACPC transformed data set: *AC*, *PC*, *AP* (the most anterior point of the cerebrum), *PP* (the most posterior point), *SP* (the superior point), *IP* (the inferior point), *RP* (the most right point) and *LP* (the most left point) ***(Figure B.29)***. Switch to the **"Talairach"** tab of the **"3D Volume Tools"** dialog.

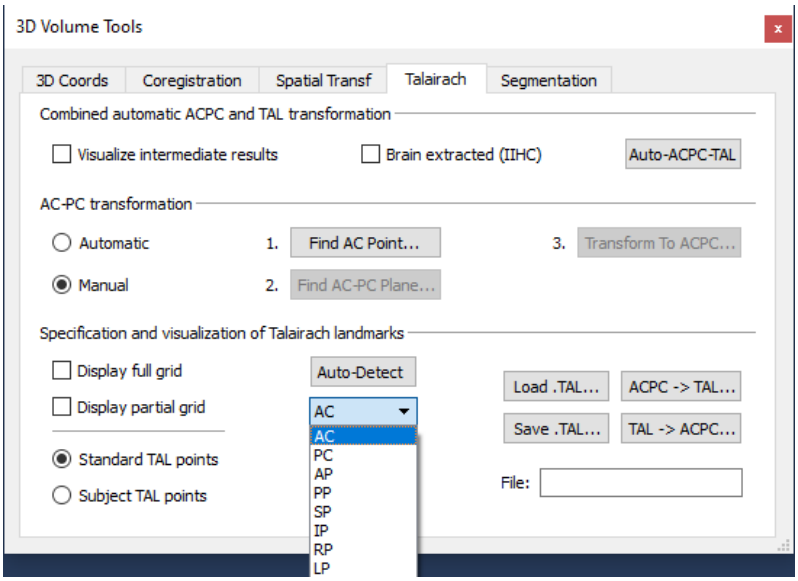

Figure B.29 *Specification and visualization of Talairach landmarks.*

Click on the **"Talairach reference points"** list box in the **"Specification and visualization of Talairach landmarks"** field. The first reference point is **"AC"**, which has not to be specified again. Select the **"PC"** reference point. This point is easy to find in the data set because it must be in the same axial plane as **"AC"**. Click the **"Set point"** button to define the **"PC"** point as the current location of the white cross. All the eight reference points are illustrated in the following figures ***(Figures B.30-B.35)***.

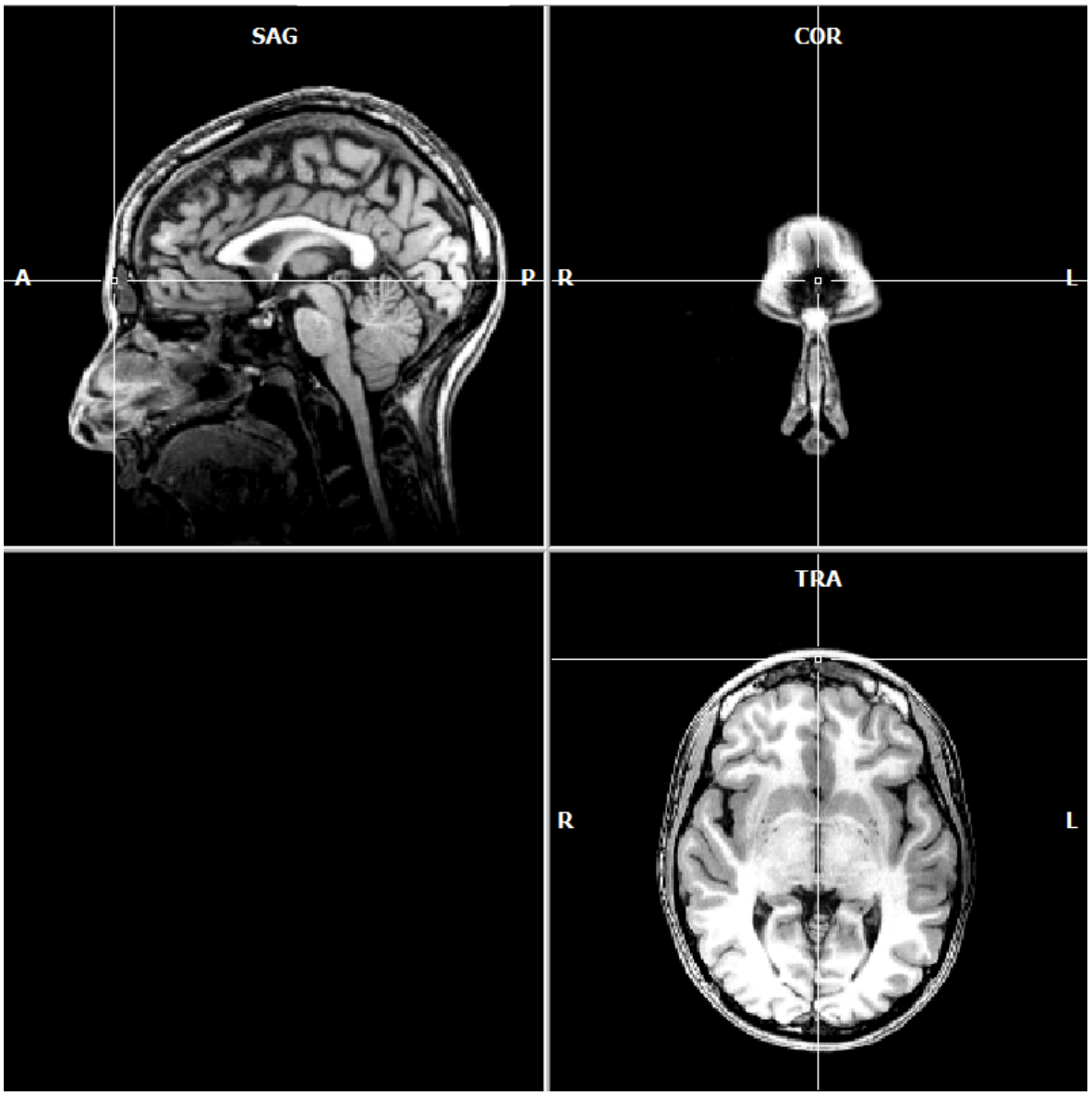

Figure B.30 *Visualization of the AP point.*

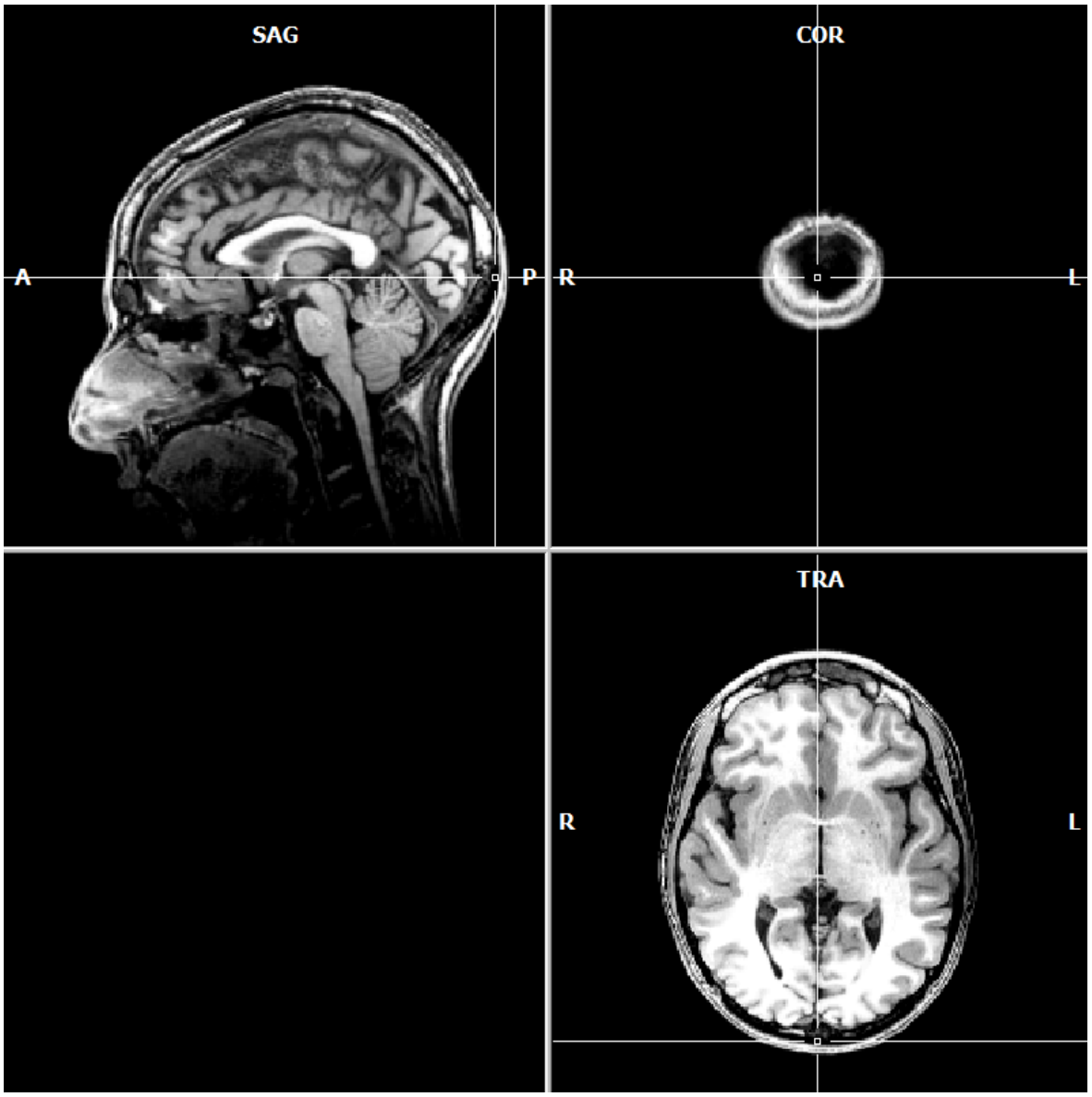

Figure B.31 *Visualization of the PP point.*

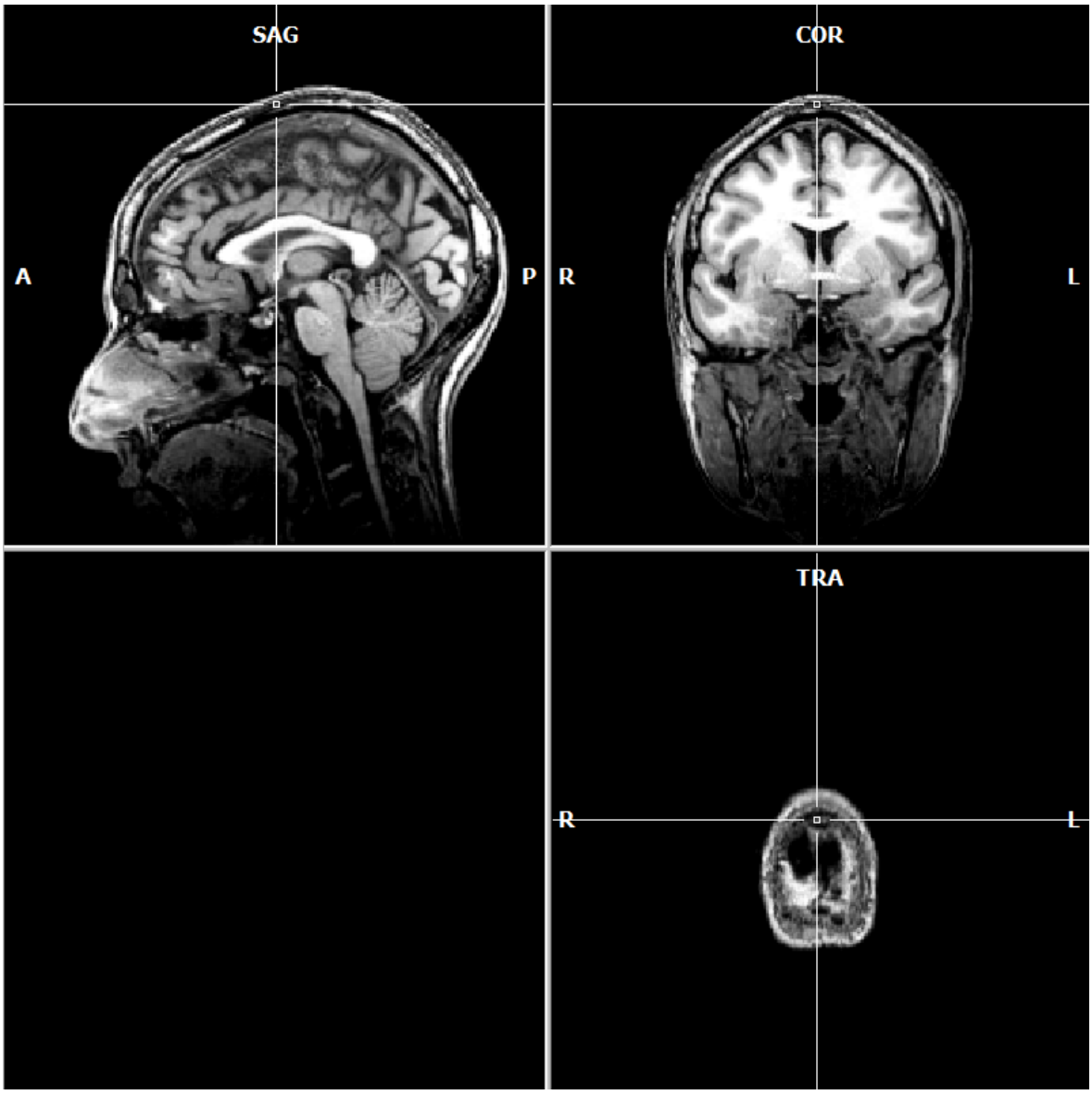

Figure B.32 *Visualization of the SP point.*

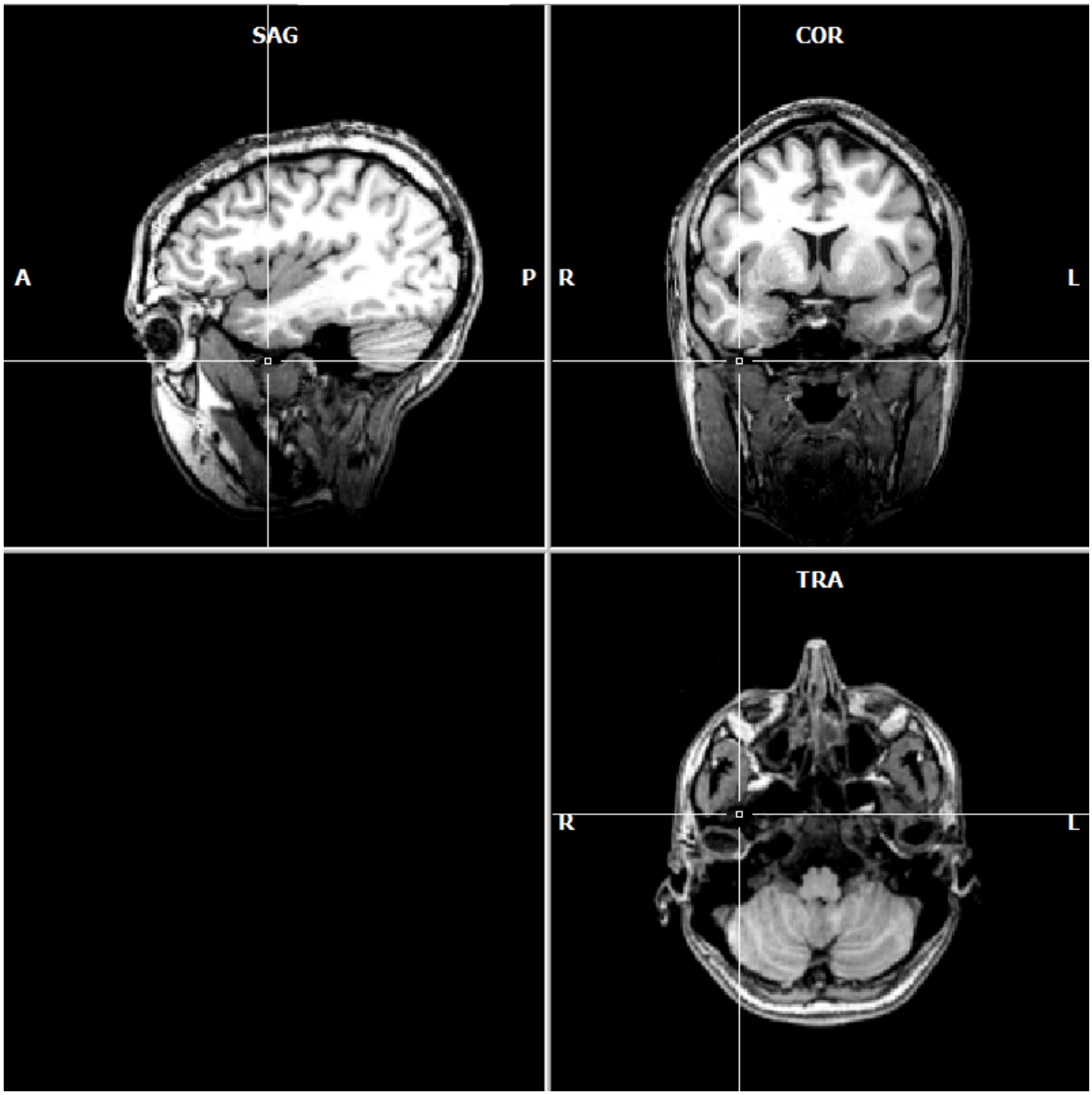

Figure B.33 *Visualization of the IP point.*

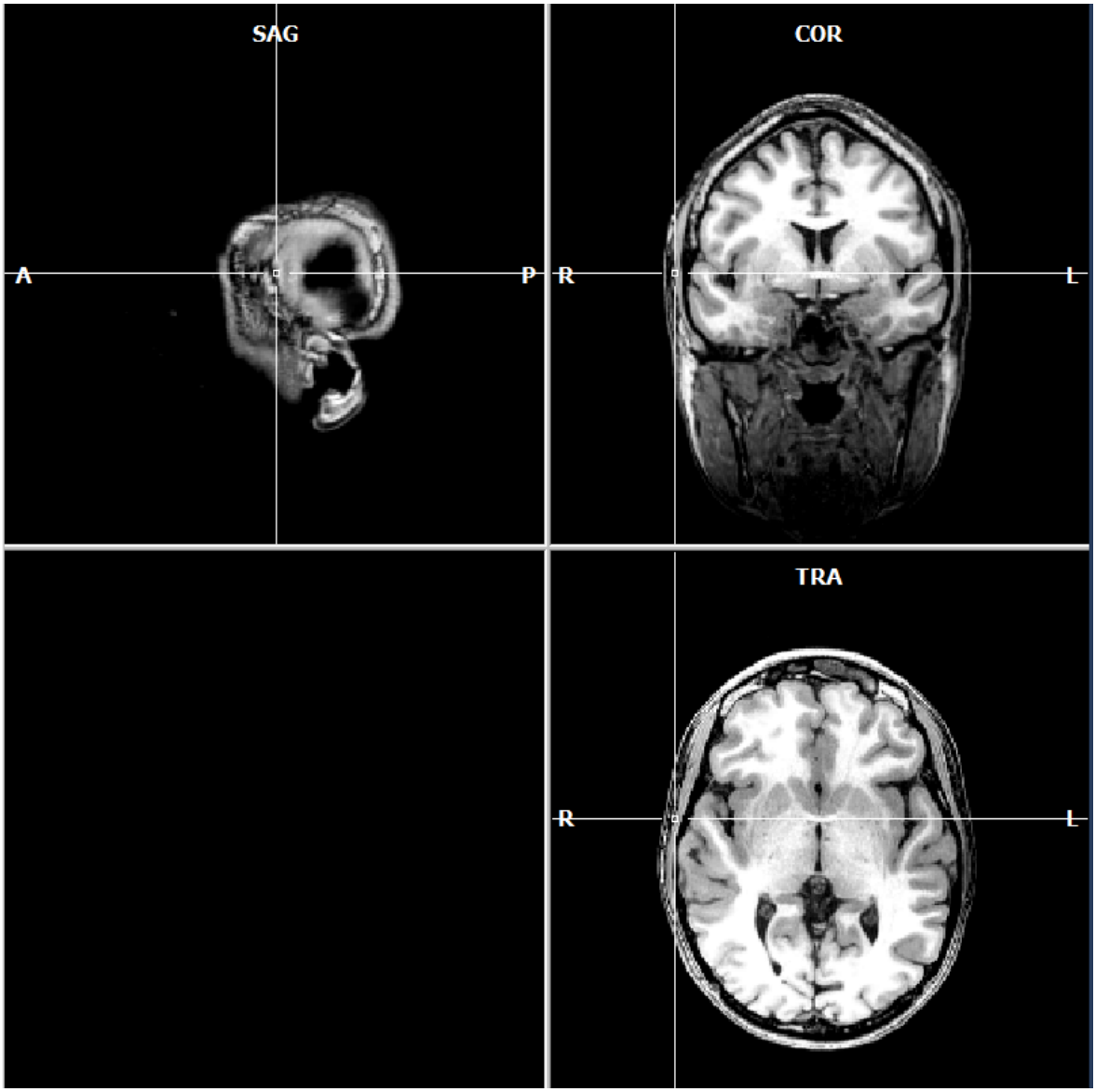

Figure B.34 *Visualization of the RP point.*

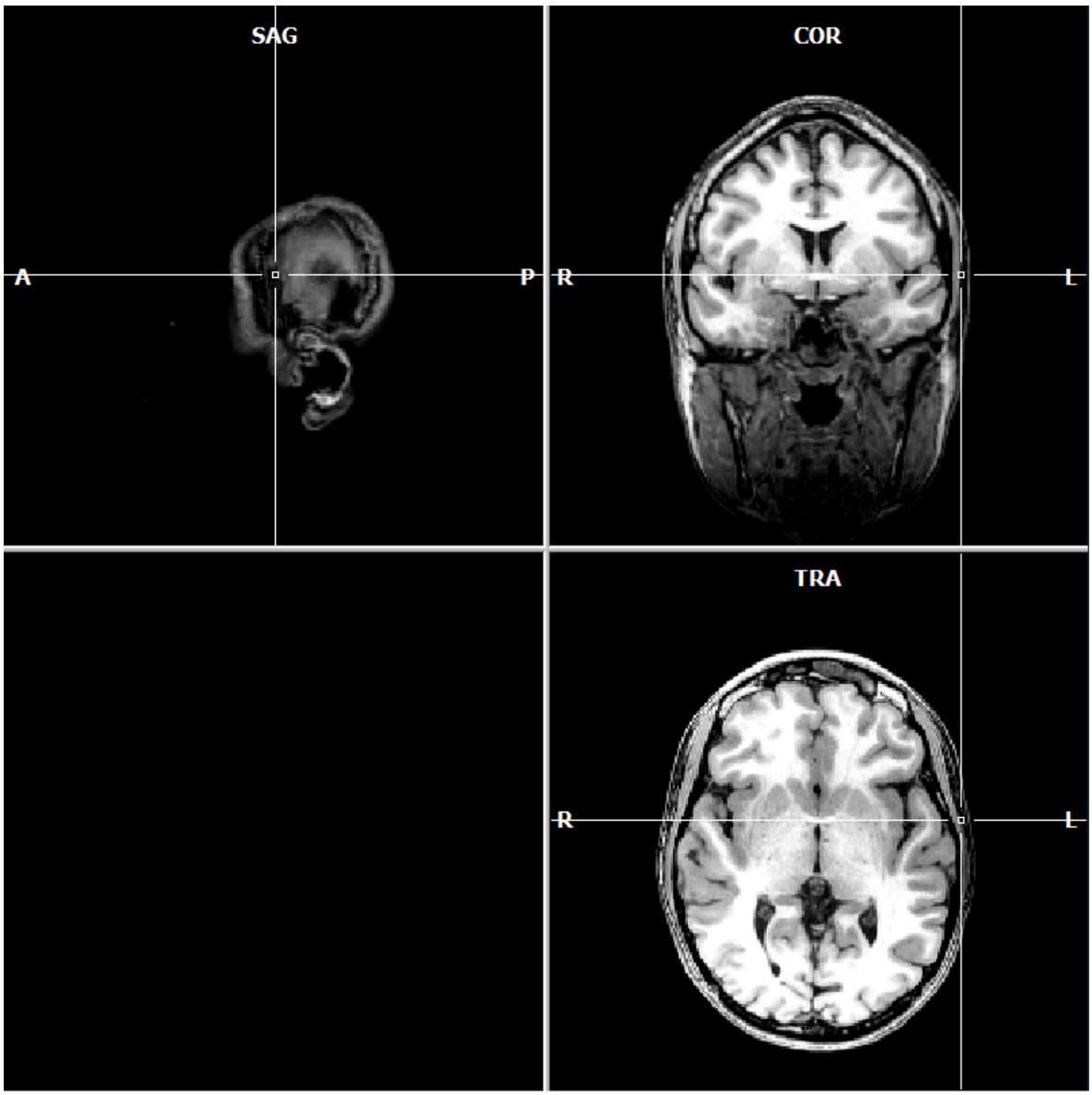

Figure B.35 *Visualization of the LP point.*

Now all Talairach reference points have been specified. Since this information is needed later, to transform functional data into Talairach space, the list of defined reference points will be saved to disk. Click the **"Save.TAL..."** button. A file .tal will be saved. Up to now, the reference points have been only specified, but the cerebrum is still in AC-PC space. To "warp" it finally into Talairach space, click the **"ACPC → TAL..."** button ***(Figure B.36)***.

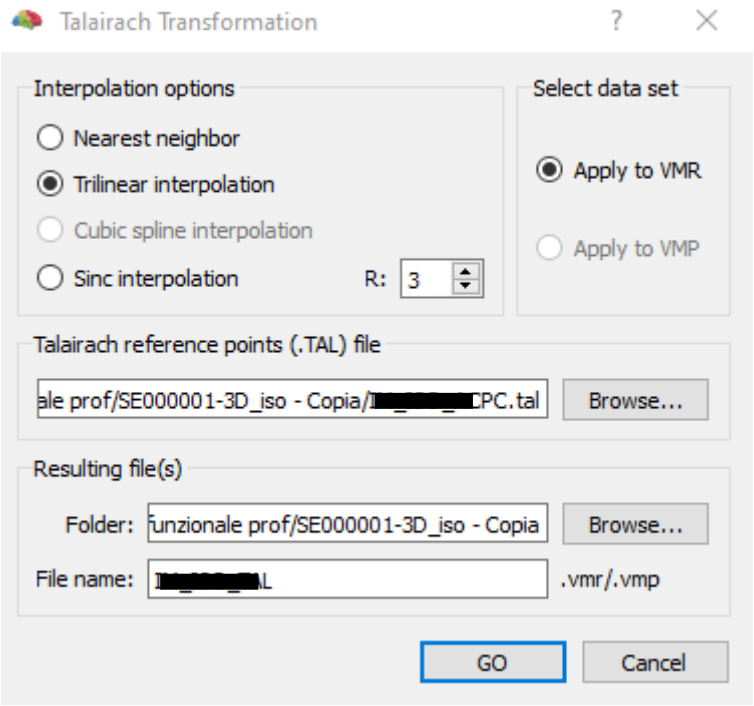

Figure B.36 *Talairach Transformation window.*

The specified reference points are now used to change the size of the brain in such a way that it fits into the size of the standard Talairach brain. After a few seconds the resulting new 3D volume has been computed and saved to disk. In addition, it is also shown automatically in a new window. The centre of the new Talairach data set is still the AC point and the brain is still located in the AC-PC plane. The cerebrum's size is, however, adjusted to fit into Talairach space ***(Figure B.37)***.

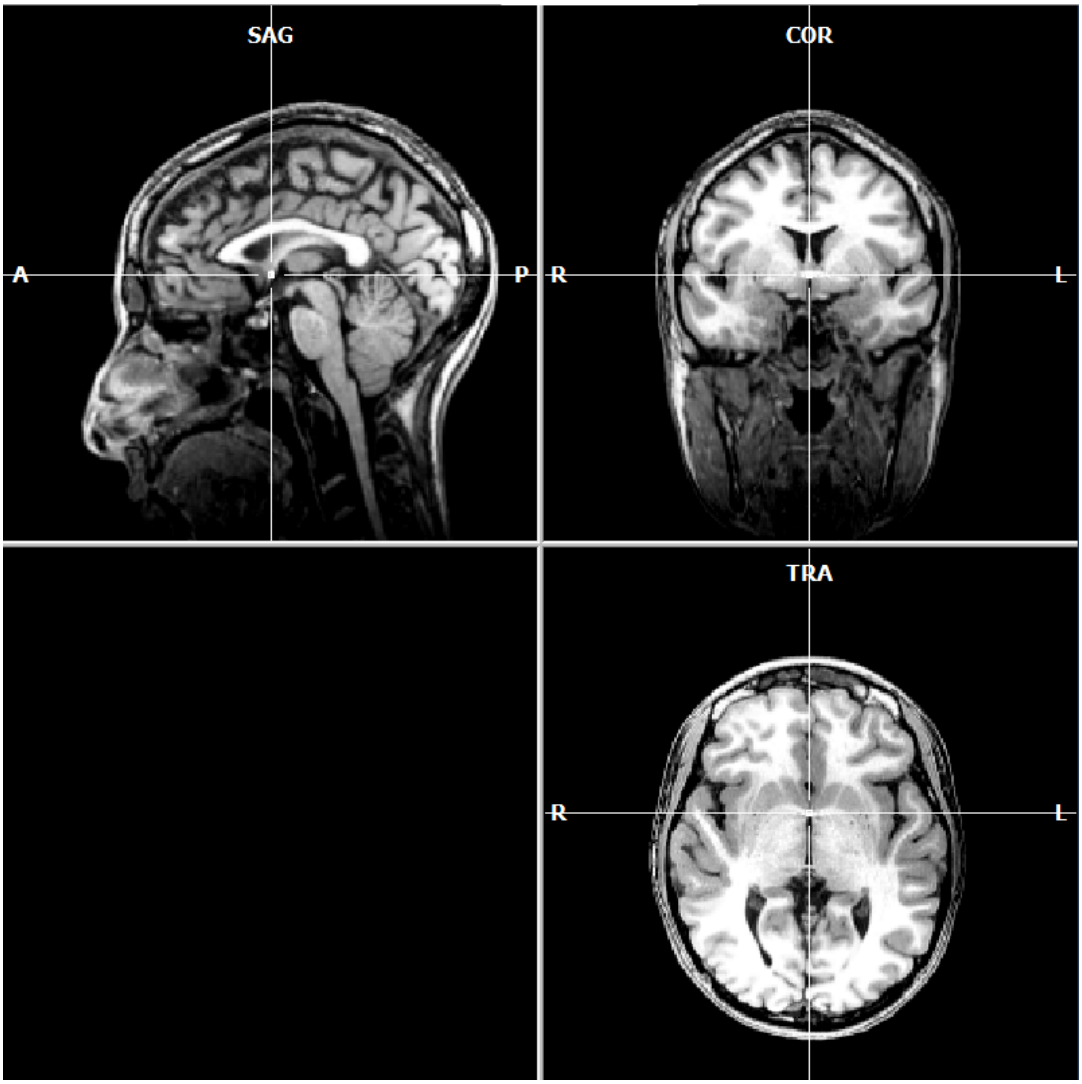

Figure B.37 *Visualization of the data transformed into Talairach space.*

B.8 Talairach transformation of functional data

In this step, functional data are transformed into Talairach space. The result of this process is a "VTC"' file (**VTC** = *v*olume *t*ime *c*ourse), containing the data from a corresponding FMR project ***(Figure B.38)***. Open the file ISO.tal obtained by the Talairach transformation. Use the menu item **"Analysis" → "Create 3D-Aligned Time Course (VTC) Data..."** to open the **"VTC File Creation"** dialog. The invoked **"VTC File Creation"** dialog contains several empty slots, which have to be filled to define the transformation "pipeline".

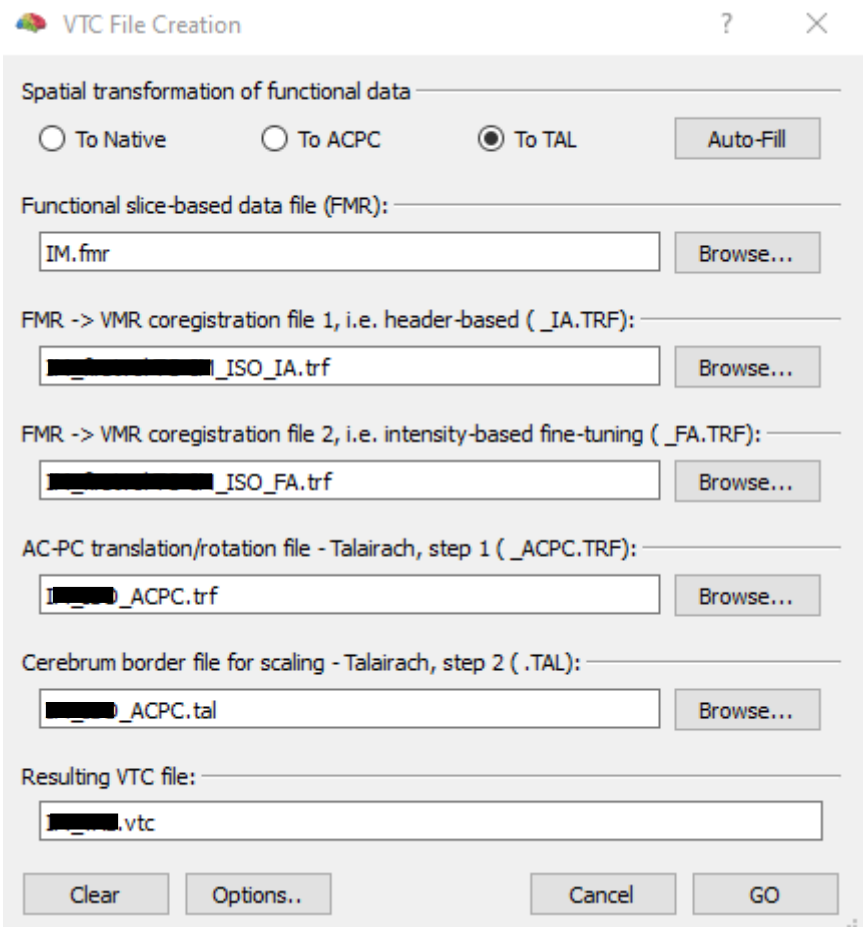

Figure B.38 *VTC File Creation window.*

Although it is possible to create a VTC in any 3D space, Talairach space allows to analyse data *across subjects*. According to this, our functional data in Talairach space can be *linked* to the anatomical data set in Talairach space. This linking possibility provides high flexibility. We can link the functional data from *any* experiment of a subject to a 3D data set and analyse across the functional data from different experiments. If all the data from the same subject has been transformed into Talairach space, detected brain activity can be located reliably and precisely (Goebel et al., 2011). In the **"Analysis"** menu, click the **"Link 3D time course (VTC) file..."** item, which invokes the **"Link 3D Volume Time Course (VTC)"** dialog ***(Figure B.39)***.

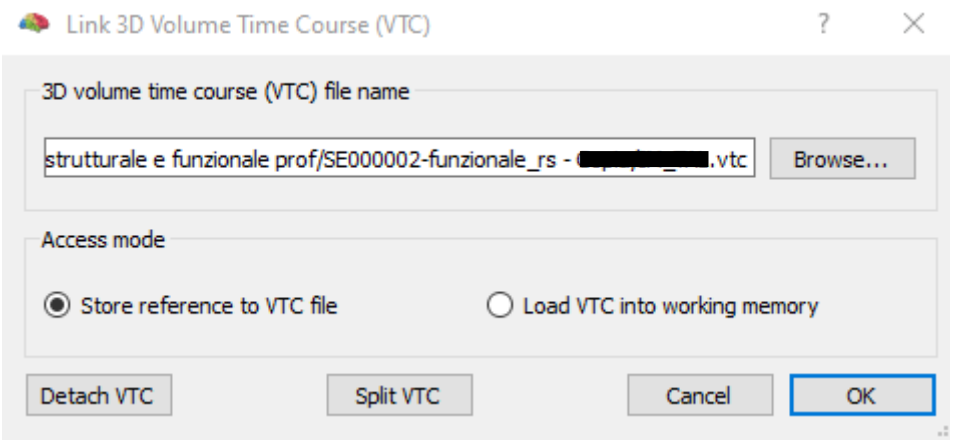

Figure B.39 *Link 3D Volume Time Course window.*

B.9 Independent Component Analysis

In BV, the spatial decomposition of the data is performed using "FastICA". To run FastICa it was used the deflation approach and Gaussian as Nonlinearity function. The number of components was by default kept 30. The input file to perform the spatial ICA is a VTC (volume time course) data set ***(Figure B.40).*** The threshold value was 10 and Z>2 ***(Figure B.41)***. The original fMRI data was pre-processed to improve the quality of data and then transformed into a normalized 3D space, known as VTC file. The VTC file was linked with the subject's normalized anatomical file. This allows to perform the ICA on a group of subjects and compare the IC across the subjects (Goebel et al., 2011).

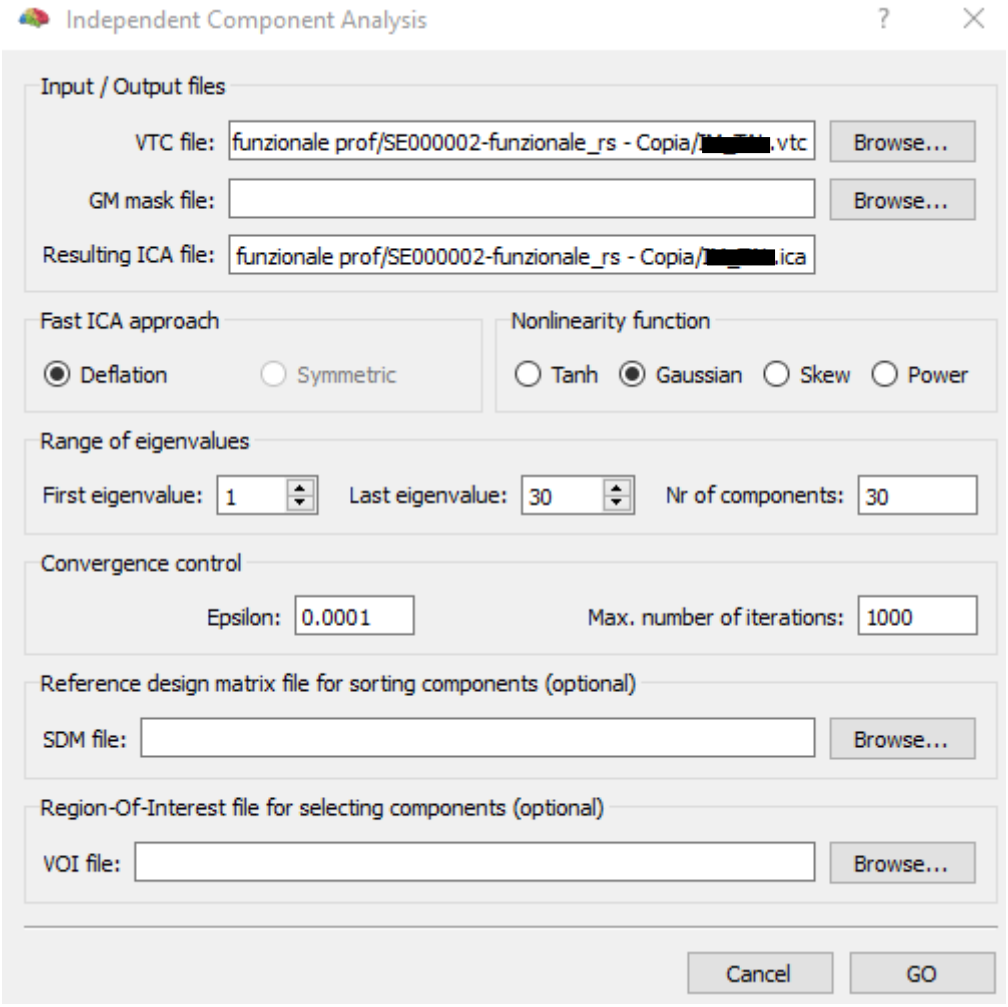

Figure B.40 *Independent Component Analysis window.*

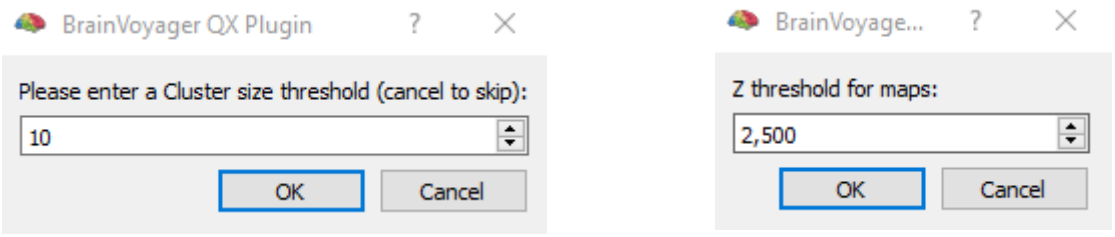

Figure B.41 *Definition of the Cluster size threshold (left) and Z threshold values (right).*

In ***Figure B.42*** the results obtained by the ICA are illustrated.

Figure B.42 *Visualization of one IC spatial map.*

Appendix C Diffusion Tensor Imaging Processing

C.1 Data

For the Diffusion-weighted (DW) data analysis the following data in ***Table 1*** are required.

Table 1 *Data needed for analysis of a DW-MRI experiment.*

Data	Type
DW-MR images	DICOM, ANALYZE, PHILIPS PAR/REC
Gradient information	Text file
Anatomical project	VMR

C.2 Creation of a Diffusion MR (DMR) Project

A new DMR Project can be created by selecting in the menu **File → Create Project Wizard**. A window will appear and the DMR project option has to be selected ***(Figure C.1)***.

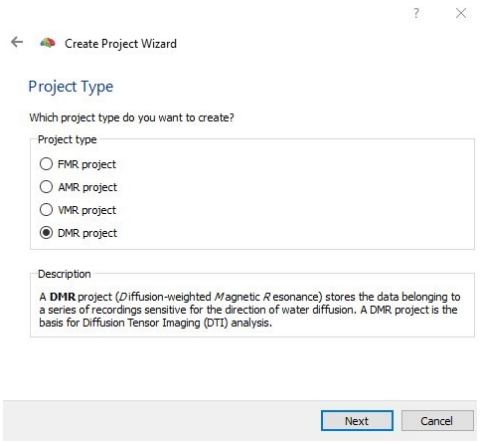

Figure C.1 *Creation of a new DMR project.*

Next step is to define the data type: in this case the data format is DICOM ***(Figure C.2)***.

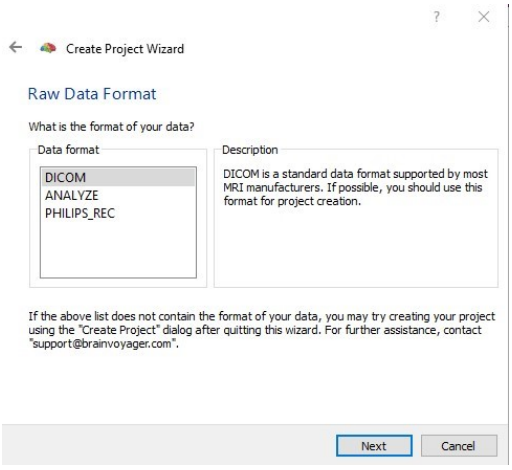

Figure C.2 *Selection of data type for the analysis.*

After choosing the correct data type, it is necessary to set the name of the project and select the folder in which data file is contained ***(Figure C.3)***. Then a window will appear in which all DICOM files are uploaded ***(Figure C.4)***.

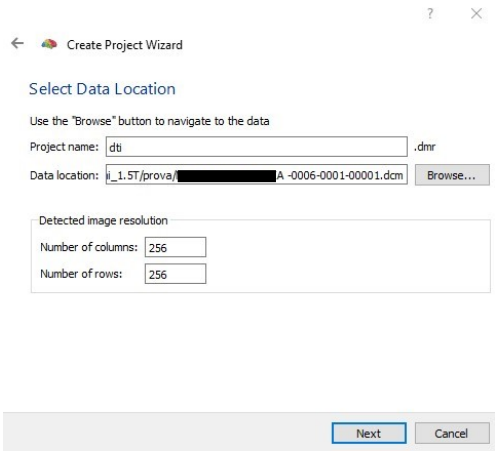

Figure C.3 *Project name creation and selection of the folder which contains the DICOM file.*

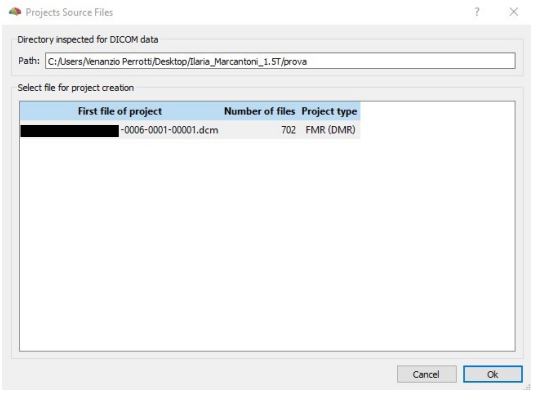

Figure C.4 *All the DICOM files necessary for the analysis.*

Afterwards the number of slices and the number of volumes must be entered. The gradient file must also be selected ***(Figure C.5)***.

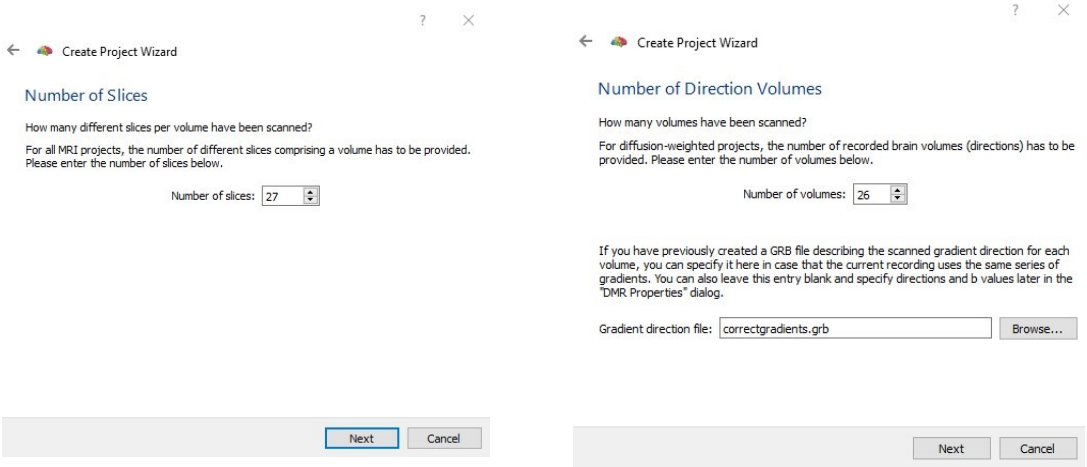

Figure C.5 *Selection of the number of slices, number of volumes and file .grb in which gradients are indicated.*

At the end of the DMR Project creation, Brain Voyager will give a summary of the project. In ***Figure C.6*** the first volume b0 is displayed. This volume contains 27 slices. The linked AMR file was created previously (Appendix B).

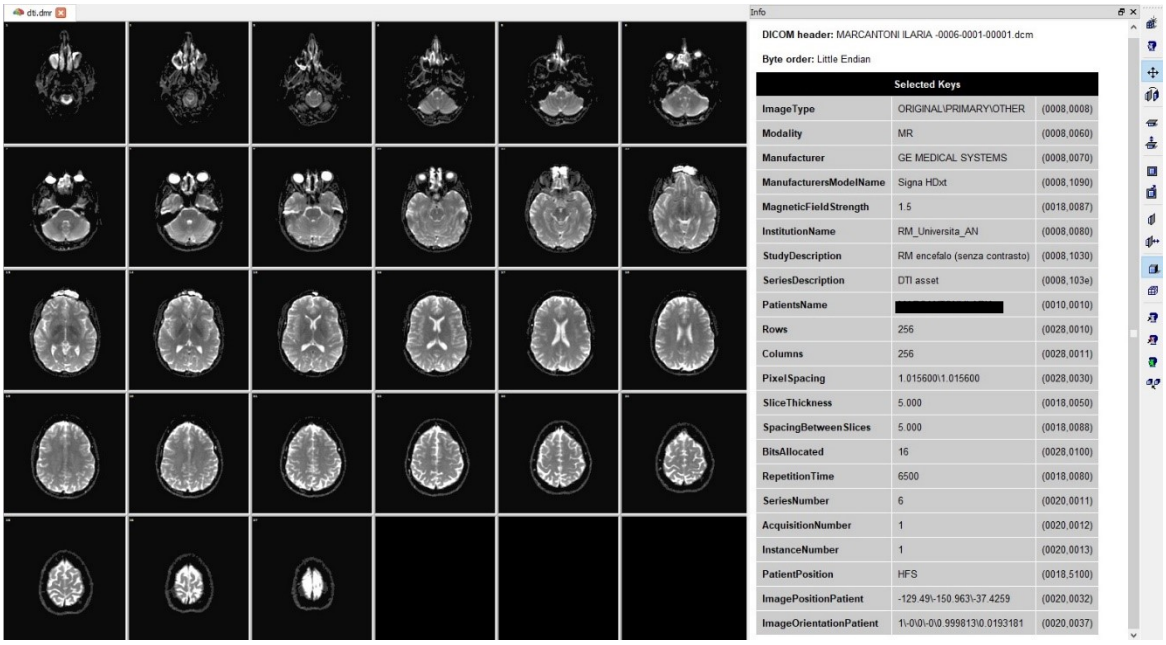

Figure C.6 *Illustration of the data and related information.*

It is also possible to select the DMR Properties ***(Figure C.7)*** to inspect if Brain Voyager has taken the correct parameters of the data and, if they are correct, select the Verified option to proceed.

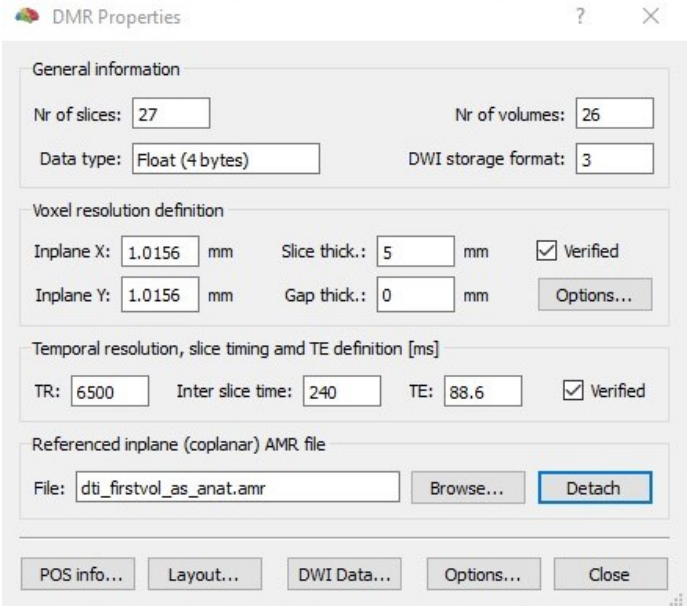

Figure C.7 *DMR Properties panel.*

C.3 Creation of Fractional Anisotropy and Mean Diffusivity maps

Based on the DMR data, it is possible to directly calculate tensors, Fractional Anisotropy and Mean Diffusivity maps.

Mean Diffusivity is defined as:

$$\mathrm{MD} = (D_{xx} + D_{yy} + D_{zz})/3 \equiv \frac{\mathrm{Tr}(D)}{3},$$

Fractional Anisotropy is defined as:

$$FA = \frac{\sqrt{3[(\lambda_1 - \lambda_2)^2 + (\lambda_2 - \lambda_3)^2 + (\lambda_3 - \lambda_1)^2]}}{\sqrt{2(\lambda_1^2 + \lambda_2^2 + \lambda_3^2)}}$$

Fully isotropic voxels have FA=0, while fully anisotropic voxels have FA=1 ***(Figure C.8)***.

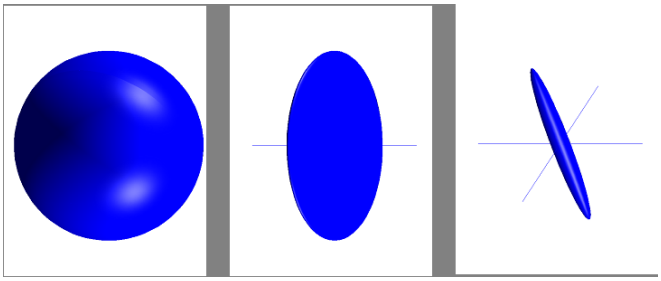

Figure C.8 *From left to right: FA=1, isotropic tensor. (λ1 = λ2) >> λ3, oblate tensor. (λ1 >> λ2, λ3, prolate tensor. FA of the oblate and prolate tensors might be the same, FA closer to 0.*

For the Tensor Calculations click **File→ DMR Properties → DWI data**. In the **Calculations** option is it possible to estimate the DDT file, MD and FA ***(Figure C.9)***.

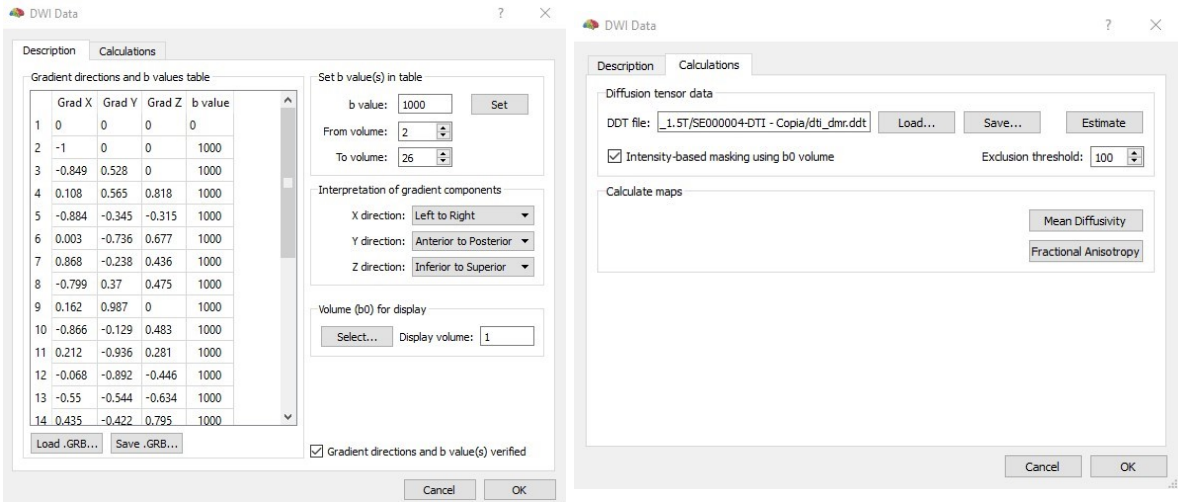

Figure C.9 *Illustration of the gradient file (left) and calculations tab (right).*

At this point it is also possible to mask the background of the image, by masking via a threshold. Clicking on the **Estimate** button, the tensor estimation is performed. After the calculations BV will ask to save the resulting DDT file, containing the tensor information. Afterwards the FA and MD are calculated and overlayed onto the DMR, by clicking on **Mean Diffusivity** and **Fractional Anisotropy** buttons ***(Figures C.10, C.11)***.

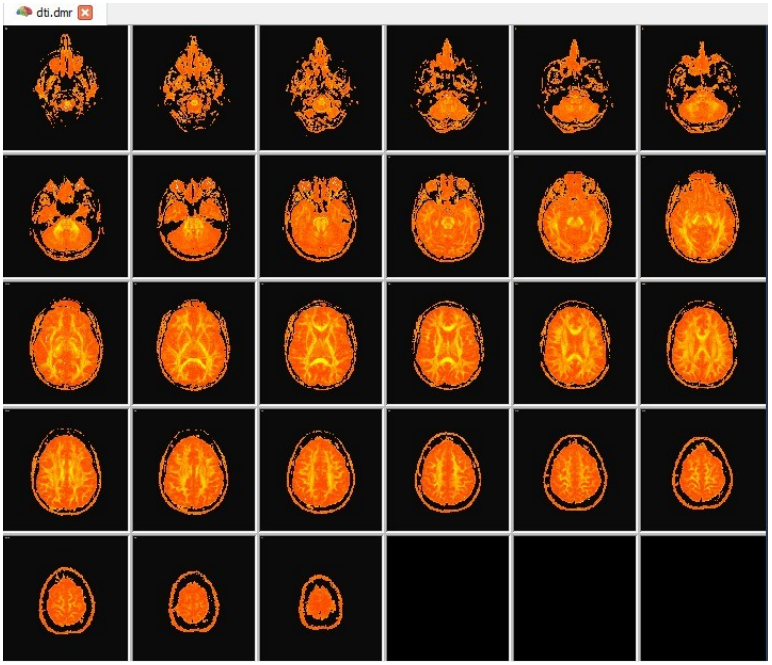

Figure C.10 *Visualization of the FA map.*

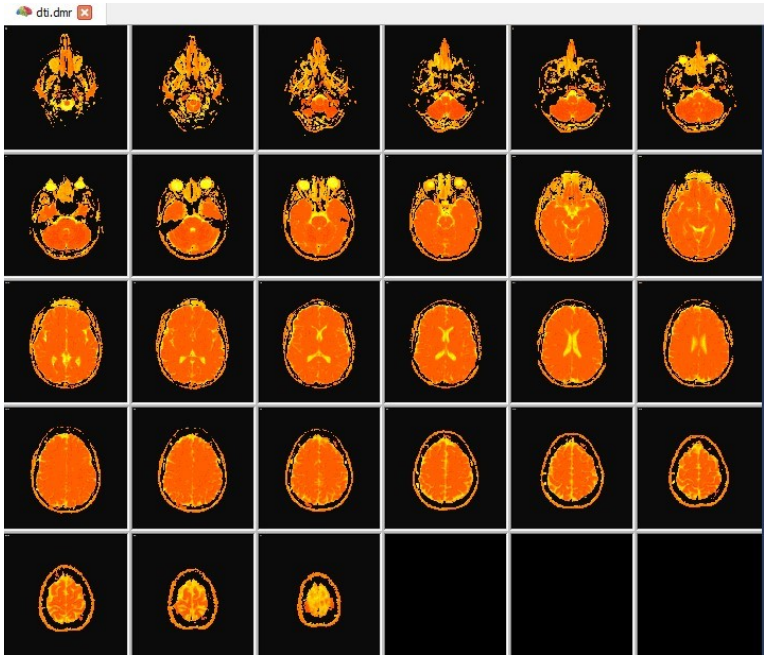

Figure C.11 *Visualization of the MD map.*

C.4 DMR-VMR co-registration

To perform the analysis in 3D, the DMR project has to be co-registered to a VMR project. The VMR acquired in the same session needs to be created and it can be brought into AC/PC or Talairach space. By selecting **DTI→ Coregister DMR-DWI to VMR**, a menu with 4 tabs appears. Click on **Browser** button to point to the previously created DMR project. BV automatically creates file names for the transformation files, i.e., <DMRname-TO-VMRname>_IA.trf and <DMRname-TO-VMRname>_FA.trf ***(Figure C.12)***.

Figure C.12 *DMR-VMR co-registration tab.*

Before running the initial and final alignment, the other tabs are inspected ***(Figure C.13)***.

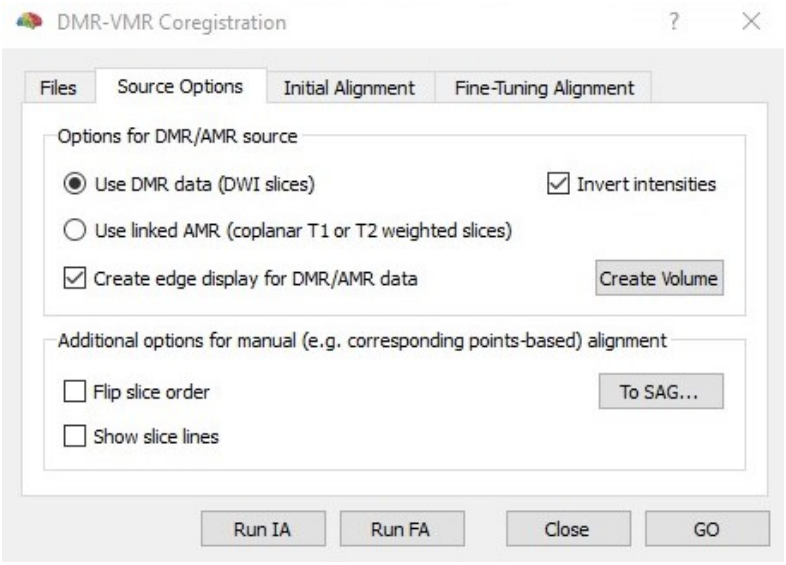

Figure C.13 *Source options tab.*

The DMR data to be used corresponds to the first volume of the DMR data b0. After choosing the option, click **Create Volume**. Then initial and final alignment are performed by clicking on **RUN IA** and **RUN FA**, leaving all the options by default ***(Figures C.14-C.16)***.

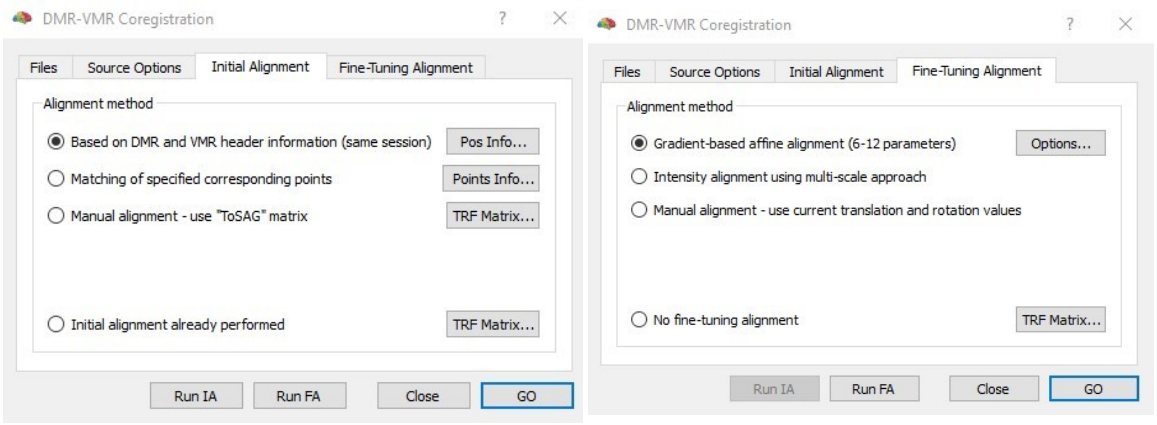

Figure C.14 *Initial and Fine-Tuning Alignment tabs.*

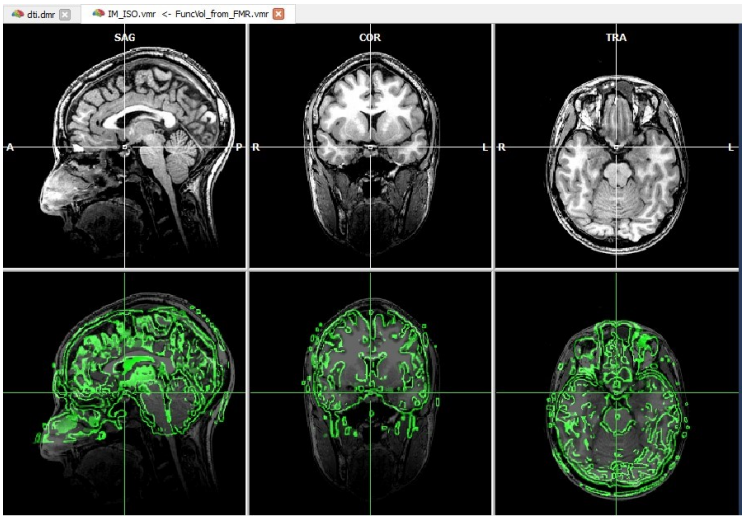

Figure C.15 *Illustration of the results of the IA. The green edges represent the DWI data.*

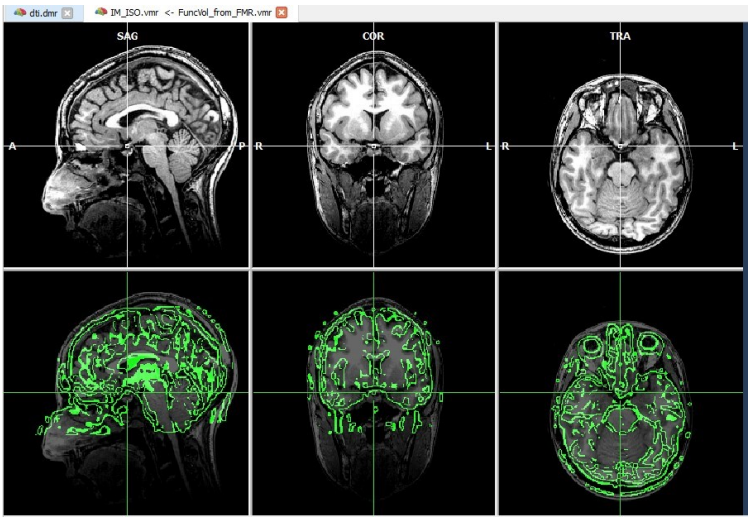

Figure C.16 *Illustration of the results of the FA. The green edges represent the DWI data.*

C.5 Creation of a Volume Diffusion Weighted (VDW) data set

A VDW data set is created by using the files obtained during the co-registration phase. By clicking on **DTI→ Create 3D Aligned Diffusion Weighted (VDW) Data**, a window appears: the **Browser** button is used to locate the DMR file and subsequently all the files necessary for the VDW creation ***(Figure C.17)***.

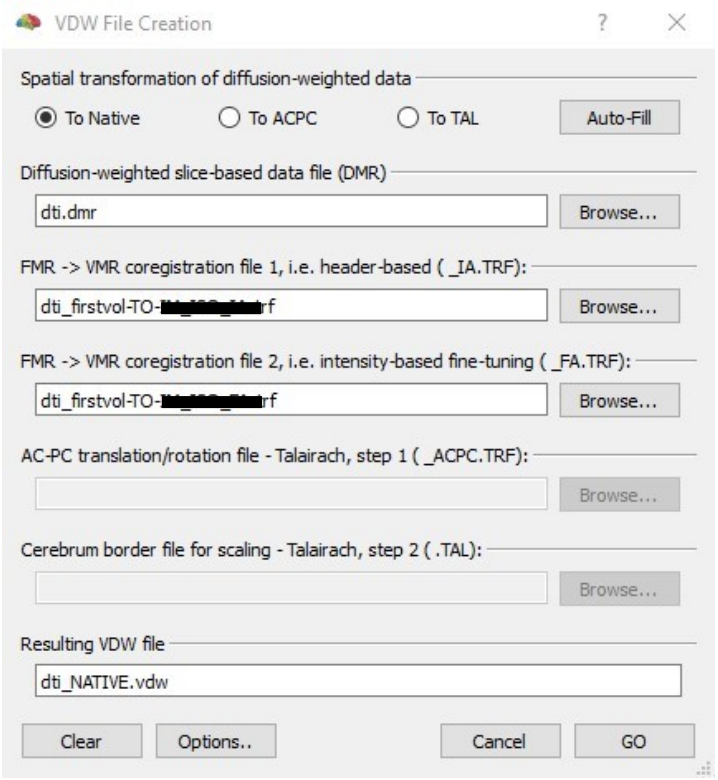

Figure C.17 *VDW File Creation window.*

In the **Options** window, is necessary to check whether **Sinc Interpolation** at **Interpolation options** is activated. DWI data is extremely sensitive to interpolation, so the best interpolation setting is required. However, Sinc interpolation may easily take hours to compute, so take the next best option, which is **Trilinear**.

C.6 Tensor, Diffusivity and FA calculation

By clicking again on **DTI→ Diffusion Weighted Data Analysis**, a **VDW Analysis** window appears. In the **Linked 3D aligned diffusion weighted data** part, clicking on the **Browser** button is it possible to point to the VDW file created previously. Clicking on the **VDW Properties** in the **VDW Analysis** window is it possible to find the gradient table. Once the VDW file and gradient information are correct, click **Estimate** in the **VDW Analysis** window. A DDT "Diffusion Tensor" file is created, and BV asks user to save this file.

C.6.1 Masking the DDT data

During the execution of the analysis the data outside the brain must be delated. In fact, due to the nature of the acquisition, there is noise present outside of the brain, which should be masked out. Besides the visual attractiveness, this also reduces the number of voxels significantly, which increases processing speed in later steps (Goebel et al., 2011).

The first step is to open the VMR corresponding to the DMR data. Remove non-brain tissue by using the **3D Volume tools →Segmentation → Options → Brain peeling** function and then hit the **Segment Brain** button ***(Figures C.18, C.19)***.

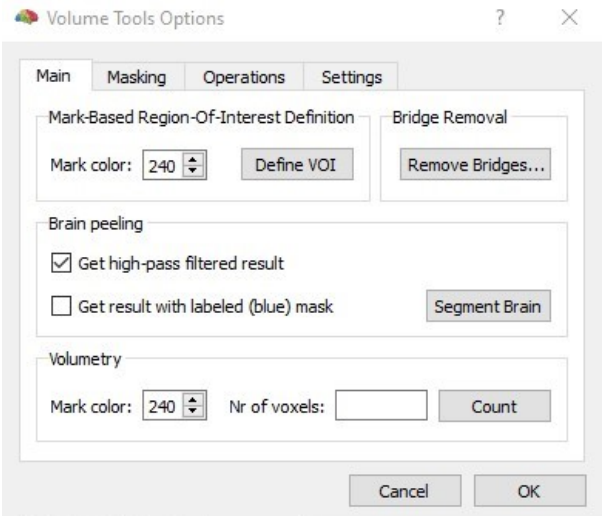

Figure C.18 *Volume Tools used for the brain segmentation.*

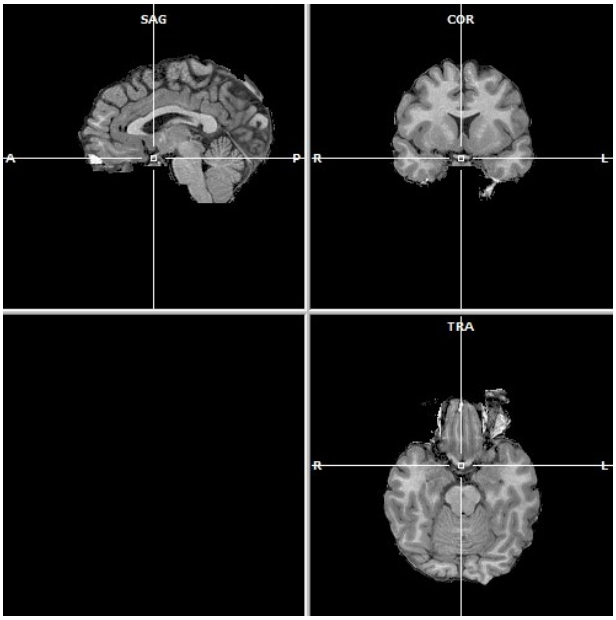

Figure C.19 *Illustration of the resulted peeled brain.*

At this point the VDW file created before has to be linked to the VMR through the following command: **DTI→ Diffusion Weighted Data Analysis**. In **the Linked 3D-aligned diffusion weighted data** section, clicking the **Browser** button the VDW file created before is located. Afterwards it is necessary to define a VOI containing all the brain voxels. To get a smooth VOI without any holes in it, click the **Gaussian** button in the segmentation tab ***(Figure C.20)***.
All brain voxels should be selected now and displayed as blue voxels. Now it's time to fill any holes which might still be present in the mask. Go to **3D Volume tools →Segmentation →Options→ Masking**, and click the **Fill Holes** button, and then **OK**. Afterwards it is possible to define a VOI in the **Option** window of the **Segmentation** tab ***(Figure C.21)***.

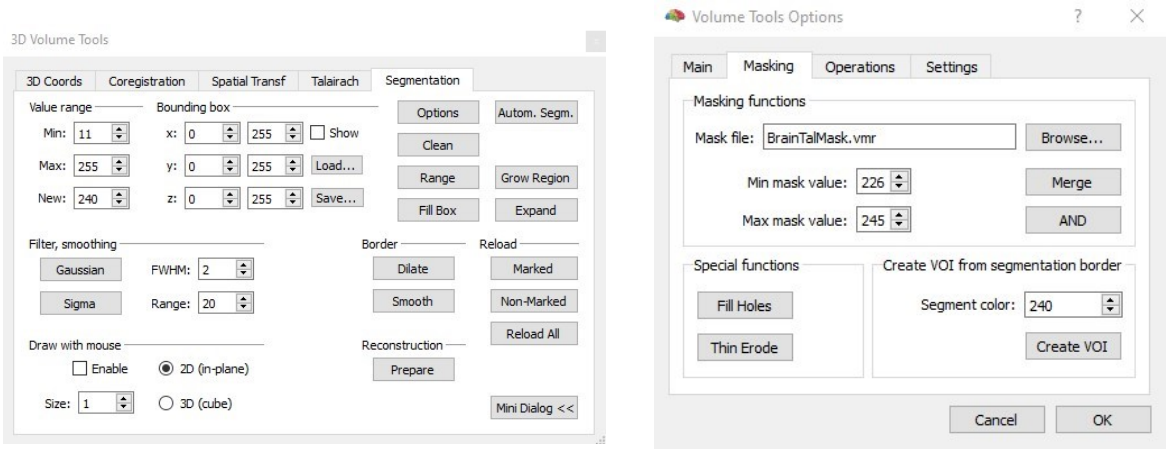

Figure C.20 *3D Volume Tools and Volume Tools Options tabs.*

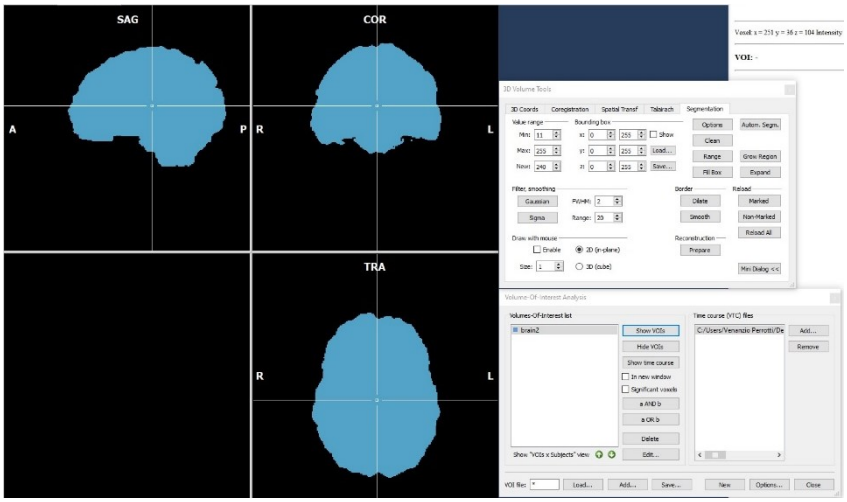

Figure C.21 *Illustration of the resulted masked peeled brain.*

The next step is to convert the VOI into a mask file, by clicking the **Region of Interest Analysis** option in the **Analysis** menu. A dialog will open in which the created VOI is found and then clicking on the **Options** button, in the **VOI Functions** tab the options must be set as follows ***(Figure C.22)***.

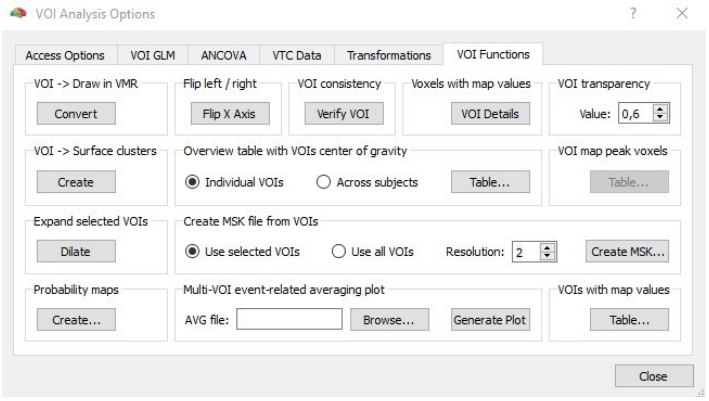

Figure C.22 *VOI Analysis Options tab.*

To apply the mask to tensor calculations, re-open the file .vmr. Go to **DTI → Diffusion Weighted Data Analysis**. The VDW previously created must be loaded and then, clicking on **Use spatial masking**, is possible to locate the mask file with the **Browser** button ***(Figure C.23)***.

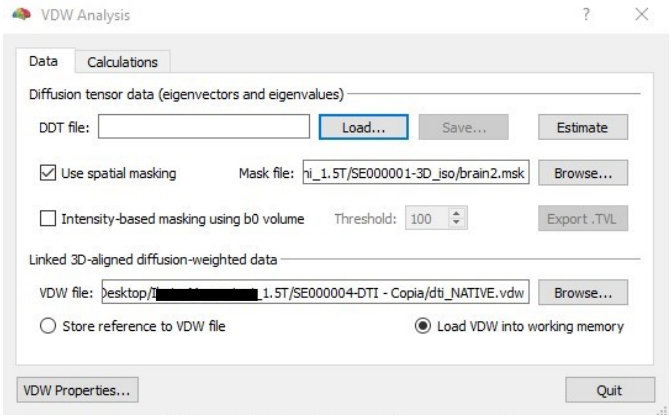

Figure C.23 *VDW Analysis tab.*

By clicking on the **Estimate** button, a masked DDT file will be created. **Fractional Anisotropy** and **Mean Diffusivity** can be calculated in the **Calculations** tab in the **VDW Analysis** window ***(Figure C.24)***. To produce a Mean Diffusivity map, overlayed on the VMR, the **Mean Diffusivity** button is used and then a map, interpolated to VMR resolution is created.

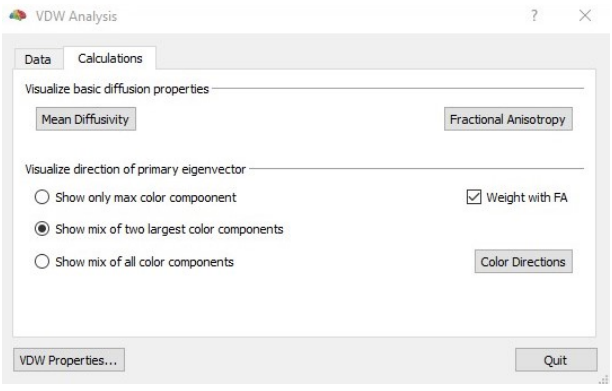

Figure C.24 *Calculations tab in the VDW Analysis window.*

Clicking on the **Fractional Anisotropy** button the FA map is calculated and overlayed on the VMR. This map is in VMR resolution. For visualisation purposes, FA is scaled up a factor 10 in BV. So, FA = 2.0 in the map is in reality FA = 0.2 (Goebel et al., 2011). In ***Figure C.25*** and ***Figure C.26*** the MD and FA maps are shown.

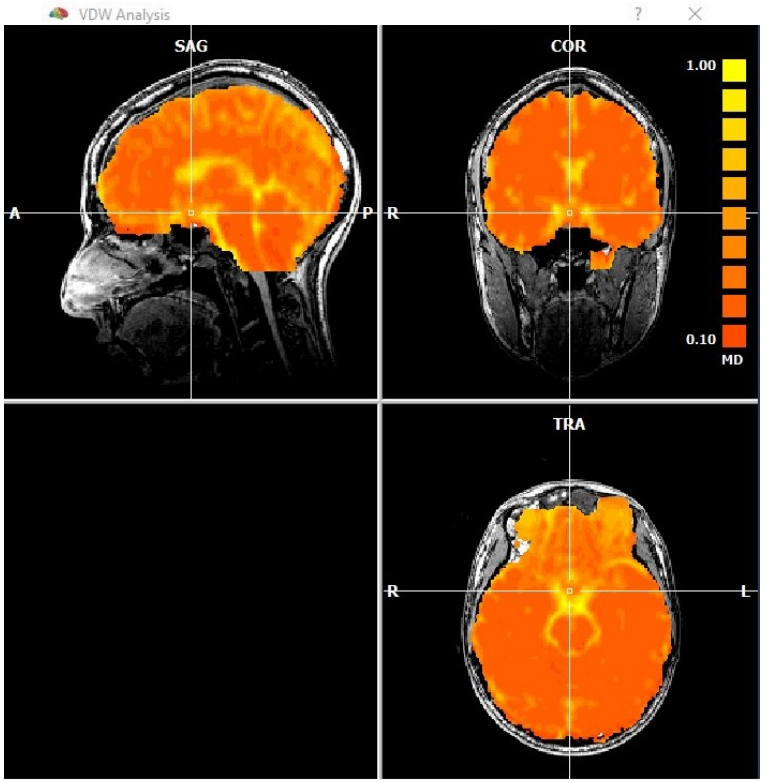

Figure C.25 *Mean Diffusivity map.*

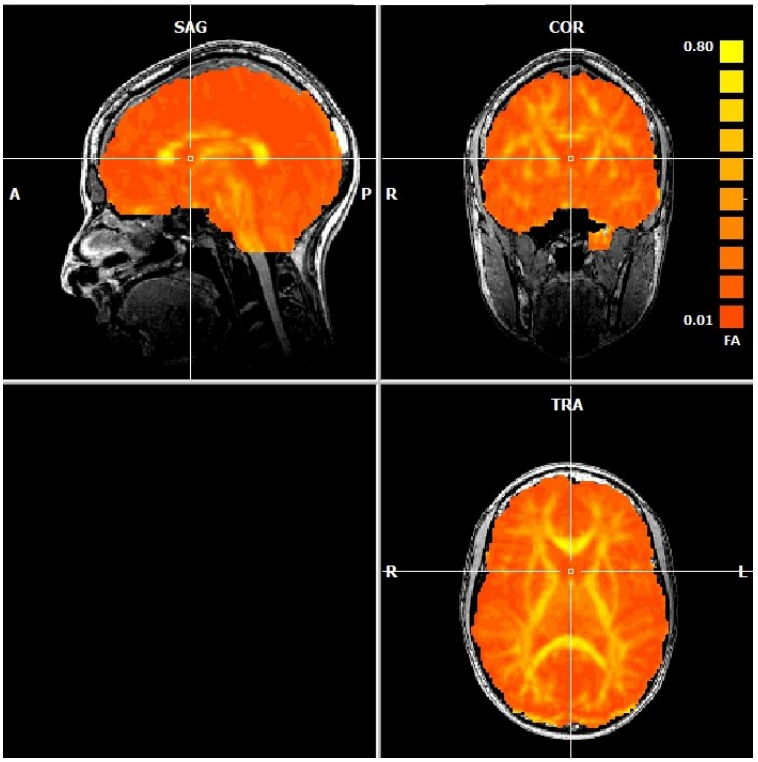

Figure C.26 *Fractional Anisotropy map*

C.6.2 Colour coded maps

Colour coded maps can be displayed by selecting one of the options in the **Visualize direction of primary eigenvector** part of the **VDW Analysis** window. It is initially recommended to choose the Weight by FA option. The color options are listed in ***Table 2.***

Table 2 *Colour coded options for the visualization of the FA map.*

option	Impact on MD	Impact on FA
Show only max colour component	In a voxel, show max (Dxx, Dyy, Dzz). If max = Dxx :=red, if max = Dyy :=green, max = Dzz :=blue	Based on eigenvector information; if the principal eigenvector is largest: in x direction, colour=red; in y direction, colour=green; in z direction, color=blue;
Show mix of two largest components	Two largest components are mixed: x + y=red+green=yellow. x + z=red+blue=purple. y + z=green+blue=cyan.	
Show mix of all colour components	Colours are yellow, purple and cyan when the mix includes 2 components; when the mix includes 3 components, the map is represented in white.	

In ***Figure C.27*** the FA map based on 3 max components is shown.

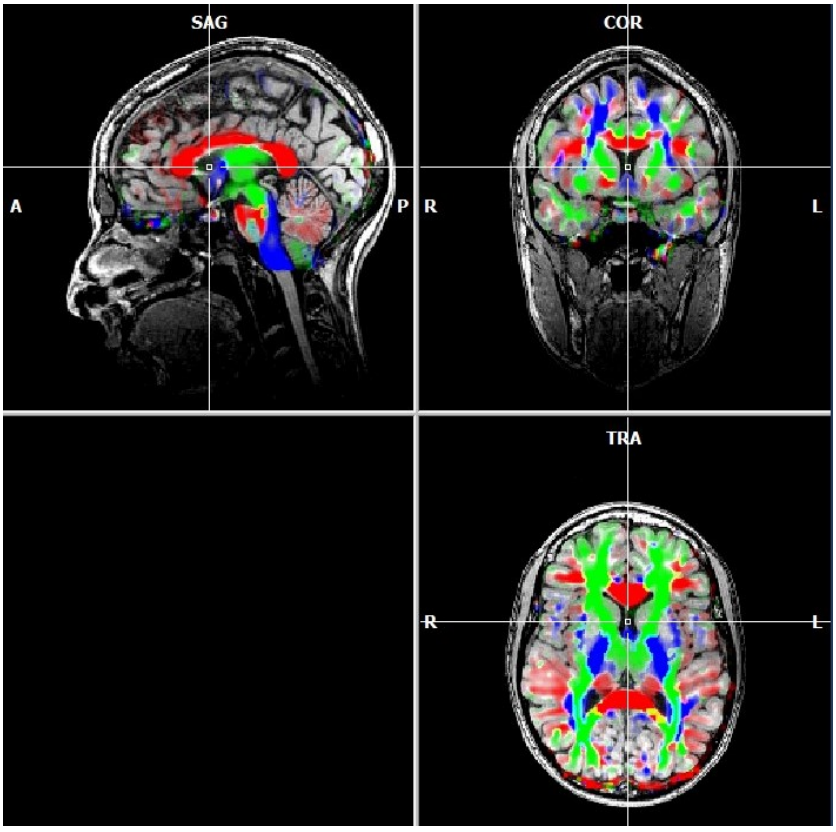

Figure C.27 *FA map based on 3 max components.*

C.7 Tensor visualization

After performing all steps until calculation of the tensors (DDT file creation), the tensors can be visualised in 3D space. At this point the file .vmr has to be opened and then the DDT file is loaded via **DTI → Diffusion Weighted Data Analysis →Browser**. Clicking on **DTI → Tensor Visualisation**, a new main window will open, and the tensor data is visualised as colour coded lines ***(Figure C.28)***. Colour coding is identical to that of a FA/MD direction colour coded map. The number of visible tensors can be adjusted by de- or increasing the FA threshold.

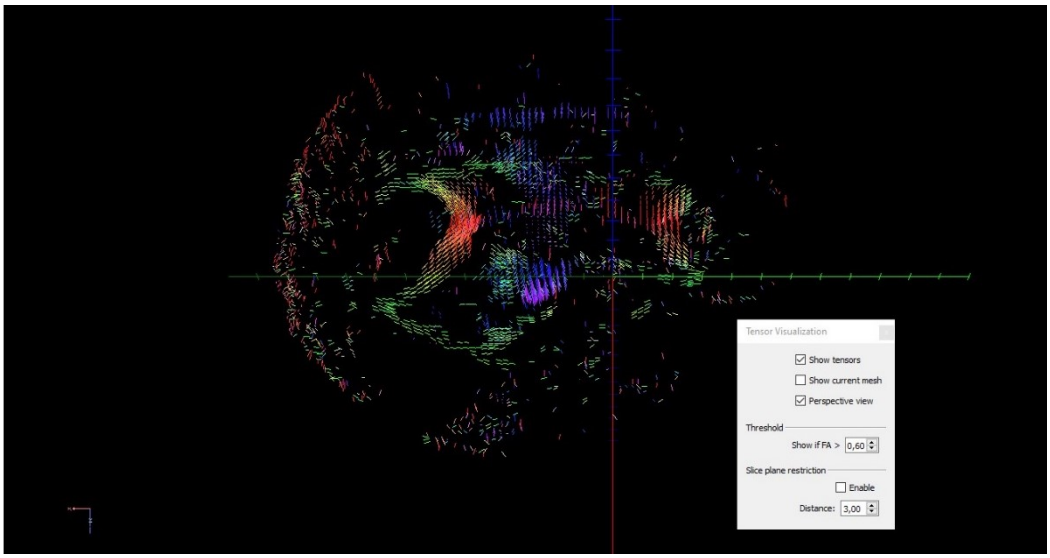

Figure C.28 *Visualization of tensors with a FA threshold= 0.6.*

The tensor view may also be limited to a slice instead of the whole volume. By clicking one of the "cut"- buttons listed below in ***Table 3***, one or more slices can be displayed.

Table 3 *Three possible slice cutting options.*

	Transversal slice cut
	Sagittal slice cut
	Coronal slice cut

BV will show the selected slice, and by checking the **Slice plane restriction** box, the tensors will be limited to the slice(s) selected.

C.8 Fiber tracking

C.8.1 Interactive Fiber Tracking

Interactive fibre tracking is useful for exploring the tracts ***(Figure C.29)***. In real-time, the user can "draw" fibres on a slice. BV puts seedpoints on the location selected by the user. This procedure is carried out by following these steps:

1. Open a VMR
2. Open a DDT file
3. (optional) calculate FA/MD maps
4. Go to DTI --> Fiber Tracking and Rendering
5. Display a slice by using the buttons from Table 3
6. use Ctrl+Alt+Left mouse click to paint fibres on the slice

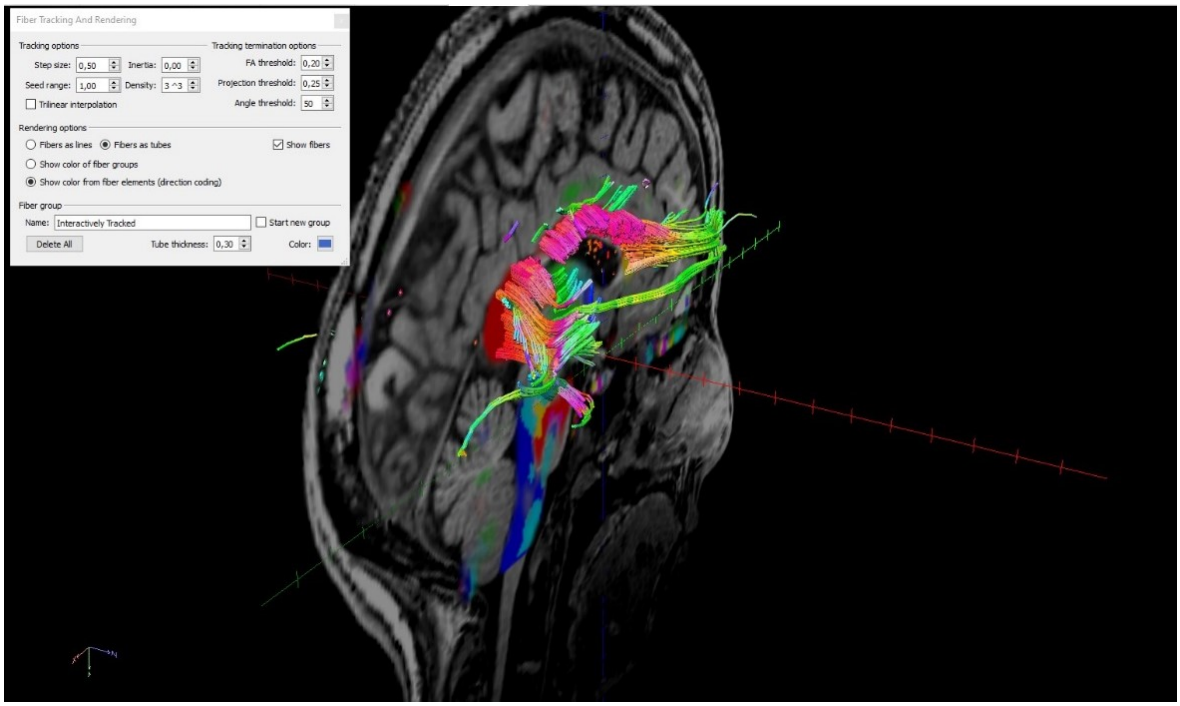

Figure C.29 *Visualization of the interactive fibre tracking results, by selecting points located on the corpus callosum.*

C.8.2 Fiber tracking from seed regions (VOI/ROI)

Fiber tracking can also be started from anatomically or functionally (fMRI) defined regions, usually termed regions of interest (ROI) or volumes of interest (VOI). Anatomical VOIs are defined by drawing them on a VMR with or without an overlayed FA/MD map. The procedure consists in opening a VMR and the DDT file, as explained before, and then overlay a FA/MD colour map. Next, go to the VMR, open the **3D Volume Tools** dialog, and click on the **Segmentation** tab ***(Figure C.30)***.

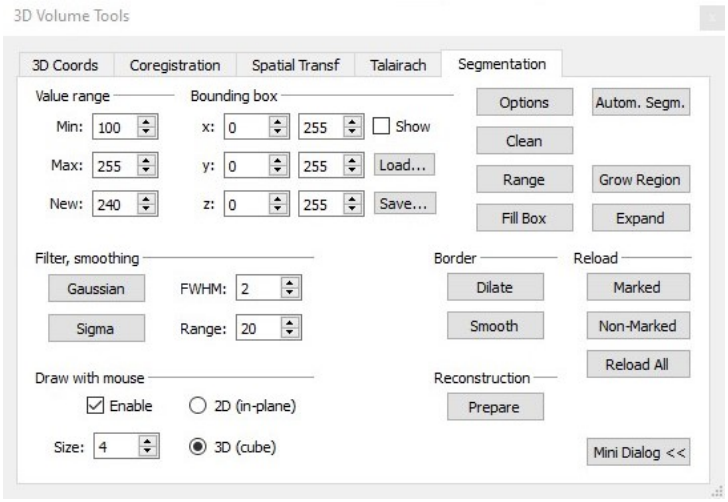

Figure C.30 *Segmentation tab in which the option Draw with mouse is enabled. The 3D cube and size =4 options are chosen.*

In the **Draw with mouse** section on the lower left of the tab, check the **Enable** box. This option allows the user to use a drawing pen, and the properties of this pen can be changed 1) by size and 2) 2D or 3D: in 2D, the pen draws a square i.e. 2×2 voxels, in 3D a cube with dimensions set by **Size**, i.e. 2 × 2 ×2 or 3 × 3 × 3 voxels. Now is it possible to draw with Ctrl+Left mouse click. A VOI can be drawn now on the corpus callosum ***(Figure C.31)*** using Ctrl+left mouse click. With Shift+left mouse click, voxels may be removed from the VOI. When drawing is finished, click the **Options** button on the **Segmentation** tab. A new window opens and, by clicking on the **Define VOI** button, a name for the VOI must be entered. Type a name and click **Ok**. The VOI analysis window is now shown, displaying all currently defined VOIs ***(Figure C.32)***.

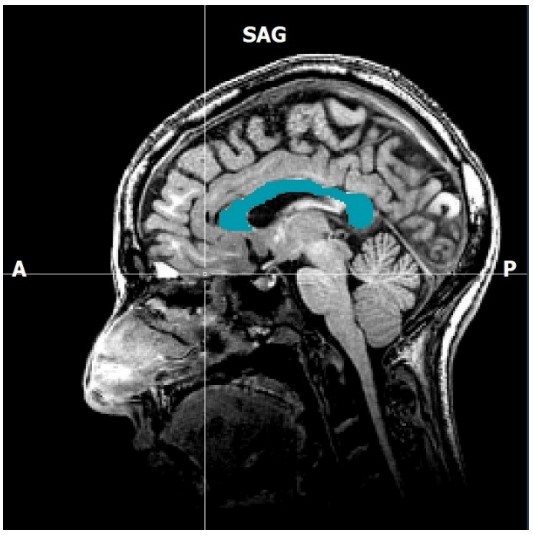

Figure C.31 *Illustration of the VOI defined on the Corpus Callosum.*

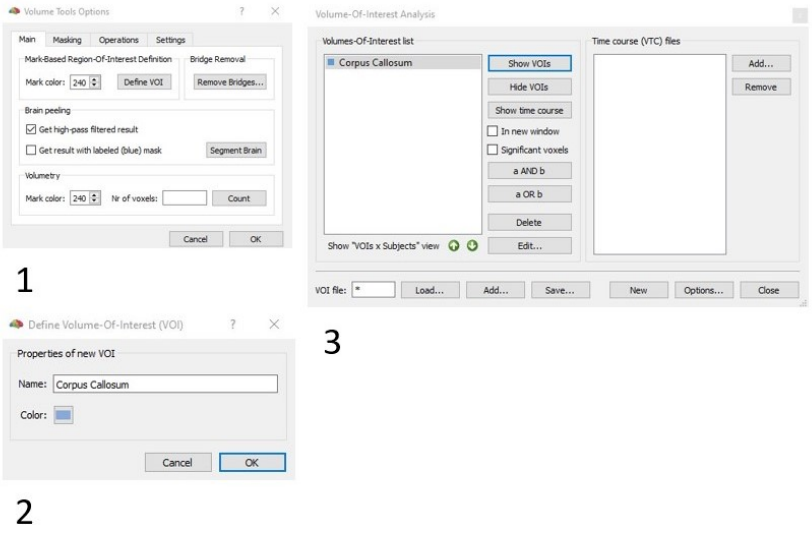

Figure C.32 *The steps necessary for the definition and creation of a VOI of the corpus callosum.*

Next, set the parameters for fibre tracking in the **DTI → Fiber Tracking and Rendering** window ***(Figure C.33)***.

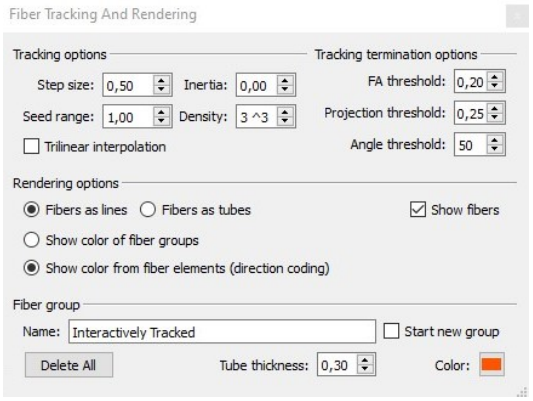

Figure C.33 Fiber Tracking and Rendering tab.

Acknowledgements

Desidero innanzitutto ringraziare la mia relatrice, la Prof.ssa Mara Fabri, per la sua disponibilità e per avermi sempre accompagnata e guidata durante questo percorso non privo di difficoltà.

Voglio inoltre ringraziare la mia correlatrice, la Dott.ssa Ilaria Marcantoni, per la sua pazienza e per avermi seguito e supportato nella realizzazione di questo elaborato.

Un grande ringraziamento alla Prof.ssa Laura Burattini, per avermi dato la possibilità di lavorare a questo progetto, permettendomi di esplorare con interesse ed entusiasmo questo nuovo campo.

Un sincero grazie a Giusi Piccolantonio per il suo lavoro pionieristico, e per avermi aiutata nella risoluzione dei problemi incontrati durante questo percorso.

Un altro ringraziamento speciale va anche a chi non ho avuto la possibilità di conoscere in prima persona, ma senza i quali non avrei mai potuto svolgere questo lavoro: il Prof. Gabriele Polonara, direttore di Neuroradiologia; le Dott.sse Mojgan Ghoushi e Nathalie Herbert, dirigenti medici di Neuroradiologia; Marco Valenti, Luca Reversi e Francesco Mariotti, fisici di Neuroradiologia; Luigi Imperiale, Lucio Montesi, Simone Marinelli e Alessio Canari, Tecnici di Neuroradiologia (acquisizione e salvataggio dati); la Dott.ssa Nicoletta Foschi, dirigente medico di Neurologia, e la Prof.ssa Simona Lattanzi, neurologa della Clinica Neurologica, referenti per i pazienti epilettici.